



University  
of Glasgow

Spathopoulos, Vassilios McInnes (2001) *The assessment of a rotorcraft simulation model in autorotation by means of flight testing a light gyroplane*. PhD thesis.

<http://theses.gla.ac.uk/797/>

Copyright and moral rights for this thesis are retained by the author

A copy can be downloaded for personal non-commercial research or study, without prior permission or charge

This thesis cannot be reproduced or quoted extensively from without first obtaining permission in writing from the Author

The content must not be changed in any way or sold commercially in any format or medium without the formal permission of the Author

When referring to this work, full bibliographic details including the author, title, awarding institution and date of the thesis must be given

**THE ASSESSMENT OF A ROTORCRAFT SIMULATION  
MODEL IN AUTOROTATION BY MEANS OF FLIGHT  
TESTING A LIGHT GYROPLANE**

**VASSILIOS McINNES SPATHOPOULOS**

Thesis submitted to the Faculty of Engineering, University of Glasgow, for the Degree of Doctor of Philosophy. All aspects of the work contained herein are original in content except where indicated.

This thesis is based on research conducted between October 1996 and March 2001 at the Department of Aerospace Engineering, University of Glasgow.

Vassilios McInnes Spathopoulos, August 2001.

© Vassilios McInnes Spathopoulos, 2001.

# Acknowledgements

It is the dream of every researcher, to reach a point in their thesis where he/she is found struggling to having the amount of space necessary to accommodate material for which he/she feels a personal enthusiasm. In commencing the expression of acknowledgement to the numerous people who contributed explicitly or implicitly to the realisation of this thesis, it seems as if I have finally encountered this difficulty..

It is *particularly* difficult for me to find the words for expressing my gratitude to both my supervisors Dr Stewart Houston and Dr Douglas Thomson for helping me survive what has been a long and often twisting road to success. I wish them the best of luck with the continuation of their gyroplane project, the visualisation and development of which required plenty of imagination and courage on their behalf.

The successful completion of this work would have never been possible without the Spartan discipline, persistence (damn right stubbornness at times!), and above all the technical brilliance of Robert Gilmour. In fact as he himself appropriately described it, 'The Albatross' would have never taken off without the fantastic support offered from the team of technicians at Spencer St., to all of which I am indebted.

I could fill the next many pages listing the huge number of friends and relatives who in one way or another contributed to the completion of my PhD work. Since I find it quite probable though that the reader is more interested in a list of Glauert's publications in autorotation than a catalogue of my own companions of the last years, I will have to limit this to the absolutely essential. This is not to say that the people not getting direct credit here will not forever stay in my mind for the support they offered both inside and outside my working environment. I could not commence from a different starting point than that of the Flight Dynamics Lab group and its many faithful followers and fans. Thanks first of all to the British connection, Sharon, Garry and Neil for their invaluable academic input, their lessons on how to apply glaswegian humour to dealing with stressful situations, and above all for helping me rid of those brain cells that were too weak to be of any use in my intellectual efforts. On a more international note, 'eskerrick asko' (thanks!) to Xab who's achievements in enduring my constant whinging and helping me understand Glauert's inflow theory merit him a degree in adult psychology and education, to Harold both for ensuring that my diet did not consist only of spicy pasta and for constantly reminding me that there are other things worth giving notice to outside the PhD, and to Fotis, who contributed to 'conversation therapy' sessions only in the way a Greek could, also stoically putting up with listening to more Greek swear words in the few months he spent sitting next to me than he did during the whole of his military service..

I would also like to thank Dano and Katitsa for some wonderful 'spirit-ual' evenings and for making autorotation theory seem relatively simple by introducing me to the world of central European politics, and to Efisio, Paul and Andi, simply for being the best flatmates I ever had. Sara deserves a special mentioning if for nothing else, just for being the first arts student ever introduced to the concept of rotorcraft model validation, and realising that the end was in sight when observing that "those two lines are close to each other!". It would also constitute an omission if I did not mention Marilena, who in one way or another made this a PhD to remember..Finally I must not forget my friends in Greece, Fatsa and Monos in

particular, for their great support offered via email and internet chat, strictly outside working hours of course!

It is said that you can choose your friends but not your relatives and family, but I have to say that with regards to the support given by the people close to me, I could not have chosen better! I thank my uncle and aunt's family for being there whenever I needed them, also offering the best B&B service in town during the final months of my work, and my Scottish grandparents simply for becoming more like my own parents but most importantly for providing some of the best Sunday meals I ever had!

If there is one thing in this thesis that I will not have disputed, it is the fact that my own family deserves the most credit for the success of my efforts. They managed to become fund raisers, advisors of study, morale boosters, all at the same time. I must therefore thank my sister Thania (for showing me that there is a life after the PhD), Isla (for helping me appreciate the true meaning of engineering approximation with her own attitude towards maths), and Fiona (for on the other hand demonstrating to me the value of perfection). I would also like to thank my father Theodoros for making it possible for me to commence my studies in the first place and for never giving up on trying to inspire me with his own unlimited enthusiasm and optimism!

Finally and most importantly, I dedicate the whole of this work for all it is worth to my mother, for simply somehow managing to contribute more, than all the above mentioned put together..

# Abstract

The simulation and flight testing of a light gyroplane aircraft is performed obtaining results regarding the flight dynamics attributes of the vehicle. The main aim of the work was to assess the ability of a mathematical model to simulate rotorcraft in the autorotative flight state. Additionally, the results acquired were to enhance the understanding of an aircraft class for which the existing database of knowledge is limited, particularly with regards to its flight mechanics characteristics.

An appropriate aircraft configuration file was obtained enabling a platform of simulation results to be generated. Parametric studies were performed primarily focusing on the influence of the vertical centre of gravity position and rotor speed degree of freedom on gyroplane longitudinal stability. A data acquisition system unique in its sophistication for this class of aircraft was developed and installed on board. The software required to drive the system was designed, and rigorous tests verifying the instrumentation functionality were conducted both on ground and in real flight.

A flight test programme capable of fulfilling the experimental aims was devised and realised, yielding results both on the steady state flight characteristics of the aircraft and its dynamic response to pilot inputs. Certain trends were established on the properties of gyroplanes by interpreting the results in terms of basic aerodynamic theory, and by comparing them to previous research findings. A comparison of the experimental data to that obtained from the simulation runs, served to fulfil the model validation aim of the work presented. The effect of model and flight discrepancies on the ability of the mathematical model to realistically emulate flight dynamics in autorotation was discussed, and possible suggestions for the reasons of mismatch were presented.

# Nomenclature

## Notes:

- i. Where a vector has both subscript and superscript, the subscript denotes the location and the superscript the axis set.
- ii. The subscript *elem* denotes the property of a blade element.
- iii. In the event of duplication the meaning of the symbol will be apparent from the context of the text.
- iv. Unless explicitly stated, all quantities are given in standard SI units.

## General

$A, B$	state-space state and control matrices
$\underline{u}, \underline{y}$	state-space input and output vectors
$x$	variable
$\underline{x}$	vector
$\underline{i}_{sub}, \underline{j}_{sub}, \underline{k}_{sub}$	unit vectors describing current axis set (denoted by subscript)

## Specific

$a$	lift curve slope
$\underline{a}$	acceleration vector
$a_x, a_y, a_z$	linear accelerations in body axes
$a_\tau$	time constant of rotor speed decay
$A$	rotor area
$c$	blade chord length
$C_0$	apparent mass factor

$C_{D0}$	blade profile drag coefficient
$Cl, Cm, Cn$	non-dimensionalised moment aerodynamic coefficient
$C_T$	non-dimensionalised thrust coefficient
$C_x, C_y, C_z$	non-dimensionalised force aerodynamic coefficients
$C_{xy}$	coherence function of output $y$ with respect to input $x$
$dD$	blade element drag
$dD_R$	rotor drag contribution of blade element
$dL$	blade element lift
$dQ$	rotor torque contribution of blade element
$dr$	blade element width
$dT$	rotor thrust contribution of blade element
$F_{par}$	partial F numbers obtained from system identification regression analysis
$F_{tot}$	total F number obtained from system identification regression analysis
$g$	gravitational acceleration
$G_{xx}, G_{yy}, G_{xy}$	power spectral density of input, output, and input/output correlation
$H$	aircraft pressure altitude
$Im, Re$	Imaginary and real parts of complex number
$I_{flap}, I_{pitch}, I_{lag}$	blade flap, pitch, lag moments of inertia
$I_R$	effective rotor inertia
$I_{xx}, I_{yy}, I_{zz}$	aircraft roll, pitch, yaw moments of inertia
$J$	cost function used for simulation trim estimation
$k$	number of discrete frequency points used for system identification application
$K_x, K_y$	gradient of longitudinal and lateral induced velocity variations
$l_b$	longitudinal distance of ballast used for aircraft centre of gravity estimation from reference point
$l_{cg}$	longitudinal distance between suspension point and the aircraft centre of gravity
$l_i$	inclinometer distance from reference point
$l_s$	vertical distance between suspension point and the aircraft x-axis
$L, M, N$	aircraft rolling, pitching and yawing moments

$[L]$	dynamic inflow static gain matrix
$m$	mass
$\underline{M}$	aircraft moment vector
$n$	number of discrete simulation time points.
$N$	number of blades
$p$	number of unknown parameters to be estimated from system identification method
$p, q, r$	aircraft roll, pitch and yaw rate perturbations from trim
$P, Q, R$	aircraft roll, pitch and yaw rates
$P_0$	profile power losses
$P_{dyn}$	dynamic air pressure
$P_{id}$	ideal power done by rotor on the air flow
$P_R$	total power done by the rotor on the air flow
$P_s$	static air pressure
$Q$	aerodynamic rotor torque
$Q_E$	torque provided by engine
$Q_{tr}$	torque required for the transmission system
$Q_{TR}$	torque required for the tail rotor
$r$	radial position
$\underline{r}_{cg}$	centre of gravity position vector
$\underline{r}_{hinge}$	rotor hinge position vector
$\underline{r}_{hub}$	rotor hub position vector
$R$	blade radius
$R^2$	multiple correlation coefficient obtained from regression analysis
$s$	rotor solidity
$s_i$	standard error of the estimated parameter $\theta_i$
$S$	reference area
$t_{DAQ}$	data acquisition time
$T$	rotor thrust
$T^{axes1/axes2}$	transformation matrix transforming from <i>axes1</i> to <i>axes2</i> axes set

$T_p$	period of oscillation of simple pendulum approach for estimating aircraft moments of inertia
$T_{temp}$	ambient air temperature
$u, v, w$	aircraft velocity component perturbations from trim
$\underline{u}_{sub}^{sup}, \underline{\omega}_{sub}^{sup}$	linear and angular velocity vectors at location <i>sub</i> in axes set sup
$U, V, W$	aircraft velocity components
$\underline{u}_{trim}, \underline{y}_{trim}$	vectors containing the trim controls and aircraft attitudes in trim flight condition
$v_h$	rotor induced velocity in hover
$v_i$	rotor induced velocity
$v_m$	dynamic inflow wake mass flow velocity
$v_0, v_{lx}, v_{lc}$	uniform, longitudinal and lateral induced velocity components
$V_c$	aircraft descent velocity
$V_f$	total airflow velocity
$V_{id}$	descent rate required for ideal autorotation
$V_{lo}, V_{la}$	longitudinal and lateral stick measuring transducer outputs
$V_p$	probe total velocity
$V_T$	dynamic inflow wake velocity
$V_x, V_y, V_z$	air flow velocity components
$W_{A/C}$	aircraft total weight
$W_b$	ballast weight used for aircraft centre of gravity calculation
$W_i$	inclinometer weight
$X, Y, Z$	forces acting along aircraft x, y, z axes
$X_{sub}, Y_{sub},$ etc.	force, moment and torque stability and control derivatives with respect to the state or control denoted by subscript
$X_{CG}$	longitudinal centre of gravity position
$X_{SP}$	x co-ordinate of suspension point
$Y_{CG}$	lateral centre of gravity position

$[\tau]$	time constant matrix
$\phi, \theta, \psi$	aircraft roll, pitch and yaw attitude perturbations from trim
$\phi_i$	rotor inflow angle for blade element analysis
$\Phi, \Theta, \Psi$	aircraft roll, pitch and yaw attitudes
$\chi$	wake skew angle
$\psi_{ax}$	shaft azimuth angle
$\omega$	angular velocity, frequency
$\omega_k$	$k_{th}$ Fourier coefficient
$\omega_{min}, \omega_{max}$	minimum and maximum frequency values used for system identification
$\omega_{ph}$	phugoid mode damped frequency
$\Omega$	rotor speed
$\Omega_0$	rotor speed at moment of power failure
$\Omega'$	rotor speed perturbation from trim
$\Omega_p$	propeller speed

### Subscripts/superscripts

<i>aero</i>	aerodynamic
<i>blade</i>	blade axes set
<i>body</i>	body axes set
<i>elem</i>	denotes the property of a blade element
<i>disc</i>	disc axes set
<i>fin</i>	denotes the force/moment contribution of the aircraft fin
<i>fuse</i>	denotes the force/moment contribution of the aircraft fuselage
<i>inertia</i>	inertial
<i>probe</i>	quantities related to air data probe
<i>rotor</i>	denotes the force/moment contribution of the aircraft rotor
<i>shaft</i>	shaft axes set
<i>tplane</i>	denotes the force/moment contribution of the aircraft tailplane

### Abbreviations

AAN	Airworthiness Approval Note
-----	-----------------------------

ADC	Analogue to Digital Converter
BCAR	British Civil Airworthiness Requirements
CAA	Civil Aviation Authority
CFD	Computational Fluid Dynamics
CP	Centre of Pressure
cg	centre of gravity
DAQ	Data Acquisition
PFA	Popular Flying Association
RASCAL	Rotorcraft Aeromechanic Simulation for Control AnaLysis
SCU	Signal Conditioning Unit

# *Contents*

## **CHAPTER 1**

<b>INTRODUCTION, MAIN AIM AND OBJECTIVES</b>	<b>1</b>
1.1 Introduction	1
1.2 An overview of the main findings of CAA sponsored study of gyroplane flight mechanics	15
1.3 Thesis aims and objectives	18
1.4 Thesis structure	21

## **CHAPTER 2**

<b>GYROPLANE HISTORICAL DEVELOPMENT AND RELATED RESEARCH</b>	<b>23</b>
2.1 Introduction	23
2.2 A historical overview of the development of the gyroplane	23
2.3 Contemporary gyroplane types	25
2.4 Review of previous gyroplane research	28
2.5 Chapter summary	30

## **CHAPTER 3**

<b>EXPERIMENTAL DESIGN FOR THE FLIGHT TESTING OF A LIGHT GYROPLANE</b>	<b>32</b>
3.1 Introduction	32
3.2 The design of an instrumentation package for the Montgomery-Parsons gyroplane	32
3.3 The flight test plan for the Montgomery-Parsons gyroplane	41

3.3.1	DAQ software programming and set-up	41
3.3.2	Ground testing	42
3.3.3	Flight test manoeuvres	43
3.3.4	Post flight considerations	46
3.4	Basic system identification data processing	47
3.5	Chapter summary	50

## **CHAPTER 4**

<b>PREDICTED CHARACTERISTICS OF THE MONTGOMERIE-PARSONS GYROPLANE</b>		<b>51</b>
4.1	Introduction	51
4.2	An overview of the RASCAL model	52
4.3	The Montgomerie-Parsons gyroplane configurational definition	53
4.4	Montgomerie gyroplane simulation results	60
4.5	Chapter summary	66

## **CHAPTER 5**

<b>VALIDATION OF RASCAL MODEL USING DATA FROM FLIGHT TESTS</b>		<b>68</b>
5.1	Introduction	68
5.2	Verification of instrumentation functionality	69
5.3	Steady state results	73
5.4	Dynamic response results	78
5.4.1	Time responses	78
5.4.2	System identification	81
5.5	Chapter summary	86

## **CHAPTER 6**

### **FLIGHT TEST RESULTS REGARDING THE MONTGOMERIE-PARSONS GYROPLANE STEADY STATE AND DYNAMIC RESPONSE CHARACTERISTICS**

**88**

6.1	Introduction	88
6.2	Steady state results	89
6.3	Dynamic response results	92
6.4	Chapter summary	102

## **CHAPTER 7**

### **RESEARCH CONCLUSIONS AND RECOMMENDATIONS FOR FUTURE WORK**

**103**

7.1	Review of research aims	103
7.2	Conclusions	104
7.3	Recommendations for future work	106
7.4	Concluding remarks	107

**APPENDICES** **108-138**

**TABLES** **139-154**

**FIGURES** **155-225**

**REFERENCES** **226-232**

# Chapter 1

## Introduction, Main Aim and Objectives

### 1.1 Introduction

Simulating any complex dynamic system such as a rotary wing aircraft presents a series of demanding challenges. For example, a challenge that must be dealt with adequately for a system model to qualify as a reliable research tool is for its validity to be established throughout the widest possible range of the system's operating conditions. In the case of a rotorcraft mathematical model those are likely to incorporate forward, ascending, and descending flight, hover, and the flight condition referred to as *autorotation*, i.e. the state at which the angular momentum of the main rotor is sustained without the need for the application of a powerplant torque, normally only achievable in descending flight. Although in recent years a series of advanced rotorcraft mathematical models have been developed and validated over several flight states (the *Helisim* simulation model developed by *Padfield [1996]*, for example), a literature review reveals that validation of the models in autorotation is extremely limited, especially when considering the static and dynamic stability attributes of the system.

Model validation can in general be performed by use of one of three methods: with analytical expressions derived from the theory governing the physical principles, with the aid of wind tunnel experiments, or by means of aircraft flight testing. Although analytical expressions relating to autorotation have been derived since the beginnings of the development of rotor aerodynamic theory (*Glauert [1926]* for example), they are mainly concerned with rotor performance characteristics. On the other hand, sustaining a stable state of autorotation in a wind tunnel presents a series of difficulties mainly caused by the high rotor rpm that the small scale model would have to achieve.

Flight testing arguably offers an effective and reliable means of validating an aircraft mathematical model. Testing of the actual aircraft as opposed to using a wind tunnel representation or expressions derived from the idealised theory significantly reduces the uncertainty bounds of the results. Although the use of error prone experimental data will introduce another degree of uncertainty, data processing tools do exist (see *AGARD [1991]*, for example) that serve to minimise this effect. Examination of the relevant literature reveals that most flight test experimental work performed on autorotating rotorcraft is limited to investigations on the quantitative *performance* characteristics of the aircraft in this mode. Examples of this are given by *Pegg [1969]*, where a flight investigation of a lightweight teetering-rotor helicopter was conducted to explore the limitations encountered in power-off flight with the collective pitch stick held in the trim level-flight position, and by *Segner [1973]* where the autorotational characteristics of the AH-56A Compound Helicopter are investigated.

Research in this area is limited since for helicopters autorotation is an abnormal mode of operation normally only experienced when a total power failure occurs, and usually lasting for a limited time period. Performing any advanced manoeuvres necessary for analysing the response of the helicopter in this state is impractical and can jeopardise pilot safety. It is therefore difficult to produce any meaningful results for the validation purposes of most rotorcraft flight dynamics simulation models, which are configured as conventional helicopters. The inherent safety implications associated with autorotation enhance the need for aircraft stability and control characteristics in this state to be modelled realistically and therefore if flight testing is to be used for validation, a technique alternative to the testing of a conventional helicopter must be employed. This research thesis presents such a method by which a generic rotorcraft model is configured as a gyroplane aircraft, a type of rotorcraft which is unique in the sense that autorotation constitutes its normal mode of operation and can therefore be tested without the practical limitations associated with the helicopter.

Before expanding on the method itself it is necessary to obtain an understanding of this non-powered rotor state of flight. This is performed by

interpreting the physical principles governing autorotation and presenting the modelling considerations associated with its simulation.

### Principles of autorotation

Autorotation is defined by *Johnson [1980]* as "the state of rotor operation with no net power requirements". This becomes possible when a component of wind flow through the rotor is sufficient to provide the energy required for overcoming both the rotor induced and profile power losses. Two viewpoints of interpreting the physical mechanism responsible for autorotation are generally presented in the literature (*Bramwell [1976]*, *Prouty [1990]*, *Sedon [1990]*, *Newman [1994]*, *Padfield [1996]*, *Leishman [2000]*, for example). With the first one, the main rotor is represented by the actuator disc model and momentum/energy principles are applied. With the second one, blade element considerations are used to derive the aerodynamic forces responsible for turning the rotor.

Although the mathematical model employed for the simulation purposes of this research activity is based on a blade element approach, actuator disc theory can provide an alternative insight into the physical processes involved. For the purposes of this analysis only the basic principles and assumptions defining the actuator disc model, will be presented. The theory assumes that the rotor can be modelled with an actuator disc, which is a circular surface of zero thickness that can generate a thrust  $T$  acting in a direction perpendicular to the disc itself, by accelerating the air particles through it. Both the induced velocity distribution and the thrust loading are assumed constant throughout the disc. Conservation of momentum, mass and energy principles can be applied to determine the thrust and power parameters.

In order to simplify the analysis consider how autorotation is predicted for a helicopter in *axial* flight. The flow model used for a vertical *descent*, is presented in Figure 1.1. For sufficiently high rates of the descent, a well defined slipstream will exist above the rotor. Far below the rotor the velocity is equal to the descent velocity  $V_c$  whereas in the far wake (above the rotor), it can be shown to be  $V_c - 2v_i$ , (*Newman [1994]*, for example), where  $v_i$  is the rotor induced velocity (always defined positive).

For the general axial flight case momentum theory can be used to predict that the induced velocity will vary with  $V_c$  in the manner depicted in Figure 1.2, where  $V_c < 0$  indicates that the aircraft is descending, whereas  $V_c > 0$  implies vertical ascent. Both velocities are non-dimensionalised with respect to,

$$v_h = \sqrt{\frac{T}{2\rho A}} \quad (1-1)$$

the induced velocity generated in hover. It is important to note that within the region,

$$-2v_h \leq V_c \leq 0$$

the physical model upon which momentum theory is based breaks down and empirical formulas must be used for predicting  $v_i$ . The significance of this will be discussed later in this analysis.

The lines  $V_c = 0$ ,  $V_c + v_i = 0$ ,  $V_c + 2v_i = 0$ , divide the plane into four regions each of which represents a different operating state. The *normal working* state covers both climbing and hovering flight. In this case both  $V_c$  and  $v_i$  are positive and therefore the ideal power added by the rotor to the air flow (i.e. not including profile power losses), is

$$P_{id} = T(V_c + v_i) > 0$$

i.e., the rotor is performing work on the air flow and therefore the aircraft is in the powered flight condition.

As the rotor moves into descent and in the region  $-2v_h \leq V_c \leq 0$ , momentum theory becomes invalid as the flow can take on two possible directions and the slipstream model used in the theory ceases to be a realistic representation of the physical situation. In the first of the two states encountered, the *vortex ring state*, re-circulation of the flow occurs and turbulence appears in the vicinity of the rotor disc,

resulting in rotor vibration. As the descent rate is further increased and  $V_c > v_i$ , the wake above the rotor starts to resemble that of a bluff body and the operating state is therefore referred to as the *turbulent wake* state. For both the vortex ring and the turbulent wake states, the flow in the vicinity of the rotor is unsteady and turbulent and empirical formulas based on experimental data must be used to predict the induced velocity. A formulation which is often used is that proposed by *Young [1978]* which gives,

$$\frac{v_i}{v_h} = k - \frac{V_c}{v_h} \quad \text{for } -1.5 \leq \frac{V_c}{v_h} \leq 0 \quad (1-2)$$

$$\frac{v_i}{v_h} = k \left[ 7 + \frac{3V_c}{v_h} \right] \quad \text{for } -2 \leq \frac{V_c}{v_h} \leq -1.5$$

where  $k$  is the induced power factor in hover, a measure of the efficiency of the rotor. On the basis of equation (1.2), and for an ideal rotor where no induced power losses occur ( $k = 1$ ),

$$\frac{V_{id}}{v_h} = -1.75$$

where  $V_{id}$  is the descent rate required to achieve *ideal* autorotation, i.e. for  $V_c + v_i = 0$ .

In reality, due to the existence of profile power losses, it can be shown (*Leishman [2000]*), that *actual* autorotation is achieved for values of  $\frac{V_c}{v_h}$  between -1.85 and -1.9. In this case it is the total power generated by the rotor,

$$P_R = P_{id} + P_0 \quad (1-3)$$

which becomes equal to zero, and therefore no external power source is required to overcome induced and profile losses and the aircraft enters non-powered flight. The quantity  $P_0$  represents the profile power losses.

As the descent velocity further increases, the slipstream re-establishes itself (although in the opposite direction to that of the normal working state), simple momentum theory can be applied again with confidence and the rotor enters the *windmill break* state.

Although the above analysis is strictly applicable to axial flight only, the physical principles are also pertinent to a gyroplane in forward flight. Consider the case where the gyroplane rotor is inclined at an angle  $\gamma$  to the incoming flow (with free stream velocity  $V_f$ ), as illustrated in Figure 1.3. It is the magnitude of the component of inflow *through* the rotor ( $V_f \sin \gamma$ ) relative to the induced velocity which determines the operating state of the rotor. As with the vertical descent case, when the component of air flow through the rotor disc becomes sufficient to overcome the induced and profile power losses, autorotation is achieved and the rotor will obtain its kinetic energy by extracting it from the air flow.

Alternatively, autorotation can be examined from a blade element perspective. With this approach, the elemental aerodynamic forces and moments are derived for an elemental blade section inclined to the incoming flow and are integrated along the blade span to calculate their overall contribution. The objective is to show that a condition is reached where the overall aerodynamic torque can actually provide the means for turning of the rotor.

For a blade element in autorotation (Figure 1.4), the incremental thrust and drag forces with respect to the rotor plane, are given by :

$$dT = dL \cos \phi_i + dD \sin \phi_i \quad (1-4)$$

$$dD_R = dD \cos \phi_i - dL \sin \phi_i \quad (1-5)$$

where  $dT$  is the incremental rotor thrust,  $dL$  is the incremental blade lift,  $dD$  is the incremental blade drag,  $dD_r$  is the incremental rotor drag and  $\phi_i$  is the rotor inflow angle.

The elemental rotor torque contribution  $dQ$  of an element of width  $dr$  at a radial distance  $r$ , is given by

$$dQ = rdD_r \quad (1-6)$$

By integrating along the blade span, *Newman [1994]* then derives the following equation for the total aerodynamic torque applied to the rotor for the case of the aircraft in steady descent,

$$Q = -\frac{1}{2} \rho N c \Omega^2 R^4 a \left[ \left( \frac{\theta_{bl}}{3} + \frac{1}{2} \frac{V_c - v_i}{\Omega R} \right) \left( \frac{V_c - v_i}{\Omega R} \right) + \frac{1}{8} \rho N c \Omega^2 R^4 C_{D0} \right] \quad (1-7)$$

where  $N$  is the number of blades,  $c$  is the mean blade chord,  $a$  is the lift curve slope,  $\Omega$  is the blade angular velocity,  $R$  is the blade radius,  $C_{D0}$  is the blade profile drag coefficient and  $\theta_{bl}$  is the local blade pitch,  $V_c$  is the descent velocity of the aircraft.

It is evident from (1-7) that if  $V_c$  is increased, a situation is reached where the total torque  $Q$  of the rotor is equal to zero, i.e. that the forward component of the blade lift becomes sufficient to overcome the blade drag. In this case the rotation is possible without the need of an external torque and therefore autorotation is achieved.

By combination of both momentum theory and blade element theory *Newman [1994]* then goes on to show that the minimum descent velocity required for a steady autorotation is given by,

$$\frac{V_c}{\Omega R} = \frac{1}{4} \frac{sC_{D0}}{C_T} + \frac{C_T^2}{sC_{D0}} \quad (1-8)$$

where,  $C_T$  is the rotor thrust coefficient and  $s$  is the rotor solidity.

When a power failure occurs in a helicopter the main rotor speed will in general not have the value required for ideal autorotation, as defined in equation (1.8). The pilot must therefore follow a certain procedure in order to ensure the safe landing of the vehicle. At the instant when the power failure occurs the elemental aerodynamic forces act in the manner presented in Figure 1.5, which is the condition required for forward powered flight. Contrary to the autorotative case, the component of lift acting in the plane of rotation will *oppose* the motion of the rotor and combined with the drag component in the same direction will produce a retarding effect. The pilot has a finite time in which he must counter this by lowering the collective control and preventing an unrecoverable rotor speed decay. A simple dynamic model for predicting the rotor speed loss before a pilot reaction, is presented by *Johnson [1980]* and *Newman [1994]*. The equation defining the value of rotor speed after time  $t$  is shown to be of the form,

$$\Omega = \frac{\Omega_0}{1 + a_r t} \quad (1-9)$$

where,  $\Omega_0$  is the rotor speed at power failure and the time constant  $a_r$  is dependent on the ratio of the rotor kinetic energy to the kinetic energy of the helicopter as a whole. Although this will obviously differ for varying aircraft configurations, typically a few seconds is the time limit within which the pilot must take the appropriate action.

Once the collective has been adjusted appropriately, and a steady descent has been established, it must be assured that sufficient rotor speed is achieved for the landing flare prior to touchdown to be performed safely. The kinetic energy stored is effectively traded for an increase in thrust obtained by an increase in collective pitch angle.

Alternative strategies are adopted by the helicopter pilot if the power failure occurs close to the ground or during forward flight. In the former case the kinetic energy stored in the rotor at the moment of the failure must be used to minimise the rate of descent, with the controls kept in their current position. The rotor speed decay will be governed by equation (1-9) and the danger therefore exists that it reduces to a value where the resulting excess blade coning could damage the aircraft. If a power failure occurs in forward flight, an inclination of the rotor to the incoming flow can be made such as to utilise a component *through* the rotor, effectively using the kinetic energy acquired from the forward motion of the aircraft to sustain the angular momentum of the main rotor. For further detail on the pilot strategies developed for each type of autorotation landing the reader is referred to *Johnson [1980]*, *Newman [1994]*, and *Leishman [2000]*.

It becomes obvious that the ability of the helicopter pilot to perform a safe landing is dependent upon the altitude and forward speed conditions encountered at the instant of the power failure. For a helicopter suffering from a total power loss, a certain set of combinations exist for which the situation can prove unrecoverable. In the altitude/forward speed graph taken from *Newman [1994]* (Figure 1.6), those areas are shaded in grey and are normally referred to as the 'Dead Man's Curve'. The most important region to avoid is the low speed one. Point B indicates the maximum height from which the helicopter can safely descend using its rotor kinetic energy. Point A is the minimum height required to build up the rotor speed needed for a safe touchdown. At point C sufficient speed and height is available to the pilot. Finally at point D the aircraft is too close to the ground to allow for a safe touchdown flare which would be required to kill off the forward speed.

It is evident that the autorotative performance of the helicopter is an important design issue which plays a major role in defining the safety level of the aircraft. It is also obvious from the above analysis that knowledge of both the steady state and transient response of variables such as the collective pitch, aircraft attitude, aircraft speed and rotor speed, is necessary in order to predict the consequence of pilot actions which in this mode of flight will have a pronounced influence on the safety of the vehicle. For example, realistic simulation of the rotorspeed response after a power failure at low altitude, can determine whether or not a 'controls fixed' descent (like the

one described previously) can be achieved without exceeding the minimum permissible rotor speed value. Validation of a rotorcraft model in autorotation is therefore necessary if aircraft simulation is to be used as a reliable means of assessing its airworthiness.

In order to realistically emulate autorotative flight, certain considerations must be taken into account which are specific to this mode of operation. Two properties which vary significantly between powered and non-powered flight are the rotor inflow and rotor speed dynamics. For the former case an air flow direction *through* the rotor is in a direction opposite to that in powered flight, whereas for the latter, rotor speed constitutes an independent degree of freedom and is allowed to vary without being governed by an engine. If a generic rotorcraft model is to be used for modelling autorotation it must be checked firstly for being able to accommodate both those properties.

#### Autorotation modelling considerations

Modelling rotor inflow can be performed in a variety of ways depending on the specific nature of the application involved. With simple momentum theory for example it is assumed that a uniform induced velocity exists throughout the rotor disc. *Glauert [1926]*, while trying to resolve the discrepancies between experimental data and the theoretically predicted lateral force of the rotor from uniform inflow, proposed the following model:

$$v_i = v_0(1 + K_x r \cos \psi_{az}) \quad (1-10)$$

where,

$v_0$  is the uniform component as predicted by simple momentum theory

$K_x$  is the gradient of the longitudinal induced velocity variation

$\psi_{az}$  is the rotor azimuth angle.

Equation (1-10) introduces a longitudinal variation in the induced velocity field, with the choice of  $K_x$  made such as to produce a small upwash at the leading

edge and an increase in downwash all along the trailing edge of the rotor. As an extension to Glauert's initial formulation, the lateral variation of the inflow can also be included giving,

$$v_i = v_0(1 + K_x r \cos \psi_{az} + K_y r \sin \psi_{az}) \quad (1-11)$$

where,  $K_y$  is the gradient of the lateral induced velocity variation.

A concise review of non-uniform inflow models developed to date can be found in *Chen [1990]*, where he states that for flight dynamics and control applications simple variants of Glauert's initial model are still used extensively, primarily due to their computational efficiency.

Static models like the one proposed by Glauert do suffer from the drawbacks of assuming that the air flow instantaneously accelerates through the plane of the disc, while also ignoring the effects of pitching and rolling motions. As a result of this, *dynamic* inflow models have been developed which aim to overcome the above limitations; *Chen [1990]* gives a definitive review of the most important ones. The particular one employed by the rotorcraft simulation model utilised in this research activity, is taken from *Chen [1990]* although it is originally based on that developed by *Pitt & Peters [1981]*, *Gaonkar & Peters [1988]* and *Peters & HaQuang [1988]* and hereafter will be referred to as the *Peters & HaQuang Inflow Model*.

With this modelling approach it is postulated that the induced velocity at any instant in time is given by,

$$v_i(r, \psi_{az}) = v_0 + \frac{r}{R} v_{1s} \sin \psi_{az} + \frac{r}{R} v_{1c} \cos \psi_{az} \quad (1-12)$$

The inflow velocities  $v_0, v_{1s}, v_{1c}$  are calculated from,

$$[\tau] \begin{bmatrix} \dot{v}_0 \\ \dot{v}_{ls} \\ \dot{v}_{lc} \end{bmatrix} + \begin{bmatrix} v_0 \\ v_{ls} \\ v_{lc} \end{bmatrix} = [L] \begin{bmatrix} T_{aero} \\ L_{aero} \\ M_{aero} \end{bmatrix} \quad (1-13)$$

which introduces the time dependence of the inflow dynamics. The matrices  $[\tau]$  and  $[L]$  are defined in Appendix 1 where a more detailed description of the model is presented.

For the purposes of this analysis two aspects of the specific formulation of the equations required for simulating autorotation, must be noted. In the presentation of the model made both by *Peters HaQuang [1988]* and *Chen [1990]*, they are expressed in their *non-dimensional* form with the velocities normalised on tip speed ( $\Omega R$ ), time normalised on rotor speed and the force and moments normalised on rotor area, tip speed, rotor radius, and the density of the air. Using the rotor speed as one of the quantities on which to normalise can only be performed for manoeuvres for which it is valid to assume that it remains of a *constant* value. If *unsteady* autorotation is to be simulated, where rotor speed is allowed to vary freely, the equations must be converted to their *dimensional* form in the manner suggested by *Peters & HaQuang [1988]*. It is for this reason that the generic rotorcraft model used for the simulation purposes of this study employs the *dimensional* form of the equations given in Appendix 1, as presented by *Houston [2000]*.

Furthermore, there is a subtle but important difference in terms of the work described in this thesis, between the original model proposed by *Peters & HaQuang [1988]* and the representation given by *Chen [1990]* regarding the definition of wake skew angle  $\chi$ . The *geometrical* difference in definition is made clear in Figures 1.7 and 1.8. In the former case (i.e. the definition given by *Peters & HaQuang [1988]*),  $\chi$  is defined from the rotor disc, where as in the latter it is measured from the thrust line.<sup>1</sup> What is of greater importance is the mathematical definition of the two angles, which in terms of the free stream and induced velocities by *Chen [1990]* is given by,

---

<sup>1</sup> Note that for both cases  $v_i$  is that derived from simple momentum theory.

$$\tan \chi = \frac{V_f \cos \gamma}{v_i - V_f \sin \gamma} = \frac{\sqrt{V_x^2 + V_y^2}}{v_i - V_z} \quad (1-14)$$

where,  $V_x$ ,  $V_y$ ,  $V_z$  are the component disc velocities.

The significance of this is that  $\tan \chi$  is allowed to acquire negative values when  $V_f \sin \gamma > v_i$ , i.e. in autorotation, implying that  $\chi > 90$  and the wake is developed *above* the rotor disc plane which is geometrically consistent with the flow in autorotative flight. This can be viewed as an extension to the Peters HaQuang formulation in which,

$$\tan \chi = \frac{|v_i - V_f \sin \gamma|}{V_f \cos \gamma} \quad (1-15)$$

This would give  $\chi > 0$  even in the case where  $V_f \sin \gamma > v_i$  which is geometrically inconsistent with the flow pattern in autorotation. If the inflow dynamics in autorotation are to be modelled therefore, it is necessary to use the representation adopted by *Chen [1990]*.

So although one must take care in choosing the appropriate formulation of the original *Peters HaQuang Inflow Model*, one can also agree with *Houston [2000]* when he states that "inspection of these equations indicates that the model will emulate physical aspects of autorotative behaviour, but its efficacy for simulation of autorotation will be defined with the validation results".

When attempting to simulate autorotative flight it must also be ensured that rotor speed dynamics constituting an independent degree of freedom, are incorporated in the model. For conventional helicopter simulations, the simplifying assumption is often made that rotor speed remains constant throughout a prescribed manoeuvre. In reality even when in powered flight, a varying need both for main rotor and tail rotor torque will result in a continuously changing rotor speed which will be controlled by an engine governor. Attempts in modelling this effect have been made by use of simple engine models (*Padfield [1996]*, *Doyle & Thomson [2000]* for example). For autorotative flight where no engine torque is available it is the torque produced by the

aerodynamic forces that will determine the (significant) rotor speed response. The generic rotorcraft model used for the simulation purposes of this research activity, models rotor speed variation by assuming that it is governed by dynamics of the form,

$$\dot{\Omega} = \frac{1}{I_R} (Q_E - Q - Q_{TR} - Q_{tr}) + \dot{R} \quad (1-16)$$

where,

$Q_E$  is the torque provided by the engine

$Q$  is the aerodynamic torque

$Q_{TR}$  is the torque required for the tail rotor

$Q_{tr}$  is the torque required for the transmission system

$I_R$  is the effective rotor inertia

$\dot{R}$  is the fuselage yaw rate.

For a gyroplane in autorotation this will reduce to,

$$\dot{\Omega} = -\frac{Q}{I_R} + \dot{R} \quad (1-17)$$

Note that when the aircraft is in trimmed flight, the net aerodynamic torque must be equal to zero which for a steady descent can be performed in the way defined by equation 1-8.

So summarising it can be said that by suitable choice of an induced velocity model and by incorporation of a rotor speed degree of freedom rotorcraft models can in principle cope with the simulation of autorotative flight without the need for applying any significant changes to the model structure. The difficulty arises when attempting to *validate* the simulation in the autorotation flight mode, particularly when studying the flight dynamics behaviour of the system.

The approach of configuring a generic rotorcraft model as a gyroplane has been adopted by Houston and Thomson in order to overcome this difficulty. It is

argued [*Houston [2000]* for example], that by validating the model in its gyroplane format (constantly autorotating), its generic nature enables the validity to be extended to other rotorcraft types (including the conventional helicopter), in autorotative flight. In other words if the model is seen to correctly predict the static and dynamic response of an autorotating gyroplane it is expected that it will perform accordingly when predicting the properties of other autorotating rotorcraft. The opportunity of putting this theoretical argument into practice was given through a CAA funded programme (*CAA [1994]*), where a conventional light gyroplane was simulated and flight tested.

## **1.2 An overview of the main findings of CAA sponsored study of gyroplane flight mechanics**

The RASCAL simulation programme developed by *Houston [1994]* was applied for the simulation and model validation purposes. It belongs to the family of rotorcraft models known as the *individual blade/blade element* type where each blade is represented separately and divided into blade elements with the elemental forces and moments determined and then integrated along the span, as described by *Rutherford [1997]*. The model is generic in its form and can be configured to simulate the flight dynamics properties of any type of rotorcraft ranging from tilt-rotors to gyroplanes. Its gyroplane representing format is described by *Houston [2000]* with any gyroplane specific characteristics of the model relating to configuration parameters. The generic nature of the model allows for the aircraft geometry (for example propeller characteristics) to be accommodated by appropriate data entries and software switches.

An aspect that does require further consideration is the emulation of the dynamics of a teetering rotor. With this type of rotor system the two blades are attached to the hub without flap or lag hinges essentially forming a single structure performing a 'see saw' (teetering) motion. A flap hinge on the rotor shaft axis allows for the flapping motion to manifest itself. Within RASCAL teetering rotor mechanics are emulated by setting the hinge offset to zero, effectively modelling a rotor with two centrally hinged blades. *Johnson [1980]* advocates that this is an acceptable approximation for the longitudinal and lateral flapping degrees of freedom. On the

other hand the coning motion of a two bladed articulated rotor is not the same as that of a teetering one, for which *Johnson [1980]* shows that the moments produced from each blade will cancel each other out. Validation results will determine if this is an acceptable simplification.

The aircraft upon which the study focused was the VPM M16 Tandem Trainer which has a maximum all-up mass of 450 kg (Figure 1.9). This is a typical design of a contemporary light gyroplane. The aims of the research activity were both to validate the RASCAL mathematical model deeming it a reliable tool for simulating other gyroplanes and rotorcraft types in autorotation but also to investigate the flight dynamic characteristics of gyroplanes for which no previous data existed. After the series of fatal accidents referred to in *Anon [1991]*, the Civil Aviation Authority was forced to produce a new airworthiness and design standard (BCAR Section T), applicable to light gyroplanes. In order to do this it was necessary to consolidate the understanding of gyroplane stability and control characteristics. As a consequence, this research program was set up with the University of Glasgow Aerospace Engineering Department. During the initial phase of the work aerodynamic data generated from wind tunnel tests (*Coton et al [1998]*)<sup>2</sup>, was used to simulate the aircraft, and the results produced are presented by *Houston [1996]*.

A flight test program was arranged and in order to facilitate the understanding of the results, the conventional 6 degree of freedom rigid body flight mechanics model was used to represent the aircraft dynamics. The gyroplane dynamics were studied using two decoupled subsets of the full system, a longitudinal set with the addition of the rotorspeed degree of freedom and a classical lateral/directional set. Results from the flight experiments are presented in *Houston & Thomson [1997]*, *Houston [1998a]*, *Houston [1998b]*, *Houston & Thomson [1999]* and *Houston [2000]*. Their implications on flight safety and airworthiness issues were summarised by the author, Houston and Thomson in *Spathopoulos et al [1998a]*.

The simulation and flight testing yielded a series of important results both with regard to the RASCAL model validity and to the understanding of gyroplane flight

---

<sup>2</sup> Although the wind tunnel data was made available in 1994 the work was not published until 1998.

dynamics issues. For the case of the key trim parameters, the model accurately predicted their trend thus providing a reliable estimate for aircraft properties such as stick speed stability. The deficiencies can be summarised as the prediction of pitch attitude at low speeds, lateral stick position over the speed range, and main rotor speed across the speed range.

The comparison of model and flight results for the aircraft stability derivatives, provided an indication of the model ability to simulate the dynamic response characteristics. The majority of the derivatives belonging to the longitudinal subset are predicted reasonably well. Important exceptions to this are the drag damping derivative  $X_u$  and the heave damping derivative  $Z_w$  which are both overpredicted. Of greatest concern is the discrepancy in  $X_u$  which results in a gross overprediction of the phugoid mode damping.

For the lateral/directional case correlation between model and experiment varies from the reasonable to poor, with the most pronounced discrepancy manifested in the yaw damping  $N_r$ , which is significantly overpredicted.

Summarising the deficiencies of the model with regard to the aircraft dynamic properties, they are seen to be overprediction in  $Z_w$  and  $X_u$ , the latter of the two resulting in a gross distortion of the aircraft phugoid response, and in the estimation of certain lateral/directional derivatives, for example  $N_r$ . Houston himself suggests that the model inadequacies warrant further investigation particularly that of  $X_u$  for which he states (*Houston [2000]*) that "it is difficult even to speculate on the source of discrepancy without further flight tests on aircraft dissimilar to that used for the present study".

The investigation conducted on the VPM gyroplane also revealed important aspects of gyroplane flight dynamics an area for which previous research is absent from the literature. Most importantly, the aircraft was seen to be stable throughout the speed range; two of the key findings regarded the influence of the vertical position of the centre of gravity position and the rotor speed mode of motion on the stability of

the phugoid. More specifically it was concluded that a cg position *above* the pusher propeller thrust line would *tend* to stabilise this mode of motion (Houston [1996]), and that the rotor speed degree of freedom is highly coupled with the phugoid also affecting its stability (Houston [1998a]). Both of these results (the former one in particular), are suggested by the authors to yield airworthiness implications if found true for aircraft of similar type, warranting further investigation.

### **1.3 Thesis aims and objectives**

The research conducted by Houston & Thomson was the first of its kind both in the sense of validating a rotorcraft model in autorotation and for investigating the flight dynamics attributes of gyroplanes. It is a natural consequence that it introduced a series of issues for which no data base of previous knowledge exists for comparison. It is important to establish whether the findings hold in a general sense or if they are limited in their scope to the particular aircraft under study. For example, are the model and flight mismatches (pitch attitude at low speed, rotor speed across the speed range, derivatives  $X_u$  and  $Z_w$ ), due to some general profound model weaknesses which will manifest themselves in other autorotation simulation cases or are they specifically related to the VPM configuration characteristics? Also, are the results indicating the effect of vertical cg position and rotor speed on the phugoid stability applicable only to the VPM aircraft or should they be taken into account when defining airworthiness criteria for all gyroplanes? Do other light gyroplanes (an aircraft class with a poor safety record), exhibit stable characteristics throughout the speed range?

For questions such as the above to be addressed with confidence the research performed on the VPM aircraft must be extended to a different aircraft of the same class. For this purpose, the Department of Aerospace Engineering at the University of Glasgow acquired a two-seater Montgomerie Parsons gyroplane, the second seat of which was removed to accommodate the on-board instrumentation. The research activity presented in this thesis involves the simulation of the aircraft static and dynamic attributes, the set-up, testing and installation of the instrumentation system required for the flight testing, the planning and realisation of flight test experiments capable of validating the RASCAL model and at the same time enhancing the

understanding of gyroplanes, and the design and application of software tools enabling efficient data processing.

The main aims and objectives of the thesis are defined as follows:

#### Thesis main aim

*Assess the ability of the RASCAL model to simulate rotorcraft in autorotation by revisiting and enhancing the results of Houston & Thomson for a second gyroplane test case.*

A successful flight test programme can provide a completely new set of experimental data for checking the validity of the RASCAL model and revisiting the key deficiencies highlighted from the previous research. Simulation results are compared to flight test data resulting both for steady and unsteady tests. For the purposes of the former a set of parameters obtained at trim conditions throughout the speed range are compared whereas for the latter, the method of comparing conventional stability and control derivatives are employed together with a presentation of aircraft state time responses to control inputs.

#### Additional aim

*Enhance the understanding of an aircraft class for which the existing database is limited to one test case.*

For a class of aircraft possessing a poor safety record it is essential to establish, if it exists, a general trend in its stability and control attributes. The stability characteristics of the Montgomerie Parsons aircraft are therefore studied across the speed range determining whether the postulates made by Houston and Thomson regarding the effect of cg position and rotor speed, apply to this type of gyroplane.

In order to realise the thesis aims the following objectives must be met:

*i) Obtain a detailed aircraft configurational file for performing a set of baseline simulations.*

In order to perform a series of aircraft simulations the RASCAL programme requires a set of configuration parameters describing the aircraft to be simulated. This includes aircraft sizing parameters, weight and balance properties, etc., obtained either from the manufacturer data sheets or by direct measurement. Detailed and accurate results are required for an aircraft type whose light weight makes it sensitive to configurational changes.

A set of baseline simulations are presented in order to provide an estimation of the aircraft's static and dynamic properties but primarily to produce a platform of results capable of being directly comparable to the flight test data. Parametric studies on parameters of particular influence on the aircraft's response are performed in addition to the baseline runs.

*ii) Develop an instrumentation and DAQ system capable of acquiring high quality data regarding the flight dynamics properties of an aircraft.*

The test vehicle was purchased in its basic form without any of the instrumentation required installed on-board. The transducer set required for obtaining knowledge of the aircraft's steady and unsteady stability characteristics is well documented (*AGARD [1995]*, for example) but research effort is needed to ensure that the most safe, cost and weight effective option is selected, particularly when testing a light aircraft with a poor class safety record. Furthermore the software required to drive the instrumentation must be designed to satisfy the bandwidth and data storage specifications of the system.

*iii) Devise and realise a flight test programme capable of yielding results appropriate for model validation and contributing to the understanding of gyroplane flight dynamics.*

As stated by several authors (*Klein [1989]*, *Murray-Smith [1991]* for example), in order to successfully realise the experimental aims a flight test schedule is required, defining the specific objectives, loading configurations, flight conditions and pilot tasks. A detailed plan is thus to be produced that will yield results appropriate both for model validation and studying gyroplane flight dynamics.

*iv) Develop the software tools capable of processing and analysing flight test data from a light gyroplane both for steady and dynamic response cases.*

The flight testing of the research aircraft yields results both regarding its static and dynamic stability properties. The data processing required for the former is minimum, restricted to basic digital filtering, mainly for data presentation and anti aliasing purposes. The dynamic characteristics of the aircraft are to be obtained by the application of a system identification technique. System identification for model validation has become increasingly popular in recent years and offers major benefits in comparison to other validation methods, as discussed by *Black [1988]*. A conventional technique is to be designed and implemented within a software environment well used for this type of application.

#### **1.4 Thesis structure**

The thesis structure follows the order in which the objectives were fulfilled. In Chapter 2 the historical development of the gyroplane is presented, together with an in-depth literature survey demonstrating the scarcity of the research activities involved with stability and control issues for gyroplanes. In Chapter 3 an illustration of the configurational aspects of the DAQ system is presented. The necessary software design required for driving the transducer set is given together with the flight test plan adopted for putting the instrumentation into use. In Chapter 4 the baseline simulation results are presented after initially having defined the configurational aspects of the specific aircraft under study. A comparison of those results complemented by a set of time responses, to the ones achieved from flight testing is presented in Chapter 5, fulfilling the model validation purposes of the research activity. In Chapter 6 the interpretation of the flight test results regarding both the steady and unsteady response of the aircraft is performed in terms of gyroplane flight

dynamics characteristics. Finally, the conclusions to the thesis are drawn in Chapter 7. It is shown that the RASCAL mathematical model can be used to simulate rotorcraft in autorotation although certain model deficiencies do exist and must be taken into account. A trend is also established in the factors affecting light gyroplane stability. Recommendations for possible avenues of future research conclude the final chapter of the thesis.

### Appendices

The dissertation is complemented with six appendices which are primarily focused on previous work that has been well documented. The second, third and sixth appendices include information on the instrumentation specifications, an overview of the flight certification process, and notes taken by the pilot during the flight testing.

# Chapter 2

## Gyroplane Historical Development and Related Research

### 2.1 Introduction

As the research work described in this thesis involves the simulation and flight testing of a gyroplane aircraft, it is considered necessary to provide an overview both of its historical development and of the research activity related to it. Presenting a description of the gyroplane's advance from its initial design to its current status provides the opportunity to highlight the unique properties of a type of aircraft belonging neither to the fixed wing nor to the conventional helicopter category. The literature survey outlining the main achievements to date presented at the end of the chapter serves to place the current research activity in its correct context.

### 2.2 A historical overview of the development of the gyroplane

The gyroplane was the first type of aircraft to use a rotary wing for direct lift generation. It is therefore regarded as the immediate predecessor to the helicopter and its historical development is described in the early chapters of several helicopter textbooks, *Johnson [1980]*, *Prouty [1990]*, *Newman [1994]*; a similar description is also provided by *Lopez-Diez et al [1999]*. The most important points in the aircraft's design advancement are illustrated in Figure 2.1.

As discussed by *Johnson [1980]*, gyroplane success preceded that of the helicopter due to the simpler mechanical design of its non-powered main rotor and to its airframe similarities to fixed wing aircraft, the technology of which was readily available early last century. Much of the initial research was closely linked to the Spanish engineer Juan de la Cierva who recognised the potential of a rotary wing aircraft when he commenced the development of the C1 gyroplane in 1919. This first

development stage was clearly the most productive, yielding several technological advancements such as the incorporation of flap and lag hinges and the use of cyclic pitch control, which have since become essential elements of most conventional helicopters. By 1927 Cierva himself had achieved several successful flights by deploying both flap and lag hinges on the main rotor of his aircraft. These innovations eliminated initial gyroplane flight problems such as the presence of a rolling moment due to main rotor lift asymmetry. An important advancement was made in 1931 when the Wilford WRK first flew, introducing the concept of cyclic pitch variation as a means of rotor control. This proved to be the last major contribution of gyroplanes to the rotorcraft field. The early thrive in gyroplane development was undermined by the production of the first helicopters in the early 1930s and the death of Cierva in 1936.

Although they were briefly used as aerial observation posts in WW II, interest in the aircraft waned until 1953, when the Bensen Gyrocopter was invented. This two-bladed rotorcraft used a teetering hub bar and rotorhead to support its main rotor. A description of the vehicle's main characteristics together with a comparison of its basic performance capabilities to those of a light aircraft, are presented by *Schad [1965]*. It was concluded that the climbing performance, the payload availability and the minimum-level-flight speed characteristics of the Bensen were considerably better than those of the fixed wing aircraft. The Bensen was also the first gyroplane to become widely commercially available and introduced the idea of using this type of aircraft for recreational flying purposes.

At around the same time, the Fairey Rotodyne Compound Helicopter project was launched. The aircraft was to combine the properties of a helicopter, a fixed wing airplane and an autogyro possessing both a main rotor and conventional fixed wings. Although not a gyroplane in the classical sense, once airborne it relied on main rotor autorotation, with the assistance of the fixed wings, for obtaining the necessary lifting force. Forward thrust would be generated by a pair of turboprop engine driven propellers. Take off and landing would be performed in the same way as the conventional helicopter by transferring the power to the main rotor.<sup>1</sup> The aircraft was intended to operate as an efficient short-haul/medium-haul aerial 'bus'. Unfortunately

---

<sup>1</sup> In fact landing could also be accomplished in autorotation.

after a series of financial letdowns, the project was abandoned in 1962. Although it was never made available commercially, it contributed to the rotorcraft field by introducing the concept of a convertible aircraft and forms the closest that any gyroplane related project has come to yielding a practical application other than recreational flying.

Interest in the aircraft again declined and was not revived until the 1980s when a trend emerged for producing ready-made gyroplane kits tailored for amateur use. It is worth noting that the configurations of these aircraft still follow the basic design concepts of the early autogyros. Several companies around the world now offer this type of service, at a cost much lower than that of conventional light helicopters. This has firmly established the gyroplane as a popular recreational aircraft and as a consequence, interest in flight safety issues has been heightened.

Finally, it is important to note a recent development in gyroplane design which is attempting to revolutionise the aircraft's performance specifications. This is the Carter Copter gyroplane, currently being developed by Carter Copters L.L.C. Much like the Fairey Rotodyne, the aircraft is a hybrid between a gyroplane and a fixed wing vehicle possessing both a main rotor and low aspect ratio wings. Vertical take off and landing are achievable through powering of the two bladed main rotor, which is switched to autorotation mode once the aircraft is airborne. The aircraft is projected to cruise at a speed of 400 mph at 45,000 ft, achieving a range of 2,500 miles. Flight testing of a prototype is currently under way.

A review of the gyroplane's historical development has indicated that since the 1930s little has changed in the aircraft's general configuration design. The following section will serve to further enhance this perception by presenting the basic attributes of the aircraft as it stands today.

### **2.3 Contemporary gyroplane types**

The fact that the fundamental airframe characteristics of the aircraft have in general not changed since the 1930s is observed when examining the illustrations of the Cierva C-29 gyroplane in Figure 2.2 and the contemporary Air Command in

Figure 2.3. In both cases, the aircraft rely on the main rotor, constantly in autorotation, to produce the required lifting force and on an engine driven propeller to acquire the propulsive force necessary to overcome the aerodynamic drag and the rearward component of the main rotor thrust. Current versions of the configuration can vary between being one or two seat, totally or partially covered to completely open frame and possessing pusher or tractor propellers. The propeller is normally powered by a low cost engine similar to those used on light aeroplanes. Roll and pitch motions are achieved through direct tilting of the main rotor whilst a conventional rudder is used for directional control. A list of the specifications of two typical types, the single seat VPM M16 Tandem Trainer and the two seat Air Command, is presented in Table 2.1. Illustrations of the aircraft are given in Figures 2.4-2.5. Contemporary gyroplanes are designed and manufactured mainly for recreational flying purposes, by several companies around the world. A catalogue of some of the most important ones is presented in Table 2.2.

Although gyroplanes are generally regarded as belonging to the family of *rotorcraft*, in the sense that they rely on a rotary wing for producing lift, they do exhibit flight performance characteristics which are unique to their aircraft type. A review of these properties for various flight states can serve to illustrate the differences between this type of vehicle and the more conventional helicopter/fixed wing aircraft.

The take-off procedure for early gyroplanes resembled that of aeroplanes in that they required a runway area. The air flow generated through the rotor was then utilised to achieve the rotor speed required for lift off. Although many contemporary gyroplanes still use this method for taking off, the need for it actually ceased to exist with the advent of the "jump" take off technique. With this approach the rotor is "pre-rotated" to a speed above normal flight rpm by a simple gear and clutch mechanism driven from the engine. This enables the aircraft to take off in a very short distance, and in some cases in a vertical manner. An immediate disengagement of the rotor is then required to avoid any fuselage torque reaction.

Although gyroplanes are therefore capable of vertical take off they do suffer from a major disadvantage when compared to the conventional helicopter, their

inability to hover. Sustaining this type of flight condition requires a powered main rotor and since gyroplane rotors rely on the incoming flow to acquire their kinetic energy a constant forward motion must be maintained if lift and thus altitude are to be preserved. This is often portrayed as the main reason why gyroplane development declined after the success of early helicopters.

When compared to fixed wing aircraft the low speed characteristics exhibited by gyroplanes are more robust. Depending on the specific wind conditions they are able to achieve speeds as low as 15 mph. It is the use of a rotary wing that enables the gyroplane to avoid the low speed limitations imposed by fixed wing stall which aeroplanes encounter at the lower end of the speed envelope. On the other hand, the more adverse drag characteristics apparent at the higher end of the envelope, limit gyroplane high speed performance when compared to that of fixed wing aircraft of similar size.

The gyroplane has one major advantage over both the helicopter and the aeroplane. In the advent of an engine failure the procedure for landing the vehicle is the same as that under normal circumstances. Since the main rotor is constantly in autorotation mode the hazards associated with the transient from powered to non-powered flight pertinent to the helicopter, do not exist. With the pilot following the normal landing procedure the aircraft should descend safely, under full control, from any altitude.

A clearer indication of the contemporary gyroplane's capabilities is presented in Table 2.3, where the basic performance specifications of the RAF 2000 gyroplane are compared to those of the Robinson R-22 light helicopter. Several important conclusions can be drawn from this comparison: most of the gyroplane's capabilities are comparable to those of a helicopter of the same mass (this includes important parameters such as maximum speed, ceiling and range). The gyroplane is obtainable at a fraction of the helicopter's cost because of the simplicity of the mechanical design of a non-powered main rotor and to the smaller engine used for powering a pusher propeller.

Although a detailed study of gyroplane flight characteristics is provided in subsequent chapters, the reader should be reminded at this point that the work of Houston & Thomson (*CAA [1994]*) demonstrated that, unusually for rotorcraft in general, the gyroplane under study displayed 'classical' longitudinal dynamic stability properties, with the rotor speed degree of freedom playing an important role. If this is to be found true for a second gyroplane case it would provide further evidence that this type of aircraft must be viewed from a different perspective than that of conventional rotorcraft.

## **2.4 Review of previous gyroplane research**

Within engineering progress in the theoretical understanding of a particular field is directly influenced by its potential to yield a practical application. A comprehensive examination of the research already accomplished for gyroplanes serves to confirm this fact. In the 1920s and 1930s when the aircraft was still regarded as a novelty capable of yielding many benefits, when compared to its contemporary fixed wing counterparts, the research activity is seen to be significant. In fact it will be demonstrated in this section that much of the work performed in this period has contributed greatly to the understanding of rotorcraft aerodynamics in general. The invention of the helicopter changed this initial gyroplane favored trend and emphasis was shifted from non-powered to powered rotor configuration development. This can be seen to have had a major degrading effect on the research into gyroplanes and, with a few noticeable exceptions, between the late 1930s and the 1990s the literature concerning it, is extremely sparse. It was not until recent years that the establishment of the aircraft as a popular type for recreational flying has revived the interest in it. The flight safety concerns already mentioned in the previous chapter, particularly in the UK, have provided the impetus for the research program regarding the aircraft's stability and control characteristics, which is partly responsible for the motivation behind the work described in this thesis. A chronological review of the most important publications in the field to date will be presented next, as this is regarded as an essential step for properly assessing the significance of the current work.

In the 1920s Glauert and Lock emerged as pioneers in the investigation of the aerodynamic properties of freely rotating rotors. Since the gyroplane was the only

rotorcraft available at the time, their research was inevitably associated with this type of aircraft. It consisted primarily of developing methods for calculating rotor loadings and estimating the flapping motion of the blades. It was shown in the previous chapter that the rotor inflow theory developed by Glauert as part of his early work, is still widely used today as a first approximation for estimating the inflow velocity.

In the first major publication on the subject to be found (*Glauert [1926]*), the force and moment characteristics of an autogyro's main rotor are examined through a series of simplifying approximations. This 'set the scene' for this first stage of the research the main purpose of which then became to enhance the fidelity of Glauert's initial representation. A first attempt at achieving this was performed by *Lock [1927]*, who disposed with some of the initial simplifications. The theoretical achievements were also complimented with wind tunnel tests, described in *Lock & Townhead [1927]*. A concise summary of the work of Glauert and Lock, including the experimental work performed on Cierva autogyros, is presented in *Glauert & Lock [1928]*. In the 1930s this research was further advanced by Wheatley, who through a series of publications developed detailed expressions for rotor aerodynamic parameters, focusing on blade flapping motion. An example of his theoretical work is presented in *Wheatley [1934]*, where the dependence of the blade flapping motion on the induced velocity distribution is demonstrated. Experimental work was also performed on the PCA-2 autogyro *Wheatley & Hood [1935]*.

This early period of research was certainly the most productive as numerous gyroplane related publications are cited in the literature. As already discussed, the foundations of what is nowadays recognised as classical rotary wing aerodynamic theory were laid. On the other hand aircraft performance and stability issues were not addressed at all at this stage. The first attempt to assess the performance attributes of a small gyroplane was made by *Schad [1965]*. A series of results were presented showing the flight speeds, power requirements, climbing capability and flight attitudes of the Bensen B-8M and the Avian 2/180 gyroplanes. Their flight performance parameters were then compared to those of the Piper Super Cub fixed wing aircraft, which is of similar size. It was concluded that the gyroplanes possessed better climbing ability, larger payload, slower minimum-level-flight speeds and reasonable descent rates.

The increased popularity of the gyroplane as a recreational aircraft in the 1990s led to a revival of the academic interest in it. In 1990 for example, *McKillip [1990]*, reports on the instrumentation required to record data from a towed gyroplane rotor. More significantly, after the series of fatal accidents referred to in the previous chapter, the Civil Aviation Authority was forced to produce a new airworthiness and design standard (*Anon [1993]*). In order to do this it was necessary to consolidate the understanding of gyroplane stability and control characteristics. As a consequence, the research program already described was set up with the University of Glasgow Aerospace Engineering Department (*CAA [1994]*). This investigation undertaken by Houston and Thomson was the first thorough examination of gyroplane properties other than that of its main rotor aerodynamics and led to the research activity described in this thesis. Results yielded from this research activity are presented in *Houston & Thomson [1997]*, *Houston [1998a]*, *Houston [1998b]*, *Houston & Thomson [1999]* and *Houston [2000]*.

As a resume of this literature review, it can be said that gyroplane related research to date is primarily concentrated into two periods, each focusing on different aspects. The first one during the 1920s and 1930s set the definitions of classical rotor aerodynamic theory. The second more contemporary one has focused on the aircraft stability and control characteristics. A major part of the work described in this thesis forms a continuation of this research.

## **2.5 Chapter summary**

This chapter provided a description of the development of the gyroplane to its current status which has demonstrated that this class of aircraft relies on autorotation to sustain lift and can therefore be used for simulating rotorcraft in autorotative flight mode, as discussed in Chapter 1. It was also shown that after the invention of the helicopter interest in developing the aircraft to a practical application disappeared, although in recent years it has been extensively used for recreational flying purposes.

A review of the related research to date indicated that it has directly contributed to the understanding of rotorcraft aerodynamics in general. In recent years this research has focused mainly on stability and control issues.

As the experimental work described in this thesis employs a Montgomerie-Parsons gyroplane it is apt to provide a presentation of the aircraft and the experimental design in advance of discussing the simulation and flight test results.

# Chapter 3

## Experimental Design for the Flight Testing of a Light Gyroplane

### 3.1 Introduction

To generate a set of experimental data, an appropriate instrumentation system had to be designed and installed on the research aircraft and a flight test plan capable of yielding the required data had to be devised and realised.

This chapter is concerned with the experimental element of the thesis work highlighting the specific considerations and problem areas associated with instrumenting and flight testing a light gyroplane. An overview of the hardware components including the transducers, filters and data recording system is provided, together with the data acquisition software. The method employed for calibrating each instrument together with an overall system performance assessment is also presented. Finally, the flight test plan that was derived is described, focusing on the selection of the pilot control inputs and the basic data processing that is necessary for the implementation of a system identification technique.

### 3.2 The design of an instrumentation package for the Montgomerie-Parsons gyroplane

The G-UNIV research gyroplane was purchased by the Department of Aerospace Engineering in 1996 and is a modified version of the two-seat Montgomerie-Parsons, manufactured by Jim Montgomerie Gyrocopters. Due to the flight test purposes of the aircraft, the second seat has been removed to accommodate the on-board data acquisition instrumentation. This is best illustrated in Figure 3.1 which provides a view of the aircraft in its basic form. For use as a flight test vehicle, the aircraft had to satisfy several performance specifications. For example, in addition

to complying with every aspect of BCAR Section T (*Anon [1993]*), it had to possess sufficient endurance and ceiling capabilities for achieving the projected flight test manoeuvres. For a summary of the basic performance specifications of the aircraft see Table 3.1, with the ones relevant to Section T sufficiently meeting its requirements. For example it is stated (*Anon [1993]*), that "the time for climb from leaving the ground up to 1000 ft above the field must be determined and when converted to the international standard day conditions at sea level, must not exceed four minutes". The specifications issued for the climb performance of the aircraft are clearly in accordance with this statement.

The instrumentation required for obtaining knowledge of aircraft states both in trimmed flight and in response to pilot inputs is now well understood and documented. An outline of the typical structure of such a system is presented in Appendix 2. In addition to the general requirements outlined in the appendix the instrumentation of the specific aircraft type, imposed further considerations:

- Restrictions on the payload capability limited the instrumentation component weights and sizing to a minimum. Small, lighter components were therefore preferred to heavier more bulky ones.
- Due to budget limitations, it was necessary for the set-up to comprise of relatively low cost instruments. A product survey was conducted to identify the most cost-effective options.
- The main instrumentation pallet was positioned as close to the aircraft centre of gravity as possible, in order to avoid a significant shift of this point in relation to the original configuration.
- The air-data probe was positioned on a 6ft stiff metal tube at the nose of the aircraft (as suggested by *Kaletka [1991]* and *Hearing [1995]*), so as to minimise the influence of aircraft vibration and flow interference both from the airframe body and the main rotor wakes.

- The main rotor and the pusher-propeller speeds  $\Omega, \Omega_p$  are essential parameters in assessing a gyroplane's performance and stability attributes. The main rotor speed in particular constitutes an independent degree of freedom and is therefore treated as a separate state when modelling the aircraft. Two electro-optical sensors were employed for recording the above parameters.
- Pilot safety is of paramount importance when flight testing an aircraft type with a poor safety record. The installation of the system was thus performed in a manner not compromising the vehicle handling qualities. As an extra precaution, the main instrumentation pallet is covered with a glass fibre fairing during all flights.

With a view to the above, a package consisting of the following sensors was designed:

- i. One mini air data probe to measure airspeed, angle of attack and sideslip.
- ii. Two temperature sensors to measure the air temperature.
- iii. One three-axes and one single axis accelerometer to measure the linear accelerations.
- iv. Three rate gyros to measure the angular velocities.
- v. Three angle indicators to measure the aircraft attitudes.
- vi. Three displacement transducers to measure the pilot control inputs (longitudinal and lateral stick and rudder deflection).
- vii. Two electro-optical sensors to measure rotorspeed and propeller speed.

A full listing of the sensors and the corresponding measured quantities are presented in Table 3.2. Basic signal conditioning techniques such as signal amplification and low pass filtering are applied to the transducer outputs. For the filtering aspect in particular, fourth order, unity gain Butterworth low pass filters with a cut-off frequency of 23Hz were used as *anti-aliasing* filters. The function of this type of filter is to alleviate the effect of any frequency components which may exist *above* the Nyquist frequency (in this case 25 Hz), and which would otherwise corrupt the acquired data. Importantly, in order not to affect the system identification results, *identical* filtering is applied to all the transducer outputs.

The data acquisition is performed by an on-board PC using a sophisticated 12-bit DAQ card driven by application software. A listing of the installed instruments, together with the corresponding manufacturers and purpose of each, is presented in Table 3.3.

In general, the overall instrumentation layout can be broken down as follows: The *main instrumentation pallet* situated at the modified second seat, the *air-data probe and associated circuitry* situated at the nose of the aircraft, a set of *position transducers* situated at the pilot controls and control surfaces and two *electro-optical transducers* situated at the main rotor and pusher-propeller.

#### Main instrumentation pack

The main instrumentation pack forms the core of the system providing the power, signal conditioning and data acquisition from all the measuring transducers. A schematic diagram of the transducer layout is provided in Figure 3.2 and a side view of the pack is illustrated in Figure 3.3. During flights, the pallet is protected through a cover constructed from glass fibre material, as illustrated in Figure 3.4.

A photo illustration of the transducer layout is provided in Figure 3.5. The three rate gyros measuring the aircraft angular velocities, are the first set of instruments to be recognised. The angular attitudes are measured by the next three sensors in line, the attitude indicators. Each of the above instruments are aligned to a particular aircraft body axis.

Both the rate gyros and the angle indicators are manufactured by British Aerospace Systems & Equipment and are based on the technology of vibrating structure gyroscopes (VSGs), the principles of which are given in *BASE [1995]*. With this type of gyroscope the Coriolis effect experienced by a vibrating solid structure is used to detect angular rotation. In particular, the sensing element (acting as an oscillator) is capable of obtaining a measure of the angular rate about its axis of alignment. In the case of the angle indicators, built-in electronics are employed to convert the rates to angular attitudes. Both sets of instruments are simple in their construction and possess low power requirements and noise characteristics.

The 3-axes accelerometer is used to record the aircraft linear accelerations. The sensing element consists of an upper fixed electrode and a lower moveable one connected to a seismic mass. The movement of the mass as a reaction to an applied acceleration causes the capacitance values to change. A mechanism of this type is enforced in each of the three axes with the device including a built-in gyroscope sensor to provide a vertical reference. The measuring range of this instrument along the aircraft z-axis ( $\pm 2\text{ g}$ ), was not considered sufficient so a single axes transducer (the last on line), with a range of  $\pm 3\text{ g}$  was also incorporated along this axis.

Finally, the main instrumentation pack also provides the power for the full instrumentation system (the computer included), and is completely independent of any of the aircraft's normal systems and power supplies. This is an important safety feature as it ensures that any problems occurring in the instrumentation system cannot affect the aircraft's own systems. The instrumentation and laptop PC are powered by two 12 V DC batteries which are charged via an existing auxiliary generator which is completely independent of the one used to start up the aircraft's engine. For the laptop PC in particular, needing 24 volts to be adequately powered, a 150 W, 12 V-24 V step-up DC-DC converter is used, which is positioned on the aircraft main mast.

#### The air-data probe and associated circuitry

A schematic diagram of the air-data probe is presented in Figure 3.6. The installation of the probe and a box containing some essential signal conditioning circuitry and the associated pressure transducers, on the aircraft, is illustrated in Figure 3.7. A bracket and bracing system was constructed in order to position the circuitry box and the air-data probe on a 6 foot stiff metal boom at the nose of the gyroplane, aligned with the aircraft body x-axis. The positioning of the bracing served the purpose of minimising the aircraft vibration transmission to the probe although due to its design configuration this was only achievable in the lateral direction. Examination of the time histories of the variables measured by the probe in subsequent chapters do indicate however that the aircraft vibration transmitted in the longitudinal direction is exhibited at high frequencies well separated from the

bandwidth of interest. In any case, the high sampling rate employed (50 Hz), facilitates the implementation of digital filtering techniques for alleviating the effect.

The positioning of the associated circuitry close to the pressure pickups serves to minimise any pneumatic lag effects which would otherwise be present due to the finite length of the pressure tubing. In particular, any changes occurring at the pressure ports will take a finite time interval before they are transmitted, through the tubing, to the relevant transducers. This time delay if significant could noticeably affect the system identification results and therefore every effort must be made to have it minimised.

#### The position transducers

The sensors used to measure the pilot control inputs (3 position transducers), are distributed in appropriate locations on the aircraft. In particular, the two displacement transducers measuring the stick deflection (longitudinal and lateral), were clamped to the keel directly beneath the pilot control as shown in Figure 3.8, with the third one mounted next to the rudder surface, the deflection of which it is designed to obtain (Figure 3.9). The position transducers essentially consist of simple potentiometers outputting a voltage proportional to their travel.

#### Electro-optical transducers

The rotor speed sensor, which is an electro-optical device, is mounted on the fixed part of the rotor head as shown in Figure 3.10. The corresponding one measuring propeller speed is situated just behind the pusher-propeller as illustrated in Figure 3.11. For the main rotor speed in particular, a reflective material is positioned on each rotor blade with the electro-optical device set up to activate a pulse on the completion of a half rotor turn. With a projected nominal rotor speed of approximately 6 Hz the instrument is effectively sampling at,

$$2 \times 6 = 12Hz$$

As the work of *Houston & Thomson (CAA [1994])* has indicated that gyroplane body modes manifest themselves at frequencies below 1 Hz, a rate of 12 Hz is considered sufficient for the purposes of this research activity.

The output from every transducer described above is fed to the SCU (Signal Conditioning Unit) which in turn then passes the data stream to the Laptop PC which logs the data. The SCU also contains all the necessary circuitry for performing the anti-aliasing filtering on each transducer output. The data is therefore logged in its filtered form with frequencies above 23 Hz being discarded. For the purposes of the flight testing it was considered that an on-board *ruggedised* PC recorder would provide the essential guarantee of safe retrieval of the data which is stored in the form of text files on the hard disk of the device, making it easily accessible for direct viewing, process and analysis.

Accurate instrument calibration, i.e. the derivation of a relationship between the physical quantity measured and the transducer (voltage) output, is an essential requirement for obtaining reliable data. Although for most sensors installed detailed calibration sheets were provided by the manufacturer, wherever possible these were verified in the laboratory.

The attitude indicators were calibrated by use of a conventional inclinometer the results verifying the supplied information. Accelerometer outputs were checked by aligning them to the Earth vertical and ensuring that they correctly indicated 1g. The position transducers measuring stick travel and rudder deflection were calibrated by applying the controls over their range and recording the corresponding voltages. For stick travel in particular a certain amount of data processing is required before the output voltages can be converted to engineering units. This is due to the coupling existing between the transducers measuring longitudinal and lateral travel, with the movement in one direction resulting in some deflection of the sensor measuring the other. This is dealt with by assuming that the actual stick positions are a function of the voltages registered on both transducers, i.e.,

$$(\eta_{ls}, \eta_{lc}) = f(V_{lo}, V_{la})$$

where,

$\eta_{lr}$  is the longitudinal stick position

$\eta_{lc}$  is the lateral stick position

$V_{lo}$  is the longitudinal stick sensor voltage output

$V_{la}$  is the lateral stick sensor voltage output

With the stick moved throughout its longitudinal and lateral range, the rotor tilt derived together with the corresponding transducer voltages are recorded and stored in the form of a lookup table. Having recorded and stored those values it is then possible to implement a 2 dimensional interpolation algorithm to calculate the rotor tilt after the completion of each flight. This is performed by fitting a surface of the form

$$z = f(x, y)$$

to the calibration data (for the longitudinal tilt calibration data, see Figure 3.12), using triangle based linear interpolation. Both the longitudinal and lateral stick position can then be obtained as a function of both sensor outputs.

The calibration of the air-data sensors was performed as follows. For the pressure transducers a Duck-DPI 610 pressure calibrator device was used to apply known pressure inputs and acquire the corresponding voltage outputs. An example of this is presented in Figure 3.13 where the calibration results for the transducer connected to the static port of the probe are displayed. The linear nature of the input/output relationship is characteristic of all the installed transducer types. The aerodynamic angle vanes were calibrated with a special protractor fixture provided by the manufacturer.

When assessing the performance of a DAQ system, accuracy, resolution, range, noise and bandwidth are major factors determining its capabilities. The accuracy is defined by the specifications of the instruments and in their selection process it was ensured that they satisfied the model validation requirements of the study. Resolution is determined by the number of bits used by the DAQ card, in this

case a National Instruments AT-MIO-64E, the specifications of which are defined in *National Instruments [1997]*. In particular for a 12 bit card like the one employed for the current application, a resolution of  $\frac{1}{2^{12}} = \frac{1}{32768}$ , is achieved. This is well within the accuracy specifications of each instrument as demonstrated when using the roll/pitch sensors possessing a range of  $\pm 45^\circ$  (i.e. a  $90^\circ$  range), as an example. The resolution achieved in this case is  $\frac{90}{32768} \approx 0.0027^\circ$ . Similar orders of resolution can be estimated for all other sensors, the specifications of which are presented in Appendix 2 and *Spathopoulos et al [1998b]*.

The range of the instruments was chosen in accordance with the projected flight manoeuvres the specific form of which will be described in the following section. Finally, a parameter which is of particular relevance to the dynamic response data is the system bandwidth. This is determined both by the DAQ hardware capabilities and the specifications of each individual instrument. For the former case the AT-MIO-64E card selected, possesses ample capability for satisfying the experimental needs. A 50 Hz sampling rate was chosen for the following reasons. It provides more than enough bandwidth for the dynamic response testing. As discussed previously, the work of Houston and Thomson (*CAA [1994]*) indicated that gyroplanes exhibit body modes of motion with a maximum damped frequency of less than 1 Hz; with a sampling rate of 50Hz a theoretical (Nyquist) maximum frequency of 25Hz can be adequately captured. Furthermore this makes it possible for a qualitative assessment on rotor induced vibration to be made the harmonics of which are predicted to appear at frequencies above 10Hz. Finally for future application, the choice of a high sampling rate would enable a study on the higher frequency flapping modes of the main rotor to be performed. As far as the performance of the individual instruments is concerned, the specifications of the transducers presented in *Spathopoulos et al [1998b]*, show that the lowest bandwidth exhibited is from the attitude indicators at 3Hz. For the purpose of assessing the body modes of motion of the aircraft this is deemed adequate.

### **3.3 The flight test plan for the Montgomerie-Parsons research gyroplane**

The preparation for the flight testing of the Montgomerie-Parsons research gyroplane consisted of the following stages:

- i. DAQ software programming and set-up
- ii. Aircraft ground tests
- iii. Flight manoeuvre scheduling
- iv. Post flight considerations

In order to maximise the planning efficiency, input was provided to the project personnel both from the aircraft technicians and from the test pilot involved.

#### **3.3.1 DAQ software programming and set-up**

In the previous section an overview of the hardware design aspects of the instrumentation system was presented, introducing the concept of acquiring and storing the transducer data on a ruggedised laptop PC. This provides the basis of a DAQ system with a sophistication unique for this type of aircraft. In order to fully exploit the capabilities of such a hardware configuration the LabView commercial software package, the main features of which are presented in *LabView [1997]*, was selected as the programming platform.

The development of the DAQ software was intended to fulfil the following purposes; through the user provided input, acquire the voltage reading from all transducer outputs at a defined sampling rate for a predetermined amount of time; by means of the provided calibration constants transform the raw voltage data into engineering units; to store the time histories of each of the measured quantities in a format easily compatible with other software packages.

The programme interface, illustrated in Figure 3.14, enables the user to directly input the desired sampling rate, sampling time and information regarding the

particular flight test conditions<sup>1</sup>. On start-up, the programme waits for the user command before enabling the actual acquisition process. This allows the computer to be safely fastened and the protective fairing to be fitted on without the loss of valuable DAQ time. The acquisition can be initiated after the aircraft start-up using a switch located on the cover protection, with a LED indicating the initiation of the process. After the predefined length of DAQ time has elapsed, the time histories of the transducer outputs are stored in the form of text files once they have been converted to the appropriate engineering units. The exception to this are the outputs from the stick position transducers (which are derived as described in the previous section), and the aircraft velocity which is calculated after each flight from the dynamic pressure output.

A flow chart diagram of the DAQ programme is illustrated in Figure 3.15, where the sequence of the tasks performed is clearly defined. The programme initially enters a loop checking the state of the DAQ initiation switch; a digital pulse indicates to the software that the switch is turned on and the DAQ process can commence. Following this, the voltage readings acquired from the pressure transducers are stored as offset values in order to be subtracted from the raw data when it is converted to engineering units. For all other transducers processing of offset (or zero reference) voltages is automated through the built-in electronics. The raw data from all sampled channels is then obtained over the predetermined DAQ time,  $t_{\text{DAQ}}$ , with the LED activated by a software generated pulse indicating that the process is under way. Once  $t_{\text{DAQ}}$  has elapsed the data is converted to the appropriate engineering units by application of the multiplying constants obtained from calibration. The time histories of each of the measured quantities are then stored as text files, as listed in Table 3.4. The file names printed in bold font indicate an actual transducer output, the others representing information such as offset values, flight conditions, etc.

### 3.3.2 Ground Testing

Starting up the aircraft and enabling the DAQ process prior to the conduct of the actual flights served the following purposes: it provided the opportunity of

---

<sup>1</sup> This can later be retrieved in the form of a simple text file

assessing both the functionality of each transducer independently and the system as a whole; valuable experience was gained in becoming accustomed to the aircraft and DAQ start-up procedures; an initial assessment of the data quality made available from the DAQ system functioning autonomously could be performed; an initial investigation was made possible on the effect of signal conditioning methods such as digital filtering, on the output time histories.

### **3.3.3 Flight test manoeuvres**

The single most important part of the preparation of a flight test plan is the specification of the flight testing manoeuvres. In particular, for the purposes of rotorcraft system identification, it has been observed by several authors (*Plaetshke et al [1979], Moulder [1985], Padfield [1986], Klein [1989], Murray-Smith [1991]*), that a critical part of the experimental design is the selection of input signals appropriate for exciting the desired aircraft modes of motion.

The flight testing was broken down into three phases each intended to meet separate objectives. Before presenting the tasks associated with each phase it is important to remind the reader of the aims of the flight test programme. The two general aims of the experiments are to validate an existing rotorcraft mathematical model in autorotation and to extend the data base of knowledge on the flight dynamics characteristics of light gyroplanes. In order to succeed with this a series of objectives have to be met.

Initially, it is necessary to ensure that the instrumentation system is functioning according to expectations, with the aircraft airborne. A series of 'shake down' flights are used not only to ascertain the proper functionality of the instrumentation but also to enhance the pilot's confidence in dealing with the test aircraft. A series of steady flight manoeuvres are then to be performed primarily to obtain a data set appropriate for validating the model over steady state conditions. In addition to this, investigation of the trim characteristics of the aircraft are able to provide information on basic performance and stability attributes such as stick/speed stability, rate of climb, minimum propeller rpm speed, main rotor induced vibration levels, etc.

Finally, time histories of the aircraft state responses to specified control inputs are to be obtained and then compared to those obtained from the model. Furthermore, the standard aircraft stability derivatives can be extracted by application of a system identification technique. Both the time responses and the stability derivative results are able to provide immediate insight to the flight dynamic characteristics of the vehicle.

With view to the above the flight testing schedule is broken down as follows:

### 'Shake down' flying

The first period of flying has the dual purpose of familiarising the pilot with the test vehicle and procedure and to check the proper functionality of the instrumentation system. More explicitly, as indicated by *Murray-Smith [1991]*, the following objectives were to be met:

- Familiarisation of the pilot with specific tests, including aircraft trim at particular flight conditions and the application of the desired control inputs.
- The training of the pilot with regard to the shape and timing of the control inputs.
- The determination of the appropriate control input amplitudes. For example, for the identification of linearised models, the inputs must be constrained by the small perturbation assumptions.
- The checking of the instrumentation system in order to detect and eliminate any measurement errors.

During this initial period there was no rigorous manoeuvre schedule imposed on the pilot who has the freedom to try out various operational conditions. A flight time of 5 hrs was allowed for the completion of this stage.

### Basic performance and trimmed flight related operation

For the model validation purposes of the experiments to be satisfied, the aircraft is to be trimmed over a speed range of 30mph to 70 mph at 5mph increments. Pilot control inputs ( $\Theta_{1s}, \Theta_{1c}$ ), and appropriate aircraft states ( $\Phi, \Theta, \Omega$ ) are recorded and directly compared to the model predictions.

A set of steady climb manoeuvres of the type described by *Vleghert [1995]*, will serve to ascertain the aircraft rate of climb. Furthermore close examination of the trim data will be used to provide information on the parameters such as stick/fixed stability, rotor induced vibration etc.

### Dynamic response

The input types to be applied by the pilot must be such as to invoke a noticeable aircraft response. Aircraft state time histories can then be examined against those obtained from the simulation runs and processed to yield estimates of the stability and control derivatives.

A series of conventional doublet and step input signals are applied to excite both the longitudinal and lateral/directional modes of motion. Doublet inputs (Figure 3.16), have been extensively used for the identification of the system dynamics of fixed wing aircraft by effectively exciting the short period and Dutch roll modes. They have the advantage of being simple and easily realised by the pilot, which is the reason that they were selected as part of the flight testing of an aircraft class with a poor safety record. However, their excitation potential is concentrated to a limited bandwidth around a specified frequency as illustrated in Figure 3.16. For helicopters which possess highly coupled dynamics using a test signal with a small bandwidth presents difficulties and therefore doublet inputs are rarely used on their own for system identification purposes. On the other hand, the work of *Houston & Thomson (CAA [1994])*, has *indicated* that they are of greater use when identifying the more 'classical' flight dynamics properties of gyroplanes. For the purposes of this research activity no rigorous definition of the pulse frequency content was made, with the pilot

given the freedom to search for the aircraft modes at frequencies at which one would expect them to manifest themselves. For the short period excitation for example, in wake of the experience gained from the VPM gyroplane study (see *Houston [1998a]*), doublets of a frequency less than 0.5 Hz are to be applied.

For the study of the longitudinal aircraft dynamics, doublet inputs are applied to the longitudinal stick position, whereas step inputs (i.e. the standard technique of displacing the stick to provoke a speed change before returning to trim), are enforced to excite any phugoid motion. For the lateral/directional case doublet inputs are applied to both the lateral stick and the rudder pedals. For safety purposes all inputs are to be made in an incremental fashion up to a maximum input of 10% when the aircraft's response reaches 5° - 10° attitude response.

Finally it should be noted that for the data analysis purposes of this stage, a pilot event button was incorporated into the instrumentation system in order to facilitate the determination of the discrete flight events. It essentially consists of an analogue switch outputting a high voltage pulse prior to the initiation of each manoeuvre.

An outline of the flight schedule sequence indicating the objectives, flight manoeuvres and flight time involved in each of the stages described above, is presented in Table 3.5. An example of a detailed description of a test flight as presented to the pilot, is given in Table 3.6, for the case of step/doublet inputs to be applied to all axis.

### **3.3.4 Post flight considerations**

A complete flight test plan must take into account the activities involved directly after a flight test, both the operational aspects of the next flight and the initial assessment of the acquired data. For the first part the general procedure adopted for all forms of flight testing, which includes the de-briefing of the pilot, a routine safety check, refuelling etc., was to be followed. Initial checking of the data is facilitated by the on-board method adopted for the recording and storing purposes. Time histories from transducer outputs are to be plotted immediately after each flight and checked

for errors such as dropouts, absence of signal, sign inversions, saturation, non-realistic noise levels etc. In addition, a detailed data inspection is used to confirm which data runs are suitable for the desired analysis.

Finally, in order to be allowed to flight test the aircraft in the first place, an official flight test permit had to be obtained from the authorised bodies. An outline of the procedure leading to this is presented in Appendix 3.

### **3.4 Basic system identification data processing**

In order to produce data which is appropriate for the implementation of a system identification technique, some basic data processing must be applied to certain transducer outputs.

For the system identification purposes, the aircraft dynamics are represented by a linear model description of the form,

$$\dot{\underline{x}} = A\underline{x} + B\underline{u}$$

The model can be examined as a longitudinal and a lateral directional subset, as shown by *Spathopoulos et al [1998a]*.

For the longitudinal case we have,

$$A = \begin{bmatrix} X_u & X_w & X_q & X_\theta & X_\Omega \\ Z_u & Z_w & Z_q & Z_\theta & Z_\Omega \\ M_u & M_w & M_q & M_\theta & M_\Omega \\ 0 & 0 & 1 & 0 & 0 \\ Q_u & Q_w & Q_q & Q_\theta & Q_\Omega \end{bmatrix}, B = \begin{bmatrix} X_{\theta_1} \\ Z_{\theta_1} \\ M_{\theta_1} \\ 0 \\ Q_{\theta_1} \end{bmatrix}$$

and

$$\underline{x} = [u \ w \ q \ \theta \ \Omega']^T, \underline{u} = [\theta_{1s}]$$

For the lateral/directional case,

$$A = \begin{bmatrix} Y_u & Y_w & Y_q & Y_\theta & 0 \\ L_u & L_p & 0 & L_r & 0 \\ 0 & 1 & 0 & 0 & 0 \\ N_u & N_p & 0 & N_r & 0 \\ 0 & 0 & 0 & 1 & 0 \end{bmatrix}, B = \begin{bmatrix} Y_{\theta_{ic}} & Y_{\theta_{rud}} \\ L_{\theta_{ic}} & L_{\theta_{rud}} \\ 0 & 0 \\ N_{\theta_{ic}} & N_{\theta_{rud}} \\ 0 & 0 \end{bmatrix}$$

and

$$\underline{x} = [v \ p \ \phi \ r \ \psi]^T, \underline{u} = [\theta_{ic} \ \theta_{rud}]^T$$

The angular attitudes and velocities, and rotor speed variables are all obtained directly from the corresponding transducers, whereas the control inputs are determined in the manner described in section 3.2. The aircraft linear velocity components  $u$ ,  $v$ ,  $w$  are derived from the probe measurements as follows:

Initially, the air density is calculated from the gas state equation,

$$P_s = \rho R T_{temp} \Rightarrow \rho = \frac{P_s}{R T_{temp}} \quad (3-1)$$

where,

$\rho$  is the air density,

$P_s$  is the barometric (static) pressure,

$T_{temp}$  is the air temperature,

$R$  is the universal gas constant.

The dynamic pressure acquired from the differential pressure transducer (measuring the difference between the total and static pressures), can then be used to determine the total velocity of the probe:

$$P_{dyn} = \frac{1}{2} \rho V_p^2 \Rightarrow V_p = \sqrt{\frac{2P_{dyn}}{\rho}} \quad (3-2)$$

where,

$V_p$  is the total velocity of the probe, and

$P_{dyn}$  is the airflow dynamic pressure.

The total probe velocity is then decomposed into aircraft body axes components as follows:

$$u_{probe} = V_p \cos \alpha_{probe} \cos \beta_{probe}$$

$$v_{probe} = V_p \sin \beta_{probe} \quad (3-3)$$

$$w_{probe} = V_p \sin \alpha_{probe} \cos \beta_{probe}$$

where,

$u_{probe}$ ,  $v_{probe}$ ,  $w_{probe}$  are the body axes components of the probe velocity, and

$\alpha_{probe}$ ,  $\beta_{probe}$  are the angles of attack and sideslip.

From equation (3-3), it is then possible to deduce the absolute velocity of the aircraft centre of gravity as follows,

$$u = u_{probe} - q(z_{probe} - Z_{CG}) + r(y_{probe} - Y_{CG})$$

$$v = v_{probe} - r(x_{probe} - X_{CG}) + p(z_{probe} - Z_{CG}) \quad (3-4)$$

$$w = w_{probe} - p(y_{probe} - Y_{CG}) + q(x_{probe} - X_{CG})$$

where,

$u$ ,  $v$ ,  $w$  are the aircraft velocity components in body axes,

$x_{probe}$ ,  $y_{probe}$ ,  $z_{probe}$  are the probe co-ordinates,

$X_{CG}$ ,  $Y_{CG}$ ,  $Z_{CG}$  are the aircraft centre of gravity co-ordinates,

$p$ ,  $q$ ,  $r$  are the aircraft angular velocity components in body axes measured by the rate gyros.

### **3.5 Chapter summary**

An overview of the experiment design involving the instrumentation and the flight test preparation of the Montgomerie-Parsons gyroplane has been presented. The experimental set-up is capable of yielding the data necessary for achieving the aims of the research work. Furthermore it is evident that the flight testing of a gyroplane involves following the conventional procedure for flight testing an aircraft in its normal mode of operation and thus eliminates the difficulties associated with conducting equivalent tests on a helicopter in autorotation.

In the next chapter the model results capable of complimenting those yielded from the flight testing will be generated in the form of baseline simulations.

# Chapter 4

## Predicted Characteristics of the Montgomerie-Parsons Gyroplane

### 4.1 Introduction

After having presented an overview of the experimental set-up, the next logical step is to provide a definitive description of the flight characteristics of the specific aircraft under study. A set of baseline simulations of the Montgomerie-Parsons research gyroplane can serve both the purpose of providing an initial understanding of the aircraft's attributes and presenting a platform of results which when compared to the data obtained from the flight tests, can be used to validate the simulation model.

The RASCAL simulation program developed by *Houston [1994]*, requires a user provided configuration file of the simulated aircraft. It is therefore necessary initially to acquire parameters such as the aircraft sizing, weight and balance properties, etc., which when grouped provide a complete configurational definition of the vehicle. Since the effect of the vertical position of the cg on aircraft stability is to be investigated, the method by which it is obtained is justifiably described in greater detail.

Results are presented both on the trim/steady flight properties and to those related to the aircraft dynamic stability; for the latter case the data is produced in the form of conventional stability derivatives. Both sets of results are checked against basic gyroplane aerodynamic theory therefore providing an initial assessment of the validity of the model.

## **4.2 An overview of the RASCAL model**

Houston [1994] reports that "the mathematical modelling of helicopters for stability, control and handling qualities has assumed increased importance in design and analysis over the last 15 years". Validation of such models can be performed in a variety of ways as discussed in Chapter 1. Two examples of models using flight test data as a validation means, can be found in *Padfield [1996]* and *Houston [1994]*. Importantly, for both activities the flight regimes examined are limited to the hover and forward flight cases. *Padfield [1996]* compares the time responses generated from simulation to those documented in the DRA Puma and DLR BO 105 helicopter flight test data bases (see *AGARD [1991]*). *Houston [1994]* on the other hand employs a small perturbation method, whereby the model under study is linearised in order to extract conventional stability derivatives which are then compared to those yielded from a system identification technique applied to the experimental data.

In recent years rotorcraft models have evolved from the actuator disc approach where the simplifying assumption is made that the rotor loading is distributed over a thrust producing surface of zero thickness and can be determined *analytically*, to the more sophisticated individual blade/blade element type where each individual blade is divided into blade elements with the elemental forces and moments calculated and then integrated *numerically* across the span. In order when classifying them to incorporate further aspects of the modelling approaches, *Padfield [1996]* has moved one step further by summarising the properties of three different modelling levels, with the introduction of blade element rotor representation still forming the distinguishing point between levels 1 and 2.

The RASCAL model used in this study was developed by *Houston [1994]* and belongs to the individual blade/blade element type. A detailed presentation of the mathematical model, together with a description of the algorithms for trimming and linearising the model, are presented in Appendix 4. It is prudent in any case before using this simulation tool in its basic form to obtain a series of baseline results for the Montgomerie gyroplane, to review some of its key elements.

Within RASCAL up to ten individually modelled rigid blades can be represented, with fully coupled flap, lag and feather motion incorporated. The blade aerodynamics are acquired through look-up tables as a function of angle of attack and Mach number. The lift and drag forces and moments of the remaining aerodynamic surfaces (fin, rudder, etc.) are determined through simple polynomial expressions.

In other words a static aerodynamic model is assumed, at least at the blade element level. It should be noted however that the incorporation of the dynamic inflow model described in Appendix 1 does introduce a more global approach to representing the unsteady effects, particularly popular for flight dynamics applications. The introduction of a time dependence of the inflow velocities which are used for the determination of the rotor forces and moments, does provide with an alternative formulation of unsteady aerodynamic modeling. *Leishman [2000]* observes that "while perhaps offering less flexibility in the ability to represent some aspects of the unsteady airfoil problem, this approach is attractive for many problems in rotor analysis, particularly those in flight dynamics and aeroelasticity".

Once the aerodynamic forces and moments have been determined, the aircraft equations of motion are formulated and solved in the conventional way and the system states at any time point can be derived. The basic features of the model are summarised in Table 4.1.

### **4.3 The Montgomery-Parsons gyroplane configurational definition**

Before presenting any results regarding the aircraft geometry parameters, it is necessary to define a co-ordinate reference system. A geometric reference point (defined on the aircraft keel), was chosen to allow movement of the centre of gravity. The x-axis was chosen along the keel and in the direction of the aircraft nose, the z-axis positive vertically down and the y-axis to complete the orthogonal system, positive in the starboard direction. Aircraft sizing parameters important to the simulation model include the positioning and sizing of the aerodynamic surfaces, the pusher propeller and, most importantly, the main rotor. The majority of the results were obtained from direct measurement or by information provided by the

manufacturer and are presented in Table 4.2. Detailed engineering drawings were produced and used for estimating the aerodynamic surface areas. An example of this is presented in Figure 4.1, where the estimation of the fuselage side-area is illustrated.

The main rotor airfoil was identified as being of NACA 8-H-12 type. Detailed information on the aerodynamic properties of this type of airfoil can be found in *Stivers & Rice [1946]*. Measurements obtained directly from the rotor were compared to those of this type of airfoil, as illustrated in Figure 4.2. The aerodynamic blade section data utilised by the model was then configured accordingly by the use of look-up tables.

Although the small discrepancies observed will have an effect on the aerodynamic properties of the rotor, it is beyond the scope of this thesis to conduct a detailed investigation into this area. Even so, the aerodynamic data utilised by the model for the Montgomerie gyroplane simulation is still considered more accurate than that for the VPM case, where a CFD analysis had to be conducted to *estimate* the aerodynamic characteristics. The significance of this will be discussed in the model validation chapter of the thesis.

#### Aircraft weight and balance calculations

The weight, centre of gravity, and moments of inertia properties of any rigid body are arguably important parameters in determining the body's stability characteristics. One of the postulates to be investigated in this thesis is that the vertical position of the centre of gravity in relation to the propeller thrust affects the longitudinal handling qualities. Detailed results are thus obtained from the aircraft in its fully instrumented form with the presence of a pilot, with a quantitative measurement error analysis included in order to assess the validity of the most important results.

### *Measuring procedure*

The aircraft weight was determined through a set of conventional scales with the configuration not including the main rotor blades assembly which was weighed separately and its effect added to the initial results.

The procedure adopted for the centre of gravity position estimation follows that used for the research conducted for the CAA [1994], on the VPM gyroplane. Due to the symmetrical layout of the airframe about the chosen y-axis, it is assumed that the y co-ordinate of the centre of gravity is equal to zero. The problem then reduces to obtaining values for the longitudinal and vertical positions.

The aircraft, including the presence of a pilot, is hung from a single suspension point. By adding the appropriate weight ballast at a point on the keel, it is then brought to a level position; this is checked through an inclinometer device. A diagram of the resulting forces acting on the system, is given in Figure 4.3. By assuming that when the system is in equilibrium,

$$\sum \underline{M} = \underline{0} \quad (4-1)$$

and by taking moments about the suspension point  $S$ , the following is obtained:

$$\begin{aligned} (X_{CG} - X_{SP}) \cdot W_{A/C} &= (l_b + X_{SP}) \cdot W_b + (l_i + X_{SP}) \cdot W_i \Rightarrow \\ X_{CG} &= X_{SP} + \frac{(l_b + X_{SP}) \cdot W_b + (l_i + X_{SP}) \cdot W_i}{W_{A/C}} \end{aligned} \quad (4-2)$$

where,

$X_{CG}$  is the longitudinal position of the centre of gravity,

$X_{SP}$  is the x co-ordinate of the suspension point,

$W_{A/C}$  is the aircraft weight,

$W_b$  is the ballast weight,

$W_i$  is the inclinometer weight,

$l_b$  is the distance of the ballast weight from the reference point,

$l_i$  is the distance of the inclinometer from the reference point.

An expression is thus produced for the longitudinal position of the centre of gravity.

The vertical position is estimated by hanging the aircraft from the same point and its angle of suspension  $\theta_s$ , measured with the inclinometer device. Once a state of equilibrium is reached, the line of action of the weight force must pass through the suspension point S, as illustrated in Figure 4.4. Simple geometry can then be used to show that,

$$\tan \theta_s = \frac{l_{cg}}{l_s - Z_{CG}} \Rightarrow Z_{CG} = l_s - \frac{(X_{CG} - X_{SP})}{\tan \theta_s} \quad (4-3)$$

where,

$Z_{CG}$  is the vertical position of the aircraft centre of gravity (in absolute value terms),

$l_s$  is the vertical distance between the suspension point and the aircraft x-axis.

$l_{cg}$  is the longitudinal distance between the suspension point and the aircraft cg position.

### *Results*

A breakdown of the components comprising the aircraft weight is presented in Table 4.3. The parameters leading to the estimation of the centre of gravity position are given in Table 4.4. The effect of the main rotor blades, which were treated as a point mass acting on the rotorhead, is illustrated in Table 4.5.

Importantly it is found that the centre of gravity point lies *above* the propeller thrust line, as illustrated in Figure 4.5, which according to Houston's postulate should benefit the aircraft longitudinal stability. Furthermore, a parametric study involving the variation of pilot weight is illustrated in Figure 4.6. Three pilot cases with weights ranging from 56 kg to 88 kg were chosen for the analysis. A best fit linear approximation is also included in the graph from which it can be deduced that each 10 kg variation in pilot weight will result in a 0.7cm change in vertical cg position. So although the aircraft weight is small, the location of the pilot seat close to the airframe cg position means that changes in pilot weights will have a negligible effect on the overall cg position.<sup>1</sup>

### *Error analysis*

The importance of the results regarding the vertical centre of gravity position suggests that consolidating the accuracy to which they are obtained, is a necessary step before using them for simulation and other purposes. The following examination of the measurement errors incurred contributes to the understanding of their effect.

By assuming that the inclinometer weight (1.3 kg), is negligible when compared to the overall system, equation (4-3) reduces to

$$Z_{CG} = l_s - \left[ \frac{(l_b + X_{SP}) \cdot W_b}{\frac{W_{A/C}}{\tan \theta_s}} \right] \quad (4-4)$$

Since  $\theta_s$  was found a relatively small angle (less than 10°), the  $\tan \theta_s$  factor in the denominator of the second term will have a magnifying effect on any errors inherent in the measurement of the parameters comprising that term. The quantities  $W_b$ ,  $W_{A/C}$  and  $l_b$  are easy to measure and therefore the results regarding them are obtained with confidence. On the other hand, due to the configuration of the airframe an indirect

---

<sup>1</sup> The variation of fuel content was shown to have a similar effect.

measurement of  $X_{SP}$  had to be made by use of a clamp positioned at the suspension point and a weight bob used to obtain its vertical projection.<sup>2</sup> It is thus important to examine the effect of  $X_{SP}$  on the overall vertical centre of gravity position result. By expanding equation (4-4) and substituting in the obtained values, the following is derived:

$$Z_{CG} = 0.62 - 1.34X_{SP} \quad (4-5)$$

It is apparent from equation (4-5) that 1cm of error in the least reliably measured quantity, will produce 1.34 cm of error in the final result. In order to have confidence in the value of  $Z_{CG}$  one must have confidence in the value of  $X_{SP}$ . The greatest effort in ensuring accuracy in the measurement of  $X_{SP}$  must be expended.

#### *Aircraft moments of inertia estimation*

The methods for estimating the aircraft moments of inertia are based on suspending it and treating it as a pendulum system, to obtain the desired results as a function of the period of oscillation. The roll and pitch inertias ( $I_{xx}$ ,  $I_{yy}$ ), are obtained from the 'simple pendulum' approach that was used on the study of the VPM gyroplane; due to the configuration design of the Montgomerie gyroplane the 'bifilar' method used for the VPM could not be adopted for the yaw inertia.

With the 'simple pendulum' approach the aircraft is hung by a single suspension point and is swung freely about its roll and pitch axes respectively. The resulting motion is assumed to be a simple harmonic oscillation defined by the dynamics illustrated in Figure 4.7. Taking moments about the suspension point S, the following is obtained:

$$\begin{aligned} \sum M &= I\ddot{\theta}_p \Rightarrow \\ -W_{A/C}(l_s - Z_{CG})\sin\theta_p &= I\ddot{\theta}_p \end{aligned} \quad (4-6)$$

---

<sup>2</sup> A similar procedure was used for the measurement of  $l_s$ , the value of which has a less pronounced

where  $I$  is the roll or pitch moment of inertia, depending on the axis about which the oscillation occurs. By using the small angle approximation

$$\sin \theta_p \approx \theta_p$$

equation (4-6) reduces to:

$$\ddot{\theta}_p = -\frac{W_{A/C}(l_s - Z_{CG})}{I}\theta_p \quad (4-7)$$

which is the equation defining simple harmonic motion with a period of

$$T_p = \sqrt{\frac{4\pi^2 I}{(l_s - Z_{CG})W_{A/C}}}$$

Rearranging the above provides an expression for the roll or pitch inertia about the suspension point,

$$I = \frac{W_{A/C}(l_s - Z_{CG})T_p^2}{4\pi^2} \quad (4-8)$$

The parallel axis theorem must then be used to obtain the moment of inertia with respect to the corresponding body axis; the rotor blade assembly is once again treated as a point mass and its effect taken into account. The results obtained for the aircraft/pilot system defined in the previous section are presented in Table 4.6.

The yaw inertia was assumed to be of the same order of magnitude as the pitch one, an assumption yielded upon examination of the configuration data available for the VPM gyroplane (CAA [1994]), an aircraft with a similar mass distribution. Furthermore, parametric studies performed demonstrated that variation in the yaw inertia had negligible effect on the aircraft parameters of interest.

---

effect on the result for  $Z_{CG}$ .

#### 4.4 Montgomerie gyroplane simulation results

Once the appropriate configuration file (see Table 4.7), is generated for the RASCAL program, it is possible to predict the aircraft trim/steady flight and dynamic stability characteristics. The simulation results are affected by model weaknesses and the judgements made in this section will therefore be revisited upon presentation of the experimental data.

##### Trim/steady flight results

The aircraft is trimmed at speeds between 35 and 75 mph, at 5 mph increments. The following parameters are recorded for each speed: longitudinal rotor tilt  $\Theta_{1s}$ , lateral rotor tilt  $\Theta_{1c}$ , roll attitude  $\Phi$ , pitch attitude  $\Theta$  and rotorspeed  $\Omega$ , with the results illustrated in Figure 4.8.

The main rotor longitudinal tilt angle<sup>3</sup> and the pitch attitude variation with speed indicate positive stability at all speeds. An increasing forward application of the stick producing a nose down pitch attitude is required to trim the aircraft as the speed increases. Interpreting this quantitatively in terms of state perturbations and taking the aircraft pitching moment equation obtainable in most flight mechanics textbooks,

$$\dot{q} = M_u u + M_w w + M_q q + M_{\theta_{1s}} \theta_{1s} \quad (4-9)$$

For level flight and assuming that the perturbations  $w$  and  $q$  are zero, we have the following,

$$\begin{aligned} \dot{q} &= M_u u + M_{\theta_{1s}} \theta_{1s} \\ 0 &= M_u u + M_{\theta_{1s}} \theta_{1s} \\ \frac{M_u}{M_{\theta_{1s}}} &= -\frac{\theta_{1s}}{u} \end{aligned}$$

---

<sup>3</sup> A decreasing tilt angle indicates a push forward of the stick.

Since  $M_{\theta_{1s}} > 0$  by definition (a positive control deflection is that which causes a positive moment), and the ratio  $\frac{\theta_{1s}}{u}$  is negative,

$$M_u > 0$$

A positive value for  $M_u$  implies a tendency for the aircraft to pitch up if an increase in forward velocity occurs, thus slowing down and reducing the perturbation in  $u$ . In other words the positive value for  $M_u$  indicated from the stick/speed graph contributes to the aircraft stability.

Converting the gradient to units of stick travel per mph<sup>4</sup> and comparing it to the corresponding results from the VPM study (*Houston [2000]*), the Montgomerie gyroplane is predicted to possess a stick/speed slope of -0.26%/mph as opposed to -0.5%/mph (approximately) for the VPM aircraft, which is indicative of the Montgomerie gyroplane being less stable in this respect.

The variables defining the lateral response of the aircraft, i.e. lateral rotor tilt and roll attitude demonstrate limited sensitivity to speed variation with the aircraft flying virtually 'wings level' throughout the range. This is consistent with the observations made on the VPM aircraft (*Houston [1998b]*) and is indicative of the fact that due to the small mass distribution about the aircraft y-axis, airframe aerodynamics have a limited role to play in influencing the overall vehicle characteristics primarily determined by the main rotor aerodynamics. It is noticed though that the model correctly predicts that a small lateral rotor tilt shift to the right is required to offset the slight rolling tendency to the left as the vehicle picks up speed.

A further indication that the model is functioning correctly is provided by the increasing trend of rotor speed which is consistent with fundamental gyroplane theory developed by Glauert [*1926*], suggesting that the model can realistically emulate this

---

<sup>4</sup> The full range of stick travel corresponds to 18.4° of longitudinal tilt.

degree of freedom. More specifically Glauert deduces that the ratio of forward velocity to the tip speed is constant and given by,

$$\frac{U}{\Omega R} = \frac{1}{3} \left[ \sqrt{\theta_{bl}^2 + \frac{3}{2} C_{D0}} - \theta_{bl} \right]$$

where,

$U$  is the aircraft axial velocity

$\Omega R$  is the blade tip velocity

$\theta_{bl}$  is the blade pitch angle

$C_{D0}$  is the profile drag coefficient

An increase in forward speed will therefore produce a corresponding increase in rotor speed, as predicted by the model. Further verification of this will be provided upon examination of the relevant rotor speed stability derivatives.

### Dynamic stability results

The results regarding the dynamic stability properties of the aircraft are presented in the form of conventional stability derivatives, discussing the significance of the values of the most important ones.

The aircraft system is represented by the following state-space model and the derivative parameters calculated numerically by the RASCAL program, as described in Appendix 4.

$$\begin{bmatrix} \dot{u} \\ \dot{v} \\ \dot{w} \\ \dot{p} \\ \dot{q} \\ \dot{r} \\ \dot{\phi} \\ \dot{\theta} \\ \dot{\psi} \\ \dot{\Omega}' \end{bmatrix} = \begin{bmatrix} X_u & X_v & X_w & X_p & X_q & X_r & X_\phi & X_\theta & 0 & X_\Omega \\ Y_u & Y_v & Y_w & Y_p & Y_q & Y_r & Y_\phi & Y_\theta & 0 & Y_\Omega \\ Z_u & Z_v & Z_w & Z_p & Z_q & Z_r & Z_\phi & Z_\theta & 0 & Z_\Omega \\ L_u & L_v & L_w & L_p & L_q & L_r & L_\phi & L_\theta & 0 & L_\Omega \\ M_u & M_v & M_w & M_p & M_q & M_r & M_\phi & M_\theta & 0 & M_\Omega \\ N_u & N_v & N_w & N_p & N_q & N_r & N_\phi & N_\theta & 0 & N_\Omega \\ 0 & 0 & 0 & 1 & 0 & 0 & 0 & 0 & 0 & 0 \\ 0 & 0 & 0 & 0 & 1 & 0 & 0 & 0 & 0 & 0 \\ 0 & 0 & 0 & 0 & 0 & 1 & 0 & 0 & 0 & 0 \\ Q_u & Q_v & Q_w & Q_p & Q_q & Q_r & Q_\phi & Q_\theta & 0 & Q_\Omega \end{bmatrix} \begin{bmatrix} u \\ v \\ w \\ p \\ q \\ r \\ \phi \\ \theta \\ \psi \\ \Omega' \end{bmatrix} + \begin{bmatrix} X_{\theta_{ls}} & X_{\theta_{lc}} & X_{\theta_{rud}} \\ Y_{\theta_{ls}} & Y_{\theta_{lc}} & Y_{\theta_{rud}} \\ Z_{\theta_{ls}} & Z_{\theta_{lc}} & Z_{\theta_{rud}} \\ L_{\theta_{ls}} & L_{\theta_{lc}} & L_{\theta_{rud}} \\ M_{\theta_{ls}} & M_{\theta_{lc}} & M_{\theta_{rud}} \\ N_{\theta_{ls}} & N_{\theta_{lc}} & N_{\theta_{rud}} \\ 0 & 0 & 0 \\ 0 & 0 & 0 \\ 0 & 0 & 0 \\ Q_{\theta_{ls}} & Q_{\theta_{lc}} & Q_{\theta_{rud}} \end{bmatrix} \begin{bmatrix} \theta_{ls} \\ \theta_{lc} \\ \theta_{rud} \end{bmatrix}$$

Derivatives which are thought to primarily influence the dynamic characteristics are shown in Figure 4.9. With regard to the X-force derivatives the most notable feature is the value of  $X_u$ , which is significantly negative. Both *Padfield [1981]* and *Houston [2001]* have developed expressions for approximating helicopter and gyroplane phugoid modes respectively which indicate that a large negative  $X_u$  will noticeably increase the damping of this mode. This is in direct accordance with the model predictions for the VPM gyroplane, predictions which were proved inaccurate when the flight test data was analysed (*Houston [1998a]*, *Spathopoulos et al [1998a]*, *Houston [2000]*, for example), showing the aircraft phugoid to be lightly damped and a value for  $X_u$  close to zero and in some cases positive; flight test data will serve to investigate if this holds for the aircraft under study.

Of particular interest are the derivatives indicating the influence of the main rotor speed which are unique for gyroplane dynamics, where the freely rotating main rotor constitutes  $\Omega$  as an independent degree of freedom. For gyroplanes where the main rotor tilt is tilted aft, the negative sign  $X_\Omega$  is indicative of the fact that an increase in rotor speed will produce an increase in the rearward component of thrust.

The Y-force derivatives results suggest that the aircraft will exhibit stable lateral dynamic stability characteristics, a fact which will be further verified on examination of the corresponding moment derivatives. The derivative  $Y_v$  is negative indicating a tendency for the aircraft to reduce any perturbation in  $v$ . The linear nature

of its variation with speed reflects the sideforce on both the fuselage and the rotor. For the latter one in particular, an increase in the lift experienced by the advancing blade will manifest itself at approximately 90° around the azimuth resulting in a stable component of sideforce. The derivative  $Y_r$  is consistent with the mean velocity of the aircraft, to which its magnitude should be approximately equal to, as demonstrated by *Padfield [1996]*.

The Z-force velocity derivatives  $Z_u$  and  $Z_w$  (in particular) have been shown in the VPM study to be poorly predicted, especially at low speeds. It is therefore considered prudent to avoid drawing any specific conclusions from their values at this stage. The derivative  $Z_q$  which should be physically equal to the mean velocity, is consistently predicted. Finally, the negative value of  $Z_\Omega$  correctly indicates that an increase in rotorspeed will tend to produce an increase in the main rotor thrust.

The most significant of the rolling moment derivatives is  $L_p$ , which is determined primarily from rotor dynamics and greatly influences the aircraft short term lateral response with a substantial negative result indicative of a stabilising effect. This also applies to the dihedral effect  $L_r$ , which is also predicted as being stabilising. This derivative is influenced both by the sideforce exerted on the fuselage and the lateral tilt of the main rotor caused by perturbation in  $v$  (as explained for derivative  $Y_r$ ). For the aircraft under study a fuselage center of pressure *below* the cg will produce a destabilising component of rolling moment. The observed net stabilising result of the rotor/fuselage combination suggests that the greatest contribution is provided by the rotor dynamics.

Although the configurational aspects of the gyroplane with a large fuselage area forward from the cg and a largely ineffective tailplane are predicted to produce instability at high speeds, at the lower speed end the aircraft exhibits classical stable characteristics ( $M_u > 0$ ,  $M_w < 0$  and  $M_q < 0$ ). It should be noted however that the destabilising fuselage effect, particularly on  $M_w$  at high speeds could be exaggerated due to the approximate nature of the fuselage aerodynamics modeling.

The reasoning for  $M_w < 0$  at low speeds even without the significant contribution of a tailplane is related to gyroplane specific configuration characteristics. For the general helicopter case, the rotor, fuselage and tailplane all contribute to the value of  $M_w$  with the latter two having a destabilising and stabilising effect respectively. The contribution of the main rotor largely depends on the longitudinal position of the aircraft cg in relation to the main rotor thrust line, as demonstrated by *Padfield [1996]* with an aft center of mass resulting in a destabilising effect. With a light gyroplane configuration the small tailplane with a short moment arm will be largely ineffective compared to the much larger fuselage. On the other hand, the *vertical* position of the cg in relation to the propeller thrust line can be made such as to introduce a positive stability effect from the main rotor as illustrated in Figure 4.10. When the pusher-propeller is positioned below the cg in order to trim the aircraft it is necessary that the main rotor thrust line passes behind the centre of gravity position. The situation can then exist for an increase in  $w$ , where the reduction in the nose down moment caused by the rotor flapping back is overcome by the effect of the increase in thrust, resulting in  $M_w < 0$ . The implications of this on aircraft longitudinal stability will be examined in Chapter 6.

The derivative  $M_\Omega$  unique to gyroplanes, being negative will have a stabilising effect as an increase in rotorspeed will result in a nose down moment, reducing the axial velocity through the rotor, and thus the rotorspeed perturbation.

The weathercock stability derivative  $N_v$  and the yaw damping derivative  $N_r$  are both stabilising ( $N_v > 0$ ,  $N_r < 0$ ). For gyroplanes, which do not possess a tail rotor, *Houston [1998b]* has postulated that the damping effect of both these derivatives is enhanced by the energising effect of the propeller positioned close to the fin and endplates. The roll/yaw coupling derivative  $N_p$ , contrary to  $L_r$  is predicted to being negligible.

The set of rotor torque derivatives, which is unique for gyroplanes, are consistent with early gyroplane theory. More specifically, the positive values of both

$Q_u$  and  $Q_w$ , indicate that an increase in airspeed and in axial velocity will tend to increase the rotorspeed, which is predicted by Glauert's seminal work. The negative value of the primary damping derivative  $Q_\Omega$  suggests that the rotorspeed mode will be damped, although it will be demonstrated that it is highly influenced by the longitudinal body degrees of freedom.

Finally, some general comments can be made for the results regarding the control derivatives. The sign of each parameter is consistent with its physical significance, for example  $M_{\delta_r} > 0$ , indicates that pulling the stick back will result in a nose up moment. Also, as expected, the aircraft response becomes increasingly sensitive to control application with airspeed.

Summarising the results in their stability derivative format, they are indicative of an aircraft with stable characteristics especially at low speeds. The absence of a tail rotor suggests that the lateral dynamics are dominated by main rotor (in particular) and configurational characteristics which are predicted to have an overall stabilising effect. Importantly with regard to the model validation aim of the thesis, the results provide a first indication that the simulation is capable of correctly predicting the characteristics of a rotorcraft in autorotation. More specifically it was seen that derivatives which are physically dominated by kinematic terms ( $Z_q$  and  $Y_r$ ), are correctly predicted. Furthermore the signs of the related derivatives are consistent with early gyroplane theory ( $Q_u > 0$  and  $Q_w > 0$ , for example), and with their physical significance ( $M_{\delta_r} > 0$ , for example).

#### **4.5 Chapter summary**

A set of baseline simulation results for the Montgomerie-Parsons research gyroplane has been produced and analysed in this chapter. The predicted trends both for the trimmed/steady flight characteristics and to those relating to the stability derivatives, are in general consistent with the ones obtained from a study conducted on an aircraft of similar type.

Furthermore the initial simulation results are consistent with early gyroplane theory and their physical significance in general, thus indicating that the model is capable of qualitatively predicting the dynamics of a vehicle in autorotation.

In the following chapter results obtained from the baseline simulations together with a set of aircraft dynamic responses will be compared to those yielded from flight test, thus fulfilling the model validation aim of the thesis.

# Chapter 5

## Validation of the RASCAL Model Using Data from Flight Tests

### 5.1 Introduction

This chapter deals with the major aim of the research activity, i.e. the validation of the RASCAL mathematical model in the autorotative flight state. This is performed by comparing the model simulation predictions for the Montgomerie-Parsons gyroplane presented in Chapter 4, complemented by a set of time responses, to the experimental data acquired from the flight testing. In order to have confidence in the flight test results, data obtained from the shakedown tests is used to verify the correct functionality of the instrumentation system. This is followed by a comparison of steady state data obtained from trimming the aircraft both in its simulated form and in real flight over its entire speed range.

For the dynamic response analysis the model is excited using the pilot generated control inputs and the resulting responses compared to those measured in flight. Furthermore, a system identification technique is employed in order to extract the derivatives and compare them to those produced by the linearisation of the mathematical model, highlighting the effect of using *doublet* type inputs on the result accuracy.

For both the steady state and unsteady cases, results are compared with those obtained from the VPM gyroplane study therefore assessing the general applicability of the model for simulating autorotative flight.

## **5.2 Verification of instrumentation functionality**

The functionality of the instrumentation system is verified in the following way. Initially the data recorded from all sensors throughout a steady climb is presented both in its raw and filtered form thus demonstrating the general overall correct system functionality. This is followed by data from manoeuvres that specifically influence variables related to the longitudinal or the lateral motion of the aircraft, thus making it possible to perform a more detailed examination of certain important aircraft parameters (such as rotor speed, vertical acceleration, etc. in the longitudinal axis and yaw rate, roll rate, etc., in the lateral axis).

### **i) Steady climb**

The raw (unfiltered) data obtained from all aircraft sensors during a steady climb to approximately 200 ft is presented in Figure 5.1. Although the quality of the data is clearly adequate for the purposes of this investigation, digital filtering is applied to enhance the clarity of the presentation.

In order to alleviate the effect of noise on the acquired data, a 4th order Butterworth filter with a cut-off frequency of 3 Hz was applied in the manner described in the previous chapter. The effect of this on the frequency response of the vertical acceleration signal is illustrated in Figure 5.2. As expected any unwanted high frequency components are filtered out from the response. The resulting filtered signals are presented in Figure 5.3, which provides a clearer indication of the variable trends.

On examination of the plots, the following can be deduced:

- **Height:** The height is zero referenced at start-up and increases to approximately 200ft, in exactly the manner in which the manoeuvre was defined. The *rate of climb* for this particular one, can be calculated from the plot as being, 534 ft/min. This value is consistent with the aircraft performance specification which was presented in Table 3.1.

- Rotor speed: The average value of the rotor speed is 370 rpm which is of the correct order for this type of aircraft. The fluctuations at the start and end of the climb come as a natural effect from the change of velocity and rotor inflow angle at these points.
- Propeller speed: Propeller speed is at a steady high power setting in order to provide the necessary power for the climb and decreases sharply (as expected) at the end point of the climb.
- Longitudinal rotor tilt: The rotor tilt (in the forward and aft direction), is fixed at roughly  $9^\circ$  throughout the climb, representing a longitudinal stick position of approximately 50%. A small push forward is performed when the aircraft reaches the level flight condition.
- Lateral rotor tilt: The lateral rotor tilt has a mean value of  $1.5^\circ$  indicating a lateral stick position slightly to the right of centre.
- Rudder tilt: Roughly  $17^\circ$  of rudder tilt to the left is required throughout the climb.
- Velocity: The velocity of the aircraft fluctuates around the 23 m/s point throughout the climb. This is consistent with the speed of 50 mph at which the pilot was instructed to perform the manoeuvre. A small increase in velocity is observed when the aircraft reaches the level flight condition.
- Angle of attack: The angle of attack has a mean value of approximately  $2^\circ$  throughout the climb.
- Angle of sideslip: The angle of sideslip varies between  $5^\circ$  and  $15^\circ$  throughout the climb.
- Roll attitude: The roll attitude has a mean value of approximately  $0^\circ$  (level wings flight), throughout the climb.

- Pitch attitude: The pitch attitude has a mean value of  $5^{\circ}$  throughout the climb and decreases sharply as the pilot pushes the nose down at the end of the climb.
- Yaw attitude: The yaw attitude is referenced to start-up and changes by less than  $10^{\circ}$  throughout the climb.
- Roll, pitch and yaw rates: All the angular rates fluctuate around the zero point during the climb.
- Longitudinal acceleration: The longitudinal acceleration starts off at a negative value which is consistent with the nose-up attitude of the aircraft which results in a component of weight being projected on the negative x-axis direction. The offset magnitude of 0.1 g is also consistent with the theoretical value for a  $5^{\circ}$  nose up attitude of

$$1 \cdot \sin \theta = 1 \cdot \sin 5 \approx 0.09$$

- Lateral acceleration: The lateral acceleration fluctuates around the zero point throughout the climb. For reasons similar to those explained for the longitudinal case, lateral acceleration acquires a more positive value as the aircraft rolls to the right during the later stages of the climb.
- Vertical acceleration: Sharp changes occur at the start and the end point of the climb; over the duration of the steady part of the manoeuvre it fluctuates round the 1 g point as expected.

The following general conclusions can be made from the above observations: The quality of the data resulting from all sensors is more than adequate for the purposes of the experiment; digital filtering can be successfully applied to rid of high frequency noise components to further enhance the clarity of the data plots; the time histories recorded by each sensor are consistent with the manoeuvre design and with each other.

In the following sections an additional two manoeuvres will be used to further confirm the above. It should be noted that for presentation purposes the signals from all transducers have been filtered in the manner described previously.

ii) Simulated engine failure

For this particular test, the pilot was instructed to simulate an engine failure by rapidly reducing the propeller (engine) rpm. This is clearly evident in Figure 5.4 where the rpm is seen to be reduced from approximately 2100 to 850 rpm over a time length of approximately 12 s. The natural resulting loss of height is also confirmed, with the aircraft descending at an approximate rate of 913 ft/min. Furthermore, the sudden loss of aircraft power is demonstrated by the sharp drop in the vertical acceleration occurring at the start of the descent, as illustrated in Figure 5.4.

Finally, the most interesting of the parameters affected by this manoeuvre is the main rotor speed. An examination of the physical principles governing this parameter has been presented in Chapter 1 and the rotorspeed variation illustrated in Figure 5.4 is consistent with Glauert's basic inflow theory. The rotor speed is gradually picked up (between the 5 and 15 second time points) as the aircraft descends and the air inflow through the rotor increases, providing a total increase of approximately 20 rpm.

iii) Yaw turns

A series of rapid yaw turns was performed by the pilot in order to test the functionality of the sensors recording the variables defining the lateral motion of the aircraft. Both the yaw pedals and the lateral stick position, with the former clearly the dominating input, were applied in order to impose this, as illustrated in Figure 5.5. The manoeuvre is initiated and concluded with a set of distinguishable yaw pedal pulses with an approximately sinusoidal motion of 0.22 Hz excited in between. The aircraft follows a combined rolling and yawing motion as demonstrated by the corresponding angular rate plots in Figure 5.5. Finally by closely examining the first of the yaw pulses, it is possible to estimate the steady rate of yaw turn at

approximately 20 deg/s which is consistent with the gradient of the yaw attitude plot, as illustrated in Figure 5.6.

As a resume of the above it can be deduced that the instrumentation sensor outputs presented from shakedown manoeuvres during the first phase of the testing such as a steady climb, a simulated engine failure and a series of yaw turns, indicate with confidence that the DAQ system is functioning according to its specification, yielding data of a quality unique for the flight testing of a light gyroplane aircraft. It is therefore possible to use this facility for the model validation purposes of this thesis.

### **5.3 Steady state results**

Results from the steady state flights performed in the first phase of the flight testing are compared to those obtained from the model configured in its baseline form, in Figures 5.7-5.11. The following observations are made for each of the individual parameters:

#### **i) Longitudinal rotor tilt:**

The trend for the longitudinal rotor tilt is modelled accurately indicating that RASCAL is capable of giving a good prediction of speed stability. The prediction does suffer from a uniform error of less than 2° corresponding approximately to 10% of stick deflection across the speed range. The uniformity of the discrepancy suggests the possibility of calibration or measurement errors. This postulate will be discussed in subsequent sections.

#### **ii) Pitch attitude:**

Simulation of pitch attitude is in excellent agreement with the flight measurements throughout the speed range. The trend is consistently predicted and the model values differ by less than 1° from the experimental equivalents.

#### **iii) Lateral rotor tilt:**

Lateral rotor tilt comparisons depict the same form as the longitudinal ones; the variation with speed is predicted consistently although a uniform error of less than 2° (10% lateral stick deflection) exists throughout the speed range. Since calibration of

the lateral rotor tilt sensor was one of the hardest to perform it is again postulated that calibration errors contribute the most to the uniform mismatch.

iv) Roll attitude:

Roll attitude is modelled very accurately for speeds up to 60 mph. At high speeds the model predicts an almost level wings flight condition whereas the flight test results indicate a right wheel down inclination. Even so, the maximum discrepancy between the two does not exceed  $2.5^\circ$ .

v) Rotor speed:

Rotor speed trend with aircraft speed is simulated correctly, although a uniform error of approximately 40 rpm is present throughout the envelope.

#### Discussion of steady state results

Generally it is observed that in all cases (apart to a small extent for roll attitude), the trends of the examined parameters with speed are simulated with great accuracy. For example stick/speed slope is an important measure for analysing stability. Here it is measured at  $-0.24 \text{ %/mph}$  from the flight test data and at  $-0.26 \text{ %/mph}$  from the model predictions. Similarly, the main rotor speed variation with aircraft velocity is measured at  $0.50 \text{ rpm/mph}$  in flight and  $0.47 \text{ rpm/mph}$  from the model output. Furthermore for all parameters examined the model predictions are made to within approximately 10% of the parameter range. The deficiencies in the validity can be summarised as a uniform mismatch of longitudinal and lateral rotor tilt and rotor speed throughout the speed range and roll attitude at high speeds.

In order to assess the capability of RASCAL in simulating steady state autorotation, it is necessary to examine the results obtained from its only previous use for modelling this flight state. The model/flight relationships obtained from the study on the VPM gyroplane are illustrated in Figure 5.12 and are extracted from *Houston [2000]*. It is observed that a consistent pattern exists between the results obtained for both aircraft cases. Importantly the trends for all variables are modelled accurately firmly establishing the RASCAL model as a reliable tool for predicting important parameters such as stick/speed stability and rotor speed sensitivity to speed. The rotor

tilt positions, in this case defined as stick deflections, are estimated with a slightly greater accuracy for the VPM case, although calibration errors will be shown to influence both sets of results. Roll attitude is predicted with much the same accuracy for both aircraft although for the VPM case it is the low speed range that suffers the most.

The trimmed flight state examined here for the gyroplane case, can be viewed as the equivalent of a steady state autorotation descent for helicopter flight. It was shown in Chapter 1 that for the majority of helicopter autorotations resulting from a power failure (with the exception of those occurring close to the ground), a steady rotor speed is established, resulting in steady rates of descent during which the pilot control inputs and aircraft attitudes are practically maintained constant. It is therefore reasonable to assume that the accuracy with which those variables are predicted in trimmed gyroplane flight will be the same as that achieved for helicopter steady state autorotation. Accurate knowledge of pilot controls and aircraft pitch attitude required for different speeds for example (seen to be predicted from reasonably to very favourably by the model), can assist in assessing the capability of the pilot to perform a safe landing. Furthermore, possessing the ability to accurately predict aircraft stick/speed stability and main rotor speed sensitivity with speed, both of which are seen to be modelled accurately by RASCAL, provides an obvious insight to the handling qualities of the aircraft during an autorotation. This in turn can provide a means of assessing the degree of difficulty for realising a particular autorotation descent.

The inability of the model to accurately predict rotor speed on the other hand, will limit the effectiveness of RASCAL in simulating autorotation. It was observed in Chapter 1 that the value of rotor speed is one of the key parameters in determining the viability of an autorotation manoeuvre. An overprediction of 40 rpm apparent from the simulation result comparison to the flight data, could for example result in assuming that an autorotation is possible, when in fact the rotor speed will have dropped below its minimum permissible value. Confirmation of this inherent modelling weakness from the investigation of a second test case now provides the impetus for an in-depth study to be performed in order to pin-point the exact sources of the discrepancy.

It is prudent however at this stage to discuss the possible sources of the observed discrepancies between model and flight which are thought to be a combination of measurement (calibration) errors and model inadequacies. The former is postulated as being the main contributor in the case of the rotor tilt position discrepancies primarily due to the difficulties arising from the calibration procedure which introduced an uncertainty in the results. There are several arguments for supporting this: First of all the model was seen to predict both parameters with greater accuracy for the VPM case, thus suggesting that measurement rather than modelling errors are resulting in the mismatch. Secondly, the uniformity of the discrepancy throughout the speed range is typical of a constant, calibration type error. Finally, the flight data depicts that a small positive (right wheel down) roll attitude induces a slightly positive (stick right), lateral rotor tilt. This finding is contrary to the results obtained from a simple trim analysis which indicate that to offset a deviation in roll, a rotor tilt in the *opposite* direction is required.

Calibration of the position sensors by use of a conventional inclinometer proved to be a particular cumbersome task. Although it is difficult to quantify the total uncertainty introduced, which will be a combination of measurement error, transducer error, and the error produced by fitting the surface described in Chapter 3 to the calibration data, 1° of calibration uncertainty will result in 5% of stick position error. It is reasonable to assume therefore, that the 10% discrepancy observed in Figure 5.7 and 5.9, is largely attributed to calibration errors.

Pitch attitude is seen to be modelled favourably for the aircraft under study with the low speed discrepancy observed for the VPM case (see Figure 5.12) having ceased to exist. The explanation provided for this is the following: At low airspeeds where the airframe areas and aerodynamic surfaces are ineffective the aircraft pitch attitude is primarily determined by the aerodynamic properties of the main rotor. As discussed in Chapter 4, airfoil aerodynamic data was obtained for the Montgomerie gyroplane whereas for the VPM case a CFD analysis was necessary to *estimate* main rotor aerodynamic characteristics. It is therefore reasonable to expect that the model will perform better at low speeds for the aircraft under study.

On the other hand, the small discrepancy observed in the high speed region for the roll case is postulated as being a result of poor modelling of airframe lateral aerodynamics. Contrary to the study on the VPM gyroplane where a complete set of wind tunnel test data base existed, simple polynomial approximations were used in this study to represent the aerodynamic forces. The diverging nature of the mismatch at higher speeds does point to a physical modelling inadequacy which in the author's view would improve if a wind tunnel data set was made available.

The inaccuracy in the rotor speed prediction observed in the VPM study repeats itself for the Montgomerie simulation case. This suggests that a modelling weakness is responsible for the error in the simulation. Rotor speed was found (*Houston [2000]*) as being very sensitive to the structural and aerodynamic characteristics of the blade, such as structural blade twisting and blade section lift and drag. The blade twisting for example which due to aeroelastic effects will appear in flight, is not modelled by the rigid-blade representation adopted by RASCAL. Furthermore, it was discussed in Chapter 4 that a simple 2-D model structure was used to represent main rotor aerodynamics. *Padfield [1996]* advocates that particularly close to the tips 3-D effects due to the interaction of the upper and lower surface flows, will result in significant changes in the chordwise lift distribution. He goes on to report that "accurate modelling of the tip aerodynamics is still the subject of intense research and renewed impetus with the advent of novel tip sections and platforms". The sensitivity of rotor speed to blade properties, suggests that unmodeled 3-D tip effects not captured by the 2-D representation could be affecting the rotor speed prediction.

Finally, it was discussed in Chapter 1 that the dynamics of the teetering rotor were approximated by those of an articulated one with a zero hinge offset. The coning motion resulting from this type of representation will not occur in reality for blades which are cantilevered to the hub. This discrepancy will influence the prediction of the total inflow through the rotor which in turn will affect the value of the rotor speed, accounting at least partially for the observed discrepancy.

## **5.4 Dynamic response results**

The ability of the model to simulate the dynamic response of the aircraft was assessed both by means of time responses and stability derivatives. For the former case, pilot control perturbations measured in flight were superimposed to the model trim values and then used to drive the simulation, whereas for the latter, derivatives extracted from a system identification technique were compared to those yielded from linearising the model at the same speed.

### **5.4.1 Time responses**

The model and flight test results obtained from a longitudinal tilt doublet input at a nominal speed of 60 mph are presented in Figure 5.13. The pitch rate (prime response), roll rate (off-axis response) and rotor speed time histories are plotted for a 35 sec period. Note that the simulation displays the high frequency periodicity inherent to individual blade modelling (see *Houston [1994]*), and that for the first few seconds of the simulation the model controls are frozen at their trim values in order for the necessary trim calculations to be performed.

Several points of interest are observed on examination of the prime (pitch rate) time history. The forced (short term) response is modelled particularly well. Both the amplitude and frequency of what appears to be a neutrally stable, steady state oscillation, are also predicted favourably. A phase shift between model and flight is seen to exist, with the model leading by approximately 2 sec. Although it is difficult to speculate on the actual source of this mismatch, it is postulated that unmodelled unsteady aerodynamic effects may have a role to play.

The off-axis response, notoriously difficult to model for rotorcraft, is surprisingly (with the exception of the short term response) well modelled. Simulation runs were used to check whether the short term inconsistency was due to a discrepancy related to the modelling of the roll rate response to lateral stick<sup>1</sup> or whether it is related to cross coupling effects. This was done by freezing the lateral tilt

---

<sup>1</sup> A small lateral stick input was applied by the pilot at the same time as the prime longitudinal control.

to its trim value throughout the time response. The characteristics of the simulation did not alter significantly, demonstrating that the deficiency is due to poor modelling of cross coupling.

The rotor speed short term response is modelled correctly although the prediction for the amplitude of the (correctly predicted in frequency) long term oscillation is poor, particularly at the time period between 15 and 30 sec. The rotor speed deviations from trim from the model, were superimposed to the flight test trim value. The phase shift seen to exist between model and flight is consistent with that observed for the pitch rate response.

The corresponding time responses for the 40 mph speed are presented in Figure 5.14. For the pitch rate the model correctly predicts that the long term response is much more subdued than for the 60 mph case, although the attenuation in the amplitude is slightly overpredicted. Once again the forced response is seen to be modelled favourably. The roll rate and rotor speed model discrepancies are consistent to those observed for the 60 mph case.

The response to the lateral rotor tilt at 60 mph is illustrated in Figure 5.15<sup>2</sup>. The prime (roll rate) forced response is well predicted, similarly to the longitudinal case. A lightly damped Dutch roll mode which is not apparent in real flight manifests itself during the first 10 sec after the application of the input. The linearisation of the model performed in the next chapter is consistent with the non-linear model results, although the flight data shows that the mode does not exist. Once again a steady state oscillatory motion is established which is well predicted in amplitude and frequency but with a 1-2 sec phase shift. The off-axis (pitch rate) response is once again surprisingly well predicted although an inconsistency still exists in phase.

Finally, the lateral tilt responses at 40 mph are displayed in Figure 5.16. The Dutch roll mode (although damping out within one cycle) is incorrectly predicted. The short term off-axis response is again well-predicted although the damping of the long term response is exaggerated.

---

<sup>2</sup> The lateral tilt inputs did not induce a significant rotor speed response.

The following general points can be made from the time response model and flight comparison: The prime forced response is modelled favourably as is the rotor speed (for the longitudinal tilt case). This implies that for helicopter autorotation the important initial reaction of the aircraft to a pilot input can be predicted with confidence. The off-axis response is modelled surprisingly well (with the exception of short term roll rate response to longitudinal tilt). This is uncharacteristic of rotorcraft simulations in general providing further indication that gyroplanes possess several attributes quite different to those of the conventional helicopter. Furthermore it is indicative of the fact that the RASCAL model is of a sophisticated type capable of emulating this type of response. A neutrally stable oscillation exhibited by all states under examination, is in general predicted well both in amplitude and in frequency, although a mismatch does exist in phase. As the important phase of helicopter transition to autorotation normally only last for a short time period, it is dominated by the (well predicted) short term response of the aircraft. The inconsistency observed in phase will therefore have little effect on the ability of RASCAL to simulate this type of flight state.

The deficiencies in the modelling can be summarised as a phase shift observed particularly for the long term response, the short term response of the off-axis roll rate, the prediction of the Dutch roll mode, and an overprediction of the damping of the oscillatory motion at lower speeds.

The phase lag between flight and model observed for most cases, points to a weakness in the modelling of the unsteady aerodynamic effects. It was discussed in Chapter 3 that the dynamic inflow model incorporated will account partially for aerodynamic lags, but it should be noted that this is its first use for simulating autorotative flight. The effect of the Peters HaQuang [1988] inflow model, particularly with regards to the prediction of the  $X_u$  derivative, will be discussed later in the analysis.

For the discrepancy in the off-axis roll rate, it was discussed earlier that simulation runs were used to verify that this is due to cross coupling modelling deficiencies, an aspect particularly common with rotorcraft flight dynamics models. The discrepancy in the Dutch roll mode on the other hand is consistent to that

observed for the VPM aircraft (see *Houston [1998b]*), and confirms that a modelling weakness exists in this aspect of the lateral dynamics.

Finally, although it is difficult to speculate on the exact source of the overprediction of the long term response damping at low speeds, it is postulated that it is related to the modelling of the main rotor. There are two reasons for supporting this, firstly at low speeds the aircraft dynamics will be dominated by the aerodynamics of the rotor, as the airframe forces and moments are relatively ineffective. Furthermore, it will be demonstrated in the following chapter that the aircraft configurational characteristics even at higher speeds have a limited role to play in the determination of the vehicle dynamic stability.

#### **5.4.2 System identification**

The time responses produced from doublet inputs were used to extract the aircraft stability and control derivatives. It is of interest to establish whether this type of manoeuvre can be used in order to obtain reliable results for gyroplane system identification, as the research performed on the VPM aircraft (*CAA [1994]*) has suggested. *Schrage [1991]*, provides a most general definition for system identification as it being "the deduction of system characteristics from measured data". It is commonly referred to as an inverse problem (*Black [1988]* for example), in the sense that instead of computing the response of a system with known characteristics, the reverse is performed, i.e. obtaining the characteristics of the system from the measured responses. In the context of aircraft and rotorcraft in particular the benefits of this are presented by several authors (*Hamel [1991]*, *McKay [1999]*, for example) and mainly relate to the validation and improvement of flight mechanics mathematical models.

A significant amount of literature exists that provides a wealth of information on system identification methodologies. *Klein [1989]* for example provides an in-depth study on the techniques developed and are applied to aircraft in general. In the reference *RTO [1999]* the state of the art developments of those techniques are presented together with their application to modern vehicles. System identification of rotorcraft, due to their aeromechanical complexity and the high level of vibration

noise encounters specific difficulties, as demonstrated in *AGARD [1991]*, *Padfield [1986]*, *Black [1988]*, *Tischler et al [1986]*, for example.

An *equation error* system identification approach in the frequency domain was implemented in the *Matlab [1996]* software environment. This type of method has been extensively used by *Black & Murray-Smith [1989]*, applied to the Puma helicopter and more significantly by *Houston & Thomson (CAA [1994])*, applied to the VPM light gyroplane. The technique essentially reduces the system identification process to a regression problem implemented in the frequency domain by obtaining the Fourier transforms from the appropriate aircraft time responses. A detailed description of the theoretical development of the technique is presented in Appendix 5.

Presentation of the results derived from the system identification software developed by the author, refer to a nominal speed of 60mph, and are presented in Tables 5.1-5.6. The results relate to derivatives for which a modelling/flight test mismatch was observed from the previous validation exercise performed on the VPM aircraft. As stated earlier, these include the values of  $X_u$ ,  $Z_w$  both of which were overpredicted in magnitude, and to a lesser extent  $N_r$  which was underpredicted.

In Table 5.1 results from applying the system identification technique to the X-force equation are presented for two concatenated doublet/phugoid cases. With this type of analysis, the time histories produced from both a doublet and a phugoid inducing input are merged as described by *Houston [2000]* in order to provide a large data record.

Frequency ranges of 0.25 Hz and 0.5 Hz were used for extracting the results. Examination both of the time histories and the signal spectral analysis (performed in the next chapter), indicate that useful rigid body mode information will be contained in frequencies of this order of magnitude. Use of larger ranges containing unmodelled vibration, noise and rotor blade dynamics would distort the quality of the estimates. A

choice of two different frequency ranges offers an assessment of the robustness of the data.

There are four primary factors that indicate one can not entrust too much confidence on the accuracy of the results. The  $R^2$  (multiple correlation coefficient) factors, a measure of goodness of fit are relatively low, with values ranging between 0.31 and 0.67. The F numbers ( $F_{tot}$ ) and partial F numbers ( $F_{par}$ ), an indication of the estimate confidence levels, are low for all cases. The value of  $X_\theta$  which is purposely left in the estimation as an indicator of result validity which physically ought to be equal to -9.81, is out by a factor of 2 (at best). Finally, results for most derivatives appear to vary significantly for the two cases. It is important to note however that from standard parameter estimation experience, force derivatives have always been harder to estimate than the corresponding moment ones. Gyroplane X-force derivative estimates possess particularly low confidence bounds as shown by *Houston [1998a]* for the VPM case.

The  $X_u$  derivative for all four cases importantly acquires a small *positive* value, as opposed to the large *negative* one (-0.23 /s) predicted by the model. This is consistent with the mismatch observed for the VPM aircraft as is portrayed in Table 5.2.

Similar observations are made for the Z-force derivative estimates and although the  $R^2$  and partial F number values are relatively higher than for the X-force case, the value of  $Z_q$  which physically ought to be approximately equal to the aircraft mean velocity, suggests that the estimates should be treated with caution. The derivative  $Z_w$  in fact displays the highest consistency for all cases. As with  $X_u$  the model/flight test mismatch is similar (although more pronounced) to that of the VPM aircraft. In particular, the model significantly overpredicts the value in the manner presented in Table 5.4.

The equation displaying the greatest confidence levels is the yawing moment one. Time responses were obtained by application of a rudder doublet input. A revised

reduced order model, containing only the  $N_v$ ,  $N_r$ ,  $N_{\theta_{rud}}$  as described by *Houston [1998b]* is deployed for this case. Both  $R^2$  and the partial F number values for the second case in particular, indicate that the results provide a good estimate for the actual values. The derivative  $N_r$ , which is of the greatest interest displays some variation between the two runs. Taking the second case as being the most reliable, it is observed from Table 5.6 that the derivative although still underpredicted is better correlated to the flight test results.

The most important observation made from the system identification results relates to the apparent inability of doublet input types to produce accurate and reliable estimates. There are two reasons for this. First of all it has been stated by several authors (*Murray-Smith [1991]*, for example), that in the case of the helicopter doublet type inputs are of limited value for identification, primarily owing to the highly coupled form of the model structure. The work of *Houston & Thomson [1999]* had indicated that for gyroplanes possessing more 'classic' dynamic characteristics doublet application could be more effective. In fact, although the standard statistical error associated with estimates for the derivatives from the doublet method were generally larger than those incurred with the frequency sweeps<sup>3</sup>, the results were seen to serve as reliable first approximations. The simulation and flight data for the Montgomerie-Parsons aircraft has shown that a greater degree of coupling exists making it respond more like a conventional helicopter in this respect, and so the estimates obtained must be treated with caution.

Furthermore, according to the pilot's own notes (see Appendix 6), with the type of doublet applied he was unable to invoke any short period response which could have provided with the data necessary for obtaining better parameter estimates. In the test pilot's own words, "the autogyro response appeared dead-beat making the doublet frequency one that did not excite/was harmonious to the autogyro's natural frequency". So both the frequency content of the applied inputs and the highly

---

<sup>3</sup> With this type of input a broad range of frequencies is applied to the control input thus exciting a broader bandwidth of the vehicle modes.

coupled nature of the aircraft dynamics are responsible for the relative ineffectiveness of the system identification method.

In any case, the estimates seem to *indicate* that a pattern of mismatches exists between model and flight test as established from the study on the VPM aircraft. It is argued that the discrepancies in  $X_u$  and  $Z_w$  can be attributed to the modelling of the induced velocity in autorotation. Padfield [1996] discusses the effect of inflow velocities on the aircraft force derivatives. He argues that since the main rotor dominates dynamics of rotorcraft, main rotor derivatives also play the greatest role in determining the corresponding stability derivatives.

For the  $X_u$  derivative for example, this can be demonstrated by considering an approximation to the rotor X-force,

$$X_{rotor} = T\beta_{1c}$$

where,  $\beta_{1c}$  is the multi-blade coordinate longitudinal flapping angle. The X rotor force derivative  $X_{rotor}$  with respect to forward velocity is given by,

$$\frac{\partial X_{rotor}}{\partial u} = \frac{\partial T}{\partial u} \beta_{1c} + T \frac{\partial \beta_{1c}}{\partial u}$$

The thrust derivative,

$$\frac{\partial T}{\partial u}$$

is a function of the changes in inflow velocities during perturbed motion, and is given by,

$$\frac{\partial T}{\partial u} = \left( \frac{\partial T}{\partial u} \right)_{v_i = \text{const.}} + \frac{\partial T}{\partial v_0} \frac{\partial v_0}{\partial u} + \frac{\partial T}{\partial v_{1s}} \frac{\partial v_{1s}}{\partial u} + \frac{\partial T}{\partial v_{1c}} \frac{\partial v_{1c}}{\partial u}$$

As the values of  $v_0$ ,  $v_{1s}$ , and  $v_{1c}$  are all derived from the dynamic inflow model, as shown in Chapter 1, there is an obvious direct connection between the inflow model and the value of the  $X_{rotor}$  derivative with respect to forward velocity which in turn will dominate the value of  $X_u$ . A corresponding analysis can be performed regarding the  $Z_w$  derivative (see *Padfield [1996]*), which demonstrates a similar dependence on the inflow modelling method.

The initial dynamic stability results from the Montgomerie-Parsons flight testing together with those obtained from the VPM study (*CAA [1994]*), suggest that the dynamic inflow model employed does not properly capture the dynamic response of the rotor to perturbations in velocity. Translating this in terms of the ability of the model to simulate the aircraft time responses, an overpredicted value of  $X_u$  in particular will have the effect of grossly overestimating the phugoid damping, thus suppressing this mode of motion. In other words, for an aircraft with a long term response dominated by a phugoid mode (such as the VPM aircraft), a lightly damped motion will appear as a heavily damped mode. Although this in itself does constitute an inherent modelling weakness, as discussed earlier in the chapter, it is the short term response normally not correlated to the phugoid motion, which is important in terms of autorotation simulation.

## **5.5 Chapter summary**

A comparison of simulation predictions and flight test results has been presented, fulfilling the model validation purposes of the research activity. For the steady state case the trends of all examined variables were seen to be accurately estimated. Uniform across the speed range discrepancies for the control angles can arguably be attributed to uncertainties resulting from the calibration process whereas

the mismatch in rotor speed was seen to emulate that incurred in the study performed on the VPM aircraft.

Comparison of model and flight time responses has indicated that RASCAL is in general capable of realistically emulating rotorcraft dynamic response in autorotation. Discrepancies observed are primarily attributed to unmodelled unsteady aerodynamic and cross-coupling effects.

Dynamic stability results produced from a system identification technique have indicated that doublet input types are of limited use for producing *accurate* estimates of the derivatives. In any case, the initial results *indicate* that the pattern established from the previous validation exercise also repeats itself for the dynamic response data. Importantly the values of the  $X_u$  and  $Z_w$  derivatives significantly influencing the phugoid behaviour in particular, are seen to be overpredicted as for the VPM gyroplane case.

In the next chapter, the flight test results complemented by a set of parametric simulation studies, will be used to assess the flight dynamics attributes of the gyroplane aircraft.

# Chapter 6

## Flight Test Results Regarding the Montgomerie-Parsons Gyroplane Steady State and Dynamic Response Characteristics

### 6.1 Introduction

In the final main chapter of the thesis a closer and more extensive examination of the flight test results is presented interpreting them in terms of the flight dynamics characteristics of light gyroplanes. The flight test programme was conducted at two locations, with the shakedown and steady state flying being performed at Carlisle airfield and the dynamic response manoeuvres requiring supervision from an authorised body, being conducted at FR Aviation, Bournemouth airport. Test flights were performed only on days where appropriate weather conditions prevailed, i.e. ones that were dry and with low winds. The aircraft ready for take off at the start of one such test at Carlisle and Bournemouth respectively is illustrated in Figures 6.1-6.2.<sup>1</sup> The procedures followed prior to, during and after each test flight were those described in Chapter 3, with most flights having a duration of 30-60 minutes.

Initially, a presentation is made of the steady state results obtained from trimming the aircraft over its speed range, yielding an assessment of parameters such as longitudinal static stability, rotor induced vibration, etc. This is followed by an illustration of the aircraft response to doublet and step inputs which serves to provide insight into its dynamic stability attributes. Results are presented both in the form of time responses and coherence plots demonstrating the dependence of each output on the applied inputs.

---

<sup>1</sup> An identical set of blades (although of different colour) was used in both cases.

Both the steady state and dynamic response results are complemented by a set of simulation runs assessing the effect of varying aircraft configuration parameters on the vehicle static and dynamic stability.

## **6.2 Steady state results**

Steady state results were produced by trimming the aircraft at speed increments of 5mph, from 30 to 70 mph, over a total flight time of 30 mins. In general the pilot managed to maintain a steady state condition at each test point, although achieving this was shown to be more demanding at the high speed end of the envelope. This is clearly apparent in Figure 6.3 when comparing the 45 mph (20 m/s) case, where constant airspeed is maintained for approximately 50 s, to the 70 mph (31 m/s) one at which maintaining the speed constant is clearly a harder task. The data recorded for parameters of interest such as longitudinal rotor tilt, pitch attitude, lateral rotor tilt, rotor speed and propeller speed, is presented in Figures 6.4-6.6.

The results on the longitudinal rotor tilt and pitch attitude indicate positive longitudinal speed stability throughout the speed range. The argument leading to this has been analysed in Chapter 4 when the corresponding model predictions were presented. Furthermore, the findings of the model regarding the level of stability in relation to that observed for the VPM gyroplane case, are verified: a Montgomerie gyroplane stick/speed slope of -0.24%/mph (calculated from the gradient of the graph and by knowing that the full stick deflection corresponds to 18.4° of longitudinal rotor tilt), is approximately half of that estimated for the VPM (*Houston [2000]*). This also confirms an anecdotal opinion expressed by the pilot indicating that the VPM aircraft is easier to handle.

The differing configuration characteristics of each aircraft are postulated to contribute to the varying degree of stability. The Montgomerie airframe is such that a significant fuselage area is located forward of the cg; more significantly, it possesses a small tailplane with a short moment arm, rendering it less effective compared to its VPM counterpart which is 3 times the size with a moment arm 1.5 times longer, as illustrated in Table 6.1. The stabilising and destabilising effect of a tailplane and large fuselage respectively is confirmed when removing their effects from the Montgomerie

simulation model, as illustrated in Figure 6.7. Remembering that for the baseline configuration the stick speed slope is *predicted* as being  $-0.26\%/mph$ , it is seen to decrease to  $-0.10\%/mph$  for the 'no tailplane' case and increase to  $-0.34\%/mph$  for the 'no fuselage' case.

So although the small size of both their area and their moment arm renders gyroplane tailplanes ineffective in comparison to their fixed wing counterparts, the results suggest that they still have a role to play in positively influencing the degree of static longitudinal stability. More specifically it is deduced that as for fixed wing aircraft, a desirable static stability light gyroplane configuration is for that with a reduced fuselage area forward of the cg and a large effective tailplane.

Examination of the aircraft roll attitude and the lateral stick required for trim reveals that it flies virtually 'wings level' throughout the speed range. Both parameters appear to be relatively insensitive to speed changes suggesting that the lateral attributes are little influenced by the aircraft airframe characteristics and are therefore dominated by main rotor dynamics; the relatively small distribution of aircraft mass along the y-axis is consistent with the above observation. It is worth noting at this point the inconsistency that exists between the roll attitude and the lateral tilt data, which as discussed in the previous chapter is attributed to calibration errors.

The rotor speed results portrayed in Figure 6.6, are consistent with Glauert's fundamental theory, with it being proportional to the aircraft airspeed. Furthermore, by use of Glauert's derivations (see *Glauert [1926]*) it can be shown that rotor speed is also proportional to rotor loading. This is confirmed by a parametric study performed on aircraft weight illustrated in Figure 6.8. The change from model minimum weight (no fuel case) to model maximum weight (maximum fuel case), represents a mass shift of 35 kg. An increase of approximately 20 rpm in rotor speed is predicted as a result, illustrating the fact that mass variation will influence light gyroplane rotor dynamics. Importantly, this also provides a further indication that the model is capable of realistically *emulating* the rotor speed characteristics for a rotorcraft in autorotation.

The propeller speed variation with aircraft speed presented in Figure 6.6 can only serve to provide a qualitative indication of aircraft performance, since no detailed specification on the engine torque/power output characteristics was provided. A 'minimum propeller rpm' speed of 45 mph (close to the aircraft cruise speed) is apparent from the data, suggesting that aircraft minimum drag and power speeds will be approximately at this point.

Finally, a qualitative assessment of the main rotor induced vibration characteristics can be made by performing a spectral analysis on the vertical acceleration response during a steady climb manoeuvre (see Figure 5.2).

Conventional rotorcraft vibration analysis has shown that rotor vibration is transmitted to the fixed frame at frequencies which are integer multiples of rotor speed. More specifically *Jones [1958]* concluded this by studying the effect of the wake generated by an oscillating blade, postulating that the additive result of the vortices disturbances experienced by each blade would tend to sustain a vibration which would reach a maximum if the vorticity below each blade is the same after each revolution. Furthermore, mathematical proofs exist (*Anderson [1999]* for example), to show that the vibration will manifest itself at harmonic frequencies which are integer multiples of the number of rotor blades. It should be noted (see *Newman [1994]*), that in the *rotor* frame of reference, rotor rolling moment will contribute forcings which are multiples of the number of blades, plus or minus one. In the fuselage however the induced vibration will be felt at integer multiples of the number of blades.

This is clearly verified for the gyroplane case where vibration components are seen to exist at 12.2, 24.4 Hz respectively. The main rotor speed for this manoeuvre is  $\frac{370}{60} \approx 6.1$  Hz, which corresponds to the fundamental frequency of the vibration. The resulting harmonics are of the form,

$$2n \times 6.1$$

where 2 is the number of rotor blades and n is an integer.

Note that a significant component of vibration also manifests itself at a frequency of 6.1 Hz (1/rev). This is a characteristic exhibited also by helicopter rotors and is due to the large 1/rev forcing resulting from forward flight and to any dissimilarity which may exist between the rotating blades.

As a resume of the study performed on the steady state results it can be said that: longitudinal and lateral trim characteristics verify the initial model predictions indicating that the aircraft is statically stable throughout the speed range; configurational characteristics are seen to influence the longitudinal response more than the lateral one which is dominated by main rotor dynamics; rotor speed characteristics are consistent to early gyroplane theory; propeller rpm dependence on speed indicates that a minimum engine output is reached at approximately the cruising speed of the aircraft; a qualitative analysis shows that the gyroplane exhibits conventional rotorcraft vibration characteristics.

The examination of a second gyroplane case has therefore confirmed that this class of aircraft possesses conventional steady flight attributes, a property attributed to the similarity with fixed wing airframe configuration characteristics. Furthermore, with regards to this aspect of the aircraft handling qualities, no adverse safety issues warranting concern have emerged, although certain configurational characteristics are seen to have a beneficial effect on the static stability.

### **6.3 Dynamic response results**

For the dynamic response case the aircraft was perturbed from trim by application of one of the following pilot input: doublet, step or phugoid inducing stick displacement. The first two input types were applied to all three controls (longitudinal/lateral stick, rudder), whereas the standard technique of displacing the longitudinal stick to provoke a speed change was used to excite any phugoid.

## Longitudinal dynamic response results

Results produced from a longitudinal stick doublet input for the 60mph speed case are presented in Figure 6.9.<sup>2</sup> The doublet input has a duration of 2.42s and a peak-to-peak amplitude of 3.25° of rotor tilt corresponding to a stick travel of approximately 18%. Examination of the pitch, roll and yaw rate responses yield the following observations: there is a strong correlation between longitudinal tilt input and pitch rate output which is confirmed by estimation of the coherence value. As illustrated in Figure 6.10, a high coherence value of close to unity is observed for frequencies below 1 Hz indicating a significant degree of linearity in the relationship in the low frequency range.

The coherence function  $C_{xy}(\omega)$  in general is an indicator of the degree of linearity between an applied input  $X(t)$  (with a Fourier transform  $X(\omega)$ ) and a resulting output  $Y(t)$  (with a Fourier transform  $Y(\omega)$ ), and is given by,

$$[C_{xy}(\omega)]^2 = \frac{|G_{xy}(\omega)|^2}{G_{xx}(\omega)G_{yy}(\omega)}$$

where,

$$G_{xx}(\omega) = |X(\omega)|^2$$

$$G_{yy}(\omega) = |Y(\omega)|^2$$

$$G_{xy}(\omega) = [X(\omega) * Y(\omega)]$$

Coherence values of less than unity are due to non-linearity effects in the input/output process or the presence of state and measurement noise. Values of coherence which are greater than 0.6 are generally considered acceptable.

---

<sup>2</sup> It is noted that results are presented in their unfiltered form.

A neutrally damped motion is induced appearing to affect most aircraft states. Interestingly this motion also manifests itself in the lateral/directional plane indicating a strong cross-coupling effect. A point of great significance is that the period of the motion, found to be 7.4s, appears to categorise the aircraft in the following BCAR Section T case: '*Any oscillation having a period between 5 and 10 seconds should damp to one half amplitude in not more than two cycles. There should be no tendency for undamped small oscillations to persist*'. Clearly the indications from this 60 mph test case suggest that the Montgomerie-Parsons *does not* conform with the stated requirements. The results obtained at lower speeds (40 and 50 mph), also exhibited this characteristic albeit with a less pronounced amplitude.

A spectral analysis performed on the probe angle of attack during this manoeuvre (Figure 6.11), also confirms the above findings, indicating that the motion will occur at a frequency of 0.137 Hz. Further confirmation of this is provided in Appendix 6, where in the pilot flight test notes it is stated that the "phugoid<sup>3</sup> was neutral to slightly/slowly divergent with a period of approximately 7 sec". It is also confirmed from the spectral analysis, that the vibration transmitted to the probe from the aircraft is done so at a frequency well separated from the bandwidth of interest, a fact that was verified upon examination of all variables measured by the data probe.

Similar observations to those made for the doublet case are derived from the response to the phugoid inducing technique of displacing the stick and then returning to trim, as illustrated in Figure 6.12. The stick is seen to be pulled back by approximately 7% stick travel (1.3° rotor tilt) and then released, inducing the oscillatory response observed for the doublet case.

Finally it should be noted that the step inputs did not induce a significant aircraft response. This was partly due to the fact that the pilot for safety reasons did not apply the large amplitude inputs that would be required for a significant vehicle reaction (see Appendix 6).

---

<sup>3</sup> Note that what the pilot refers to as a 'phugoid' is in fact a highly coupled mode affecting all states the characteristics of which will be discussed later in the chapter.

### Lateral/directional dynamic response results

For the lateral/directional case, doublet and step inputs were applied to the lateral stick position and rudder respectively, with the former (doublet) inducing a more effective aircraft response.

Application of a lateral stick doublet is illustrated in Figure 6.13. The duration of the input is 2.5 s and its peak-to-peak amplitude  $4^\circ$  (22% of stick travel). The roll rate response is seen to be highly correlated to this control which induces the same neutrally damped motion observed for the longitudinal stick case. Its effect on the directional plane of motion is apparent in the yaw rate response, although the smaller amplitude of the motion suggests that it is less correlated to lateral stick inputs. The cross-coupling effect of this motion is further depicted by the pitch rate plot which portrays a significant response in pitch resulting from a lateral stick deflection.

The coherence plots illustrated in Figure 6.14 serve to confirm the above. Roll rate is seen to be highly correlated to lateral stick with coherence values of greater than 0.6 observed for most frequencies below 0.8 Hz. Yaw rate on the contrary is seen to be largely incoherent with respect to lateral stick inputs.

The converse observations are made when studying the time response and coherence plots resulting from the rudder inputs, presented in Figures 6.15-6.16. A rudder doublet with a peak-to-peak amplitude of approximately  $10^\circ$  is applied over a duration of 3.7s, resulting in a relatively subdued roll rate response and a much more pronounced yaw rate motion. Once again observation of the pitch rate response verifies the existing coupling between the longitudinal and lateral directional motions.

The coherence plots indicate a relatively strong relationship between roll rate and rudder for frequencies below 0.6 Hz. An even stronger linear relationship indicated by coherence values close to unity exists for the yaw rate/rudder case for approximately the same frequency range.

## Discussion of dynamic response results

Several general points can be deduced from the presentation of the results. Doublet inputs are seen as the more effective than step/phugoid inputs as a means of inducing an aircraft response in all axes of motion. The presence of a fast, neutrally stable mode of motion contributes to the effectiveness of a relatively high frequency input signal.

A significant degree of cross coupling exists between longitudinal and lateral/directional motions, an observation consistent with the model predictions. So although gyroplanes are seen to possess static stability attributes similar to those of fixed wing aircraft, the presence of a main rotor introduces a significant degree of coupling in the dynamic response characteristics.

Both the longitudinal and lateral/directional dynamics are dominated by a fast, neutrally stable mode whose period/damping characteristics appear to defy the BCAR Section T standards. This final observation holds the most significant airworthiness and handling qualities implications and therefore warrants some further discussion. The relatively fast nature of this mode makes it particularly sensitive to most pilot control deflections, a fact apparent in all aircraft time responses presented. A fast, non stable mode induced by almost any type of pilot control deflection and influencing most aircraft states will significantly increase pilot workload throughout the performance of any dynamic manoeuvre. Although this observation applies only to the Montgomerie-Parsons G-UNIV aircraft, which due to its research purposes possesses unique configuration characteristics, it does provide the impetus for similar flight testing to be conducted on light gyroplane types with a poor safety record, in order to investigate the existence of similar behaviour.

The conclusions drawn from the flight test results can be verified and further extended by use of the model simulations. The eigenvectors of the aircraft body modes obtained from linearising the model at a speed of 60 mph are presented in Table 6.2. The more 'classic' phugoid and Dutch roll modes are fairly easy to identify from their trademark characteristics (for example, the forward velocity dominance pertinent to the phugoid case). The rotor speed degree of freedom unique to

gyroplanes is also clearly identified and in accordance to Houston's [2000] observations for the VPM case, is seen to be coupled with the body modes of motion.

The remaining two modes exhibit characteristics which are unconventional in the sense that they manifest a high degree of coupling between longitudinal and lateral/directional aircraft states. Examination of the corresponding eigenvalues in frequency/damping ratio format (see Table 6.3), indicates that it is the first of the two coupled modes with a frequency of 0.908 rad/s and a damping ratio of 0.209, that is responsible for the oscillatory motion affecting most states as observed from the flight test data. It is thus important to establish the effect of varying configuration parameters on the stability of this dominant mode. It is argued that since the model was seen to accurately predict the dynamic characteristics of the baseline configuration at this speed (see Chapter 5), it is also able to correctly simulate the vehicle in its modified form.

Both the aircraft fuselage and the tailplane were seen to affect the static stability attributes of the aircraft. The corresponding effect on the dynamic response is illustrated in Figure 6.17, where the pitch rate model simulation is presented for the 60 mph case. The effect of the fuselage has been removed by setting all the aerodynamic forces generated by it to zero, whereas the tailplane effectiveness has been increased by doubling its area size. Significantly, it is observed that although the magnitude of the response is attenuated, the dynamic characteristics remain unchanged with the oscillatory motion persisting throughout the time interval under examination. The same effect was also observed for the off-axis (roll rate) response of the aircraft. Furthermore a second, higher frequency response which is attributed to the second coupled mode identified in Table 6.2, is seen to manifest itself more clearly than for the baseline case, immediately after the application of the input. The configurational changes have thus decreased the damping of this mode therefore deteriorating the short term handling qualities. The above results suggest that an increase in tailplane effectiveness in relation to the de-stabilising influence of the fuselage does not benefit the dynamic response of the aircraft in the same way as it does for the static case.

The result of varying the vertical cg position relative to its baseline position is illustrated in Figures 6.18-6.19. It is observed that a 10cm shift below the baseline position adversely affects the stability of the dominant coupled mode making it unstable. This is consistent with the conclusions drawn by *Houston & Thomson (CAA [1994])*, which indicated that a low cg position would tend to deteriorate gyroplane stability. A 10 cm shift above the baseline position on the other hand, although seen to benefit the dominant mode damping, de-stabilises the rotor speed mode as illustrated in Figure 6.19 and Table 6.4. The significance of this is important as the coupling between this mode and the body degrees of freedom means that this instability will adversely affect the overall handling qualities of the aircraft. Simulation runs performed, demonstrated that a closed range of vertical cg positions exists for which the aircraft remains dynamically stable. The limits of this range were determined at approximately 3cm below the thrust line for the lower end (below which the oscillatory mode became unstable) and 11cm above the thrust line for the upper end (above which the rotor speed mode became unstable). This is consistent with the pattern observed for the VPM aircraft (see *Houston [1996]*), although in that case the study focused on the implications of *lowering* the cg below the thrust line. It is now evident from the study performed on the Montgomery-Parsons gyroplane that it is equally important to impose an upper limit on the vertical cg position. The reason that a high cg position can de-stabilise the rotor speed mode will be discussed later in the analysis.

Although the highly coupled nature of the dominant oscillatory mode means that it is difficult to obtain transparent physical insight to the parameters affecting its stability, the significant correlation of the mode with the vertical cg position does suggest that the  $M_w$  derivative has an important role to play. Simulation runs confirmed the theory developed in Chapter 4 which showed that  $M_w$  is highly sensitive to variations of the vertical cg position. For the reasons explained in Chapter 4, an upward shift of the cg will stabilise  $M_w$  (making it more negative) which in turn is seen to benefit the stability of the dominant mode.

For the phugoid and rotor speed modes *Houston [2001]* has developed expressions approximating their dynamic characteristics which can serve to interpret

the simulation results. Assuming that the state-space equation governing the dynamics is of the form,

$$\begin{bmatrix} \dot{u} \\ \dot{\theta} \\ \dot{\Omega}' \end{bmatrix} = A \begin{bmatrix} u \\ \theta \\ \Omega' \end{bmatrix} + B \underline{u}$$

The state matrix is given by,

$$A = \begin{bmatrix} X_u - \frac{X_w(M_q Z_u - Z_q M_u) + X_q(M_u Z_w - Z_u M_w)}{Z_w M_q - M_w Z_q} & X_\theta & X_\Omega - \frac{X_w(M_q Z_\Omega - Z_q M_\Omega) + X_q(M_\Omega Z_w - Z_\Omega M_w)}{Z_w M_q - M_w Z_q} \\ \frac{M_u Z_w - Z_u M_w}{Z_w M_q - M_w Z_q} & 0 & \frac{M_\Omega Z_w - Z_\Omega M_w}{Z_w M_q - M_w Z_q} \\ Q_u - \frac{Q_w(M_q Z_u - Z_q M_u)}{Z_w M_q - M_w Z_q} & 0 & Q_\Omega - \frac{Q_w(M_q Z_\Omega - Z_q M_\Omega)}{Z_w M_q - M_w Z_q} \end{bmatrix}$$

Given that the system characteristic equation is of the form,

$$(\lambda - \lambda_\Omega)(\lambda^2 + 2\zeta_{ph}\omega_{ph}\lambda + \omega_{ph}^2) = 0$$

it is clear that all terms determining the rotor speed and phugoid modes of motion are dependent on the body/rotor speed coupling derivatives,

$$X_\Omega, Z_\Omega, M_\Omega, Q_u, Q_w$$

which play an important role in gyroplane flight dynamics. Furthermore it is deduced from the expression for the state matrix that both modes of motion will also be influenced by the  $M_w$  derivative, i.e. by the vertical position of the cg.

An investigation of the effect of those parameters is presented in the following sections.

#### i) Rotor speed/phugoid coupling effect

A first indication of the existence of coupling between rotor speed and phugoid modes of motion was provided in Table 6.2 where the eigenvectors corresponding to these modes are presented, with significant magnitudes of forward velocity, pitch and rotor speed apparent in both cases. The coupling effect becomes more obvious when examining Table 6.5, with its influence effectively removed by setting all phugoid/rotor speed derivatives in the full system matrix to zero. An aircraft speed of 45 mph, close to the cruising speed of the vehicle, is chosen for this case study. For the decoupled state the rotor speed eigenvalue is simply equal to  $Q_\Omega$ , the rotor speed damping derivative. The effect of the body modes are to increase it from -0.08 to -0.38, producing a significant benefit for rotor speed damping. A clue to the reason for this is provided by the state matrix of the system dynamics where it is observed that  $Q_\Omega$  is augmented by the term,

$$-\frac{Q_w(M_q Z_w - Z_q M_\Omega)}{Z_w M_q - Z_q M_w}$$

Further examination of Table 6.5 indicates that the coupling also has a beneficial effect on phugoid stability. More specifically the phugoid damping is increased from 0.45 to 0.75 and the frequency decreased from 0.58 to 0.28 rad/s, resulting in a slower and more highly damped phugoid motion. The trend is consistent with that observed in the study of the VPM gyroplane indicating that gyroplane dynamics are benefited by the cross coupling between body and rotor speed degrees of freedom.

## ii) Vertical cg effect

The derivative most influenced by the vertical cg position is  $M_w$ , as illustrated in Table 6.6. This in turn will affect both the stability of the phugoid and the rotor speed mode of motion, as indicated by the state matrix. More specifically for a cg shift from 5 cm below the baseline position to 5 cm above the phugoid damping is slightly increased and the frequency almost halved producing a slower, slightly more damped oscillation. For the rotor speed case where the relationship between  $M_w$  and

the mode eigenvalue is more transparent it is possible to deduce that an increase in the magnitude of the negative value of  $M_w$  (produced by an upward shift of the cg position), will reduce the effect of the augmenting factor (presented in the rotor speed analysis), thus decreasing the overall damping of the mode as depicted in Table 6.6. This also explains the time response characteristics presented in Figure 6.19.

As with the rotor speed/phugoid coupling effect, the trends observed for both the phugoid and rotor speed stability with regard to vertical cg position are consistent with those established for the VPM study.

Before concluding this final main chapter of the thesis it is felt necessary to make some final comments on the presence of the neutrally damped, relatively fast mode which appears to dominate the aircraft's response especially at higher speeds. An aircraft which the official testing procedure deemed as satisfying all requirements of BCAR Section T, according both to the data acquired from a thoroughly tested instrumentation system and the predictions made by a sophisticated rotorcraft mathematical model, evidently fails the basic dynamic stability requirement. The effect of installing the on-board instrumentation (weighing approximately 25 kg) on the vertical cg, which was shown to be the parameter with the most pronounced effect on the vehicle dynamic stability properties, is negligible (see Table 6.7). It is therefore reasonable to argue that the stability characteristics of the vehicle have not been significantly modified by the installation of the DAQ system.

It seems as if an erroneous judgement has been made during the original flight testing of the uninstrumented aircraft. According to the pilot involved (who was not a qualified test pilot), the aircraft met the relevant criteria. However, when flown by a qualified test pilot for the experimental purposes of this thesis, it clearly did not demonstrate compliance. It is therefore the opinion of the author that the authorised bodies should take appropriate action by revisiting the newly defined process leading to gyroplane certification.

#### **6.4 Chapter summary**

An examination of flight test and simulation data has demonstrated that a second light gyroplane possesses conventional steady state stability properties with the degree of stability being influenced by the vehicle configurational characteristics.

The dynamic response of the aircraft is seen to be dominated by a highly coupled, neutrally damped, relatively fast mode, which appears to defy the standards set by BCAR Section T. In order for the vehicle to remain stable, the vertical cg position must be situated between a set of lower and upper limits.

In the next and final chapter of this thesis, the overall conclusions drawn from the research activity will be presented together with suggestions for future development of the work.

# Chapter 7

## Research Conclusions and Recommendations for Future Work

### 7.1 Review of research aims

Before assessing the conclusions drawn from the research work it is apt to remind the reader of the predefined aims and objectives. The main aim was to assess the ability of the RASCAL model to simulate rotorcraft in autorotation by revisiting and enhancing the results of Houston and Thomson for a second gyroplane case. Additionally, by use of data acquired both from the model simulation and the experimental testing, it was aimed to enhance the understanding of an aircraft class for which the existing data base was limited to one case. In order to achieve the above a series of baseline simulations was to be performed and an instrumentation system unique in its sophistication for this class of aircraft was to be developed. Furthermore it was necessary to devise and realise an appropriate flight test programme and to design the software tools capable of analysing the experimental data.

In the subsequent section it will be shown that the above aims were met, highlighting the importance of the work both in assessing the RASCAL model and to contributing to the understanding of gyroplane flight dynamics.

## 7.2 Conclusions

In a summary, the following conclusions can be drawn from the work performed:

### i) Assessment of RASCAL model

The ability of the RASCAL model to simulate autorotation has been assessed by use of steady state and dynamic response data. For the former case the model was seen to accurately predict the trends of all variables examined. The important in terms of handling qualities stick/speed stability parameter, was seen to be simulated correctly for a second gyroplane case and can therefore be used as a reliable means of assessing rotorcraft static stability in autorotation.

Furthermore, all trim variables were seen to be predicted within 10% of range for the control inputs and 2.5° for the attitudes. Confirmation that the model can successfully emulate those parameters in steady state gyroplane flight, enables its use to be extended to the prediction of control and attitude values in steady autorotation descent. The exception to this was rotor speed, particularly sensitive to blade aerodynamic and structural properties, for which a significant discrepancy was observed for a second gyroplane case. As this parameter plays an important role in determining the viability of an autorotation manoeuvre, if RASCAL is to be used as a reliable tool for assessing handling qualities in this flight state, every effort must be expended in resolving this modelling weakness.

The comparison of simulation and flight test aircraft time responses to doublet inputs, yielded a series of important results. The short-term prime responses were in general, seen to be modelled favourably. A long term, neutrally stable oscillation, appearing to affect all aircraft states, was modelled correctly in amplitude and frequency particularly at higher speed. The trend with speed of the dynamic characteristics is also consistently predicted.

The time response comparisons in general have demonstrated, that the important in terms of helicopter autorotation initial reaction of the aircraft to pilot

inputs, is realistically emulated. A mismatch observed in phase for the long term response will have little effect on the ability of RASCAL to assess handling qualities in autorotation.

Although the input signal type employed (conventional doublet), was seen to be relatively ineffective for an aircraft exhibiting highly coupled dynamics, the application of a system identification technique *indicated* that the model/flight discrepancies observed for the VPM aircraft case are also pertinent to the Montgomerie-Parsons aircraft. There is yet more evidence therefore to suggest that the overprediction of both the  $X_u$  and  $Z_w$  derivatives is due to some generic model inadequacy thus eliminating the possibility speculated by Houston and Thomson that it may have been aircraft specific. Since both the derivatives are correlated to the calculation of rotor induced velocities, it is postulated that the dynamic inflow model adopted by RASCAL is unable to correctly emulate all aspects of autorotation flow. For an aircraft with a long term response dominated by a classical phugoid mode (like the VPM gyroplane for example), this modelling discrepancy will have the effect of grossly overpredicting the damping of this mode, thus suppressing the aircraft long term response.

## ii) Flight dynamics characteristics of gyroplanes

The realisation of this research work has defined a second point in the learning curve regarding gyroplane flight dynamics characteristics. Several important results have been derived or confirmed. A second gyroplane has been found to exhibit classic stable static stability characteristics with configuration parameters such as tailplane and fuselage areas seen to affect the degree of stability. Rotor speed characteristics are found consistent with Glauert's early aerodynamic theory. For the first time main rotor induced vibration has been investigated for a gyroplane case, the results showing that it is consistent with conventional rotorcraft theory.

Dynamic stability results have confirmed that the vertical cg and rotor speed degree of freedom play an important role in determining the aircraft response. For the former in particular it has been found that a closed range of cg positions exists for

which the aircraft is dynamically stable. Configurational characteristics on the other hand appear to have a limited effect. It is noted that for the first time presented in the literature, parametric studies using *time responses* produced by RASCAL were employed in order to investigate the dynamic stability attributes of gyroplanes.

Finally, the dynamic response time histories indicate that contrary to the results provided from the flight testing incorporated in the official certification procedure, the aircraft under study does not satisfy the dynamic stability requirements imposed by BCAR Section T. It is therefore suggested that there is cause for the method of implementing gyroplane certification proceedings to be revisited by the authorised bodies.

### **7.3 Recommendations for future work**

Due to the specific nature of the research activity described in this thesis, a platform now exists, both in means of specialised software and experimental apparatus, for the work to be further progressed and enhanced.

#### **i) Investigation into rotor speed and derivative modelling discrepancies**

Both the steady state and dynamic response time histories have indicated that discrepancies exist in rotor speed and the  $X_u$  and  $Z_w$  derivative predictions. In order for the fidelity of the model to be increased, investigations must be made to pinpoint the exact sources of the mismatches which are postulated to be connected to modelling of the rotor blades and the dynamic inflow model employed.

#### **ii) Instrumentation installation on other gyroplane types**

The autonomous nature of the instrumentation system facilitates its removal from this particular aircraft and its efficient installation on vehicles of similar type. A transducer set with its functionality thoroughly verified can therefore be directly deployed for acquiring data from an aircraft class of a poor safety record, contributing to the understanding of its flight characteristics. Furthermore the extension of the data

set can be used to further validate rotorcraft mathematical models in autorotation, such as the RASCAL one described in this thesis.

### iii) Instrumentation enhancement suitable for rotor blade study

The modular design nature of the instrumentation system enables it to be enhanced in order to study further aspects of the aircraft's dynamic performance. In particular, the DAQ bandwidth and channel redundancy capabilities exist for a series of appropriate sensors to be installed on the aircraft blades, acquiring data related to the main rotor response in flight. An in-depth investigation of rotor dynamics can thus be conducted much in the same fashion as the basic airframe stability and control characteristics were derived.

## **7.4 Concluding remarks**

The research activity described in this thesis involved the successful set up and realisation of a major flight test programme involving a gyroplane aircraft. As a result the validation of a rotorcraft mathematical model has been performed for a second autorotative flight mode case, revealing that it can be used in principle for simulating rotorcraft in autorotation. Limitations in its fidelity do exist, and these must be taken into account when using it as a simulation tool. Further insight into gyroplane performance and flight mechanics issues has also been gained thus enhancing the understanding of an aircraft type with a poor safety record. The instrumentation and software developed can now be used on aircraft of the same class, complementing the results obtained by the author of this thesis.

It is hoped that the above have been realised and presented in such a way, as to prove beneficial not only for the understanding of light gyroplanes, but for rotorcraft in general.

# Appendix 1

## The Peters HaQuang Dynamic Inflow Model

The dynamic inflow model presented here, was developed by *Peters & HaQuang [1988]*, although the original model introduction is attributed to *Pitt & Peters [1981]*. A concise review of this modelling approach is also provided by *Chen [1990]* who introduces the definition of wake skew angle  $\chi$  used here. Furthermore the inflow equations are formulated in their *dimensional* form in order to account for rotor speed variation, as presented by *Houston [2000]*.

The rotor induced velocities are expressed in the form:

$$v_i(r, \psi_{az}) = v_0 + \frac{r}{R} v_{1s} \sin \psi_{az} + \frac{r}{R} v_{1c} \cos \psi_{az} \quad (\text{A1-1})$$

where  $v_0, v_{1s}, v_{1c}$  are the uniform, longitudinal and lateral velocity variations respectively. The contribution of  $v_i(r, \psi_{az})$  to the blade element kinematics will be highlighted in Appendix 2.

The three inflow states can then be calculated from:

$$[\tau] \begin{bmatrix} \dot{v}_0 \\ \dot{v}_{1s} \\ \dot{v}_{1c} \end{bmatrix} + \begin{bmatrix} v_0 \\ v_{1s} \\ v_{1c} \end{bmatrix} = [L] \begin{bmatrix} T_{aero} \\ L_{aero} \\ M_{aero} \end{bmatrix} \quad (\text{A1-2})$$

where,

$[\tau]$  is the time constant matrix

$[L]$  is the dynamic inflow static gain matrix

$T_{aero}, L_{aero}, M_{aero}$  are the rotor thrust, roll and pitching aerodynamic moments respectively.

Note that all the parameters included in equations (A1-1) and (A1-2), are referred to *wind* axes. The time constant  $[\tau]$  and the dynamic inflow static gain matrix  $[L]$ , are defined as:

$$[\tau] = \begin{bmatrix} \frac{4R}{3\pi V_T C_0} & 0 & \frac{-R \tan(\chi/2)}{12u_m} \\ 0 & \frac{64R}{45\pi u_m (1 + \cos \chi)} & 0 \\ \frac{5R \tan(\chi/2)}{8V_T} & 0 & \frac{64R \cos \chi}{45\pi u_m (1 + \cos \chi)} \end{bmatrix}$$

and,

$$[L] = \frac{1}{\rho\pi R^3} \begin{bmatrix} \frac{R}{2V_T} & 0 & \frac{15\pi \tan(\chi/2)}{64u_m} \\ 0 & -\frac{4}{u_m (1 + \cos \chi)} & 0 \\ \frac{15\pi \tan(\chi/2)}{64V_T} & 0 & -\frac{4 \cos \chi}{u_m (1 + \cos \chi)} \end{bmatrix}$$

If  $u_{mom}$  is the momentum theory induced velocity and  $V_x, V_y, V_z$  are the component disc velocities, the remaining undefined variables are defined as follows:

$$V_T = \sqrt{(V_x^2 + V_y^2 + (V_z - u_m)^2)}$$

$$u_m = \frac{[V_x^2 + V_y^2 + (u_{mom} - V_z)(2u_{mom} - V_z)]}{V_T}$$

$$\chi = \tan^{-1} \left( \frac{\sqrt{V_x^2 + V_y^2}}{u_{mom} - V_z} \right)^1$$

---

<sup>1</sup> Note that the skew angle is defined here in terms of the *component* disc velocities rather than free stream velocity and disc inclination, as in Chapter 1.

Finally,  $C_0$  is the apparent mass factor and is given values of 1 or 0.64 depending on whether untwisted or twisted blades are to be modelled.

## Appendix 2

### Instrumentation Set-up

#### A2.1 The basic principles of flight testing instrumentation

The purpose of any flight test experiment is to acquire and store data about the operation and environment of the test aircraft. The design of the instrumentation performing this depends greatly on the particular focus of the testing, which in turn defines the parameters of interest. In the case of determining both the steady and unsteady stability and control characteristics of the aircraft, the states and controls in trimmed flight and in response to pilot inputs, must be obtained. In other words, we require knowledge of the state variables

$$U V W P Q R \Phi \Theta \Psi$$

and their rates, in response to control inputs

$$\Theta_{1s}, \Theta_{1c}, \Theta_{rud}$$

The transducer set required for this is now well understood and documented (AGARD [1991], AGARD [1995], for example) and can be summarised as follows:

i. Air-data transducers

In order to obtain the aircraft velocity components, i.e.  $U, V, W$ , an air-data probe consisting of static and total head pressure pickups and two vanes for measurement of aerodynamic angles  $\alpha_{probe}, \beta_{probe}$ , is usually employed. A temperature sensor is used to record the air temperature.

## ii. Rate gyros

This group of transducers, mounted orthogonally to each other and aligned to the aircraft body axes, are used to measure  $P, Q, R$ , the roll, pitch and yaw angular velocities<sup>1</sup>. It is stated by *Kalètkà [1991]*, that for rotorcraft in particular, responses to control inputs are primarily rates and therefore it is essential that rate gyro data are accurately measured.

## iii. Attitude indicators

The Euler angles  $\Phi, \Theta, \Psi$  are measured through a set of attitude indicators mounted in the same way as their rate gyro counterparts. The aircraft heading  $\Psi$  is usually referenced to the aircraft orientation at start-up.

## iv. Linear accelerometers

Although not normally treated as aircraft states, the linear accelerations are recorded in order to calculate the velocity rates  $\dot{U}, \dot{V}, \dot{W}$  and for data compatibility checking purposes. Linear accelerometers are considered as the most reliable component of flight testing instrumentation; they are mounted in the same manner as the rate and attitude gyroscopes.

## v. Rotational accelerometers

Rotational accelerometers exhibit high noise characteristics and are therefore not often used. In most cases, the rotational accelerations  $\dot{P}, \dot{Q}, \dot{R}$  are calculated by numerically differentiating the corresponding angular velocities (although this in itself introduces inaccuracies).

---

<sup>1</sup> As opposed to the Euler rates  $\dot{\Phi}, \dot{\Theta}, \dot{\Psi}$ .

vi. Control input measuring transducers

The pilot control inputs ( $\Theta_{1s}$ ,  $\Theta_{1c}$ ,  $\Theta_{rud}$  for the gyroplane case), are normally measured by a set of position transducers. When the control surface deflection is not obtained directly, it is necessary to accurately calibrate the relationship between the deflection and the pilot command (control stick, pedals, etc.). Also, for conventional flight dynamics applications the control inputs are usually small to allow for a linearised model formulation. It is therefore important that the range of data is sufficiently resolved and transducers with high signal to noise ratios are chosen.

vii. Miscellaneous transducers

Finally, for rotorcraft applications in particular, it is often necessary to record parameters such as the main rotor speed, and for the gyroplane the propeller speed is also required. Transducer types such as induction coils and photoelectric sensors are employed for this set of measurements.

## **A2.2 Specifications of the Montgomerie gyroplane instrumentation**

The specifications of the most important instruments installed on the Montgomerie-Parsons gyroplane are as follows:

### **The C3A-02 3-Axes Accelerometer**

#### *General information*

<b>Part Number</b>	C3A-02
<b>Serial Number</b>	702111
<b>Manufacturer</b>	British Aerospace & Equipment
<b>Purpose</b>	Measurement of linear accelerations
<b>Description</b>	Solid state acceleration sensor

*Technical specifications*

<b>Number of Axes</b>	3
<b>Acceleration Range</b>	$\pm 2g$
<b>Output</b>	DC unipolar (0-5V)
<b>Sensitivity</b>	1g/V
<b>Non-linearity</b>	x,y axes 0.5 % full scale z-axis 1.5% full scale
<b>Ready Time</b>	0.3s
<b>Bandwidth</b>	x,y axes 30 Hz z-axis 7Hz
<b>Operating temperature</b>	-30°C to +75°C
<b>Shock Resistance</b>	Drop to concrete floor from 1m height
<b>Vibration Survival</b>	$\pm 4.5g$ 5 to 200Hz

The Seika B1 Single-axis Accelerometer

*General information*

<b>Part Number</b>	NB43R10, Seika B1
<b>Serial Number</b>	A7659
<b>Manufacturer</b>	Seika Kempton
<b>Purpose</b>	Measurement of vertical acceleration
<b>Description</b>	Capacitive accelerometer

*Technical specifications*

<b>Number of Axes</b>	1
<b>Acceleration Range</b>	$\pm 3g$
<b>Output</b>	DC unipolar (2.4 - 2.6V)
<b>Sensitivity</b>	120.8 mV/g

<b>Non-linearity</b>	1% full scale
<b>Bandwidth</b>	200 Hz
<b>Operating temperature</b>	-40°C to +85°C
<b>Shock Resistance</b>	10000g

The VSG 2000 Rate Gyro

*General information*

<b>Part Number</b>	VSG 2000
<b>Serial Number</b>	30206, 30201, 30202
<b>Manufacturer</b>	British Aerospace & Equipment
<b>Purpose</b>	Measurement of angular rates
<b>Description</b>	Solid state rate gyro

*Technical specifications*

<b>Number of Axes</b>	1
<b>Angular Rate Range</b>	$\pm 100 \text{ deg/s}$
<b>Output</b>	DC unipolar (0.5 - 4.5V)
<b>Sensitivity</b>	not available
<b>Non-linearity</b>	0.5% full scale
<b>Ready Time</b>	0.3s
<b>Bandwidth</b>	70Hz
<b>Operating temperature</b>	-40°C to +85°C
<b>Shock Resistance</b>	1000g
<b>Vibration Survival</b>	10g rms 20 to 1000Hz

The AD01-Y, AD01-RP Angle Detectors

*General information*

<b>Part Number</b>	AD01-Y (yaw), AD01-RP (roll/pitch)
--------------------	------------------------------------

<b>Serial Number</b>	6062350, 7053204, 7053155
<b>Manufacturer</b>	British Aerospace & Equipment
<b>Purpose</b>	Measurement Euler angles
<b>Description</b>	Solid state angle indicator
<i>Technical specifications</i>	
<b>Number of Axes</b>	1
<b>Angle Range</b>	± 45 deg (roll, pitch) ± 180 deg (yaw)
<b>Output</b>	DC unipolar (0.5 - 4.5V)
<b>Sensitivity</b>	20mV/deg (pitch/roll), 11.1mV/deg (yaw)
<b>Non-linearity</b>	1% full scale
<b>Ready Time</b>	0.3s
<b>Bandwidth</b>	3Hz
<b>Operating temperature</b>	-20°C to +70°C

The 144SC0811BARO, HCXM020D6 Sensortechincs Pressure Transducers

*General information*

<b>Part Number</b>	144SC0811BARO, HCXM020D6
<b>Serial Number</b>	not available
<b>Manufacturer</b>	Sensortechincs
<b>Purpose</b>	Measurement of barometric and dynamic pressure
<b>Description</b>	Precision pressure transducers

*Technical specifications*

<b>Pressure Range</b>	800-1100mb (barometric) 0-20mb (dynamic)
<b>Output</b>	DC unipolar 0-5V (barometric) DC unipolar 0.5-4.5 (dynamic)
<b>Linearity</b>	0.005% full scale

**Power Consumption**

70mW (barometric)

50mW (dynamic)

## Appendix 3

### Overview of the Aircraft Certification Process

It is thought necessary to provide an overview of the process required for certifying the aircraft for its flight testing purposes as it forms an integral part of the flight test plan development since without the appropriate permission clearance it is impossible to conduct any testing. A flow diagram illustrating the process from the issue of the basic Permit to Fly for the aircraft in its unmodified form to the issue of an updated one allowing for the aircraft to be flown fully instrumented, is presented in Figure A3.1. The basic Permit to Fly was obtained by the PFA (reference, PFA-G/08-390) and the aircraft was assessed against all requirements of BCAR Section T (*Anon [1993]*). Once a modification has been applied to the aircraft at this stage, authorisation of it must be performed in one of two ways: If the modification is characterised as minor, this can be obtained through the existing permit to fly; if it is deemed as a major one, a new permit must be issued. Installation of aircraft instrumentation is characterised as a major modification and thus requires the second, more cumbersome route, to be followed. A modification statement which included a detailed description of the mechanical installation of each instrument, the electrical installation and power supply and most importantly the effect on the weight and balance properties, was submitted to the CAA. This in turn led to the issue of an Airworthiness Approval Note (AAN), which officially stated all the modifications presented in the modification statement. The last paragraph of the AAN stating that "This aircraft is eligible for the issue of a Permit to Fly to Test and, when the Flight Testing in accordance with Flight Test Schedule No. 301, detailed in paragraph 5, is complete to the satisfaction of CAA Permit to Fly provided that it is operated in accordance with limitations, procedures, pilot notes and maintenance publications referenced in this AAN", effectively provides with a Permit to Fly to Test allowing the flight test schedule to be performed.

On completion of the testing, an application must be made requesting the issue of a new full Permit to Fly which will incorporate all the current changes.

## Appendix 4

### The RASCAL Mathematical Model

#### A4.1 Model overview

The RASCAL (Rotorcraft Aeromechanic Simulation for Control AnaLysis) simulation software was developed by *Houston [1994]* at the University of Glasgow. Due to its generic form can be used to simulate almost any rotorcraft configuration. The method of modelling the aircraft main rotor categorises it as a non-linear, individual blade/blade element model type. Detailed information on this modelling approach is presented by *Johnson [1980]*.

The aircraft system is represented by

$$A\dot{\underline{x}} = f(\underline{x}, \underline{u})$$

where  $\underline{x}$  is the state vector which includes the aircraft translational and angular velocities, the feather, flap and lag angles and their corresponding rates for each blade on each rotor, the induced velocity states derived from the rotor wake as well as the angular velocities and corresponding moments for each rotor and the engine torques. The matrix  $A$  contains terms associated with the airframe moments of inertia, the dynamic inflow model and the blade equations of motion. Finally, the input vector  $\underline{u}$  consists of the control positions i.e. in the case of the gyroplane, the main rotor longitudinal and lateral tilt and the rudder angular deflection.

By assuming the rotorcraft to be a rigid structure, the motion of the aircraft's centre of gravity can then be simulated by using the conventional Euler rigid body and kinematic equations:

$$m\dot{U} = -m(WQ - VR) + X - mg \sin \Theta$$

$$m\dot{V} = -m(UR - WP) + Y + mg \cos \Theta \sin \Phi$$

$$m\dot{W} = -m(VP - UQ) + Z + mg \cos \Theta \cos \Phi$$

$$I_{xx}\dot{P} = (I_{yy} - I_{zz})QR + I_{xz}(\dot{R} + PQ) + L$$

$$I_{yy}\dot{Q} = (I_{zz} - I_{xx})RP + I_{xz}(R^2 - P^2) + M$$

$$I_{zz}\dot{R} = (I_{xx} - I_{yy})PQ + I_{xz}(\dot{P} - QR) + N$$

$$\dot{\Phi} = P + Q \sin \Phi \tan \Theta + R \cos \Phi \tan \Theta$$

$$\dot{\Theta} = Q \cos \Phi - R \sin \Phi$$

$$\dot{\Psi} = Q \sin \Phi \sec \Theta + R \cos \Phi \sec \Theta$$

The starting point for any modelling exercise is the formulation of the external forces and moments, denoted by  $X$ ,  $Y$ ,  $Z$ ,  $L$ ,  $M$  and  $N$  respectively and expressed in conventional aircraft *body* axes. For convenience they can be treated as the sum of the contributions from each of the relevant aircraft components as follows:

$$X = X_{rotor} + X_{fuse} + X_{fin} + X_{iplane}$$

$$Y = Y_{rotor} + Y_{fuse} + Y_{fin} + Y_{iplane}$$

$$Z = Z_{rotor} + Z_{fuse} + Z_{fin} + Z_{iplane}$$

$$L = L_{rotor} + L_{fuse} + L_{fin} + L_{iplane}$$

$$M = M_{rotor} + M_{fuse} + M_{fin} + M_{iplane}$$

$$N = N_{rotor} + N_{fuse} + N_{fin} + N_{iplane}$$

where the subscripts *rotor*, *fuse*, *fin*, *iplane*, denote the main rotor, fuselage, fin and tailplane respectively.

The system of the non-linear Euler equations is integrated numerically (by a Runge-Kutta technique), in order to obtain the orientation of the aircraft at each time point. The Euler transformation can then be applied to define this orientation in an earth-fixed axes system.

The key elements of the model have already been presented in Table 4.1. Special reference should be made to the main rotor representation, as the most significant part of the modelling effort is devoted to this. Depending on the number of rotor blades, there can be up to 100 non-linear, periodic ordinary differential equations describing the coupled rotor airframe dynamics, which can be modelled with up to 10 individually modelled rigid blades incorporating fully coupled flap, lag and feather motion. The aerodynamic forces are represented by up to 10 elements per blade and look-up tables are used to calculate the lift and drag properties as a function of Mach number and angle of attack. Since the forces and moments applied to the main rotor dominate the modelling of any rotorcraft configuration, a significant portion of this appendix is devoted to their derivation.

#### **A4.2 Determination of rotor forces and moments**

With the blade element approach, the problem of calculating the rotor forces and moments is formulated by determining the contribution of each blade element. The incremental lift and drag forces are obtained from aerodynamic data, which usually exists in the form of look-up tables produced from wind-tunnel tests. In order to facilitate the corresponding calculations, it is necessary to obtain the linear and

angular velocities and accelerations of a general blade element in *blade* axes, through a series of appropriate axes transformations. Once this procedure is completed it is possible to calculate the loadings on each individual blade and by summing the blade contributions, to instantaneously determine the total rotor force and moment. The procedure for achieving this goal, starting with a basic analysis of blade element kinematics, is outlined in the following sections.

### Blade element kinematics

The purpose of the following analysis is to derive the velocity vector of a general blade element in a blade fixed axes system, from the aircraft's velocity vector represented in an aircraft body axes system.

Initially, the effect of the kinetic terms due to the airframe's rotation is added to the aircraft velocity vector, in order to obtain the absolute velocity of the rotor hub:

$$\underline{u}_{hub}^{body} = \underline{u} + \underline{\omega} \times [\underline{r}_{cg} - \underline{r}_{hub}] \quad (A4-1)$$

where ,

$\underline{u}_{hub}^{body}$  is the hub absolute velocity vector in aircraft body axes

$\underline{u}$  is the aircraft velocity vector in aircraft body axes

$\underline{\omega}$  is the aircraft angular velocity in aircraft body axes

$\underline{r}_{cg}$  is the centre of gravity position vector

$\underline{r}_{hub}$  is the rotor hub position vector

Assuming that the rotor shaft is inclined with respect to the body axes at an angle  $\gamma_{disc}$ , a new *disc* set of axes can be defined, centred at the rotor hub and obtained by rotating through an angle  $\gamma_{disc}$  about the  $\underline{j}$  body axis. The hub velocity expressed in this new axis system is obtained from

$$\underline{u}_{hub}^{disc} = [T^{body / disc}] \underline{u}_{hub}^{body} \quad (A4-2)$$

where,

$$T^{body / disc} = \begin{bmatrix} \cos \gamma_{disc} & 0 & -\sin \gamma_{disc} \\ 0 & 1 & 0 \\ \sin \gamma_{disc} & 0 & \cos \gamma_{disc} \end{bmatrix}$$

is the transformation matrix from body to disc axes and  $\underline{u}_{hub}^{disc}$  is the hub velocity expressed in disc axes.

The disc set of axes is fixed geometrically and is of little use when studying the dynamics of a rotating blade. A new rotating set of axes, referred to as *shaft* axes, must therefore be defined. It is obtained by rotating the disc axis system about its  $\underline{k}$  axis, through the shaft azimuth angle  $\psi_{az}$ . The hub velocity in this new axis system is then given by:

$$\underline{u}_{hub}^{shaft} = [T^{disc / shaft}] \underline{u}_{hub}^{disc} \quad (A4-3)$$

where,

$$T^{disc / shaft} = \begin{bmatrix} \sin \psi_{az} & -\cos \psi_{az} & 0 \\ \cos \psi_{az} & \sin \psi_{az} & 0 \\ 0 & 0 & 1 \end{bmatrix}$$

is the transformation matrix needed to be applied and  $\underline{u}_{hub}^{shaft}$  is the hub velocity expressed in shaft axes.

Assuming that the rotor is modelled with a hinge offset, it is then necessary to include both the kinematic terms due to the offset presence and the induced velocity terms due to the rotor wake. If no hinge modelling is included, the kinematic terms can be ignored.

The absolute velocity of the hinge in shaft axes is thus given by:

$$\underline{u}_{hinge}^{shaft} = \underline{u}_{hub}^{shaft} + \underline{\omega}_{hinge}^{shaft} \times \underline{r}_{hinge}^{hub} + [0 \quad 0 \quad -v_i[r, \psi_{az}]]^T \quad (A4-4)$$

where,

$\underline{u}_{hinge}^{shaft}$  is the hinge absolute velocity in shaft axes

$\underline{\omega}_{hinge}^{shaft}$  is the hinge angular velocity in shaft axes

$\underline{r}_{hinge}^{hub}$  is the position vector of the hinge relative to the hub

$v_i(r, \psi_{az})$  is the radially and azimuthally varying wake induced velocity

The hinge angular velocity in shaft axes is derived from:

$$\underline{\omega}_{hinge}^{shaft} = [T^{disc / shaft}] [T^{body / dist}] \underline{\omega} + [0 \quad 0 \quad \Omega]^T \quad (A4-5)$$

where  $\Omega$  is the angular velocity of the rotating blades.

The term  $v_i(r, \psi)$  in equation (A4-4) is obtained from the wake model dynamics. The manner in which it is derived is described in Appendix 1. By transforming from shaft to *blade* axes, through the sequence of lag ( $\zeta_{lag}$ ) and flap ( $\beta_{flap}$ ) angles, the translational velocity of the hinge expressed in blade axes is given by:

$$\underline{u}_{hinge}^{blade} = [T^{shaft / blade}] \underline{u}_{hinge}^{shaft} \quad (A4-6)$$

where,

$$T^{shaft / blade} = \begin{bmatrix} \cos \zeta_{lag} & \sin \zeta_{lag} & 0 \\ -\cos \beta_{flap} \sin \zeta_{lag} & \cos \beta_{flap} \cos \zeta_{lag} & \sin \beta_{flap} \\ \sin \beta_{flap} \sin \zeta_{lag} & -\cos \beta_{flap} \sin \zeta_{lag} & \cos \beta_{flap} \end{bmatrix}$$

is the transformation matrix from hub to blade axes and  $\underline{u}_{hinge}^{blade}$  is the hinge velocity in blade axes.

Finally, the absolute velocity of a general blade element in blade axes, is calculated from:

$$\underline{u}_{elem}^{blade} = \underline{u}_{hinge}^{blade} + \underline{\omega}_{elem}^{blade} \times \underline{r}_{elem}^{blade} \quad (A4-7)$$

where,

$\underline{u}_{elem}^{blade}$  is the absolute velocity of the blade element in the blade axes set

$\underline{\omega}_{elem}^{blade}$  is the angular velocity of the blade element

$\underline{r}_{elem}^{blade}$  is the position vector of the blade element with respect to the hinge.

The blade element angular velocity is calculated from

$$\underline{\omega}_{elem}^{blade} = T^{shaft / blade} \underline{\omega}_{hinge}^{shaft} + \begin{bmatrix} \dot{\beta}_{flap} & \dot{\theta}_{feath} & \dot{\zeta}_{lag} \end{bmatrix} \quad (A4-8)$$

where  $\dot{\beta}_{flap}$ ,  $\dot{\theta}_{feath}$ ,  $\dot{\zeta}_{lag}$  are the flap, feather and lag rates respectively.

### Rotor aerodynamic forces

Once the absolute velocity vector of the blade is calculated it is possible to estimate the aerodynamic lift and drag acting on it. Given that the blade element velocity vector can be defined as,

$$\underline{u}_{elem}^{blade} = \begin{bmatrix} u_{blade}^x & u_{blade}^y & u_{blade}^z \end{bmatrix}$$

the local angle of attack will be given by

$$\alpha_{elem} = \theta_{elem} + \tan^{-1} \left( \frac{u_{blade}^z}{u_{blade}^x} \right)$$

where,

$\theta_{elem}$  is the local geometric pitch angle.

Assuming two dimensional aerodynamic theory and by defining

$$V_{elem} = \sqrt{(u_{blade}^x)^2 + (u_{blade}^z)^2}$$

the lift and drag forces can then be calculated as

$$L_{elem} = \frac{1}{2} \rho V_{elem}^2 c_{elem} r_{elem} a(\alpha_{elem}, M_{elem}) \alpha_{elem} \tag{A4-9}$$

$$D_{elem} = \frac{1}{2} \rho V_{elem}^2 c_{elem} r_{elem} \delta(\alpha_{elem}, M_{elem})$$

where,

$L_{elem}$   $D_{elem}$  are the lift and drag forces acting on the blade element

$c_{elem}$  is the chord of the blade element

$r_{elem}$  is length of the blade element

$a(\alpha_{elem}, M_{elem})$  is the lift curve slope as a function of  $\alpha_{elem}$  and local Mach number

$\delta(\alpha_{elem}, M_{elem})$  is the drag coefficient as a function of  $\alpha_{elem}$  and local Mach number

Equation (A4-9), specifies the aerodynamic forces in a frame of reference which has its x-axis aligned to the local flow  $V_{elem}$ . In order to obtain the forces in the blade fixed axis system the following must be applied:

$$X_{aero}^{blade} = L_{elem} \sin \alpha_{elem} - D_{elem} \cos \alpha_{elem}$$

$$Y_{elem}^{aero} = 0 \quad (A4-10)$$

$$Z_{aero}^{blade} = -L_{elem} \cos \alpha_{elem} - D_{elem} \sin \alpha_{elem}$$

where  $X_{aero}^{blade}$ ,  $Y_{aero}^{blade}$ ,  $Z_{aero}^{blade}$  are the rotor aerodynamic forces in the x, y, z blade axis respectively. It is noted again that ,

$$Y_{elem}^{aero} = 0$$

as a consequence of two dimensional aerodynamic theory being applied.

In order for the total forces and moments to be calculated, the loads produced from the absolute acceleration of the blade element, referred to as inertial loads, must be obtained; their derivation is presented in the following section.

### Inertial forces

The inertial forces acting on a blade element are determined from Newton's Second Law:

$$\underline{X}_{inertia}^{blade} = -m_{elem} \underline{a}_{elem}^{blade} \quad (A4-11)$$

where,

$\underline{X}_{inertia}^{blade}$  is the vector of inertial forces in blade axes

$m_{elem}$  is the mass of the blade element

$\underline{a}_{elem}^{blade}$  is the absolute acceleration of the blade element

The derivation of the absolute acceleration  $\underline{a}_{elem}^{blade}$  is performed in the same manner as for the absolute velocity, and by neglecting angular acceleration terms is obtained from:

$$\underline{a}_{elem}^{blade} = T^{shaft / blade} \left( \begin{aligned} & \left[ T^{disc / shaft} \left[ T^{body / disc} \left[ \dot{\underline{u}} + \underline{\omega} \times \underline{u} + \underline{\omega} \times (\underline{\omega} \times \underline{r}_{hub}) \right] \right] + \underline{\omega}_{hinge}^{shaft} \times \left[ \underline{\omega}_{hinge}^{shaft} \times \underline{r}_{hinge}^{hub} \right] \right] \\ & + \underline{\omega}_{elem}^{blade} \times \left( T^{shaft / blade} \left[ \underline{\omega}_{hinge}^{shaft} \times \underline{r}_{hinge}^{hub} \right] \right) \end{aligned} \right) \quad (A4-12)$$

Equations (A4-11) and (A4-12) can therefore be used to define the inertial forces which combined with the aerodynamic loads comprise the total forces and moments acting on the rotor blade element.

#### Total forces and moments acting on the rotor

The total force acting on a blade element in blade fixed axes is given by

$$\underline{X}_{elem}^{blade} = \underline{X}_{aero}^{blade} + \underline{X}_{inertia}^{blade} \quad (A4-13)$$

It is then possible to sum the forces (and their moment effect), to produce the total force and moment acting on a rotor expressed in aircraft body axes:

$$\underline{X}_{rotor} = \left[ T^{body / disc} \right]^{-1} \sum_{j=1}^N \left( \left[ T^{disc / shaft} \right]^{-1} \left[ T^{shaft / blade} \right]^{-1} \left\{ \sum_{i=1}^{n_{elem}} \underline{X}_{elem} \right\} \right) \quad (A4-14)$$

$$\underline{L}_{rotor} = \left[ T^{body / disc} \right]^{-1} \sum_{j=1}^N \left( \left[ T^{disc / shaft} \right]^{-1} \left( -\underline{r}_{hinge} \times \left( \left[ T^{shaft / blade} \right]^{-1} \left\{ \sum_{i=1}^{n_{elem}} \underline{X}_{elem} \right\} \right) \right) \right) + (\underline{r}_{hub} - \underline{r}_{cg}) \times \underline{X}_{rotor}$$

where,

$\underline{X}_{rotor}$  is the rotor force vector in aircraft body axes

$\underline{L}_{rotor}$  is the rotor moment vector in aircraft body axes

$N$  is the number of rotor blades

$n_{elem}$  is the number of elements on a blade.

### Blade equations of motion

The blade equations of motion are based on the derivation by *Bramwell [1976]* and are given by:

$$\begin{aligned} I_{flap} (\dot{\omega}_x^{blade} + \omega_y^{blade} \omega_z^{blade}) - m_{blade} y_{cg}^{blade} a_z^{hinge} &= M_{flap}^{blade} \\ I_{pitch} (\dot{\omega}_y^{blade} + \omega_x^{blade} \omega_z^{blade}) &= M_{pitch}^{blade} \\ I_{lag} (\dot{\omega}_z^{blade} + \omega_x^{blade} \omega_y^{blade}) - m_{blade} y_{cg}^{blade} a_x^{hinge} &= M_{lag}^{blade} \end{aligned} \quad (A4-15)$$

where,

$I_{flap}$ ,  $I_{pitch}$ ,  $I_{lag}$  are the blade flap, pitch and lag inertias

$\omega_x^{blade}$ ,  $\omega_y^{blade}$ ,  $\omega_z^{blade}$  are the components of the blade angular velocity

$M_{flap}^{blade}$ ,  $M_{pitch}^{blade}$ ,  $M_{lag}^{blade}$  are the aerodynamic and spring restoring moments

The blade angular velocity and acceleration terms are obtained from blade element kinematic principles described in the previous section. It is evident from the above analysis that the model structure supports fully coupled flap and lag degrees of freedom for its rotor representation.

### A4.3 Fuselage, tailplane, rudder fin forces and moments

The forces and moments produced from the aerodynamic surfaces are obtained from data existing in one of two forms: look-up tables of forces and moments produced from wind-tunnel data measured at a series of angles of attack and sideslip or polynomial functions of angle of attack and sideslip, with the polynomial coefficients estimated from simple two dimensional aerodynamic theory. The later of the two methods was in fact adopted for all calculations involving the Montgomerie gyroplane's aerodynamic surfaces, for which there was no wind tunnel data available. This approach is used in the following section to demonstrate the manner in which the fuselage forces and moments are estimated. The loads on the remaining aerodynamic surfaces are calculated in a similar way.

The fuselage aerodynamic forces and moments are given by,

$$X_{fuse} = \frac{1}{2} \rho V_{fuse} S_{fuse} (Cx_{fuse0} + Cx_{fuse1} \alpha + \dots)$$

$$Y_{fuse} = \frac{1}{2} \rho V_{fuse} S_{fuse} (Cy_{fuse0} + Cy_{fuse1} \beta + \dots)$$

$$Z_{fuse} = \frac{1}{2} \rho V_{fuse} S_{fuse} (Cz_{fuse0} + Cz_{fuse1} \alpha + \dots)$$

$$L_{fuse} = \frac{1}{2} \rho V_{fuse} S_{fuse} (Cl_{fuse0} + Cl_{fuse1} \beta + \dots)$$

$$M_{fuse} = \frac{1}{2} \rho V_{fuse} S_{fuse} (Cm_{fuse0} + Cm_{fuse1} \alpha + \dots)$$

$$N_{fuse} = \frac{1}{2} \rho V_{fuse} S_{fuse} (Cn_{fuse0} + Cn_{fuse01} \beta + \dots)$$

where,

$V_{fuse}$  is the fuselage local velocity

$S_{fuse}$  is the fuselage reference area

$\alpha_{fuse}$  is the fuselage angle of attack

$\beta_{fuse}$  is the fuselage angle of sideslip

$Cx_{fuse}, Cy_{fuse}, Cz_{fuse}$  etc. are the force and moment aerodynamic coefficients

Since  $\alpha_{fuse}$  and  $\beta_{fuse}$  are small angles, it is usual for high order expressions for these quantities to be ignored.<sup>1</sup> Simple two dimensional aerodynamic theory is applied in order to determine the remaining aerodynamic constants. The force and moment coefficients for the tailplane, fin and rudder are estimated in a similar manner. Hence, the total forces and moments acting on the airframe are determined and the equations of motion, described in section A4.1, can be solved.

#### **A4.4 Trim and linearisation algorithms**

The general trim problem for a conventional rotorcraft is described in most helicopter text books and is defined by a set of prescribed steady state flight conditions. The purpose of the trim algorithm is to calculate the control inputs and

---

<sup>1</sup> Note that in theory up to 5th order terms can be incorporated. For the purposes of this study only first order term were considered.

aircraft attitudes required to maintain this steady state condition. Hence, assuming that,

$$\sum_{i=1}^n \dot{\underline{x}}_i = f(\underline{y}_{trim}, \underline{u}_{trim})$$

where,

$\dot{\underline{x}}$  is the vector containing the rates of change of the aircraft states

$\underline{y}_{trim}$  is a vector containing the variables defining the flight condition

$\underline{u}_{trim}$  is a vector containing the trim controls and aircraft attitudes

$n$  is the number of discrete simulation time points

the objective is to chose  $\underline{u}_{trim}$  such that

$$J = \sum_i^n \dot{\underline{x}}_i \rightarrow 0$$

In all cases, the subscript  $i$  denotes the  $i$ th point in a discrete time history of  $n$  points, where

$$n = \frac{(t_2 - t_1)}{\Delta t}$$

The algorithm used to perform this is simple but has proved to be effective (*Houston [1994]*). The cost function

$$J = \sum_i^n \dot{\underline{x}}_i$$

is minimised using a standard least squares method. An initial value for  $\underline{u}_{trim}$  is selected from which  $J$  is calculated. If the value for  $J$  lies outside the predefined tolerance, the steepest descent path from the current solution is used to update  $\underline{u}_{trim}$ . The process is repeated until the cost function is reduced to the desired value. It is noted by *Houston [1994]*, that during the time interval  $(t_2 - t_1)$  an integer number of rotor revolutions must be performed, in order for the mean values of the forces and

moments to be calculated. Also during this interval the acceleration terms of the aircraft states are suppressed, i.e. it is assumed that the linear and angular velocities remain constant throughout the trimming process when in fact they will vary according to the rigid body modes of the aircraft. This approximation does not have a significant effect on the overall results of the simulation.

The cost function  $J$  can be used further to obtain a linear small perturbation representation of the aircraft system about a specified trim condition. Assuming that the linear model is of the conventional state-space form

$$\dot{\underline{x}} = A\underline{x} + B\underline{u}$$

where

$$\underline{x} = [u \ v \ w \ p \ q \ r \ \phi \ \theta \ \psi \ \Omega]^T$$

$$\underline{u} = [\theta_{ls} \ \theta_{lc} \ \theta_{rud} \ \theta_{th}]^T$$

$$A = \left( \frac{\partial F}{\partial x} \right)_{x=x_{trim}}$$

$$B = \left( \frac{\partial F}{\partial u} \right)_{x=x_{trim}}$$

then the cost function  $J$  is calculated with each state and control in the 6 DOF model sequentially perturbed by a small predefined amount ( $\delta \underline{x}_j$  or  $\delta \underline{u}_j$ ). The elements of the state-space matrices are then calculated from

$$A_j = \sum_1^i \dot{\underline{x}}_i \left( \frac{\delta \underline{x}_j}{n \delta \underline{x}_j} \right)$$

$$B_j = \sum_1^i \underline{u}_i \left( \frac{\delta \underline{u}_j}{n \delta \underline{u}_j} \right)$$

## Appendix 5

### Equation Error System Identification Method in the Frequency Domain

The synthesis of the model to be identified is based on the linearised, decoupled longitudinal and lateral, 6-DOF state space form of the dynamic equations,

$$\dot{\underline{x}} = A\underline{x} + B\underline{u}$$

For the longitudinal case we have,

$$A = \begin{bmatrix} X_u & X_w & X_q & X_\theta & X_\Omega \\ Z_u & Z_w & Z_q & Z_\theta & Z_\Omega \\ M_u & M_w & M_q & M_\theta & M_\Omega \\ 0 & 0 & 1 & 0 & 0 \\ Q_u & Q_w & Q_q & Q_\theta & Q_\Omega \end{bmatrix}, B = \begin{bmatrix} X_{\theta_1} \\ Z_{\theta_1} \\ M_{\theta_1} \\ 0 \\ Q_{\theta_1} \end{bmatrix}$$

and

$$\underline{x} = [u \ w \ q \ \theta \ \Omega']^T, \underline{u} = [\theta_{1s}]$$

For the lateral/directional case,

$$A = \begin{bmatrix} Y_u & Y_w & Y_q & Y_\theta & 0 \\ L_u & L_p & 0 & L_r & 0 \\ 0 & 1 & 0 & 0 & 0 \\ N_u & N_p & 0 & N_r & 0 \\ 0 & 0 & 0 & 1 & 0 \end{bmatrix}, B = \begin{bmatrix} Y_{\theta_{1c}} & Y_{\theta_{rud}} \\ L_{\theta_{1c}} & L_{\theta_{rud}} \\ 0 & 0 \\ N_{\theta_{1c}} & N_{\theta_{rud}} \\ 0 & 0 \end{bmatrix}$$

and

$$\underline{x} = [v \ p \ \phi \ r \ \psi]^T, \underline{u} = [\theta_{1c} \ \theta_{rud}]^T$$

The equations converted to the frequency domain acquire the form,

$$j\omega x(\omega) = Ax(\omega) + Bu(\omega)$$

with  $x(\omega)$  and  $u(\omega)$  calculated from the Discrete Fourier Transform, given by,

$$x(\omega_k) = x(k\Delta\omega) = \Delta t \sum_{n=0}^{N-1} x_n \exp[-j2\pi(kn)/N] \quad (A5-1)$$

$$k = 0, 1, 2, \dots, N-1$$

where,

$x(\omega_k)$  = Fourier coefficients

$x_n = x(n\Delta t)$  = data points

$\Delta t$  = time increment

$N$  = number of discrete frequency points

Each degree of freedom is then treated as a separate regression problem and least squares estimates are produced for the unknown stability and control derivatives. In order to demonstrate the mechanism for this, the formulation for the pitching moment equation will be demonstrated in this section. The other degrees of freedom are analysed in a similar manner.

Converted to the frequency domain the pitching moment equation is given by,

$$\dot{q}(\omega) = M_u u(\omega) + M_w w(\omega) + M_q q(\omega) + M_\theta \theta(\omega) + M_\Omega \Omega'(\omega) + M_{\theta_{1s}} \theta_{1s}(\omega) \quad (A5-2)$$

Separating real and imaginary parts,

$$\begin{aligned}
 -\omega \operatorname{Im}[q(\omega)] &= M_u \operatorname{Re}[u(\omega)] + M_w \operatorname{Re}[w(\omega)] + M_q \operatorname{Re}[q(\omega)] + M_\theta \operatorname{Re}[\theta(\omega)] + \\
 &M_\Omega \operatorname{Re}[\Omega'(\omega)] + M_{\theta_{1s}} \operatorname{Re}[\theta_{1s}(\omega)] \\
 \omega \operatorname{Re}[q(\omega)] &= M_u \operatorname{Im}[u(\omega)] + M_w \operatorname{Im}[w(\omega)] + M_q \operatorname{Im}[q(\omega)] + M_\theta \operatorname{Im}[\theta(\omega)] + \\
 &M_\Omega \operatorname{Im}[\Omega'(\omega)] + M_{\theta_{1s}} \operatorname{Im}[\theta_{1s}(\omega)]
 \end{aligned}
 \tag{A5-3}$$

The unknown parameters must simultaneously satisfy both equations defined by (A5-3) and their least squares estimate obtained for the discrete frequency values of  $[\omega_{\min} \dots \omega_{\max}]$ . The frequency  $\omega_{\min}$  is the lowest non-zero discrete frequency; excluding the zero value eliminates the need for estimating values associated with measurement zero shift, as explained by *Black & Murray-Smith [1989]*. The maximum frequency  $\omega_{\max}$  is selected through examination of the spectral densities of the relevant states.

Defining,

$$\underline{y}(\omega_i) = \begin{bmatrix} -\omega_i \operatorname{Im}[q(\omega_i)] \\ \omega_i \operatorname{Re}[q(\omega_i)] \end{bmatrix}$$

$$\underline{x}(\omega_i) = [u(\omega_i) \quad w(\omega_i) \quad q(\omega_i) \quad \theta(\omega_i) \quad \Omega'(\omega_i) \quad \theta_{1s}(\omega_i)]$$

$$\underline{\theta}_{par} = [M_u \quad M_w \quad M_q \quad M_\theta \quad M_\Omega \quad M_{\theta_{1s}}],$$

and making the assumption that no measurement noise exists and that the state noise is random with a zero mean value, the least squares estimate for the unknown parameters is given by:

$$\underline{\theta}_{est} = (\underline{x}^T \underline{x})^{-1} \underline{x}^T \underline{y}
 \tag{A5-4}$$

The covariance of the estimated parameter vector is given by

$$E[(\underline{\theta}_{est} - \underline{\theta}_{par})(\underline{\theta}_{est} - \underline{\theta}_{par})^T] = \sigma^2 (\underline{x}^T \underline{x})^{-1} \quad (A5-5)$$

where,

$$\sigma^2 = \frac{1}{N-n} \sum_{i=1}^N \varepsilon_{est}(\omega_i)$$

$$\varepsilon_{est}(\omega_i) = y(\omega_i) - y_{est}(\omega_i)$$

$$y_{est}(\omega_i) = (\theta_{est})_1 x_1(\omega_i) + \dots + (\theta_{est})_{n-1} x_{n-1}(\omega_i)$$

In addition to the above, the multiple correlation coefficient  $R^2$  providing a measure of the fit accuracy, and the total and partial F-remove ratios, providing a measure of confidence of the fit, are given by the following:

$$R^2 = \frac{(\underline{x}\underline{\theta}_{est})^T (\underline{x}\underline{\theta}_{est})}{\underline{y}^T \underline{y}}$$

$$F_{tot} = \frac{\frac{R^2}{p-1}}{(1-R^2)(k-p)}$$

$$F_{par_i} = \frac{(\theta_{est})_i^2}{s_i^2}$$

where,

$p$  is the number of parameters to be identified

$k$  is the number of discrete frequency points

$s_i$  is the standard error of the parameter  $\theta_i$ .

# Appendix 6

## Pilot Flight Test Notes

The following is an extract from the pilot's<sup>1</sup> flight test notes, taken from a test at 60 mph investigating the longitudinal response of the aircraft:



### FRA Post Flight Report

FTS No. : MP2-00-01  
 Flight No. : FTPO4 Date : 28<sup>th</sup> February 2001  
 Aircraft Type : Montgomerie 2-seat Aircraft Reg : G-UNIV  
 Pilot : C CHADWICK Co-pilot : —  
 Observer (ground) : C. HANLEY Other POB : NONE  
 Loading : Stores Port : } NONE  
 Stbd : }  
 Take-Off Time : 1654 Land Time : 1722 (0:40:30)

OVERALL TEST OBJECTIVE:  
 STABILITY TESTS AT 60 MPH

Test No.	Test To Be Performed
1	TRIM CHECK 40, 45, 50, 55, & 60 MPH
2	PHUGON FROM 60 MPH
3	LONGITUDINAL STEP INPUTS AT 60 MPH
4	LONGITUDINAL DOUBLETS AT 60 MPH
5	LATERAL STEP INPUTS AT 60 MPH
6	LATERAL DOUBLETS AT 60 MPH
7	RUDDER STEP INPUTS AT 60 MPH
8	RUDDER DOUBLETS AT 60 MPH
9	
10	

**Data and Comments**

**Test No.1**

Test sequence carried out as briefed in cold air with light turbulence. Tests commenced at 2000ft over airfield on airfield QFE.

TRIM CHECKS Test sequence flown with events at 40mph, 45mph, 50mph, 55mph. Autogyro in slight rate of climb. Re-established level flight at 50mph with event, followed by 55mph and 60mph.

<sup>1</sup> Chris Chadwick, FR Aviation, Bournemouth.

2. Phugoid Initial speed of 60mph. Reduced to 50mph and reset stick to nominal 60mph position. Allowed oscillation to continue over 3-4 cycles. Repeated phugoid tests with events. Phugoid was neutral to slightly/slowly divergent with a period of approximately 7 seconds. Control regained by positive pilot input to stop the motion. Manoeuvring the autogyro felt that the phugoid (incipient) was always waiting in the background to be excited.
3. LONG STEP INPUTS 3 or 4 aft step inputs. May have arrested the pitch rate too soon. Very small sharp step inputs could generate a fast pitch rate. With forward step inputs may have been a little shy and reversed with size of input and arrested the motion too soon. These test points may need to be repeated.
4. LONG DOUBLETS 3 pairs of doublets. The autogyro response appeared to be death-beat making the doublet frequency one that did not excite / was harmonious to the autogyro's natural frequency.

The pilot remarks both on the dynamic characteristics of the neutrally stable long term response, and those regarding the aircraft short term reaction to doublet inputs are consistent with the results extracted from both the flight test data and the simulation time responses.

<b>Specifications</b>	<b>VPM M16 Tandem</b>	<b>Air Command Tandem</b>
Engine	40 hp Rotax 447	75 hp Rotax 618
Propeller	66" x 68", wood	Warp Drive 68" 2 blade
Rotor Blades	23' x 7' aluminium /composite	27' x 8" Sky Wheels composite
Min Speed	10 mph	20 mph
Cruise Speed	40 mph	75 mph
Max Speed	70 mph	105 mph
Empty Weight	230 lbs.	400 lbs.
Useful Load	300 lbs.	775 lbs.
Gross Weight	530 lbs.	1155 lbs.
Width	7'4"	5'7"
Height	7'8"	8'10"
Length	12'	13'5"
Cost	unknown	\$17935

**Table 2.1: Basic properties of VPM and Air Command gyroplanes**

<b>GYROPLANE</b>	<b>DESCRIPTION</b>	<b>MANUFACTURER</b>
Air Command 147A	Two-seat, fully enclosed	Air Command International, Inc.
Air Command Single Place	Single-seat, partially enclosed	Air Command International, Inc.
Air Command Tandem	Two-seat, partially enclosed	Air Command International, Inc.
Air Command Side-by-Side	Two-seat, partially enclosed	Air Command International, Inc.
Air & Space 18A	Two-seat, fully enclosed	Air & Space America, Inc.
Bumble Bee	Single-seat, open frame	Aircraft Designs, Inc.
Sportster HA-2M	Two-seat, partially enclosed	Aircraft Designs, Inc.
Barnett J4B	Single-seat, partially ( fully) enclosed	Barnett Rotorcraft
Barnett J4B2	Two-seat, fully enclosed	Barnett Rotorcraft
Cricket	Single-seat, partially enclosed	British Gyroplanes, Ltd.
SnoBird Explorer	Single-seat, open frame	Calumet Motorsports, Inc.
SnoBird Exciter	Single-seat, open frame	Calumet Motorsports
Sycamore MK1	Two-seat, fully enclosed	Chayair Manufacturing & Aviation
Twinstar	Two-seat, partially enclosed	Farrington Aircraft Corp.
Midnight Hawk	Single-seat, partially enclosed	Gyro-Kopp-Ters
Montgomerie Merlin	Single-seat, partially enclosed	Jim Montgomerie Gyrocopters
Super Bandit	Two-seat, partially enclosed	Joe Souza Gyroplanes, Inc.
Brock KB-2	Single-seat, open frame	Ken Brock Manufacturing, Inc.
Brock KB-3	Single-seat, open frame	Ken Brock Manufacturing, Inc.
Little Wing Rotor-Pup	Single-seat, partially enclosed	Little Wing Autogyros, Inc.
Little Wing LW-2	Single-seat, fully enclosed	Little Wing Autogyros, Inc.
Little Wing LW-3	Single-seat, fully enclosed	Little Wing Autogyros, Inc.
Little Wing two-place	Two-seat, fully enclosed	Little Wing Autogyros, Inc.
Mad Max	Single(two)-seat open frame	Mad Max Aero
Magni M-18 Spartan	Single-seat, partially enclosed	Magni Gyro
Magni M-14 Scout	Two-seat, partially enclosed	Magni Gyro
Magni M-16 Trainer	Two-seat, partially enclosed	Magni Gyro
Marchetti Avenger	Two-seat, open frame	Marchetti Engineering
Pitbull	Single-seat, partially enclosed	North American Rotorwerks
Gyrobee	Single-seat, open frame	Ralph Taggart
RAF 200	Two-seat, fully enclosed	Rotary Air Force
Sport Copter Lightning	Single-seat, partially enclosed	Sport Copter, Inc.
Sport Copter Vortex	Single-seat, partially enclosed	Sport Copter, Inc.
Skyhook	Single-seat, partially (fully) enclosed	The Australian Autogyro Co.

**Table 2.2: A catalogue of contemporary gyroplane types**

<b>Properties</b>	<b>RAF 2000</b>	<b>ROBINSON R-22</b>
Maximum Airspeed (mph)	100	118
Maximum Cruise (mph)	80	110
Maximum Range (miles)	250	200
Fuel Consumption G..P.H	6	7.5
Rate of Climb (feet/min)	1000	1000
Maximum Ceiling (feet)	10,000	14,000
Empty Weight (lbs)	830	826
Gross Weight (lbs)	1540	1370
Useful Load (lbs)	600	544
Cost	\$21500	\$125000

**Table 2.3: RAF 2000 and Robinson R-22 comparison<sup>1</sup>**

<sup>1</sup> Table extracted from Rotary Air Force commercial brochure

PROPERTY	SPECIFICATION
Cruise speed	60 knots
Maximum speed	80 knots
Range	150 km
Endurance	2h 30min
Time-to-climb	5 min to 3000 feet / 10 min to 5000 feet, at ISA +10 deg C
Maximum weight	280 kg
Payload provision	80 kg
Power supply	12 V electrical system

**Table 3.1: Montgomerie-Parsons gyroplane technical specification**

PARAMETER	DESCRIPTION	UNITS	SENSOR
$a_x$	Longitudinal Acceleration	g	Accelerometer
$a_y$	Lateral Acceleration	g	Accelerometer
$a_z$	Normal Acceleration	g	Accelerometer
$P$	Roll Rate	deg/s	Rate Gyro
$Q$	Pitch Rate	deg/s	Rate Gyro
$R$	Yaw Rate	deg/s	Rate Gyro
$\Phi$	Roll Attitude	deg	Angle Indicator
$\Theta$	Pitch Attitude	deg	Angle Indicator
$\Psi$	Yaw Attitude	deg	Angle Indicator
$V_f$	Airspeed	m/s	Air Data Probe
$P_s$	Static Pressure	mbar	Air Data Probe
$H$	Altitude	m	Air Data Probe
$T_{temp}$	Air temperature	deg Celsius	Temperature Sensors
$\alpha_{probe}$	Angle of Attack	deg	Air Data Probe
$\beta_{probe}$	Angle of Sideslip	deg	Air Data Probe
$\Theta_{ls}$	Longitudinal Rotor Tilt	deg	Position Transducer
$\Theta_{lc}$	Lateral Rotor Tilt	deg	Position Transducer
$\Theta_{rud}$	Rudder deflection	deg	Position Transducer
$\Omega$	Rotorspeed	rpm	Photoelectric Sensor
$\Omega_p$	Propeller speed	rpm	Photoelectric Sensor

**Table 3.2: Sensors and measured parameters**

INSTRUMENT	MANUFACTURER	MEASURED QUANTITY
Angle indicators	British Aerospace Systems & Equipment	Aircraft angular attitudes
Rate gyroscopes	British Aerospace Systems & Equipment	Aircraft angular rates
1-axis accelerometer	Seika, Scientific Electro Systems Ltd.	Aircraft vertical acceleration
3-axis accelerometer	British Aerospace Systems & Equipment	Aircraft linear accelerations
Air data probe	Space Age Control, Inc.	Aircraft velocity, height aerodynamic angles
Thermocouple	RS components	Atmospheric temperature
Position transducers	Space Age Control, Inc.	Pilot controls
Electro-optical sensors	RS components	Main rotor, propeller speed
PC recorder	Kontron Elektronik	Record and store sensor outputs

**Table 3.3: Instrumentation list**

File name	Channel No.	Measured quantity
<b>accel1.dat</b>	<b>11</b>	<b>Vertical Acceleration</b>
accelref.dat	24	Vertical acceleration zero reference
<b>accelx.dat</b>	<b>12</b>	<b>X-axis acceleration</b>
<b>accely.dat</b>	<b>13</b>	<b>Y-axis acceleration</b>
<b>accelz.dat</b>	<b>14</b>	<b>Z-axis acceleration</b>
<b>alpha.dat</b>	<b>16</b>	<b>Alpha vane deflection</b>
attref.dat	23	Angle attitudes zero reference
<b>beta.dat</b>	<b>17</b>	<b>Beta vane deflection</b>
<b>height.dat</b>	<b>21</b>	<b>Vertical height position</b>
info.dat	No channel	Information on flight conditions
monitor.dat	28	Event button pulse
<b>pitch.dat</b>	<b>5</b>	<b>Pitch attitude</b>
<b>pitchr.dat</b>	<b>9</b>	<b>Pitch rate</b>
<b>pos1.dat</b>	<b>26</b>	<b>Forward stick position</b>
<b>pos2.dat</b>	<b>2</b>	<b>Lateral stick position</b>
<b>pos3.dat</b>	<b>1</b>	<b>Rudder deflection</b>
prateref.dat	3	Pitch rate zero reference
<b>pressure.dat</b>	<b>19</b>	<b>Atmospheric pressure</b>
<b>prop.dat</b>	<b>0</b>	<b>Propeller speed</b>
<b>roll.dat</b>	<b>4</b>	<b>Roll attitude</b>
<b>rollr.dat</b>	<b>8</b>	<b>Roll rate</b>
<b>rotor.dat</b>	<b>25</b>	<b>Rotorspeed</b>
rrateref.dat	22	Roll rate zero reference
<b>temp1.dat</b>	<b>15</b>	<b>Air-temperature 1</b>
<b>temp2.dat</b>	<b>20</b>	<b>Air-temperature 2</b>
<b>velocity.dat</b>	<b>18</b>	<b>Dynamic pressure</b>
<b>yaw.dat</b>	<b>6</b>	<b>Yaw attitude</b>
<b>yawr.dat</b>	<b>10</b>	<b>Yaw rate</b>
yrateref.dat	27	Yaw rate zero reference

**Table 3.4: Transducer signal output file names**

<b>Test Phases</b>	<b>Task Title</b>	<b>Objectives</b>	<b>Manoeuvres</b>	<b>Flight time</b>
Stage 1	Shakedown Flying	To assess instrumentation functionality and to familiarise pilot with flight test vehicle	No rigorous manoeuvre schedule imposed	5 hr
Stage 2	Basic performance and trim flying	To assess basic performance and static stability characteristics	Perform climbs and descents at varying speeds  Trim aircraft at 5 mph speed increments between 30 and 70 mph	5 hr
Stage 3	Dynamic response (step/doublet inputs)	To assess dynamic stability characteristics by means of step and doublet pilot inputs	Step and doublet inputs applied to longitudinal stick  Doublet inputs applied to lateral stick and rudder	5 hr

**Table 3.5: Flight manoeuvre scheduling**

### FLIGHT TEST PLAN

1. Carry out normal take-off
2. At a nominal height of 2,000 ft, carry out level flight trims at 40, 45, 50, 55, 60 mph
3. At a speed of 60 mph and a nominal height of 2,000 ft, excite the aircraft's phugoid by reducing the airspeed by 5-10 mph and noting the aircraft's open loop response.
4. At a speed of 60 mph and a nominal height of 2,000 ft, carry out a series of aft and forward step inputs on the longitudinal control. Inputs are to be made in an incremental fashion up to a maximum input of 10% when the aircraft's response reaches  $5^{\circ}$  -  $10^{\circ}$  attitude response.
5. At a speed of 60 mph and a nominal height of 2,000 ft, carry out a series of doublet inputs on the longitudinal control both with an aft and forward input first. Inputs are to be made in an incremental fashion up to a maximum input of 10% when the aircraft's response reaches  $5^{\circ}$  -  $10^{\circ}$  attitude response.
6. At a speed of 60 mph and a nominal height of 2,000 ft, carry out a series step inputs on the lateral control both left and right. Inputs are to be made in an incremental fashion up to a maximum input of 10% when the aircraft's response reaches  $5^{\circ}$  -  $10^{\circ}$  attitude response.
7. At a speed of 60 mph and a nominal height of 2,000 ft, carry out a series of doublet inputs on the lateral control with both left and right inputs first. Inputs are to be made in an incremental fashion up to a maximum input of 10% when the aircraft's response reaches  $5^{\circ}$  -  $10^{\circ}$  attitude response.
8. At a speed of 60 mph and a nominal height of 2,000 ft, carry out a series step inputs on the pedals both left and right. Inputs are to be made in an incremental fashion up to a maximum input of 10% when the aircraft's response reaches  $5^{\circ}$  -  $10^{\circ}$  attitude response.
9. At a speed of 60 mph and a nominal height of 2,000 ft, carry out a series of doublet inputs on the pedals both with left and right inputs first. Inputs are to be made in an incremental fashion up to a maximum input of 10% when the aircraft's response reaches  $5^{\circ}$  -  $10^{\circ}$  attitude response.
10. Carry out normal landing

**Table 3.6: Flight test pilot instructions**

<b>Rotor Dynamics</b>	<ul style="list-style-type: none"> <li>• Up to 10 individually modelled rigid blades</li> <li>• Fully coupled flap, lag and feather motion</li> <li>• Blade attachment of offset hinges and springs</li> <li>• Linear lag damper</li> </ul>
<b>Rotor loads</b>	<ul style="list-style-type: none"> <li>• Aerodynamic and inertial loads represented by up to 10 elements per blade</li> </ul>
<b>Blade aerodynamics</b>	<ul style="list-style-type: none"> <li>• Lookup tables for lift and drag as function of angle of attack and Mach number</li> </ul>
<b>Wake model</b>	<ul style="list-style-type: none"> <li>• Peters HaQuang dynamic inflow model</li> </ul>
<b>Transmission</b>	<ul style="list-style-type: none"> <li>• Coupled rotor speed and engine dynamics</li> <li>• Up to 3 engines</li> <li>• Geared or independently controlled rotor torque</li> </ul>
<b>Airframe</b>	<ul style="list-style-type: none"> <li>• fuselage, tailplane, fin and rudder aerodynamics by lookup tables or polynomial functions</li> </ul>
<b>Atmosphere</b>	<ul style="list-style-type: none"> <li>• International Standard Atmosphere</li> <li>• Provision for variation of sea-level temperature and pressure</li> </ul>

**Table 4.1: Key elements of RASCAL model**

<b>Fuselage data</b>		
Side area		0.798 m <sup>2</sup>
Plan area		0.916 m <sup>2</sup>
Frontal area		0.448 m <sup>2</sup>
Centre of pressure co-ordinates		(1.626,0,-0.480)
<b>Tailplane data</b>		
Area		0.356 m <sup>2</sup>
Centre of pressure co-ordinates		(-1.020,0,-0.057)
<b>Fin data</b>		
Area		0.281 m <sup>2</sup>
Centre of pressure co-ordinates		(-1.00,0,-0.268)
<b>Rudder data</b>		
Area		0.368 m <sup>2</sup>
Centre of pressure co-ordinates		(-1.633,0,-0.392)
<b>Endplate data</b>		
Area		0.107 m <sup>2</sup>
Centre of pressure co-ordinates		(-1.090,0.45,-0.057)
<b>Main rotor data</b>		
Radius	3.81 m	
Chord	0.197 m	
Flapping inertia	63.62 kgm <sup>2</sup>	
Mass	13.15 kg	
Airfoil	NACA 8-H-12	
Hub pivot point co-ordinates		(-0.038,0,-2.105)
<b>Propeller data</b>		
Radius	0.787 m	
Chord	0.09 m	
Hub pivot point co-ordinates		(-0.950,0,-0.795)
Orientation of thrust line	1 deg nose down	

**Table 4.2: Montgomerie-Parsons gyroplane sizing parameters**

PARAMETER	RESULT
Airframe weight	220.3 kg
Blade assembly weight	32.2 kg
Pilot weight	85.1 kg
Total weight	337.6 kg

**Table 4.3: Aircraft weight results**

PARAMETER	RESULT
$W_b$	67.8 kg
$l_b$	1.11 m
$W_i$	1.3 kg
$l_i$	0.94 m
$l_s$	2.105 m
$X_{SP}$	0.038 m
$\theta_s$	9° 25'
$X_{CG}$	<b>0.196</b>
$Z_{CG}$	<b>-0.695</b>

**Table 4.4: Centre of gravity results (not including rotor blades)**

ITEM	Longitudinal CG			Vertical CG		
	Weight (kg)	Arm (m)	(Moment) (kgm)	Weight (kg)	Arm (m)	(Moment) (kgm)
Aircraft	305.4	0.196	59.858	305.4	- 0.695	-212.253
Blades	32.19	-0.038	-1.052	32.19	- 2.105	-67.670
Total	337.59		58.806	337.59		-279.923
cg co-ordinates		<b>0.174</b>			<b>- 0.830</b>	

**Table 4.5: Blade mass effect**

PARAMETER	ROLL INERTIA	PITCH INERTIA
Period (s)	2.4	2.8
Moment of inertia (kgm <sup>2</sup> )	72.96	297.21

**Table 4.6: Roll and pitch moment of inertia results**

## Configurational Data for the Montgomerie Gyroplane

<i>Gross Mass</i>	337.6 kg	<i>Fuselage Data :</i>	
		Side Area	0.798 m <sup>2</sup>
<i>Moments of Inertia</i>		Plan Area	0.916 m <sup>2</sup>
lxx	72.96 kg m <sup>2</sup>	Frontal Area	0.448 m <sup>2</sup>
lyy	297.21 kg m <sup>2</sup>	Lift curve Slope	3.5/rad
lzz	300 kg m <sup>2</sup> *		
		<i>Tailplane Data :</i>	
<i>Co-ordinates (in metres) for :</i>		Area	0.356 m <sup>2</sup>
Centre of Gravity	(0.174,0,-0.83)	Setting Angle	0 deg
Hub Plate Pivot Point	(-0.038,0,-2.105)	Lift curve Slope	3.5/rad
Propeller Hub	(-0.950,0,-0.795)		
Fuselage C.P.	(1.626,0,-0.480)	<i>Fin Data :</i>	
Tailplane C.P.	(-1.02,0,-0.057)	Area	0.281 m <sup>2</sup>
Fin C.P.	(-1.00,0,-0.268)	Setting Angle	0 deg
End Plate C.P.	(-1.09,0.45,-0.063)	Lift curve Slope	3.5/rad
Rudder C.P.	(-1.633,0,-0.392)		
		<i>Endplate Data :</i>	
<i>Rotor Blade Parameters :</i>		Area	0.107 m <sup>2</sup>
Radius	3.81 m	Setting Angle	0 deg
Chord	0.197 m	Lift curve Slope	3.5/rad
Mass	13.15 kg		
Flapping Inertia	63.62 kg m <sup>2</sup>	<i>Rudder Data :</i>	
Shaft Length	0.137	Area	0.368 m <sup>2</sup>
		Setting Angle	0 deg
		Lift curve Slope	3.5/rad
		<i>Propeller Data :</i>	
Cd (frontal area)	1	Blade Radius	0.787 m <sup>2</sup>
Cy (side area)	-2	Blade Chord	0.09 m
Cz (plan area)	2	Blade Twist	0 deg
		Blade Mass	unknown
		Orientation of Thrust Line	1 deg

\* Estimated value

**Table 4.7: Configuration file for baseline simulations**

Case 1, f = 0.25Hz			Case 1, f = 0.5Hz		
Parameter	Value	$F_{par}$	Parameter	Value	$F_{par}$
$R^2$	0.67		$R^2$	0.47	
$F_{tot}$	21.54		$F_{tot}$	19.14	
$X_u (1/s)$	0.0355(0.0210)	2.87	$X_u (1/s)$	0.0377(0.0219)	2.97
$X_w (1/s)$	-0.0097(0.0339)	0.08	$X_w (1/s)$	0.0009(0.0350)	0.0006
$X_q (m/s)$	-3.7574(0.8542)	19.35	$X_q (m/s)$	-4.1768(0.8923)	21.91
$X_\theta (m/s^2)$	-4.9099(1.7592)	7.79	$X_\theta (m/s^2)$	-5.3823(1.8880)	8.13
Case 2, f = 0.25Hz			Case 2, f = 0.5Hz		
$R^2$	0.49		$R^2$	0.31	
$F_{tot}$	18.21		$F_{tot}$	17.87	
$X_u (1/s)$	0.0219(0.0306)	0.51	$X_u (1/s)$	0.0203(0.0301)	0.45
$X_w (1/s)$	-0.0704(0.052)	1.82	$X_w (1/s)$	-0.0801(0.0511)	2.46
$X_q (m/s)$	-1.0959(1.14150)	0.92	$X_q (m/s)$	-0.6771(1.1201)	0.36
$X_\theta (m/s^2)$	-0.9038(2.3552)	0.15	$X_\theta (m/s^2)$	-0.3153(2.3148)	0.0186

**Table 5.1: X-force derivative values**

Aircraft	Model	Flight
VPM	-0.22 (1/s)	0.047(0.025) (1/s)
Montgomerie	-0.23 (1/s)	0.036(0.021) (1/s)

**Table 5.2: Comparison of VPM, Montgomerie results for  $X_u$**

Case 1, f = 0.25Hz			Case 1, f = 0.5Hz		
Parameter	Value	$F_{par}$	Parameter	Value	$F_{par}$
$R^2$	0.79		$R^2$	0.59	
$F_{tot}$	38.52		$F_{tot}$	31.51	
$Z_u (1/s)$	0.0024(0.0176)	0.02	$Z_u (1/s)$	0.0043(0.0187)	0.05
$Z_w (1/s)$	-0.1252(0.0284)	19.41	$Z_w (1/s)$	-0.1231(0.0300)	16.84
$Z_q (m/s)$	5.2741(0.7170)	54.11	$Z_q (m/s)$	5.3572(0.7643)	49.13
$Z_\theta(m/s^2)$	4.3892(1.4766)	8.84	$Z_\theta(m/s^2)$	4.7430(1.6172)	8.60
Case 2, f = 0.25Hz			Case 2, f = 0.5Hz		
$R^2$	0.79		$R^2$	0.61	
$F_{tot}$	73.17		$F_{tot}$	60.76	
$Z_u (1/s)$	-0.0017(0.0168)	0.01	$Z_u (1/s)$	0.0032(0.01719)	0.0317
$Z_w (1/s)$	-0.1350(0.0286)	22.21	$Z_w (1/s)$	-0.1267(0.0305)	17.28
$Z_q (m/s)$	4.7935(0.6260)	58.64	$Z_q (m/s)$	4.7436(0.6681)	50.42
$Z_\theta(m/s^2)$	3.4490(1.2916)	7.13	$Z_\theta(m/s^2)$	3.7825(1.3807)	7.51

**Table 5.3: Y-force derivative values**

Aircraft	Model	Flight
VPM	-0.93 (1/s)	-0.565(0.057) (1/s)
Montgomerie	-1.19 (1/s)	-0.135(0.029) (1/s)

**Table 5.4: Comparison of VPM, Montgomerie results for  $Z_w$**

Case 1, f = 0.25Hz			Case 1, f = 0.5Hz		
Parameter	Value	$F_{par}$	Parameter	Value	$F_{par}$
$R^2$	0.78		$R^2$	0.76	
$F_{tot}$	98.57		$F_{tot}$	175.39	
$N_v (m/s)$	0.0059(0.0004)	230.62	$N_v (m/s)$	0.0059(0.0002)	406.81
$N_r (1/s)$	-0.1637(0.0197)	69.01	$N_r (1/s)$	-0.1639(0.0148)	122.93
$N_{\theta_{rud}} (m/s^2 deg)$	0.0095(0.0008)	138.83	$N_{\theta_{rud}} (m/s^2 deg)$	0.0095(0.0006)	247.67
Case 2, f = 0.25Hz			Case 2, f = 0.5Hz		
$R^2$	0.97		$R^2$	0.96	
$F_{tot}$	433.50		$F_{tot}$	625.02	
$N_v (m/s)$	0.0090(0.0005)	276.40	$N_v (m/s)$	0.0090(0.0004)	394.22
$N_r (1/s)$	-0.2460(0.0125)	385.38	$N_r (1/s)$	-0.2450(0.0105)	547.30
$N_{\theta_{rud}} (m/s^2 deg)$	0.0124(0.0004)	1026.60	$N_{\theta_{rud}} (m/s^2 deg)$	0.0124(0.0003)	1471.60

**Table 5.5: N-moment derivative values**

Aircraft	Model	Flight
VPM	-0.098	-0.931(0.044)
Montgomerie	-0.14	-0.246(0.013)

**Table 5.6: Comparison of VPM, Montgomerie results for  $N_r$**

AIRCRAFT	VPM	MONTGOMERIE-PARSONS
Tailplane Area (m <sup>2</sup> )	0.9	0.36
Tailplane CP (m)	1.5	1.02
Fuselage Area (m <sup>2</sup> )	1.6	0.92
Fuselage CP (m)	1.2	1.63

**Table 6.1: VPM and Montgomerie-Parsons tailplane and fuselage parameters**

STATES	PHUGOID	DUTCH ROLL	ROTORSPEED	COUPLED MODE 1	COUPLED MODE 2
U	0.9590	0.1257	0.1478	0.4606	0.2309
V	0.1153	0.9519	0.3348	0.2416	0.4776
W	0.2213	0.2403	0.3861	0.6505	0.7832
P	0.0026	0.0919	0.0167	0.0168	0.0698
Q	0.0007	0.0276	0.0011	0.0308	0.0342
R	0.0048	0.0692	0.0096	0.0042	0.0407
$\Phi$	0.0151	0.0382	0.0400	0.0186	0.0346
$\Theta$	0.0039	0.0117	0.0027	0.0340	0.0170
$\Psi$	0.0260	0.0293	0.0225	0.0046	0.0203
$\Omega$	0.1304	0.0623	0.8453	0.5510	0.3090

**Table 6.2: Eigenvectors at 60 mph**

EIGENVALUE PARAMETERS	PHUGOID	DUTCH ROLL	ROTORSPEED	COUPLED MODE 1	COUPLED MODE 2
Frequency (rad/s)	0.18	2.37	0.43	0.91	2.01
Damping ratio	0.98	0.16	1.00	0.21	0.72

**Table 6.3: Frequency and damping of modes at 60 mph**

CG POSITION	ROTOR SPEED EIGENVALUE
10cm below	-0.65
10cm above	+0.06

**Table 6.4: Effect of cg shift on rotor speed mode (60 mph)**

SYSTEM MATRIX	PHUGOID	ROTOR SPEED EIGENVALUE
Full	$\zeta_{ph}=0.75, \omega_{ph}=0.28\text{rad/s}$	-0.38
Decoupled	$\zeta_{ph}=0.45, \omega_{ph}=0.58\text{rad/s}$	-0.08

**Table 6.5: Effect of coupling on phugoid and rotor speed modes (45 mph)**

CG POSITION	$M_w$	PHUGOID	ROTOR SPEED EIGENVALUE
5cm below	0.013	$\zeta_{ph}=0.79, \omega_{ph}=0.35\text{rad/s}$	-0.46
5cm above	-0.011	$\zeta_{ph}=0.86, \omega_{ph}=0.19\text{rad/s}$	-0.34

**Table 6.6: Effect of vertical cg position on phugoid and rotor speed modes (45 mph)**

PARAMETER	BASIC AIRCRAFT	INSTRUMENTED AIRCRAFT
Pilot weight	88 kg	85 kg
Long. cg position	0.156	0.174
Vertical cg position	-0.854	-0.830
Thrust line/cg margin	78 mm	55 mm

**Table 6.7: Effect of instrumentation on cg position**



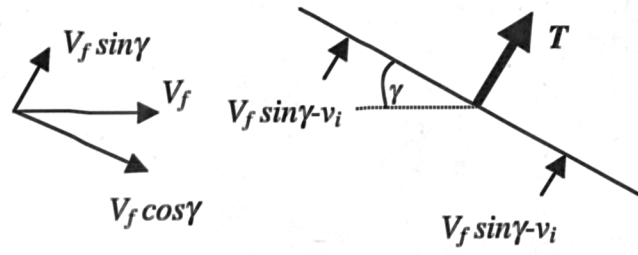


**Figure 1.3: Actuator disc in autorotation**

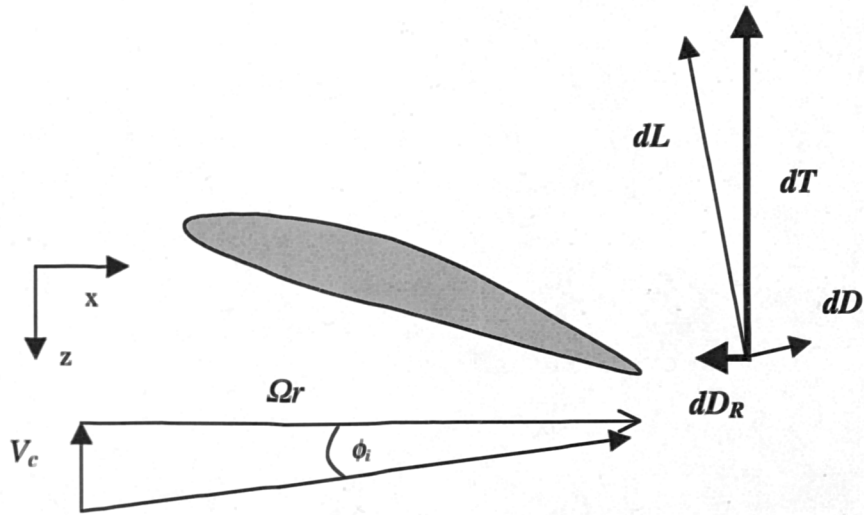


**Figure 1.4: Blade element in autorotation**

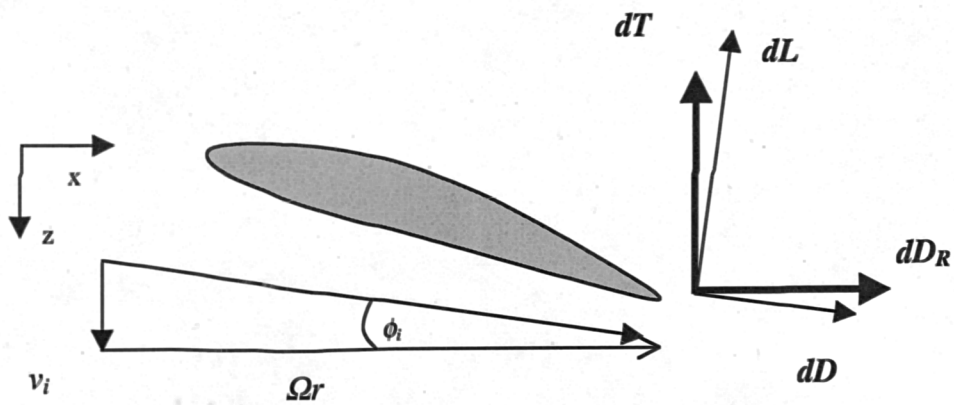


**Figure 1.5: Blade element at power failure instant**

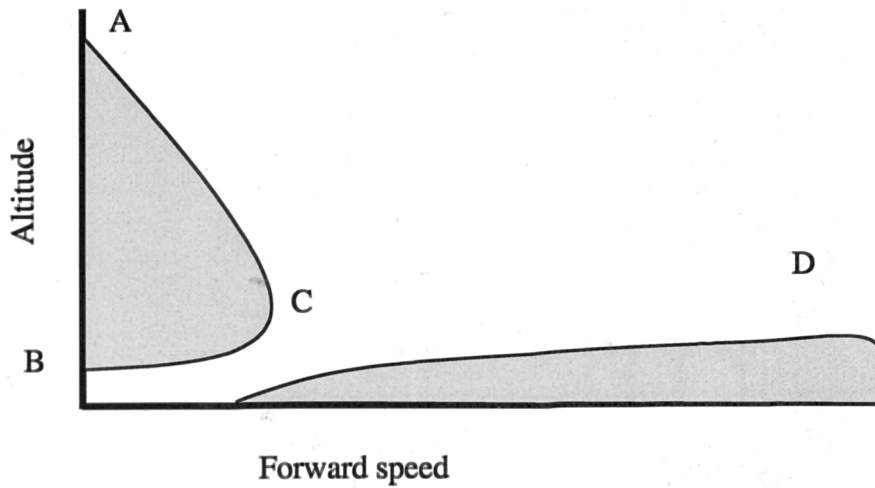


Figure 1.6: Dead man's curve<sup>2</sup>

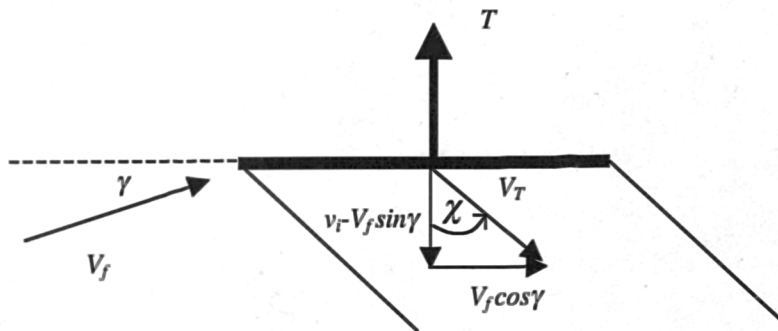


Figure 1.7: Chen's definition of wake skew angle

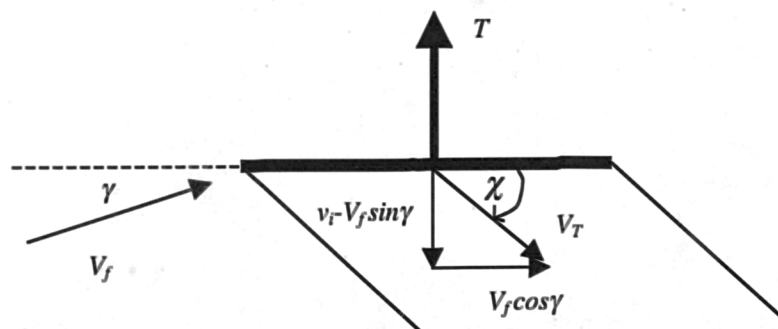
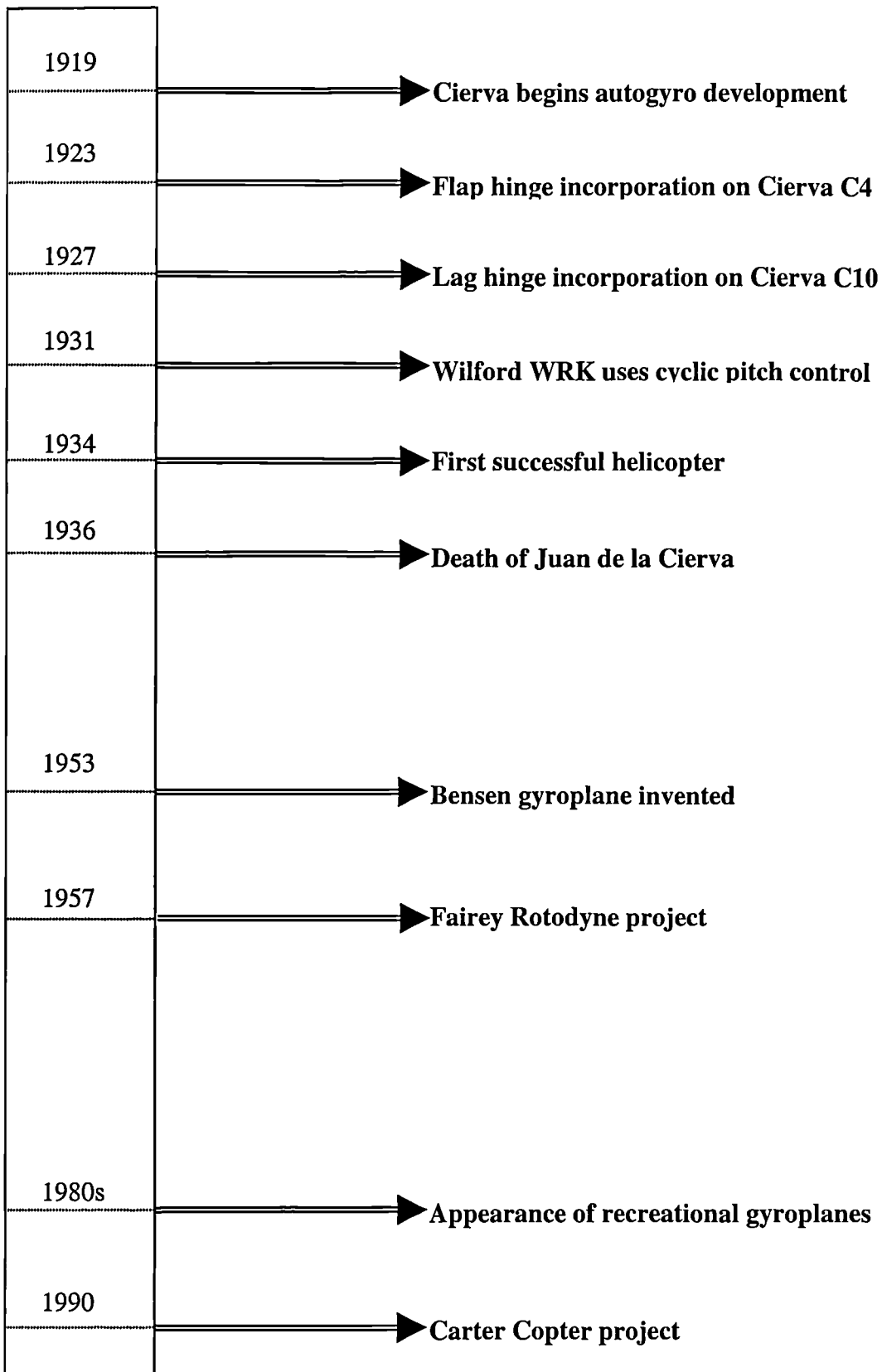


Figure 1.8: Peters HaQuang definition of wake skew angle

<sup>2</sup> Adapted from Newman [1994].



**Figure 1.9: Fully instrumented VPM research gyroplane**



**Figure 2.1: Gyroplane historical development**

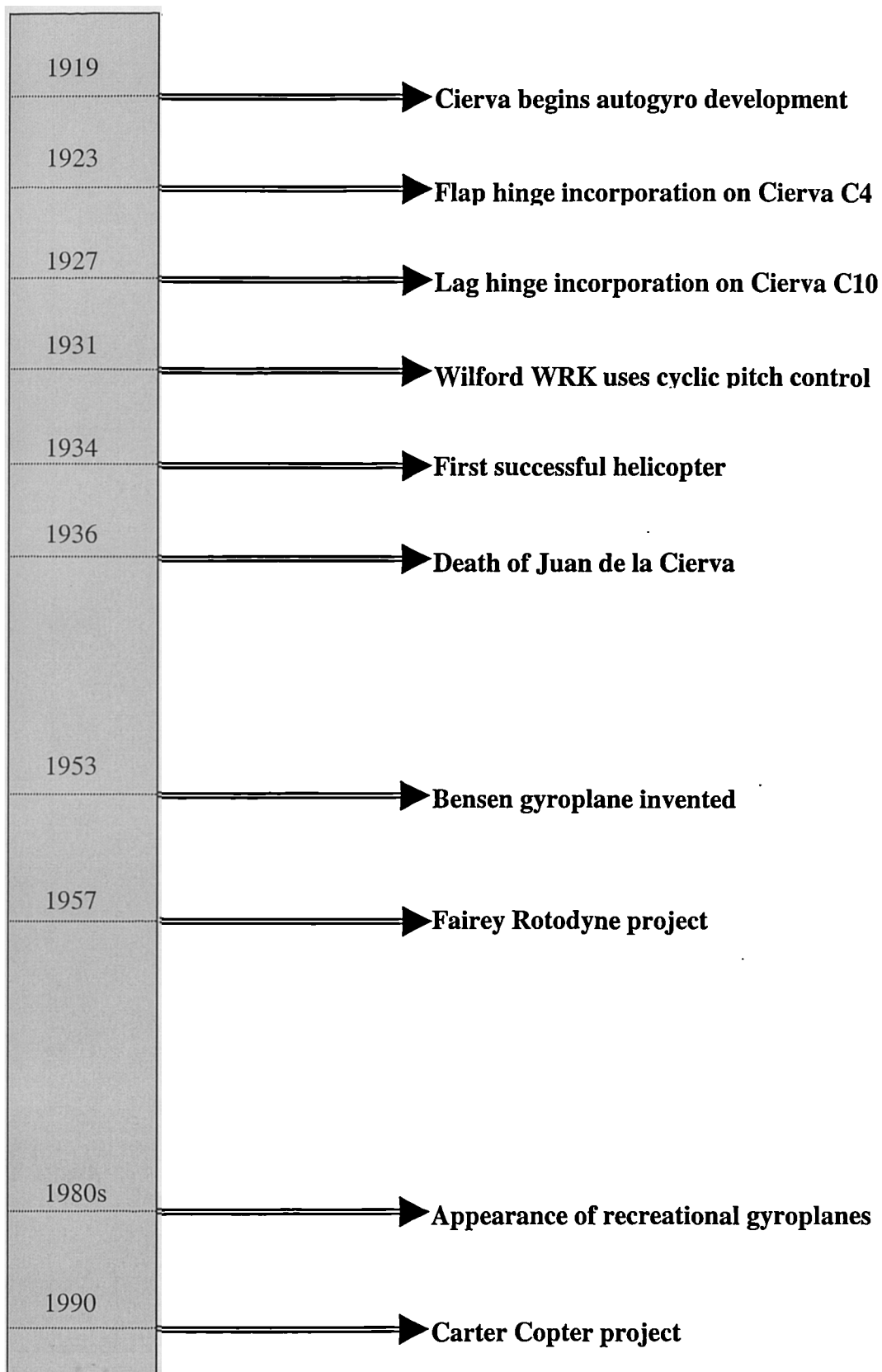


**Figure 2.1: Gyroplane historical development**



**Figure 2.2: The Cierva C-29 gyroplane<sup>1</sup>**



**Figure 2.3: The single seat Air Command gyroplane**

---

<sup>1</sup> Extracted from the Helicopter History Web Site: <http://www.helis.com/default/>



**Figure 2.4: The Air Command two seat gyroplane**



**Figure 2.5: VPM M16 Tandem gyroplane**

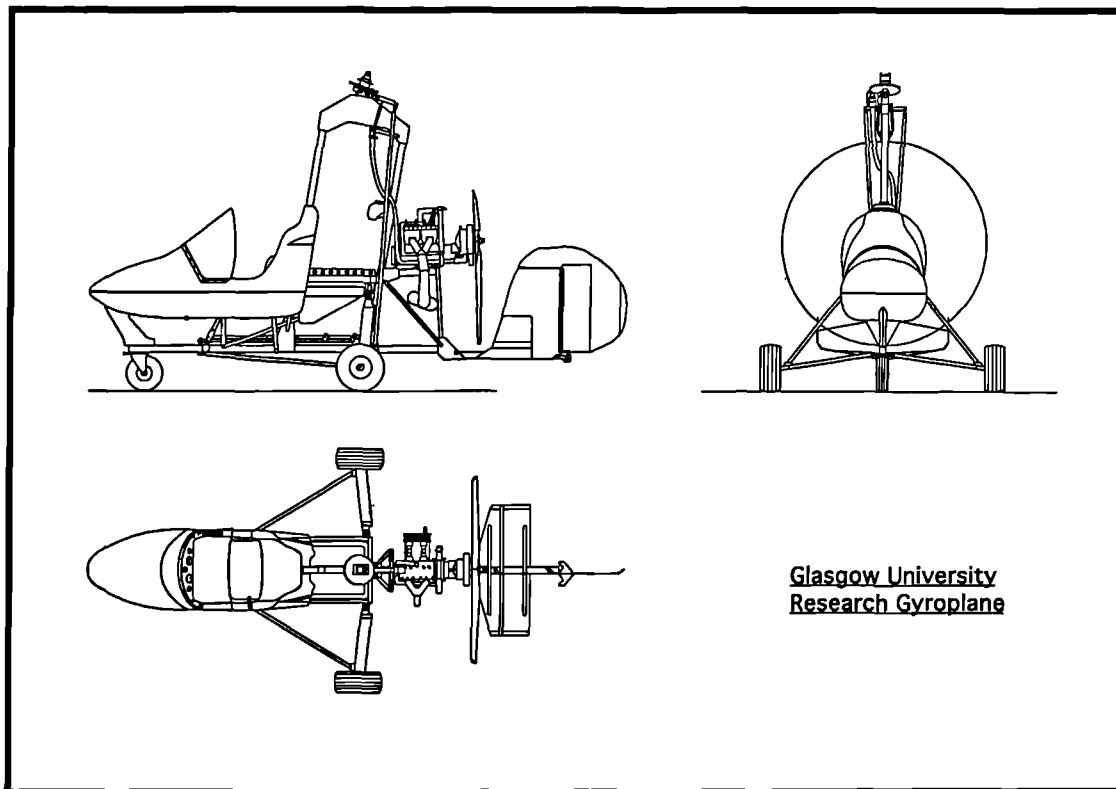


**Figure 3.1: 3-Side view of the Montgomery-Parsons gyroplane**

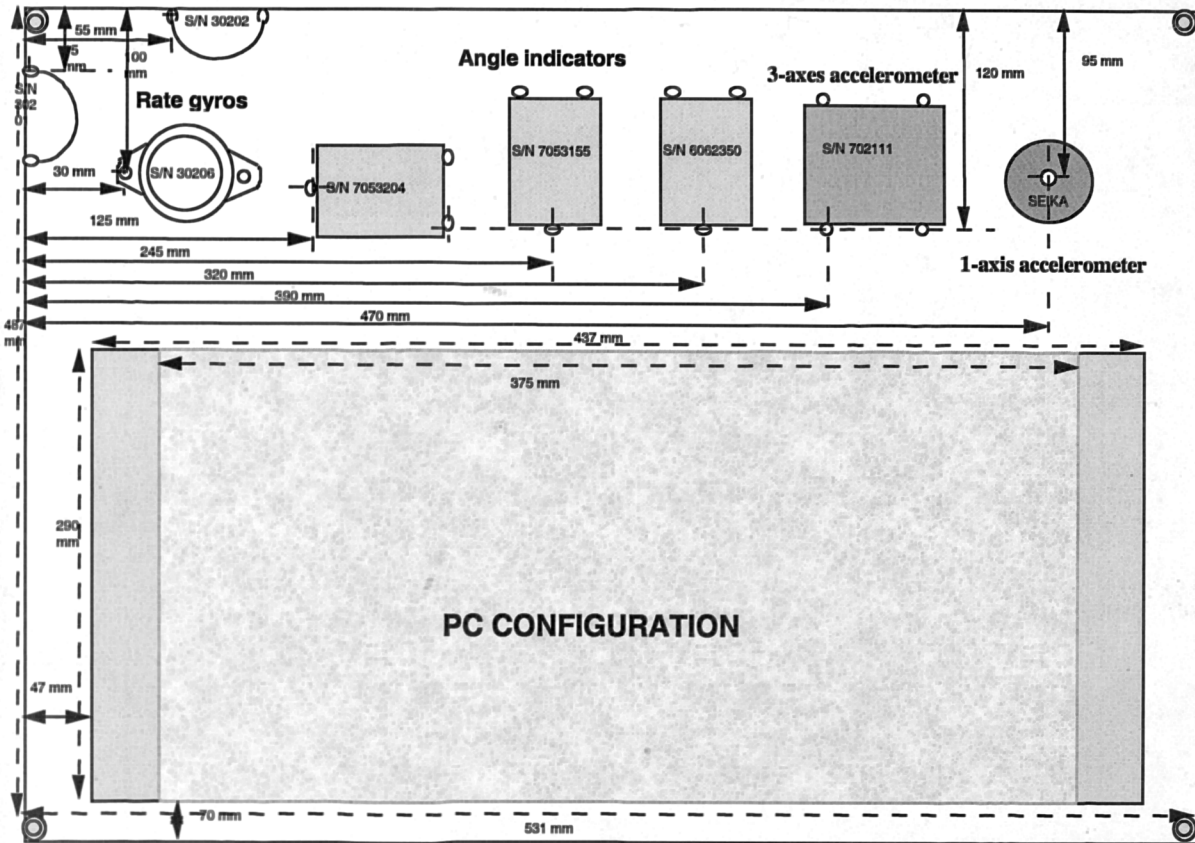
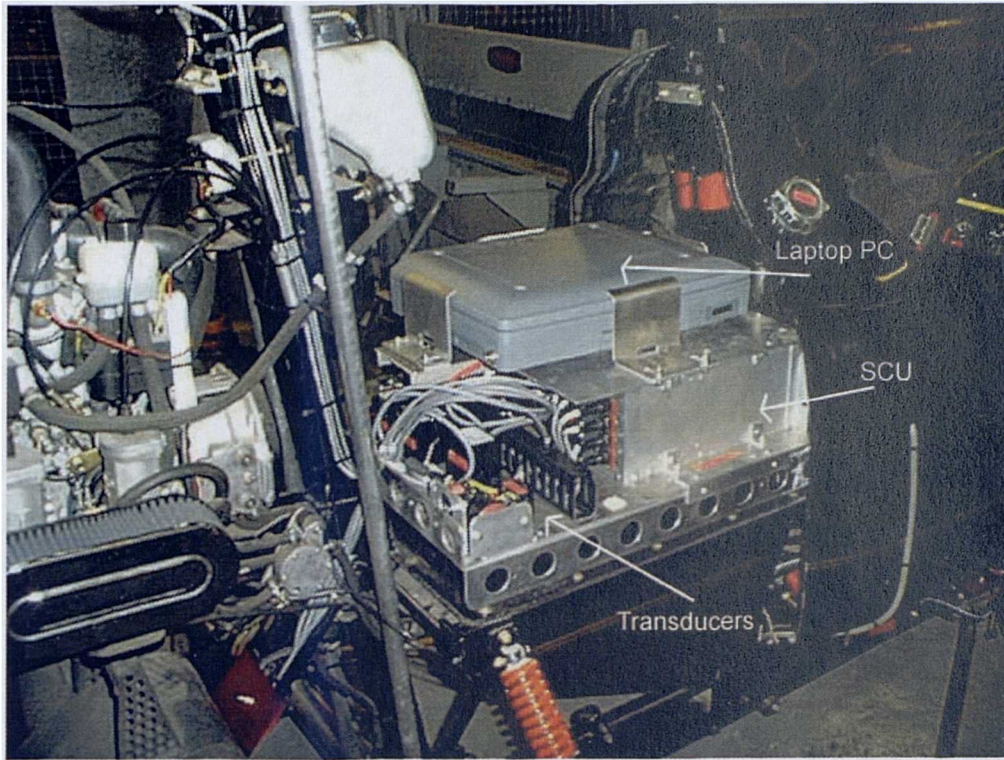
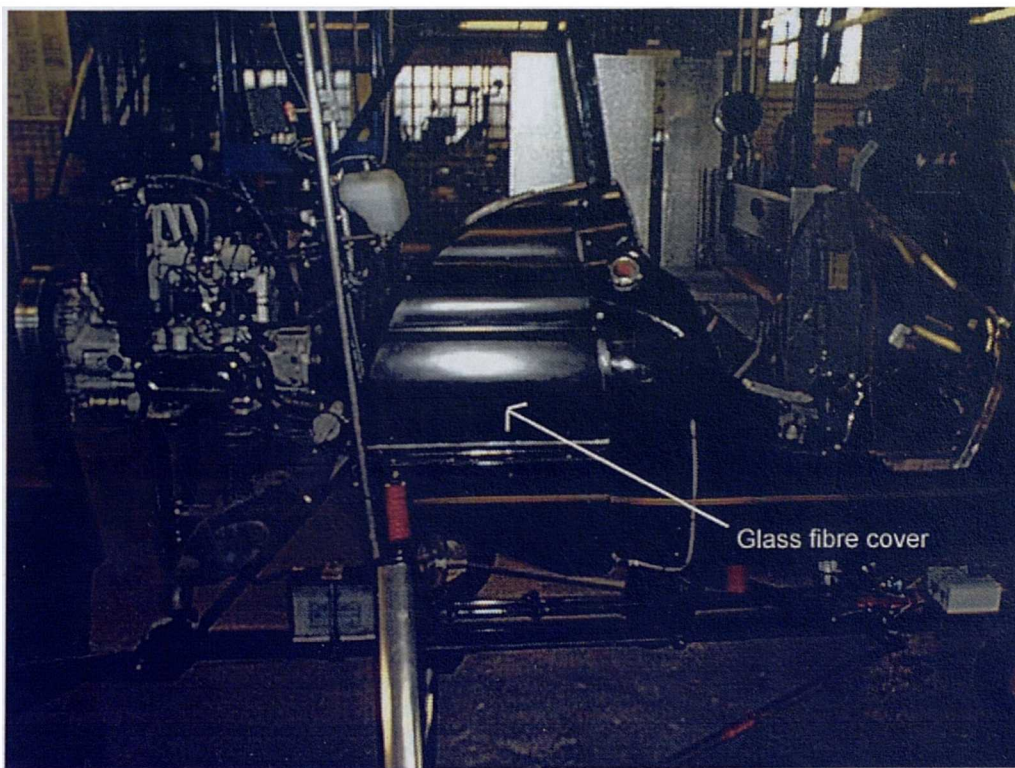


Figure 3.2: The main instrumentation pallet layout



**Figure 3.3: Main instrumentation pallet side-view**



**Figure 3.4: The glass fibre instrumentation cover**

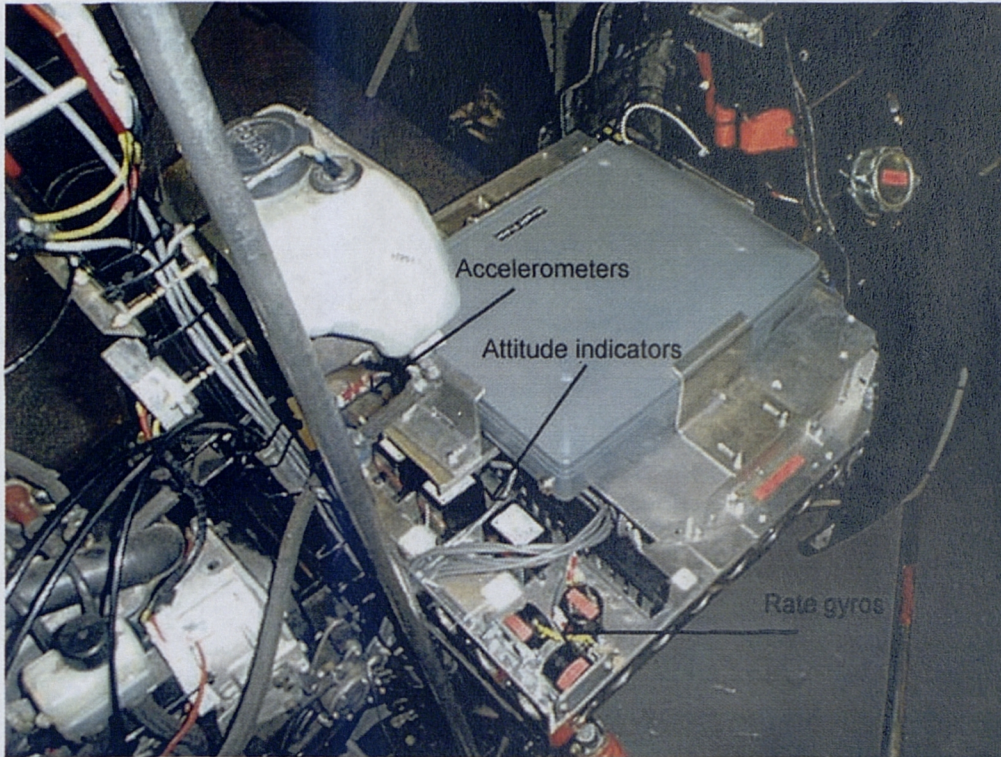


**Figure 3.5: Individual transducers**

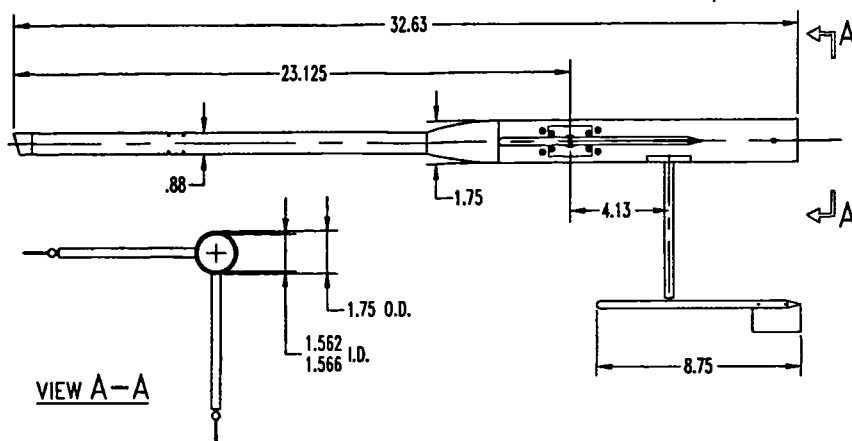


**Figure 3.6: Schematic diagram of air data probe<sup>2</sup>**

<sup>2</sup> Extracted from SpaceAge Control, Inc., air data products catalogue



**Figure 3.7: The air-data probe installation**

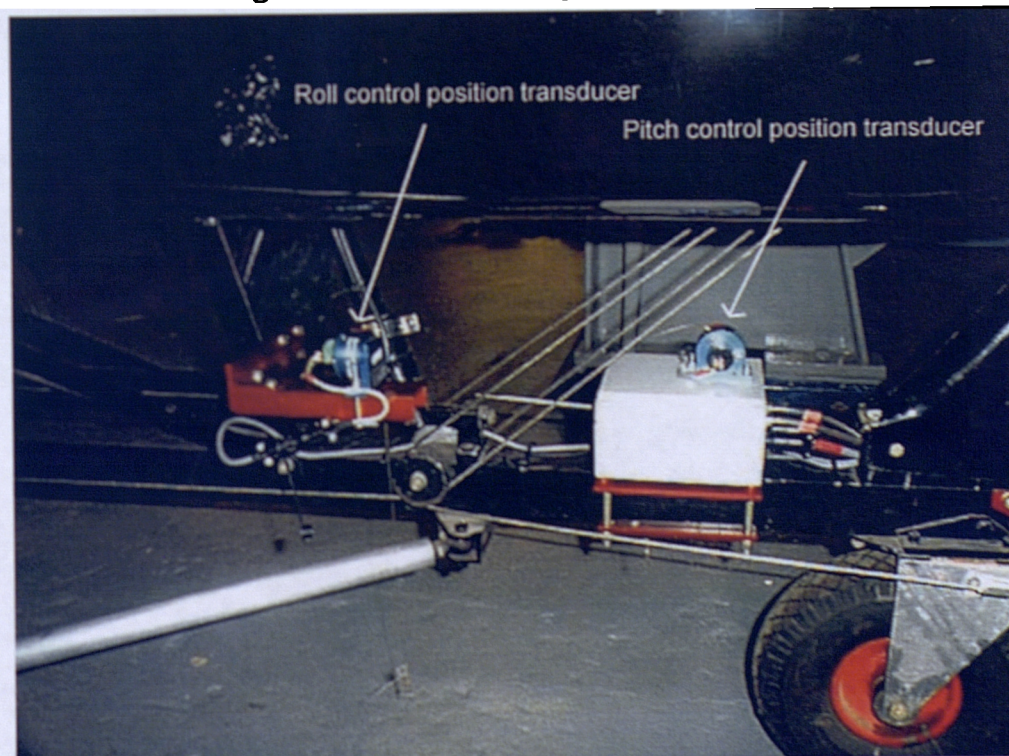


**Figure 3.8: Roll and pitch control position sensors**

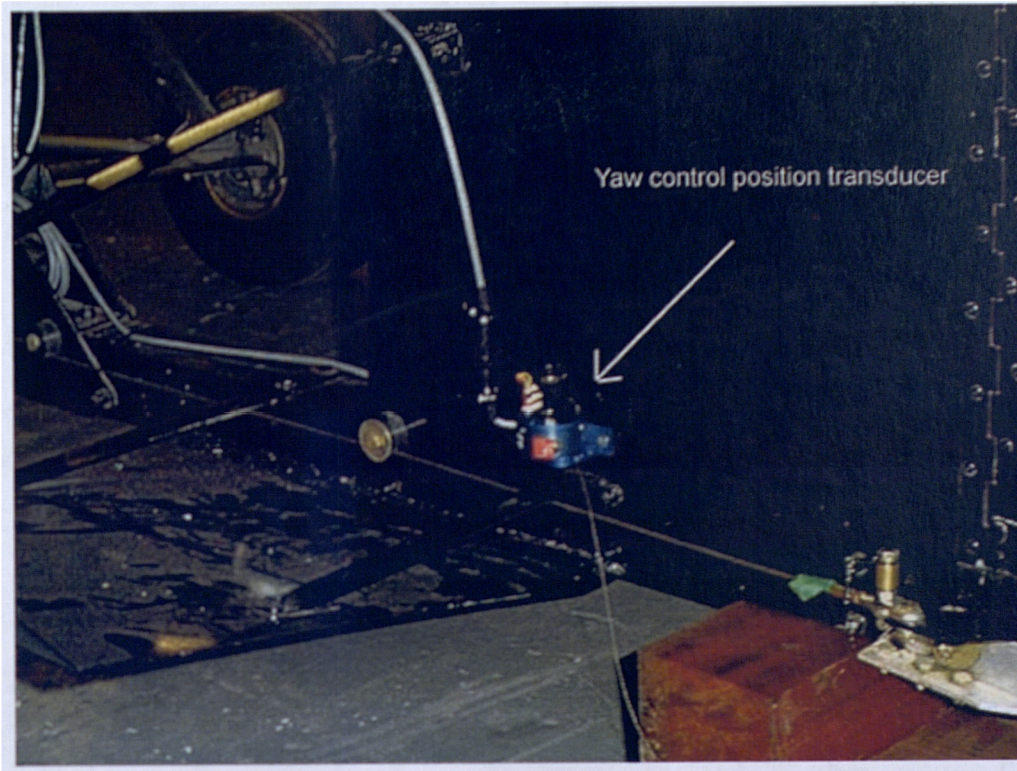


**Figure 3.9: Yaw control position sensor**

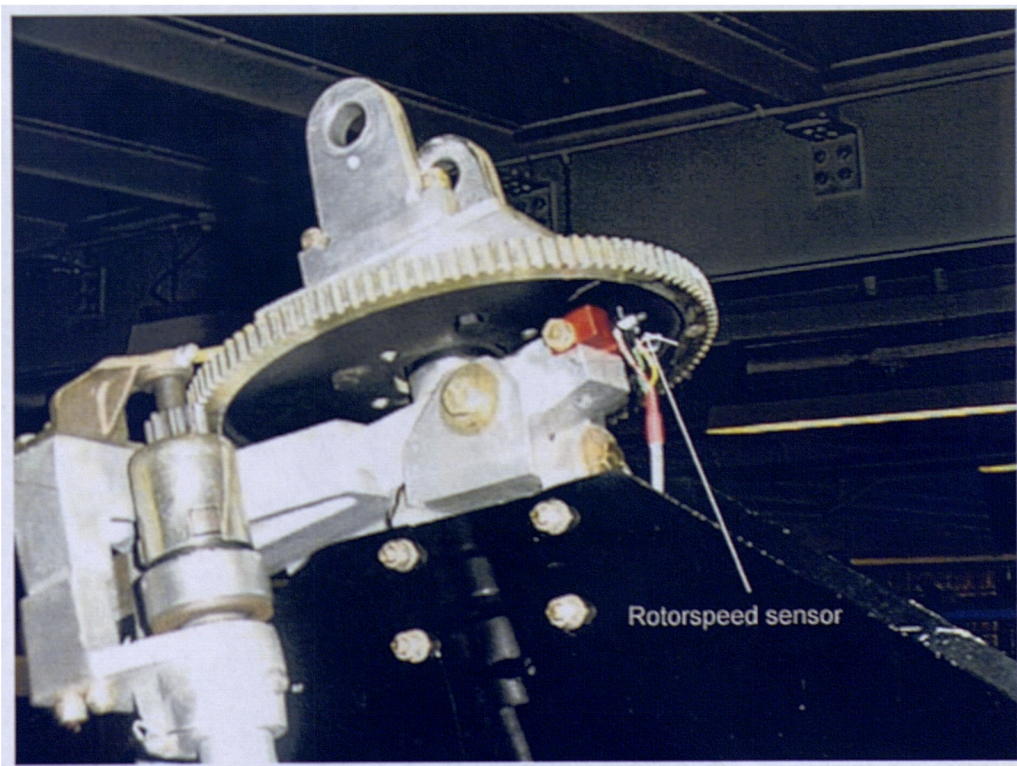


**Figure 3.10: Rotor speed sensor**

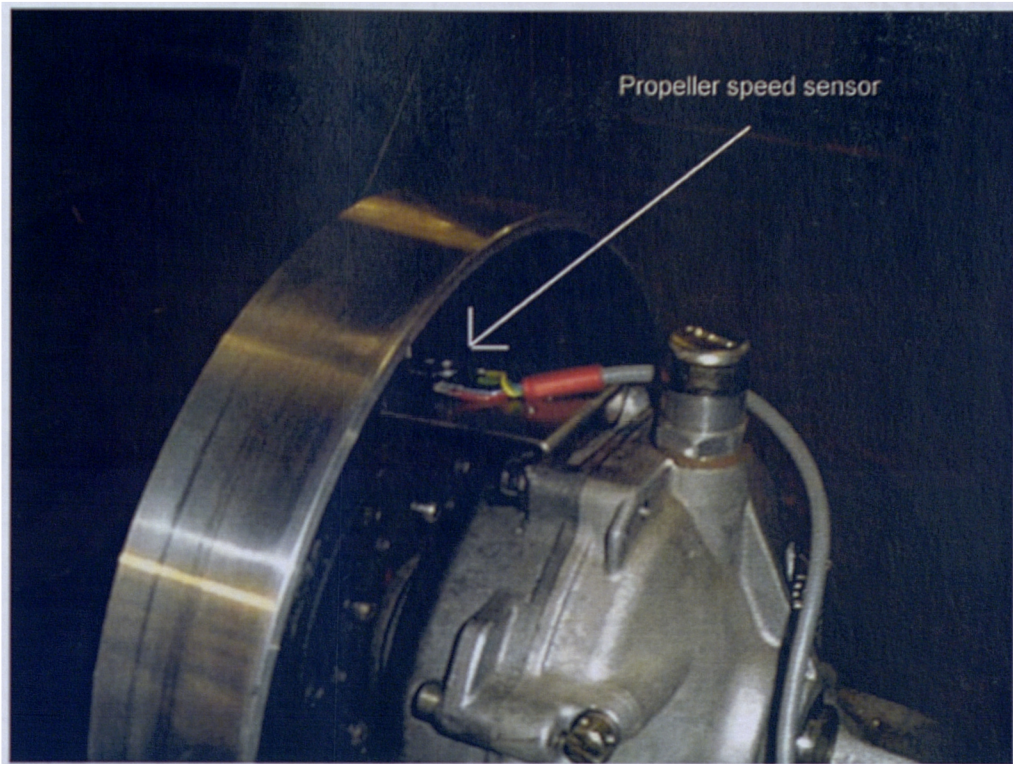


**Figure 3.11: Propeller speed sensor**

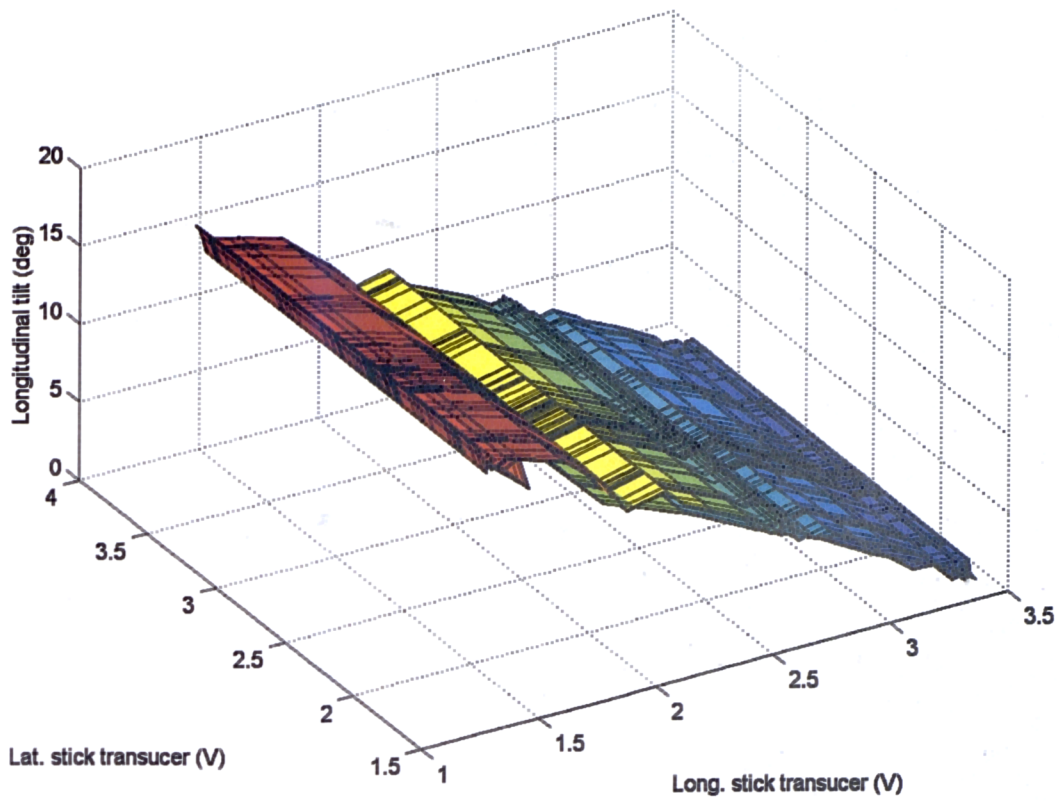


**Figure 3.12: Pilot stick transducer calibration curve**

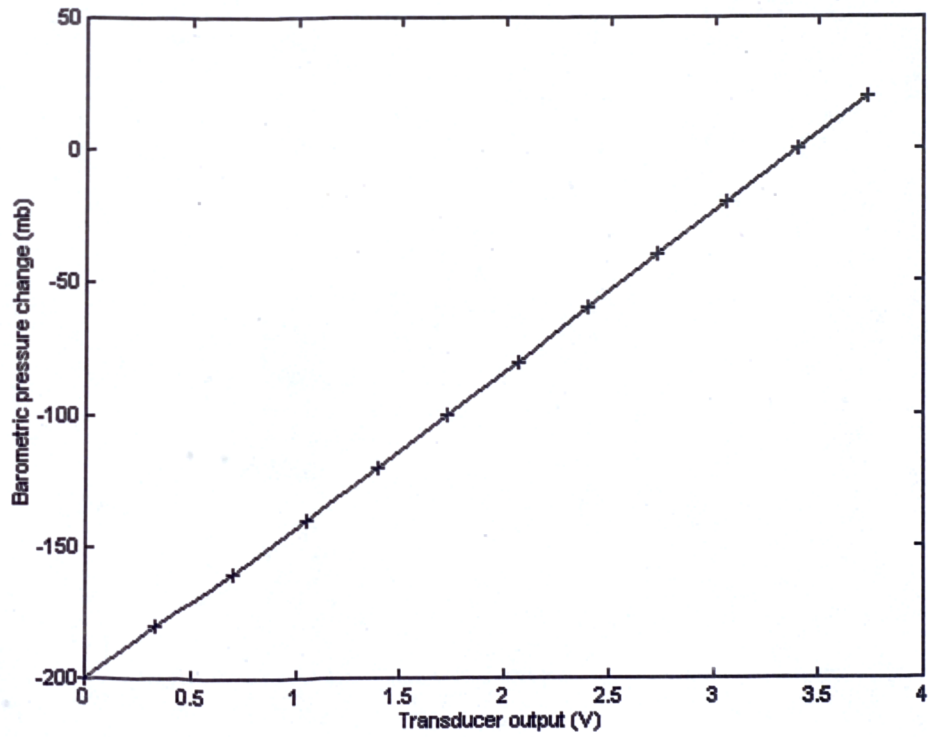


**Figure 3.13: Static pressure transducer calibration curve**

**DATA ACQUISITION SOFTWARE FOR THE MONTGOMERIE RESEARCH GYROPLANE  
(C) VASSILIOS M. SPATHOPOULOS 1999**

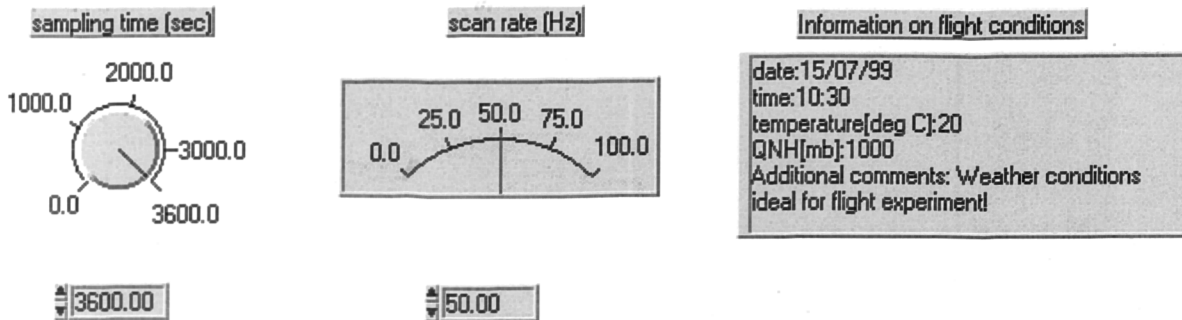


**Figure 3.14: DAQ software user interface**

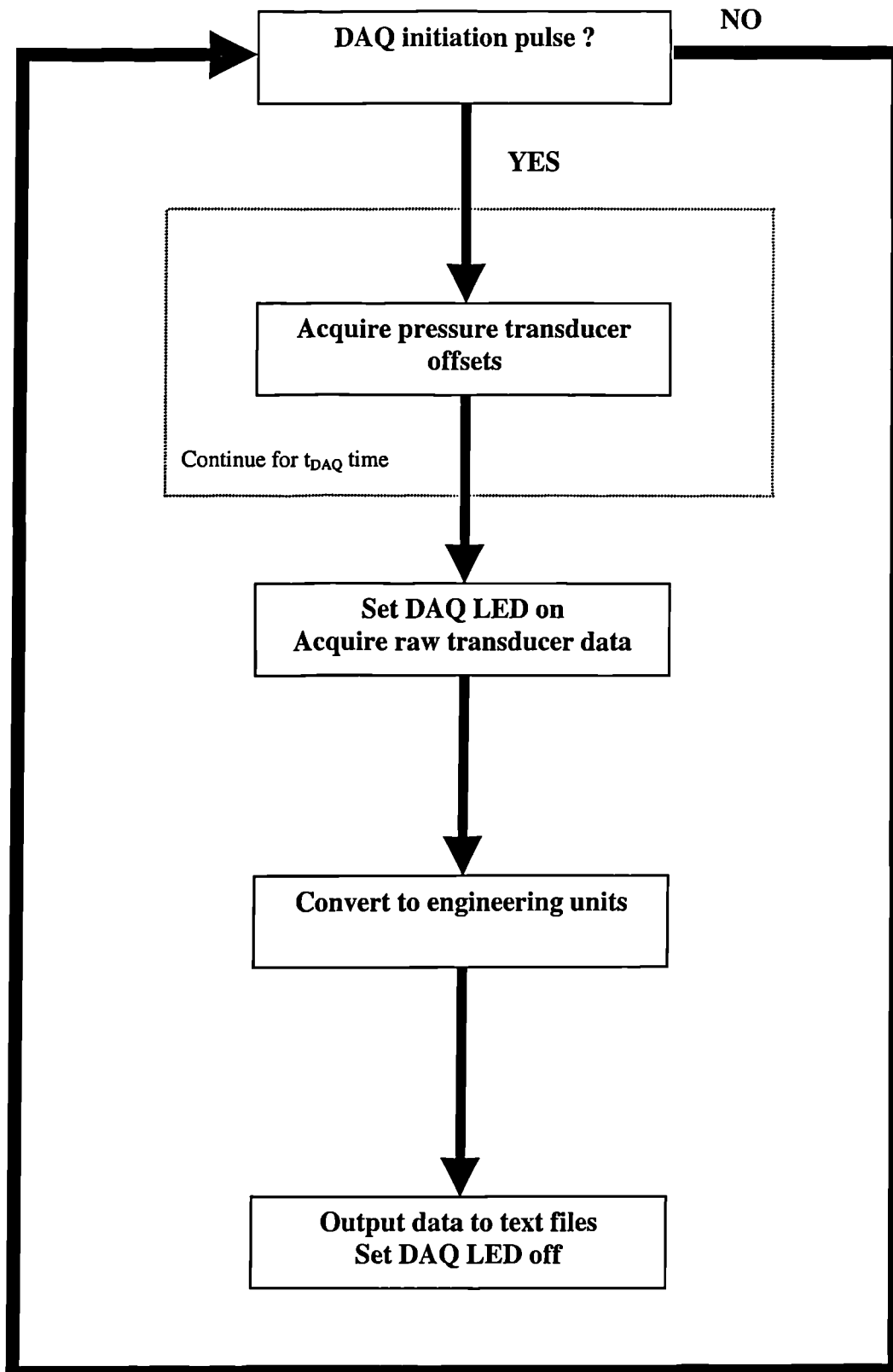


Figure 3.15: DAQ software flow chart

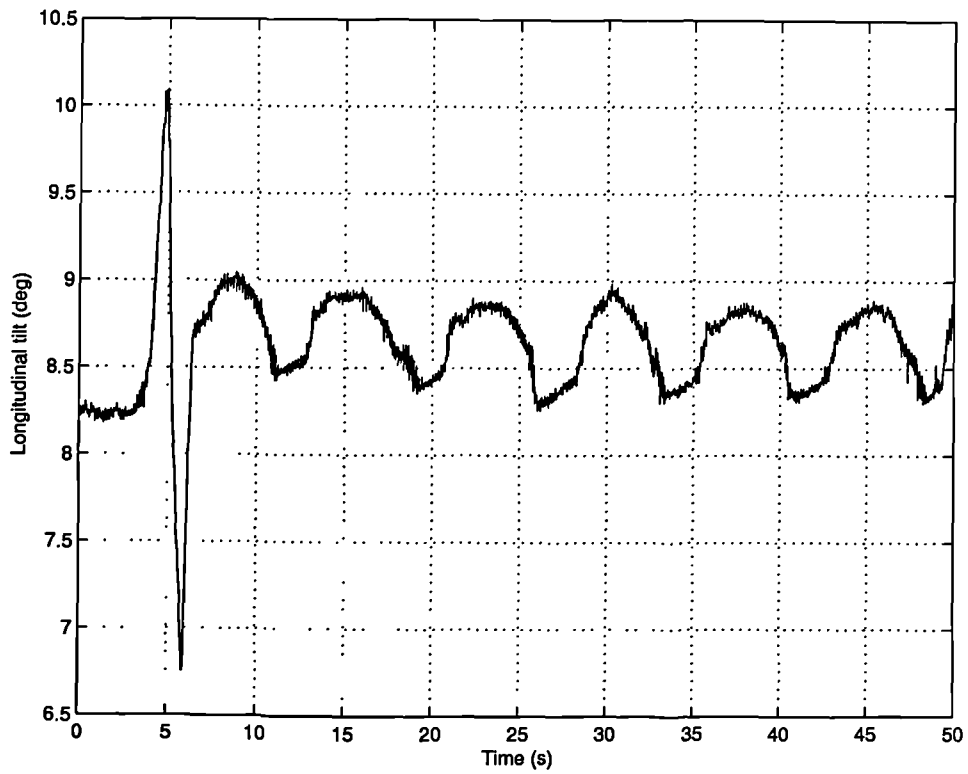


Figure 3.16: Doublet input

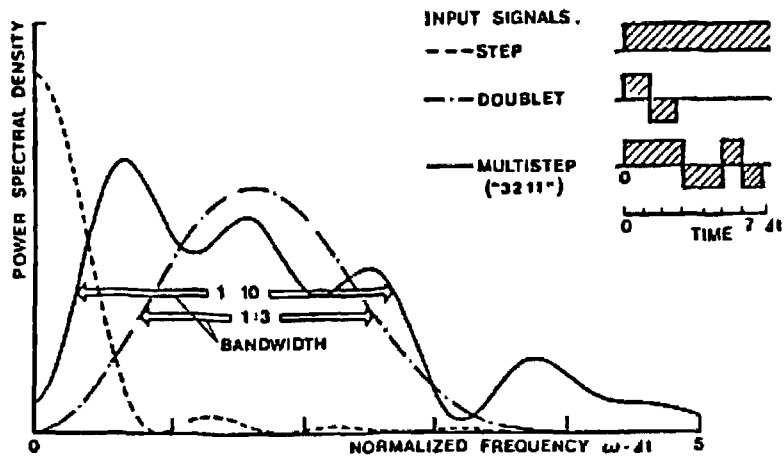
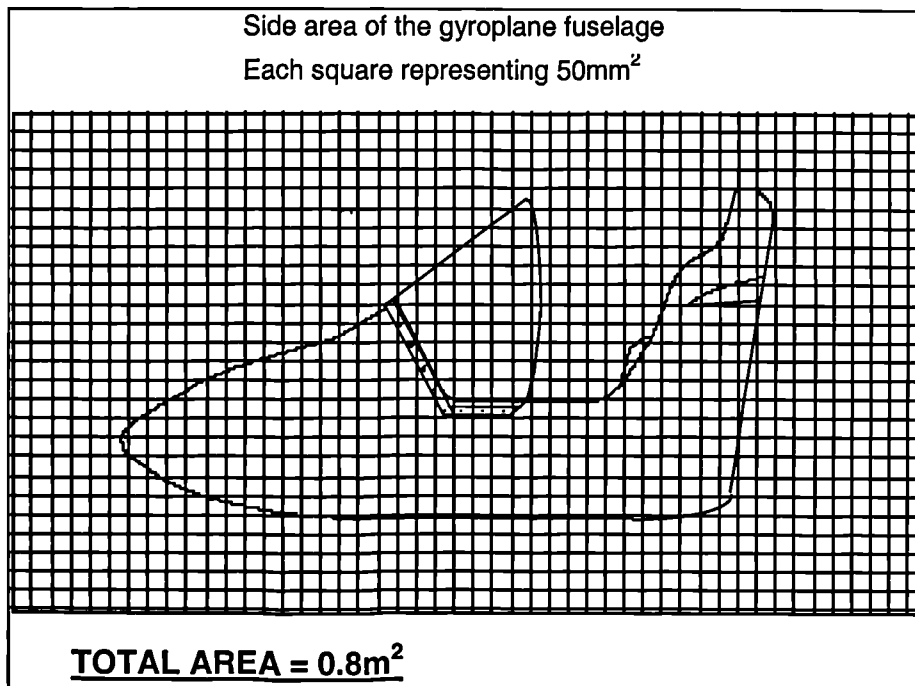
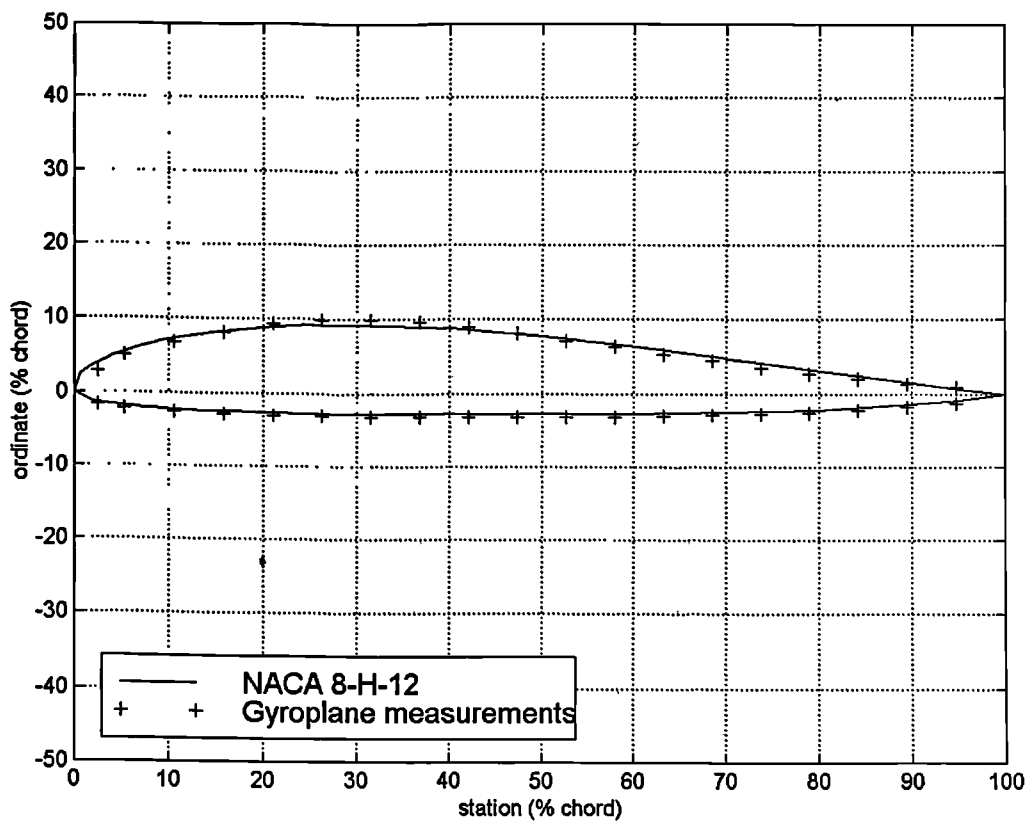


Figure 3.17: Doublet input frequency content<sup>1</sup>

<sup>1</sup>Reproduced from Klein [1989].



**Figure 4.1: Calculation of fuselage side area**



**Figure 4.2: Main rotor airfoil identification**

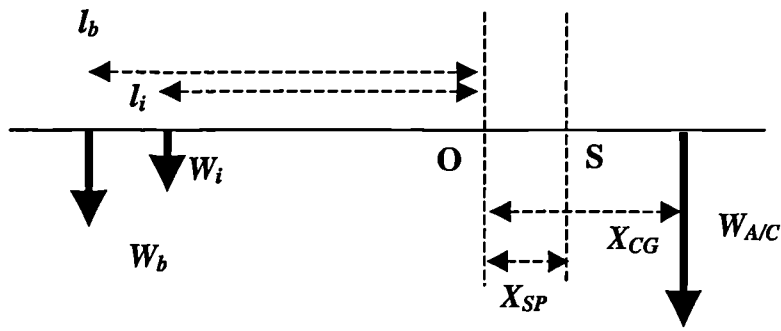


**Figure 4.3 : Force diagram for calculation of longitudinal centre of gravity position**

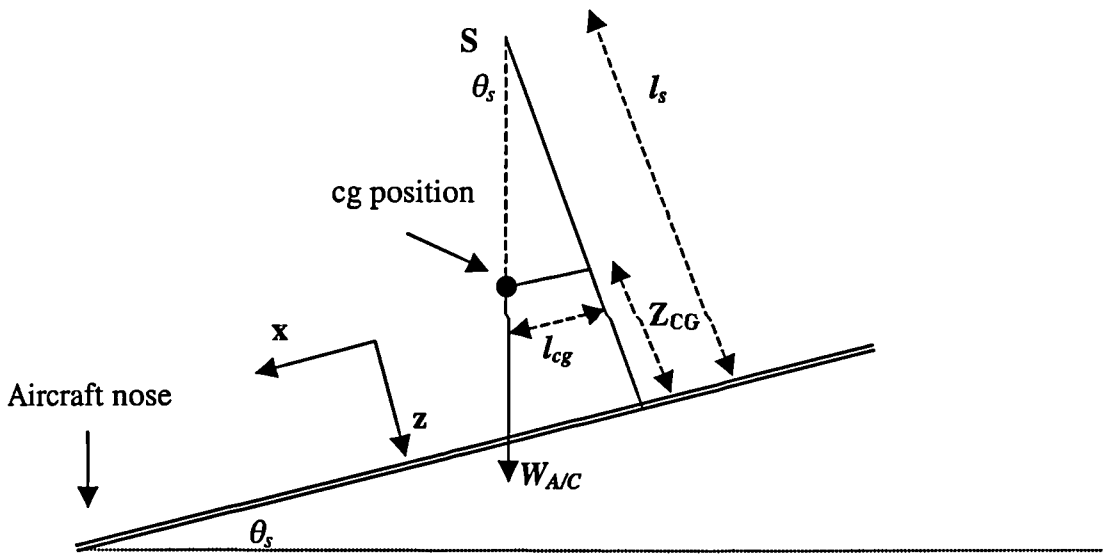


**Figure 4.4: Calculation of vertical centre of gravity position**

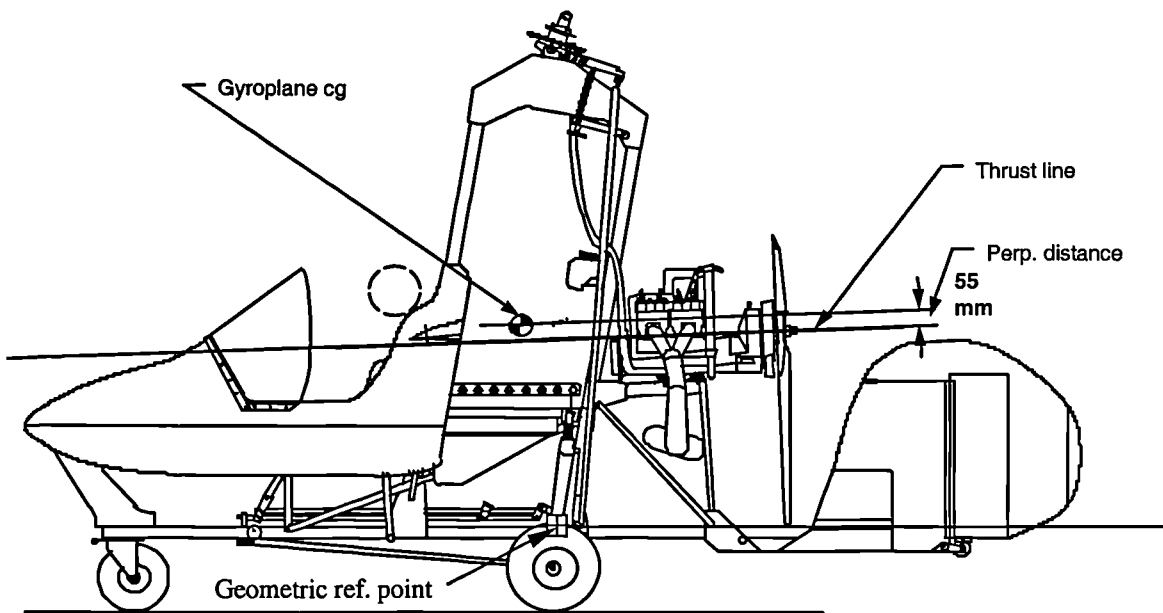


**Figure 4.5: Thrust line and centre of gravity relative positions**

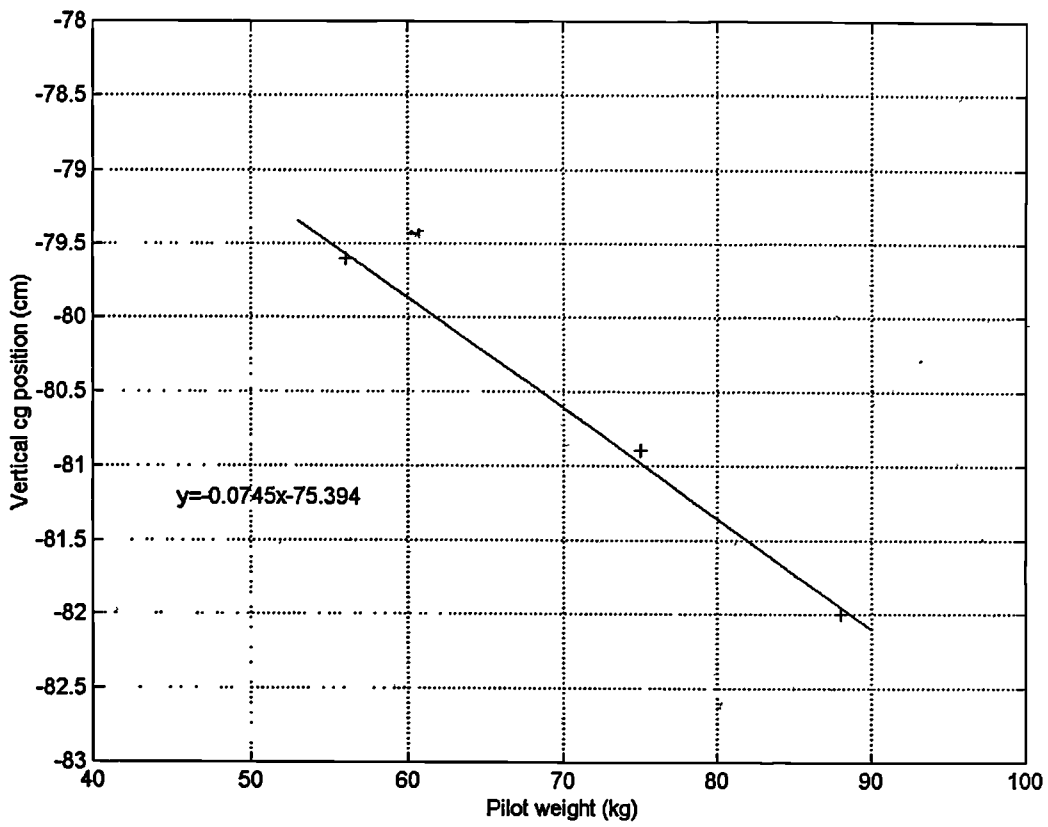


Figure 4.6: Effect of pilot weight on vertical cg position<sup>1</sup>

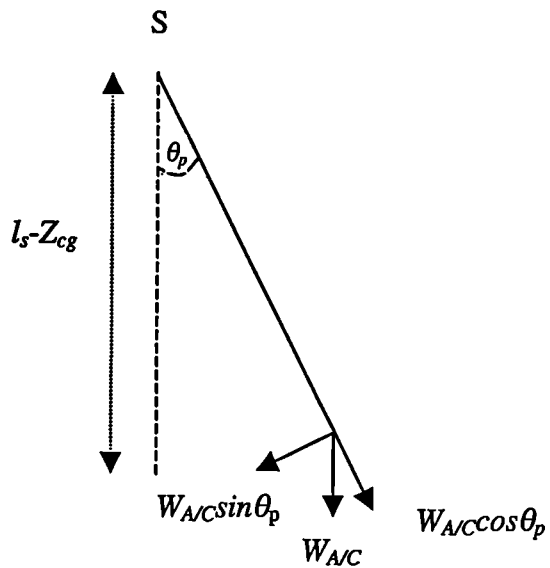
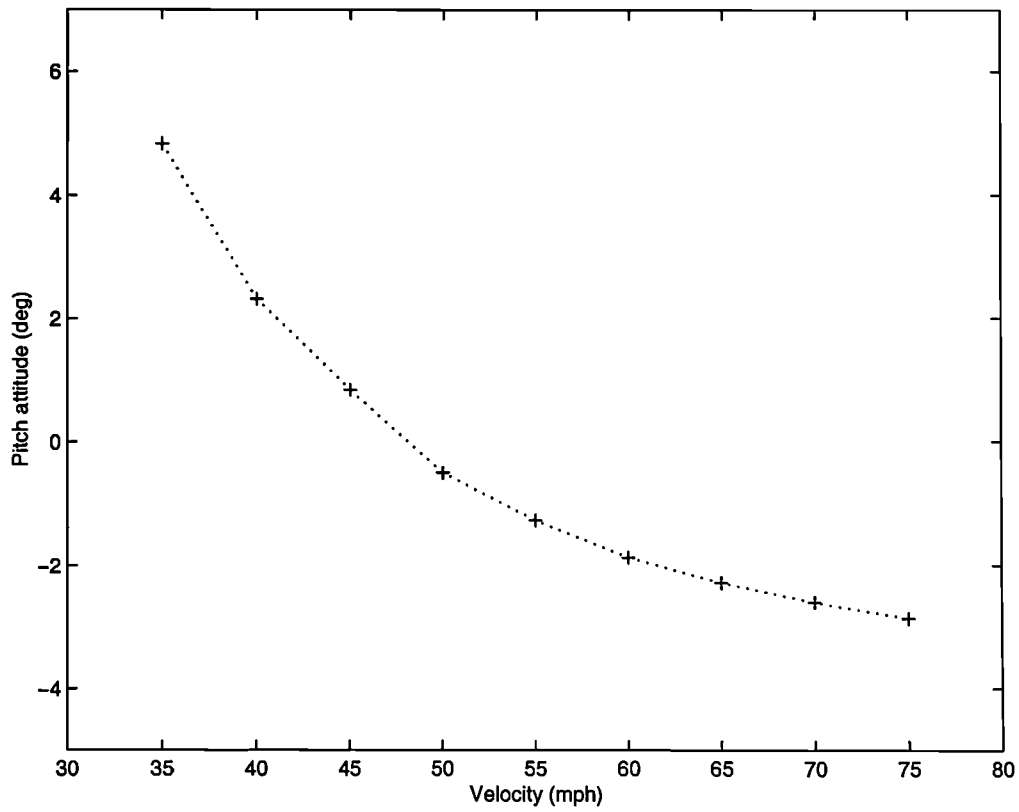
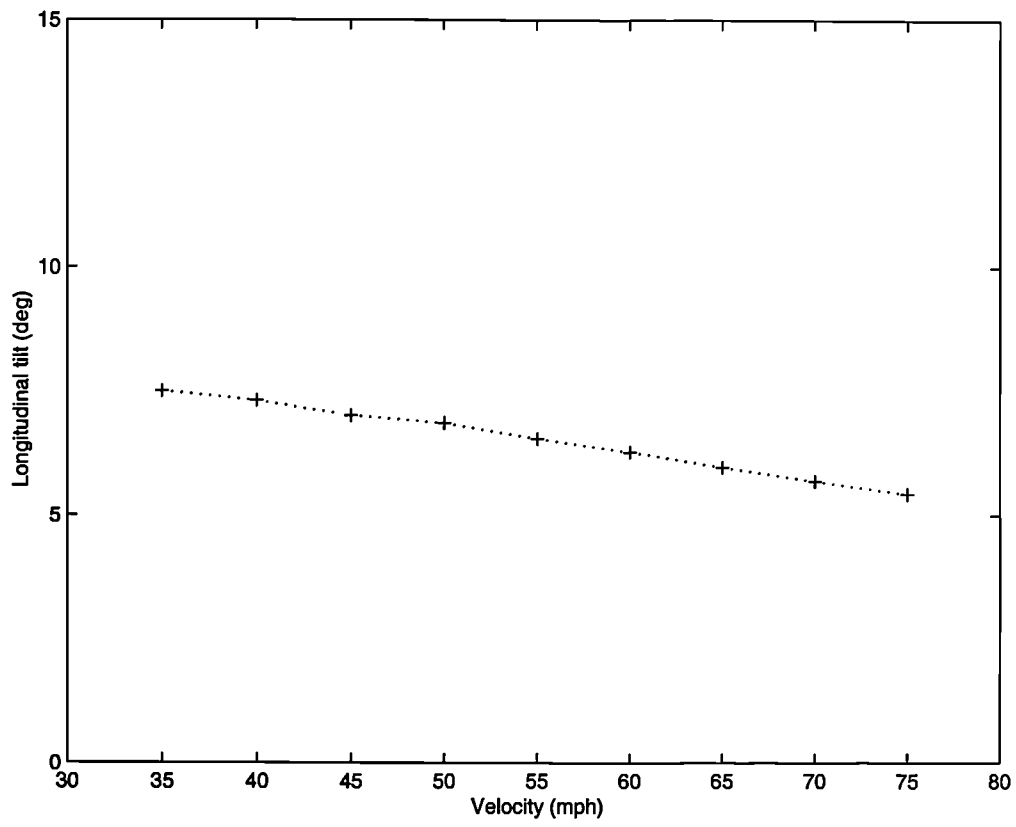
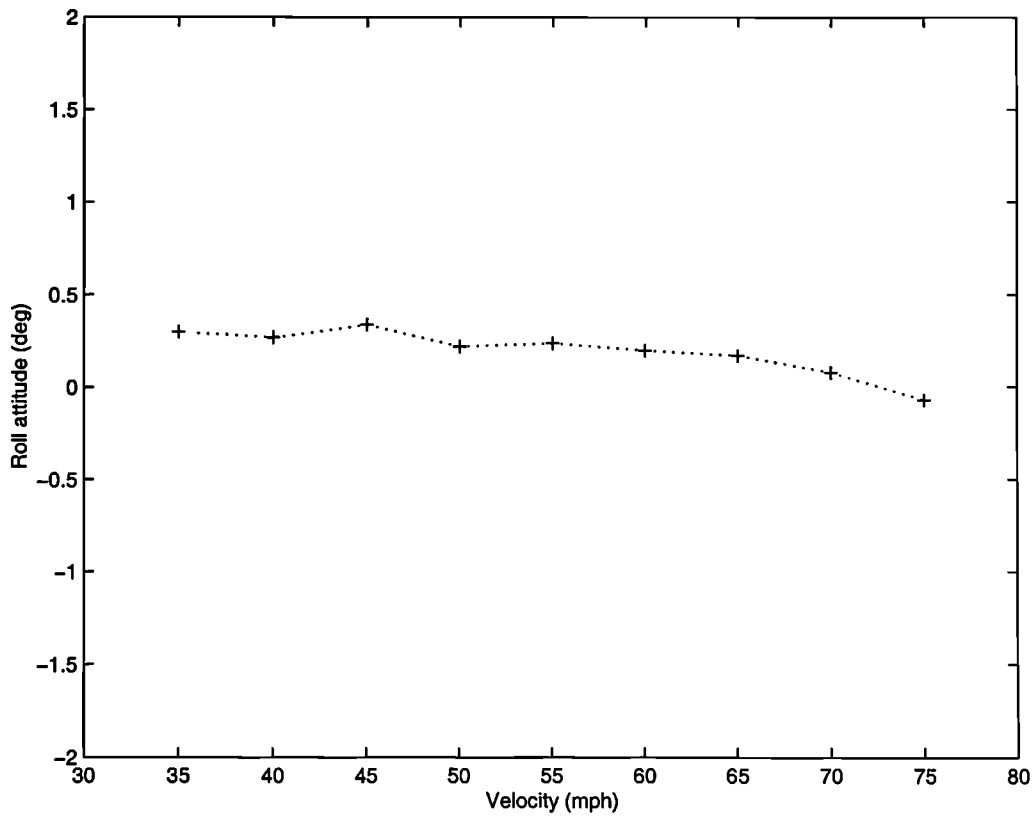
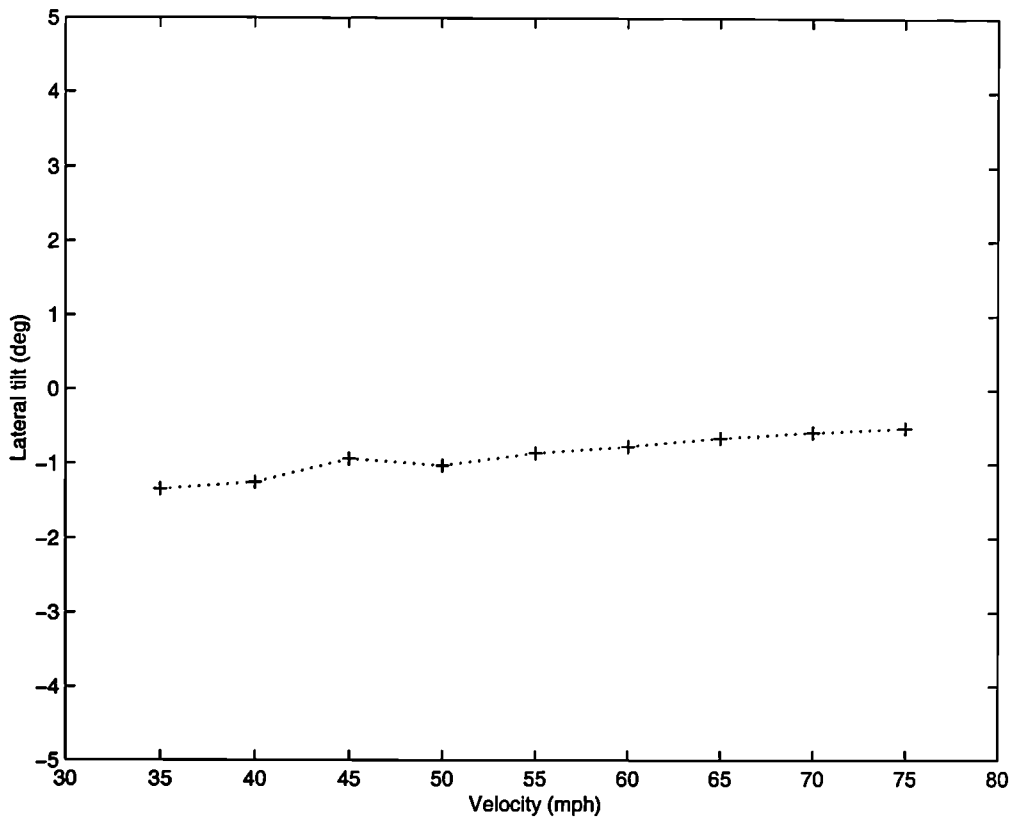


Figure 4.7: 'Simple pendulum' force diagram

<sup>1</sup> Negative cg position co-ordinate indicates that cg is above the aircraft keel.



**Figure 4.8: Trim parameters**



**Figure 4.8 (cont.)**

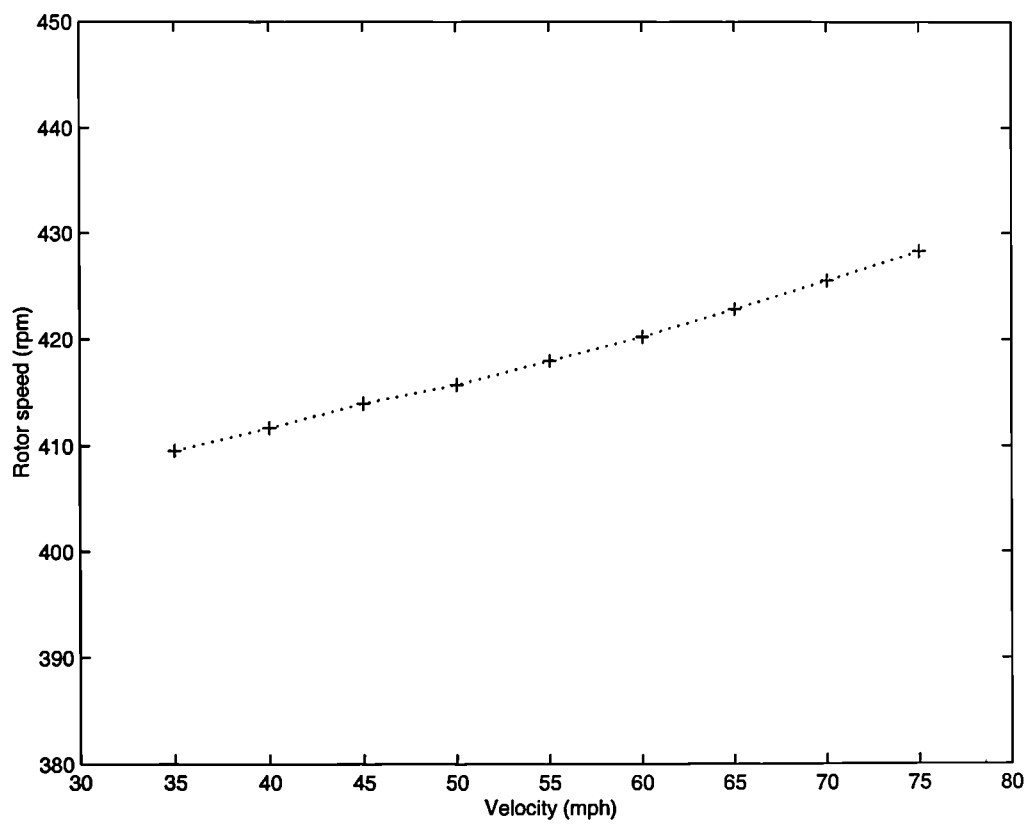


**Figure 4.8 (cont.)**

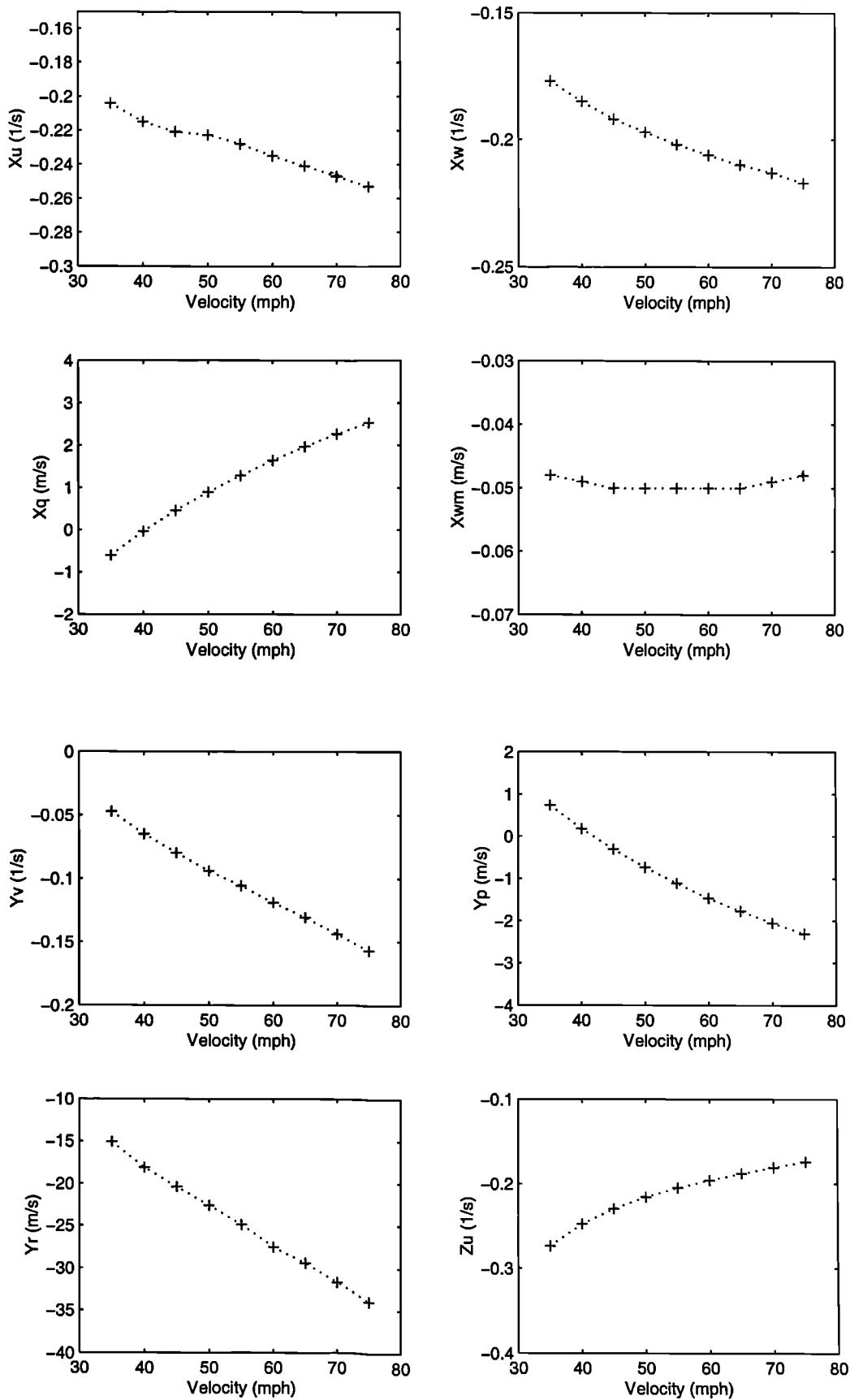


**Figure 4.9: Derivative values**

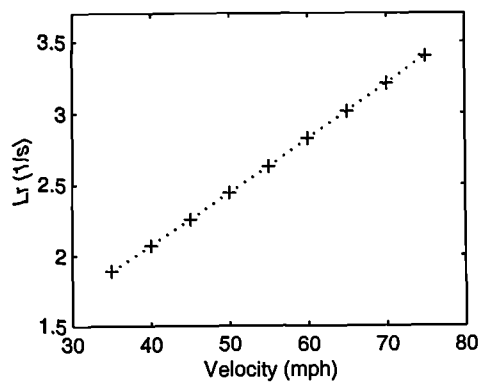
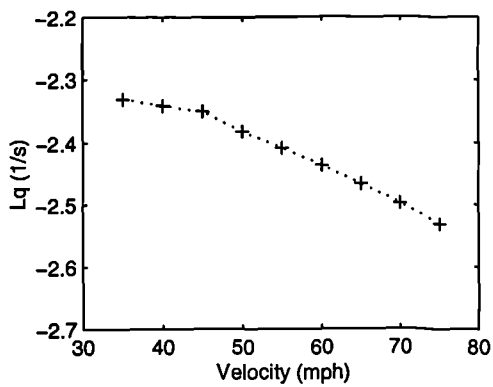
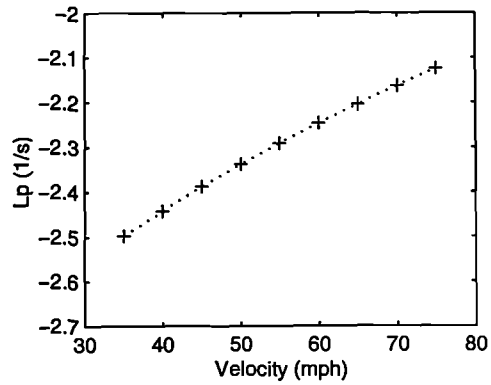
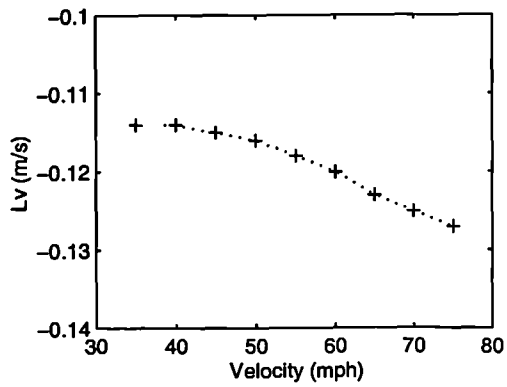
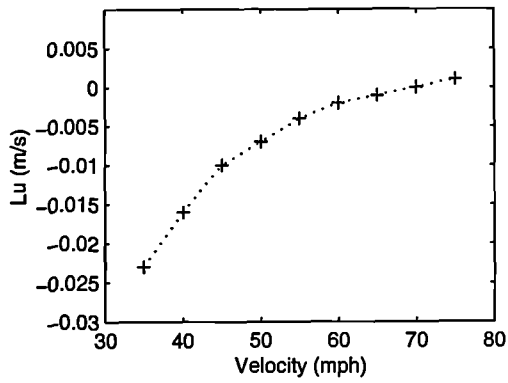
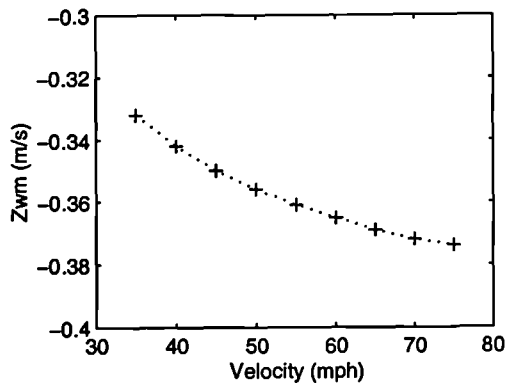
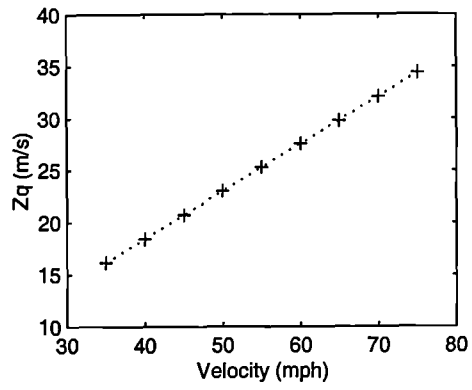
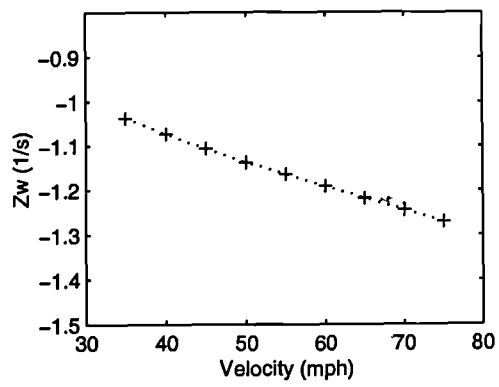


Figure 4.9 (cont.)

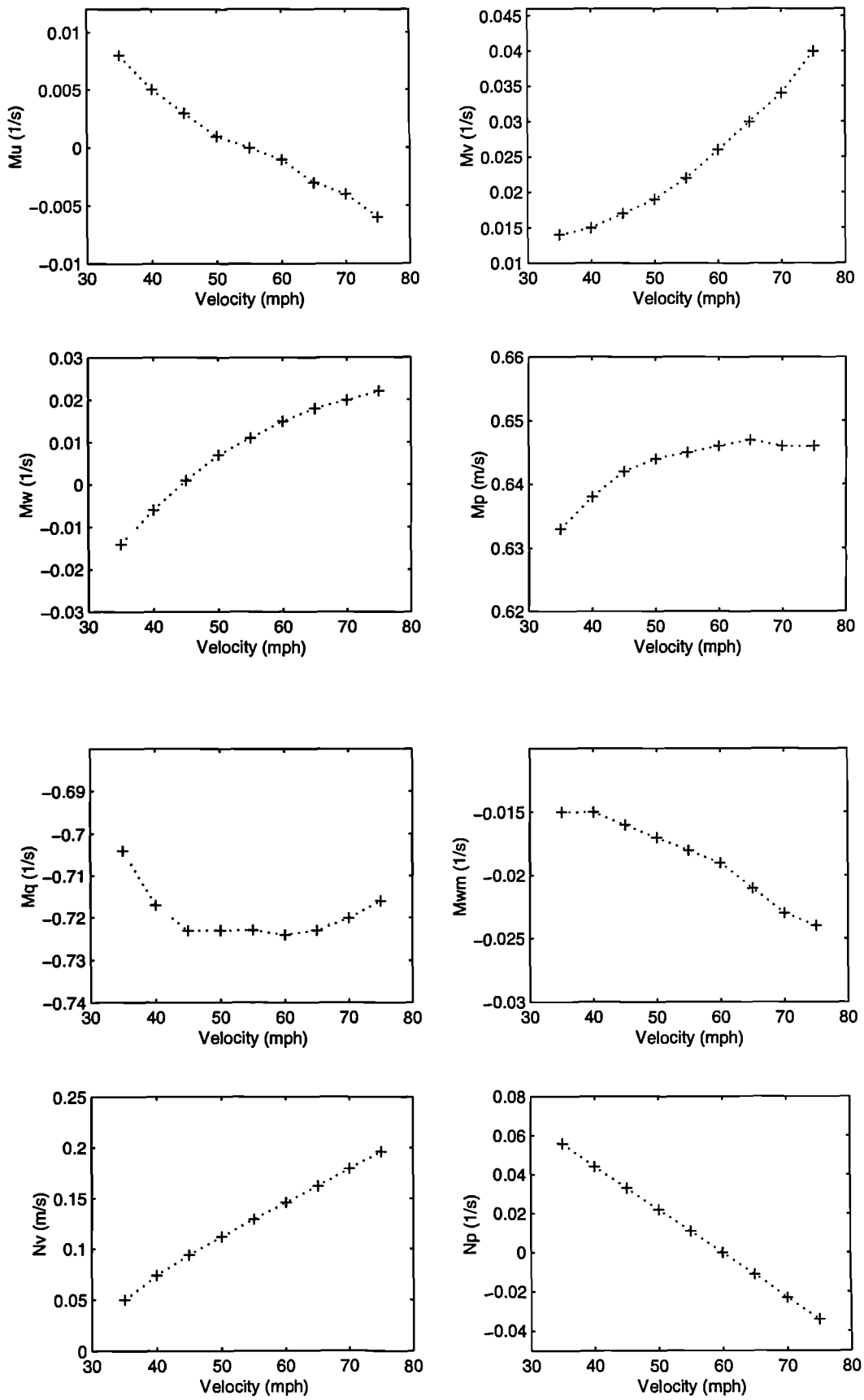


Figure 4.9 (cont.)

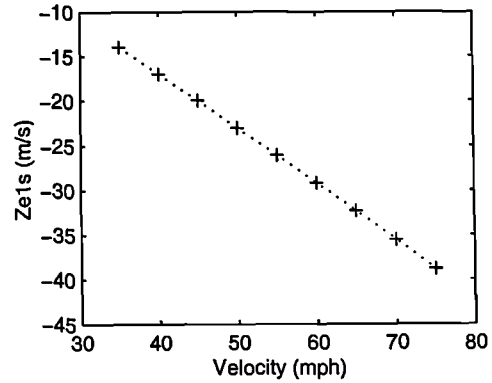
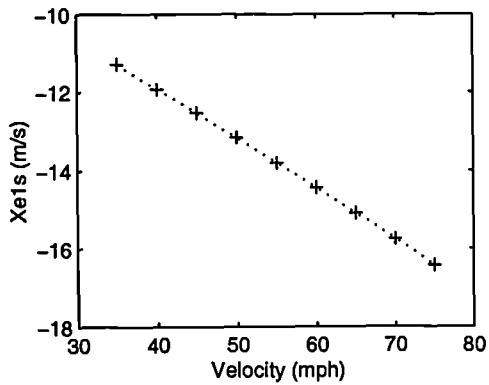
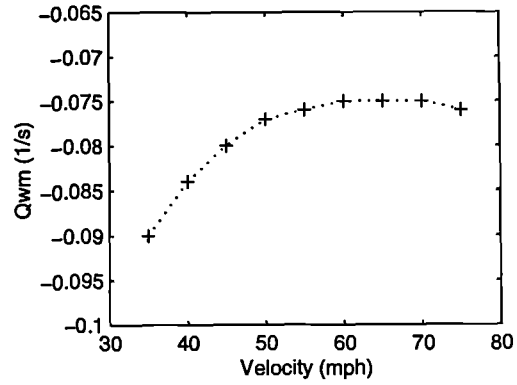
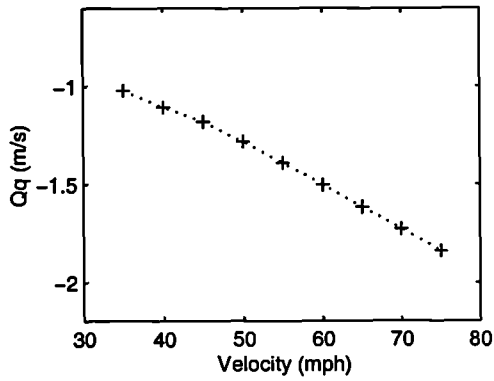
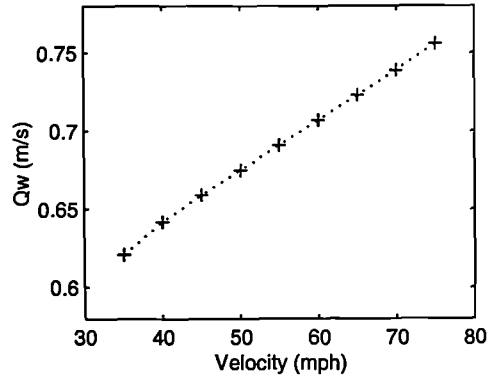
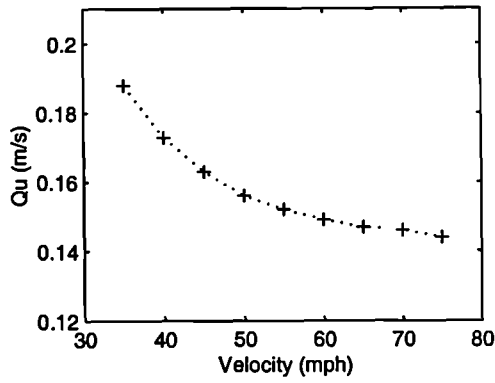
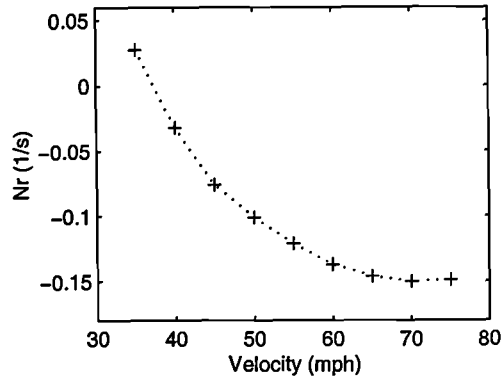
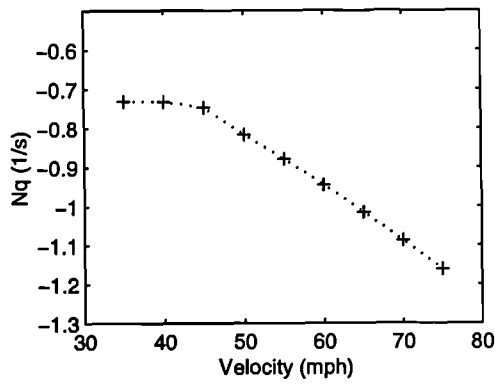


Figure 4.9 (cont.)

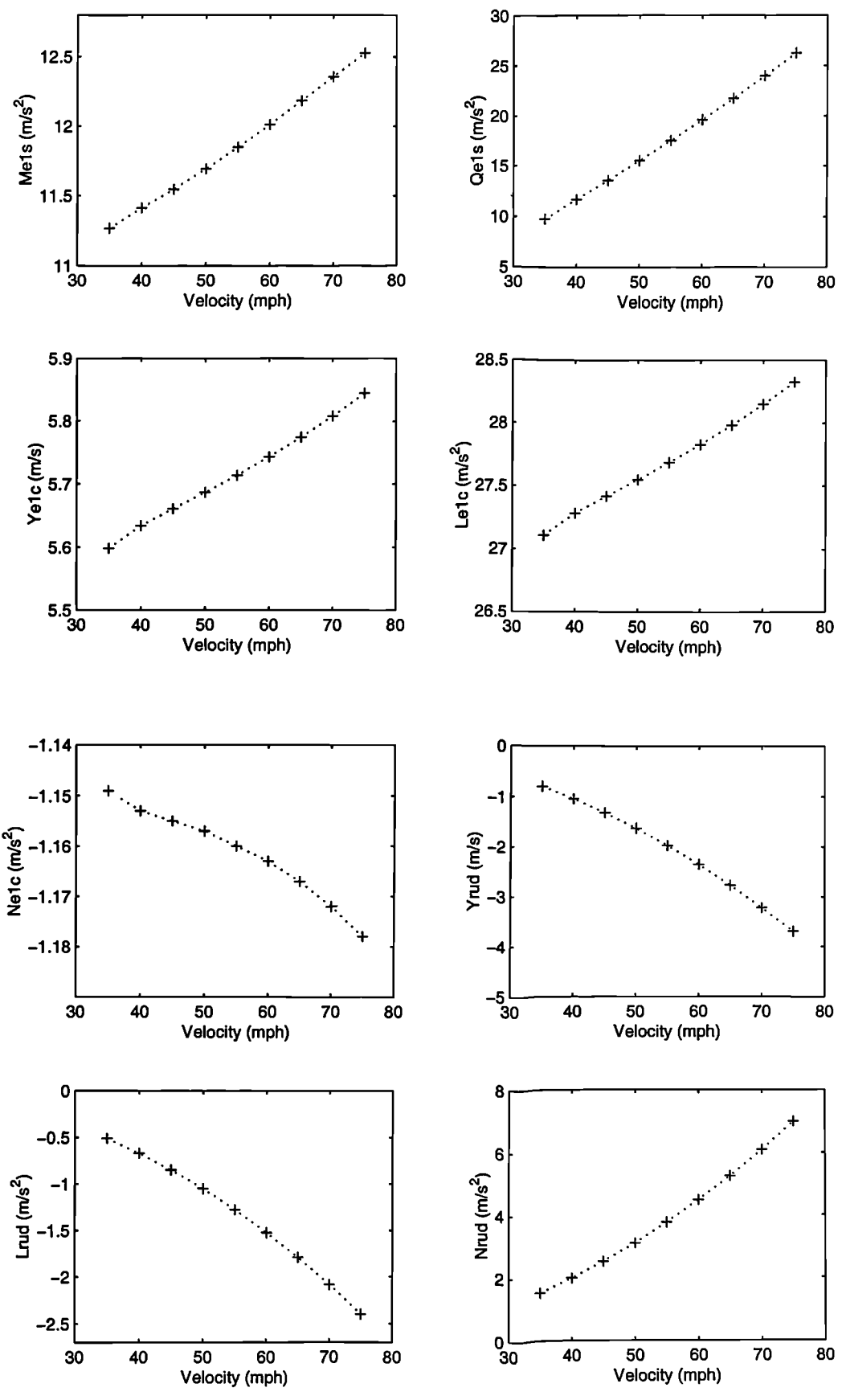
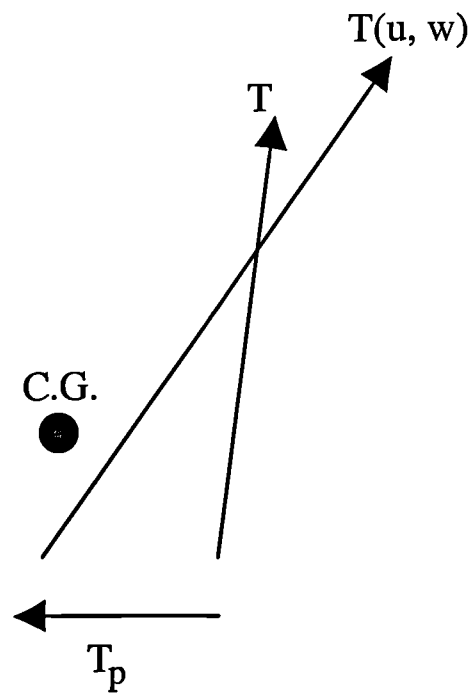
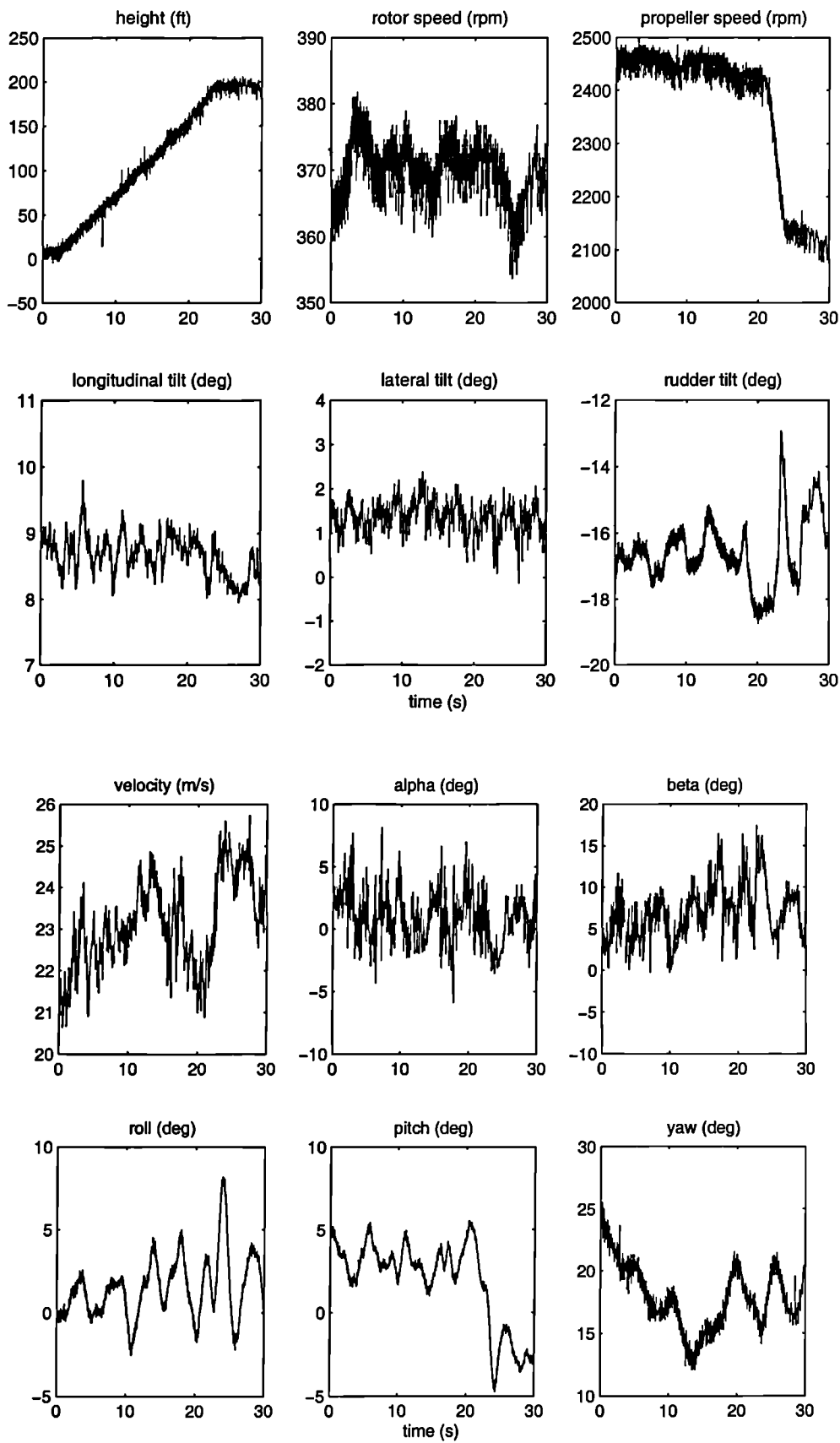


Figure 4.9 (cont.)



**Figure 4.10: Rotor and propeller forces in equilibrium and disturbed flight**



**Figure 5.1: Raw sensor data during steady climb**

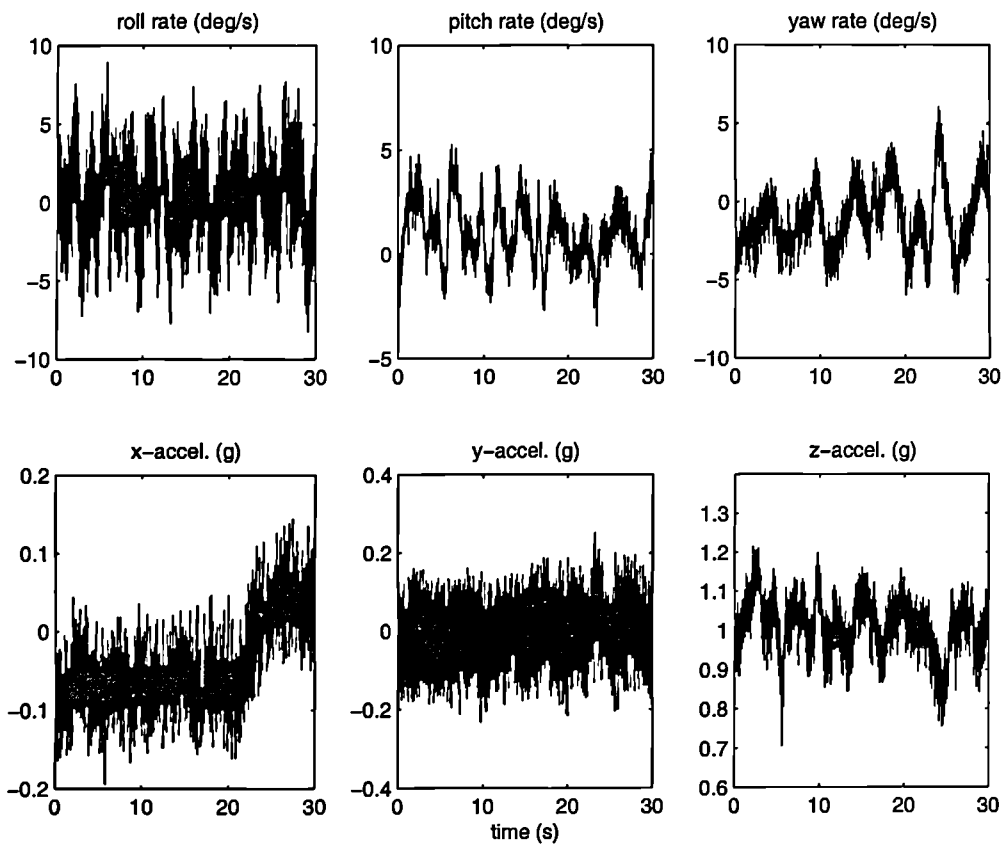


**Figure 5.1 (cont.)**

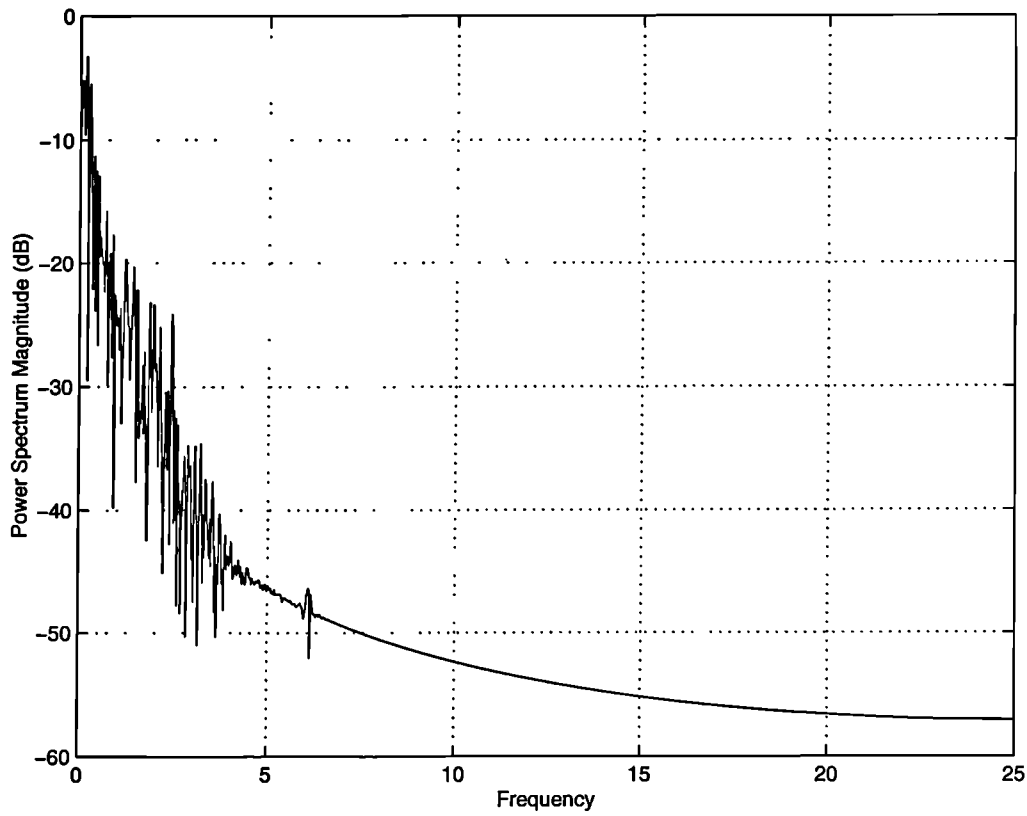
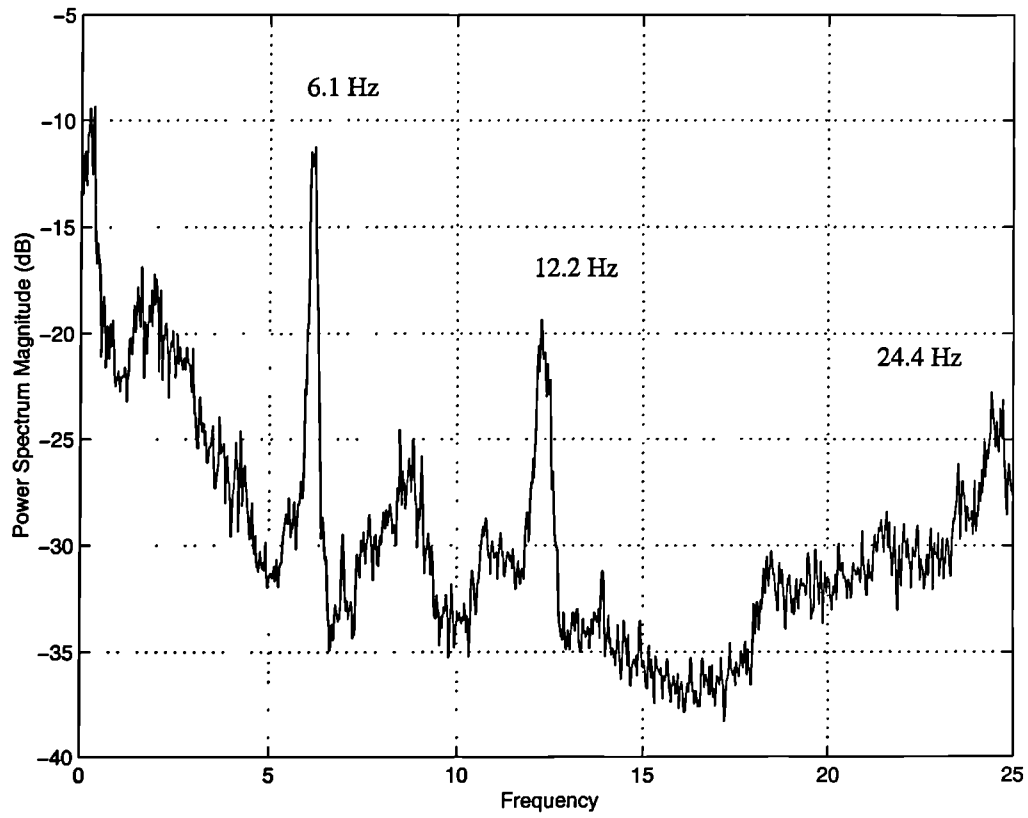


**Figure 5.2: Raw and filtered vertical acceleration PSD**

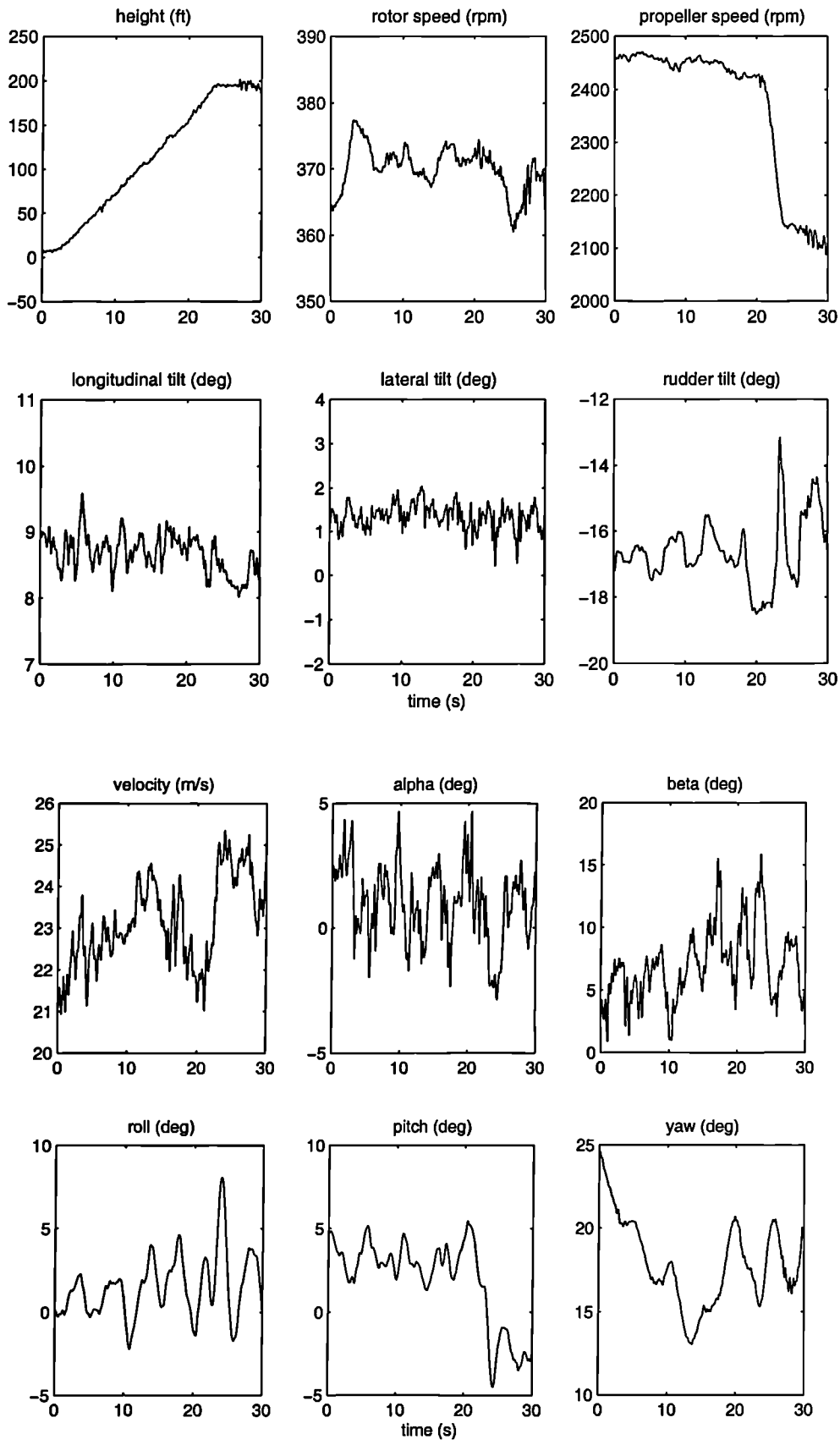


**Figure 5.3: Filtered sensor data during steady climb**

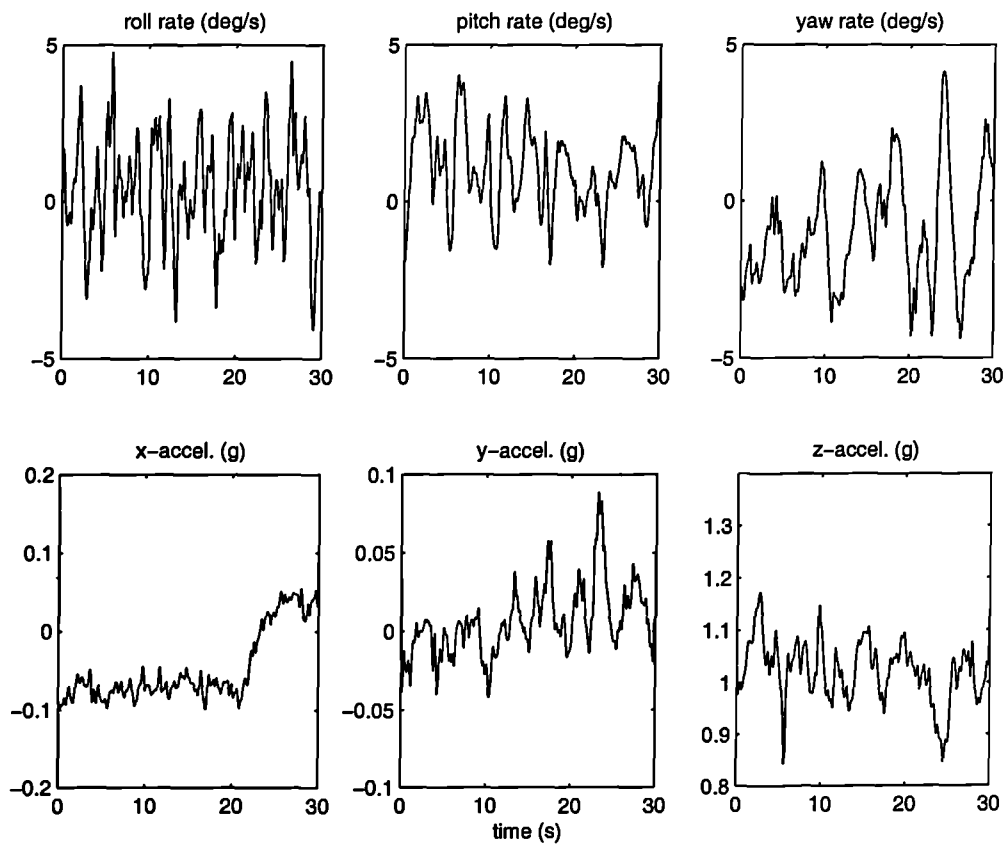
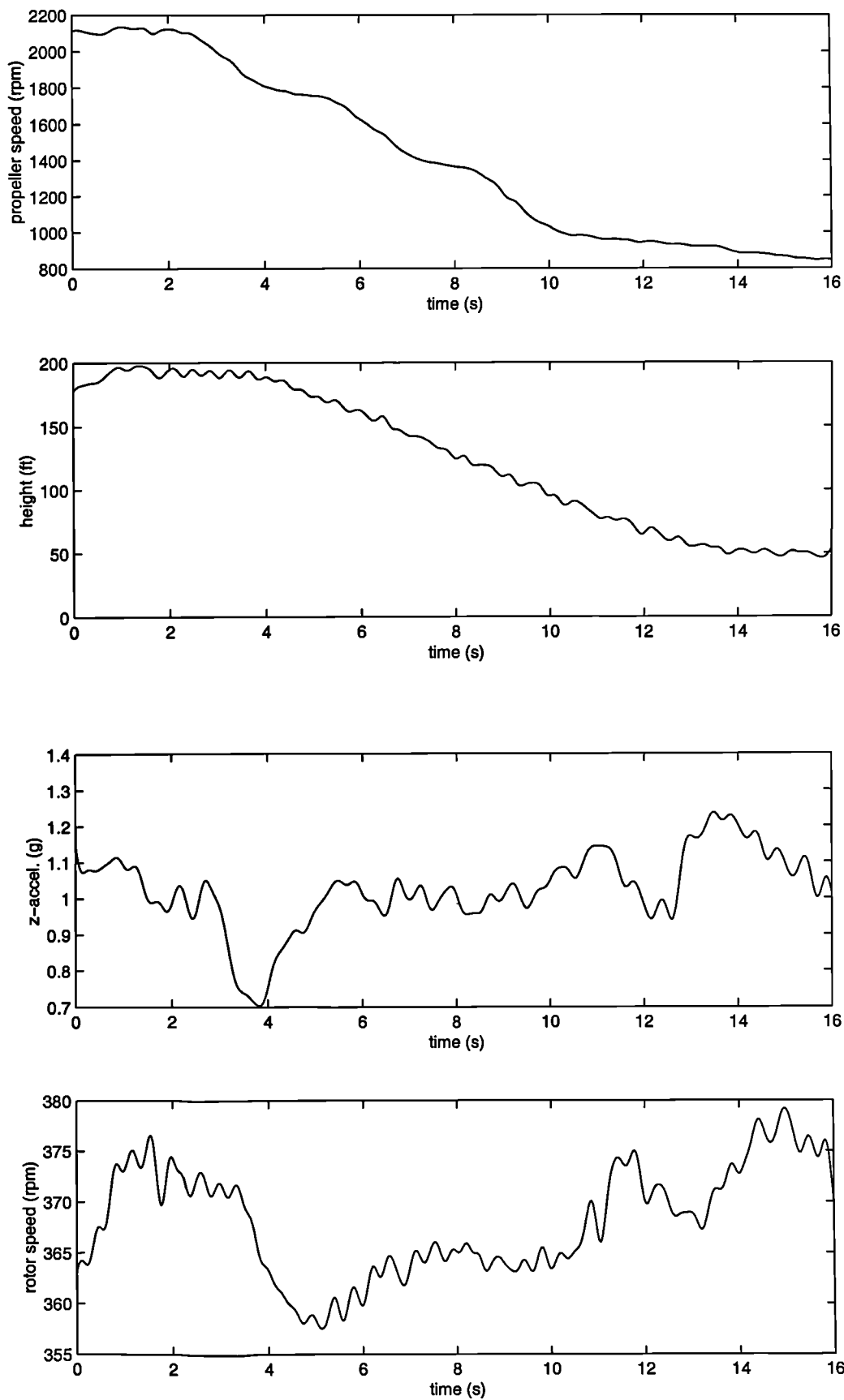
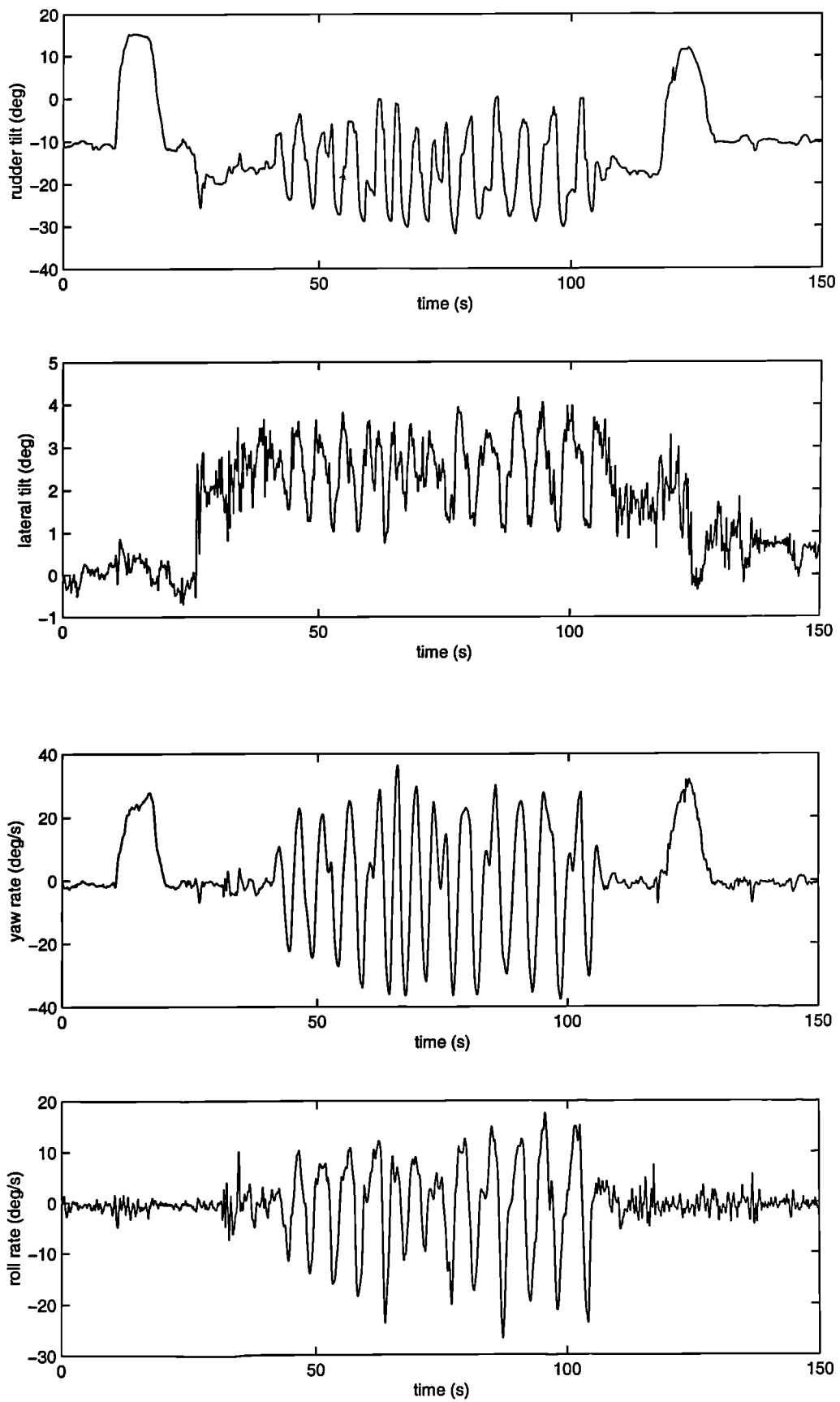


Figure 5.3 (cont.)



**Figure 5.4: Sensor readings during simulated engine failure**



**Figure 5.5: Sensor readings during 'yaw turns' manoeuvre**

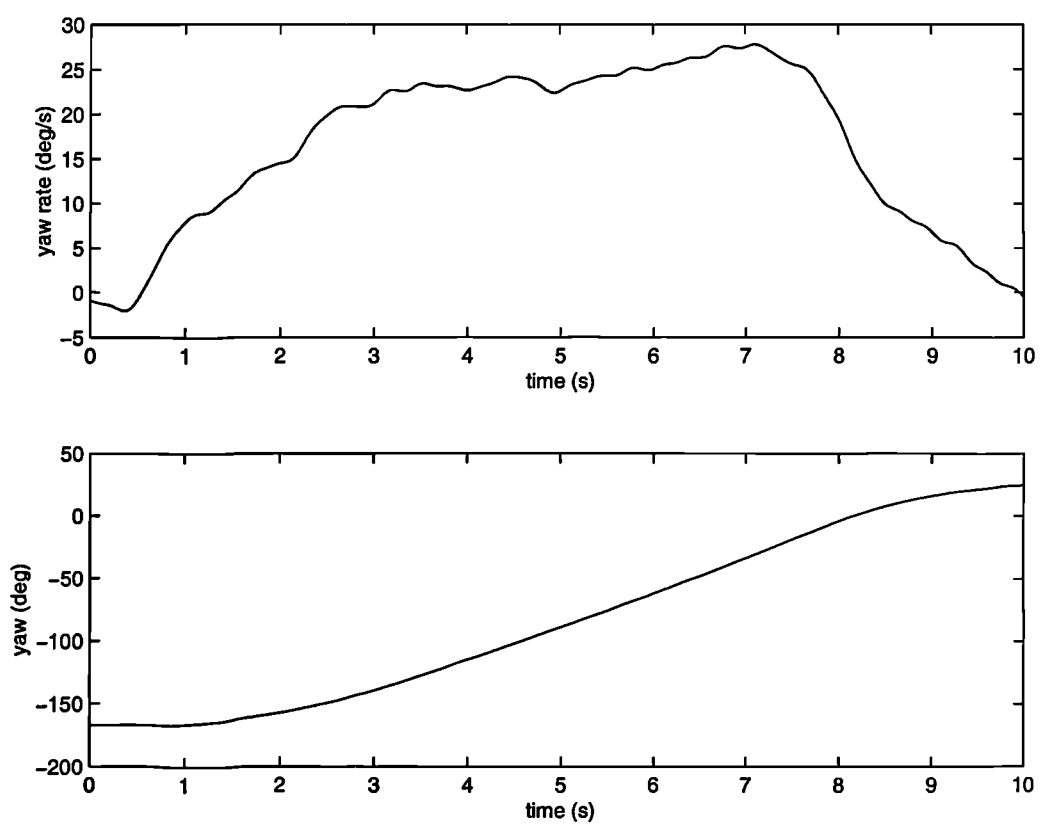


**Figure 5.6: Yaw rate and yaw attitude comparison during 'yaw pulse'**

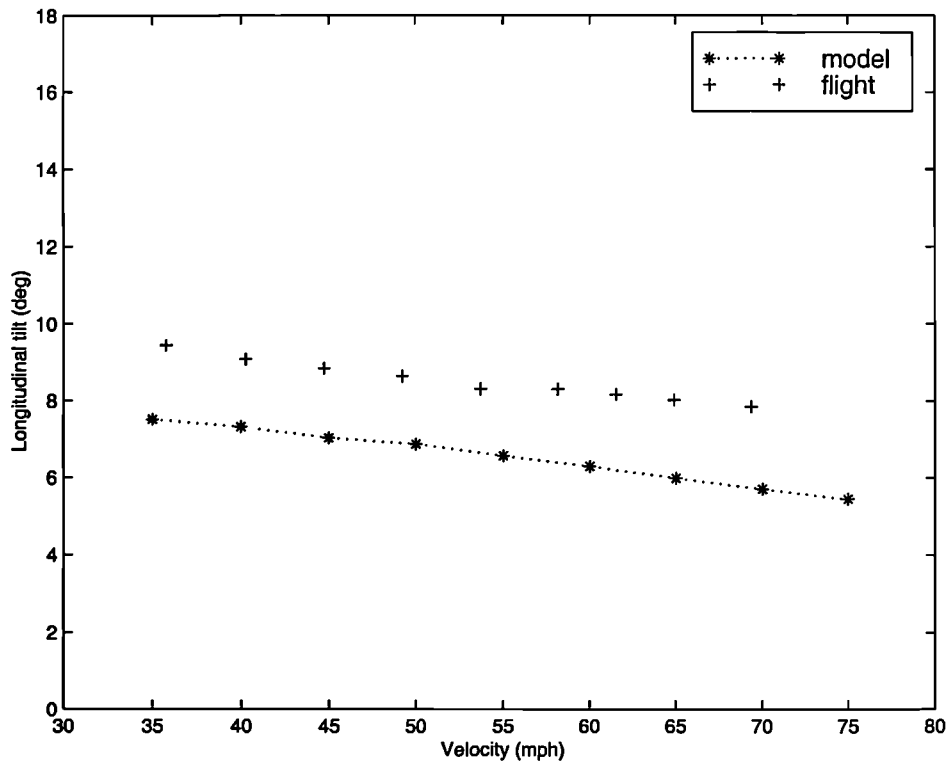


**Figure 5.7: Longitudinal tilt model/flight comparison**

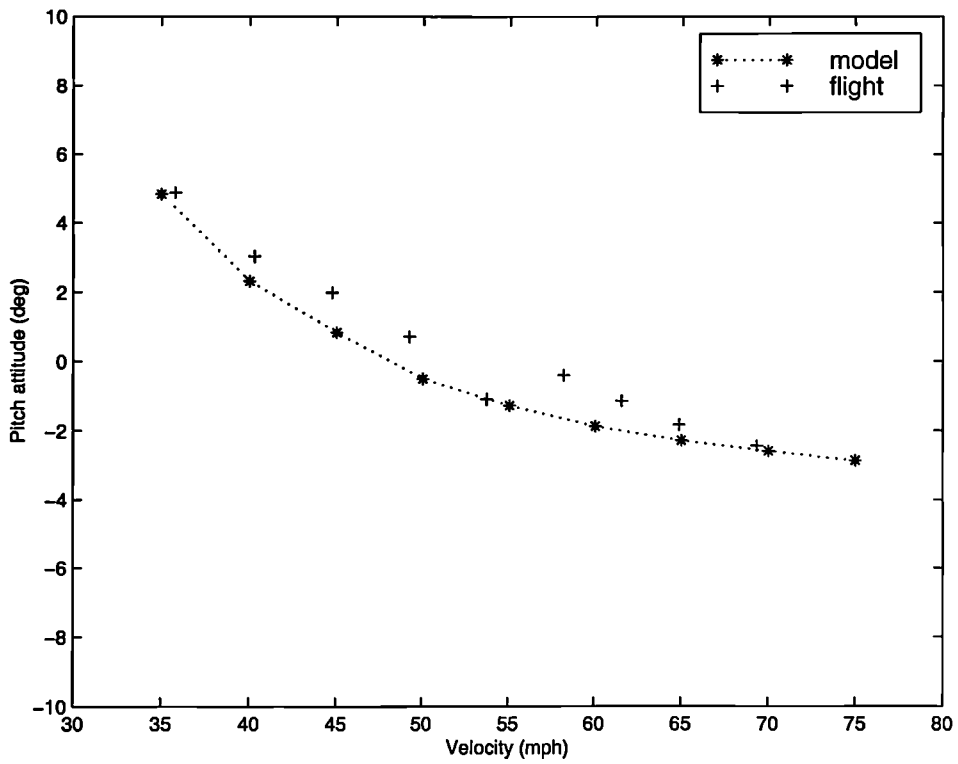


**Figure 5.8: Pitch attitude model/flight comparison**

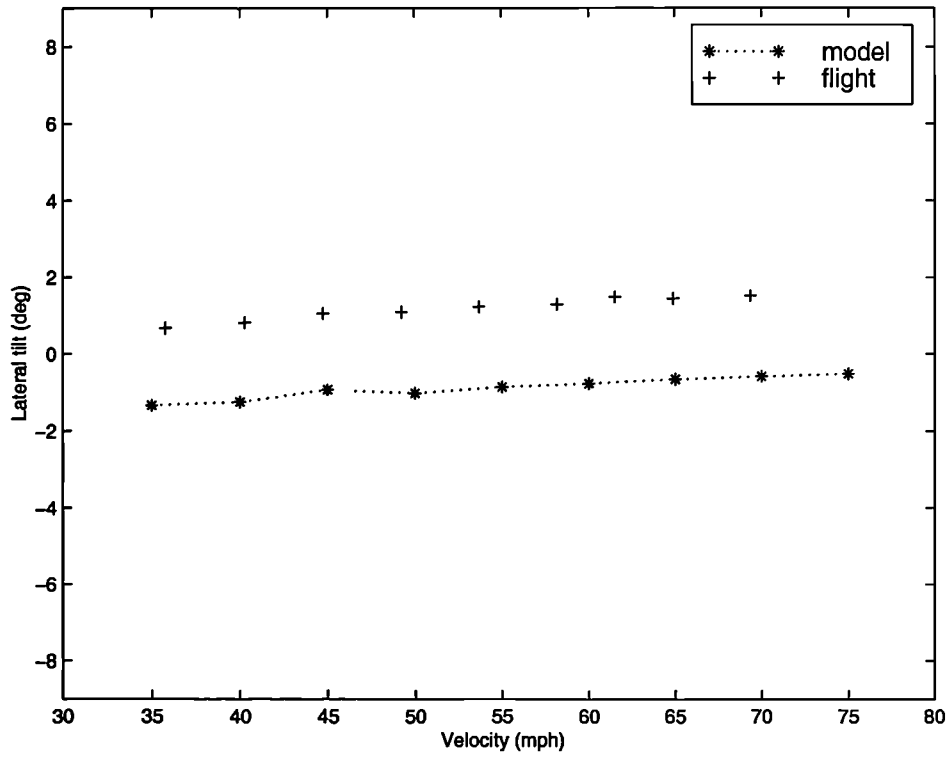


**Figure 5.9: Lateral tilt model/flight comparison**

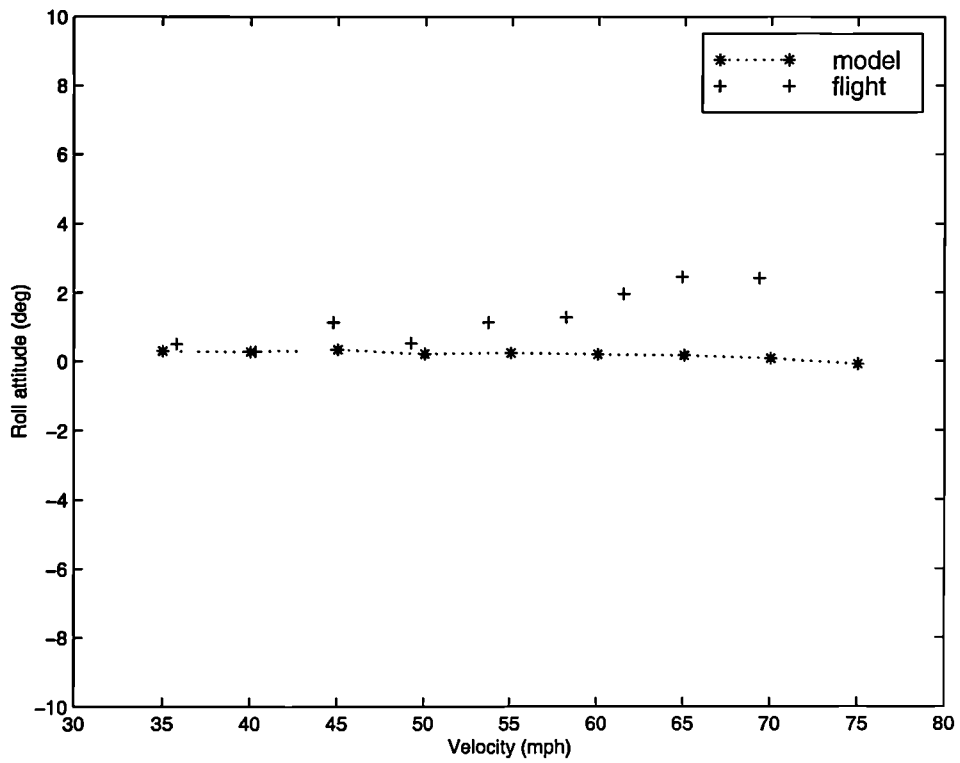


**Figure 5.10: Roll attitude model/flight comparison**

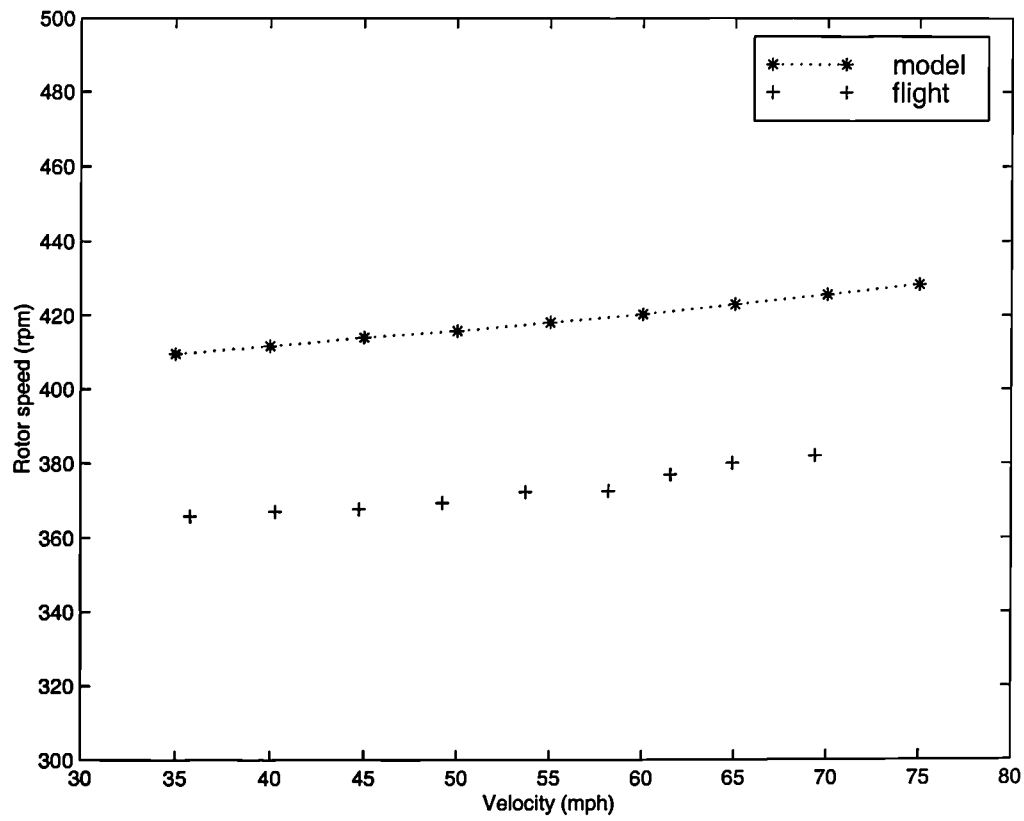


**Figure 5.11: Rotor speed model/flight comparison**

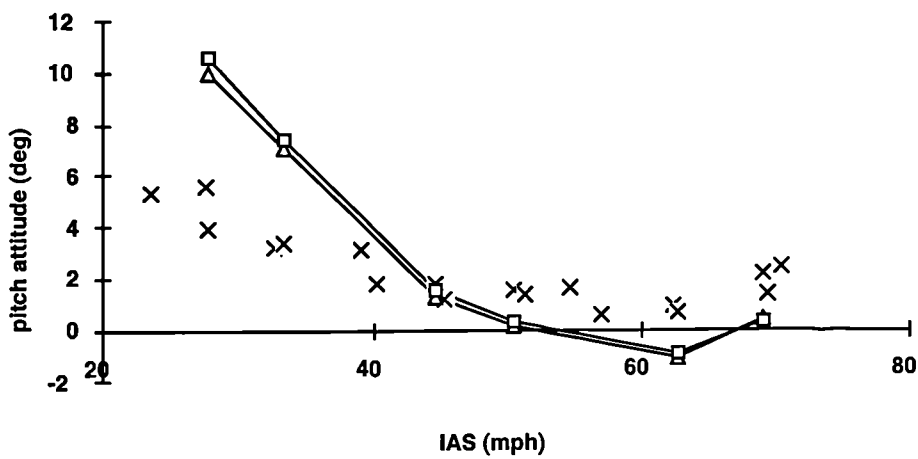
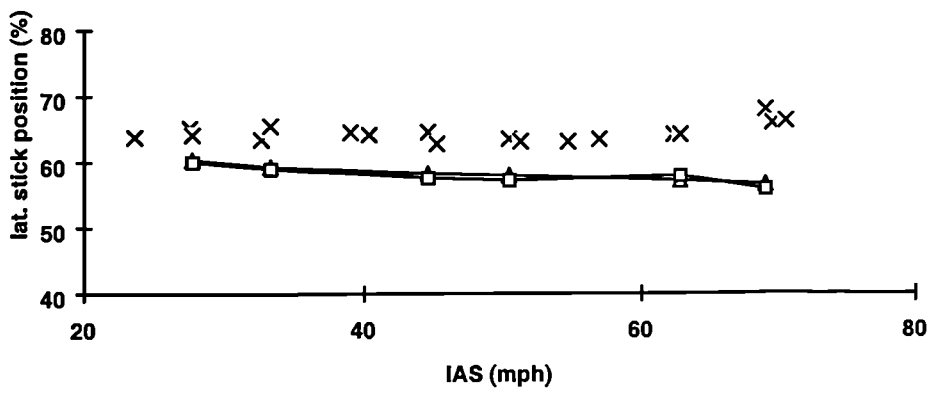
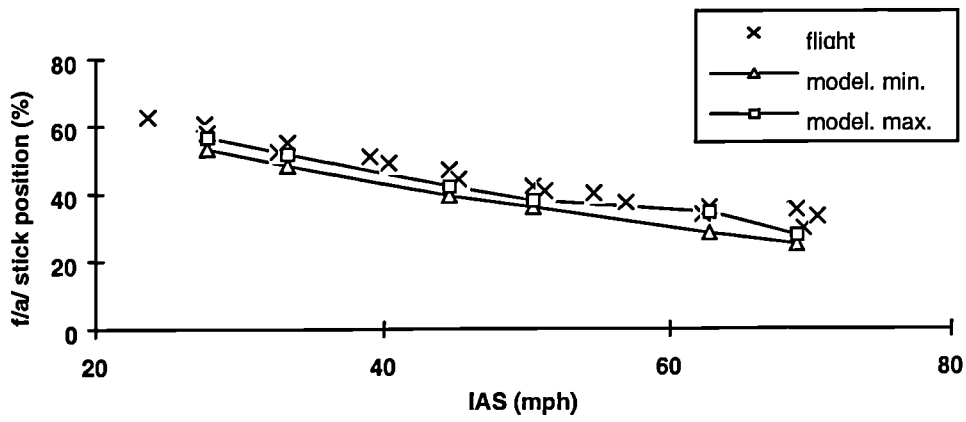


Figure 5.12: VPM model validation results<sup>1</sup>

<sup>1</sup> Reproduced from Houston [2000].

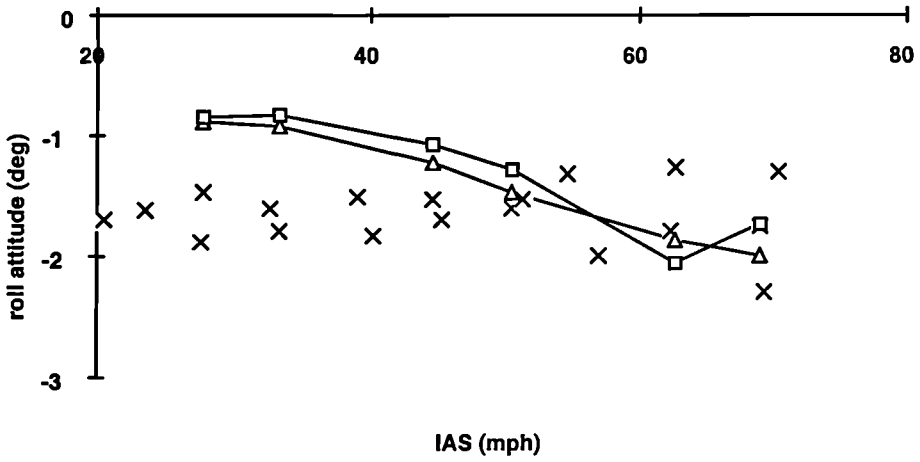
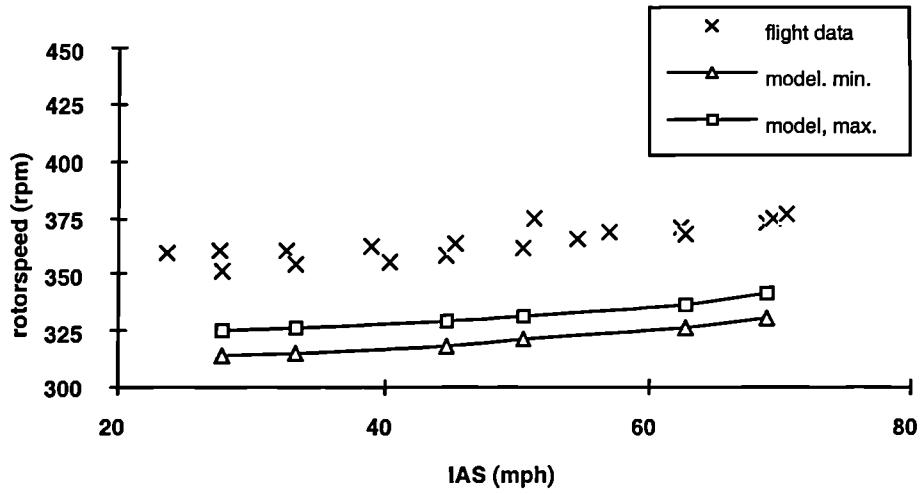
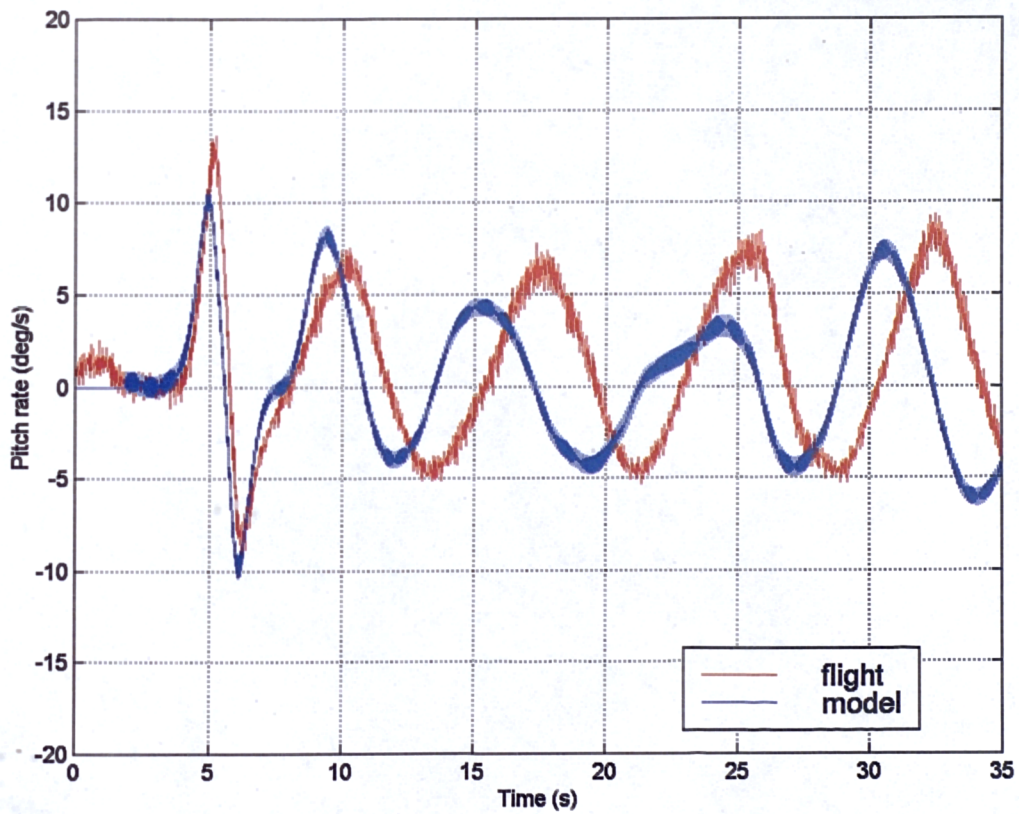
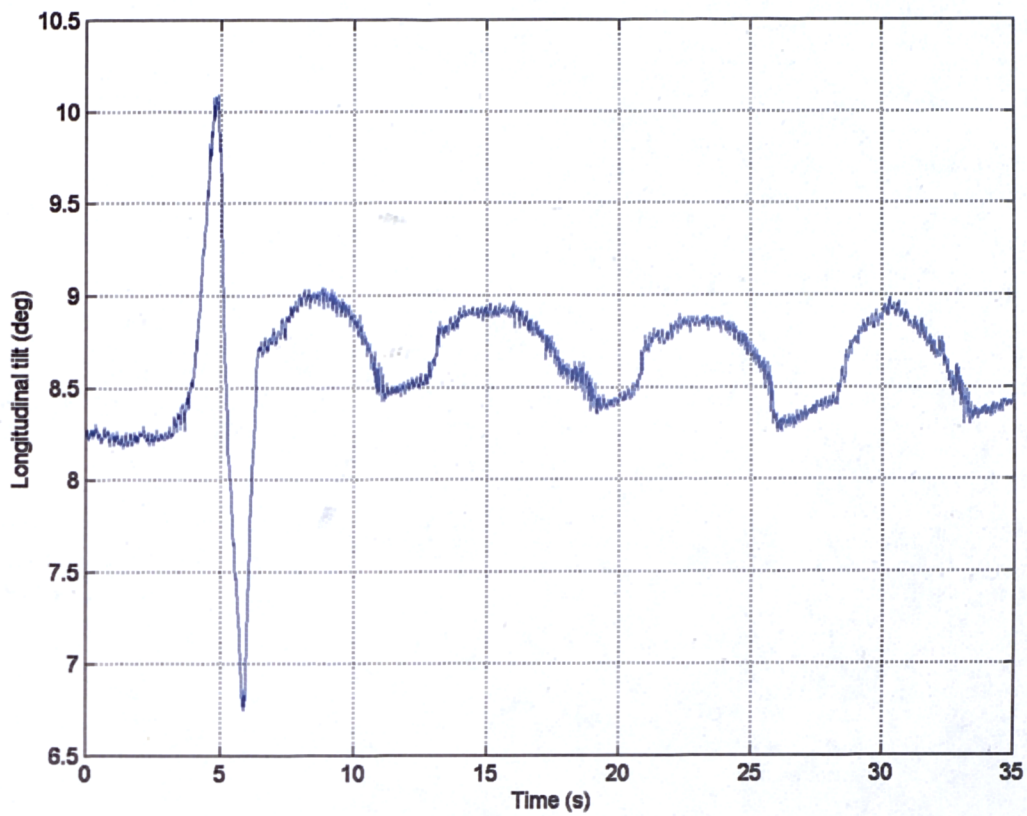


Figure 5.12 (cont.)



**Figure 5.13: Model and flight data response to longitudinal tilt (60 mph)**

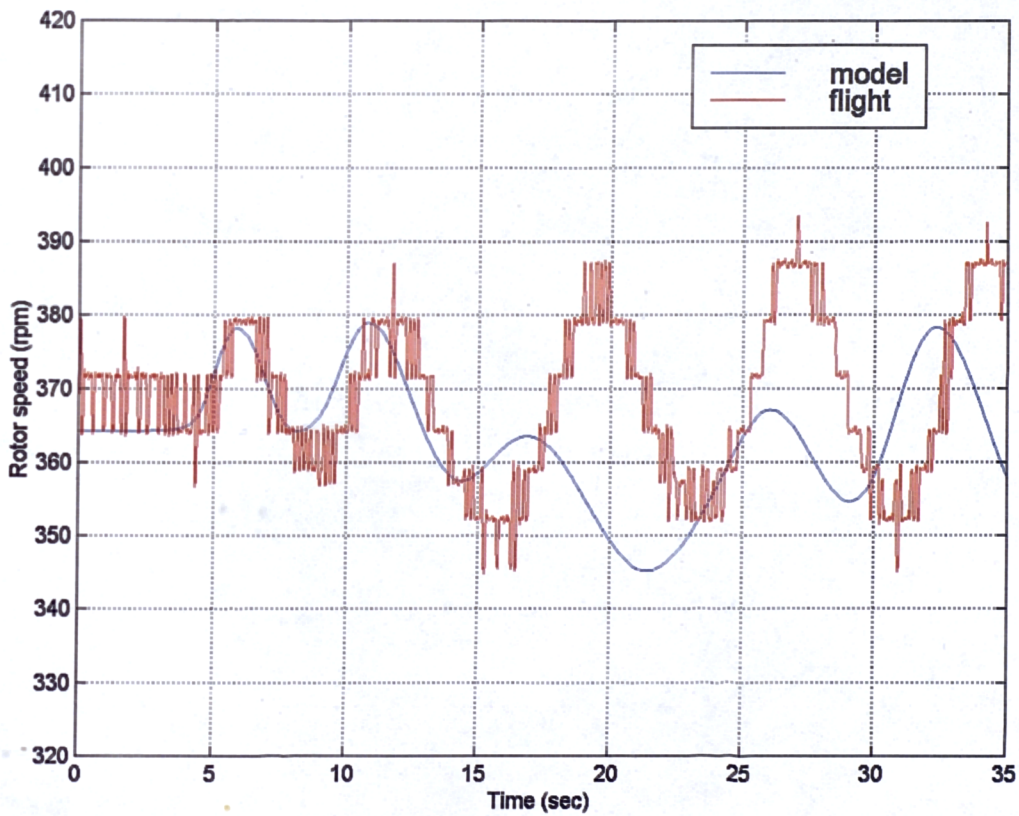
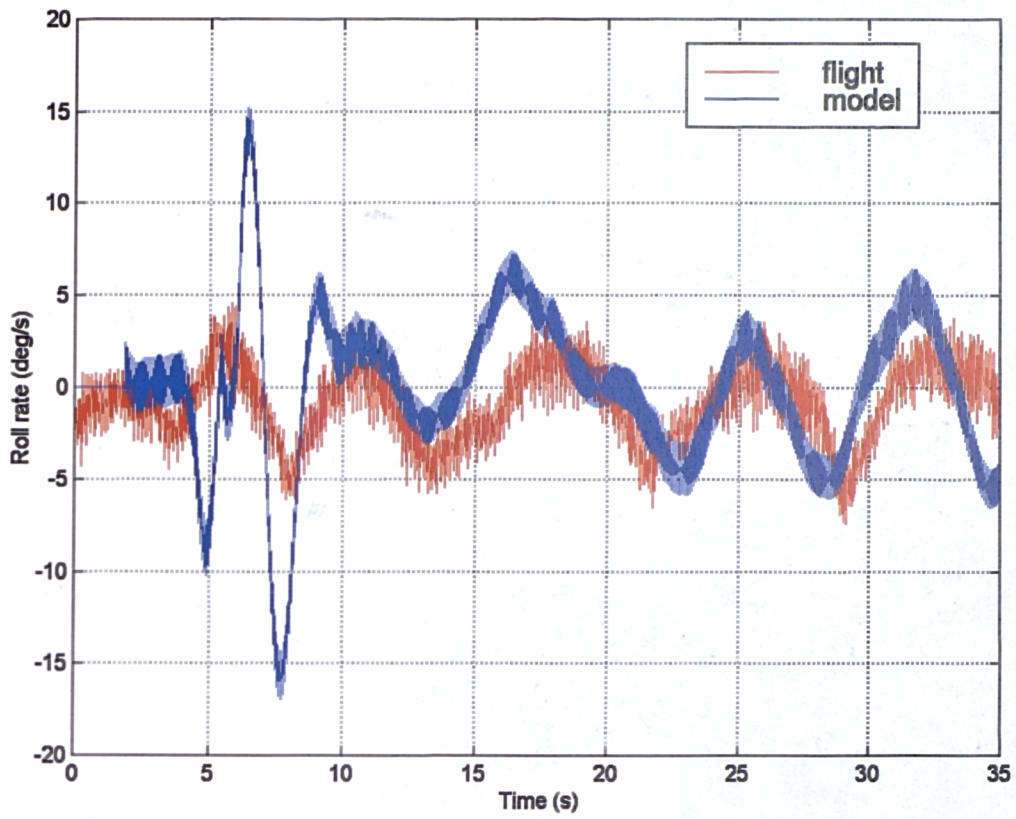
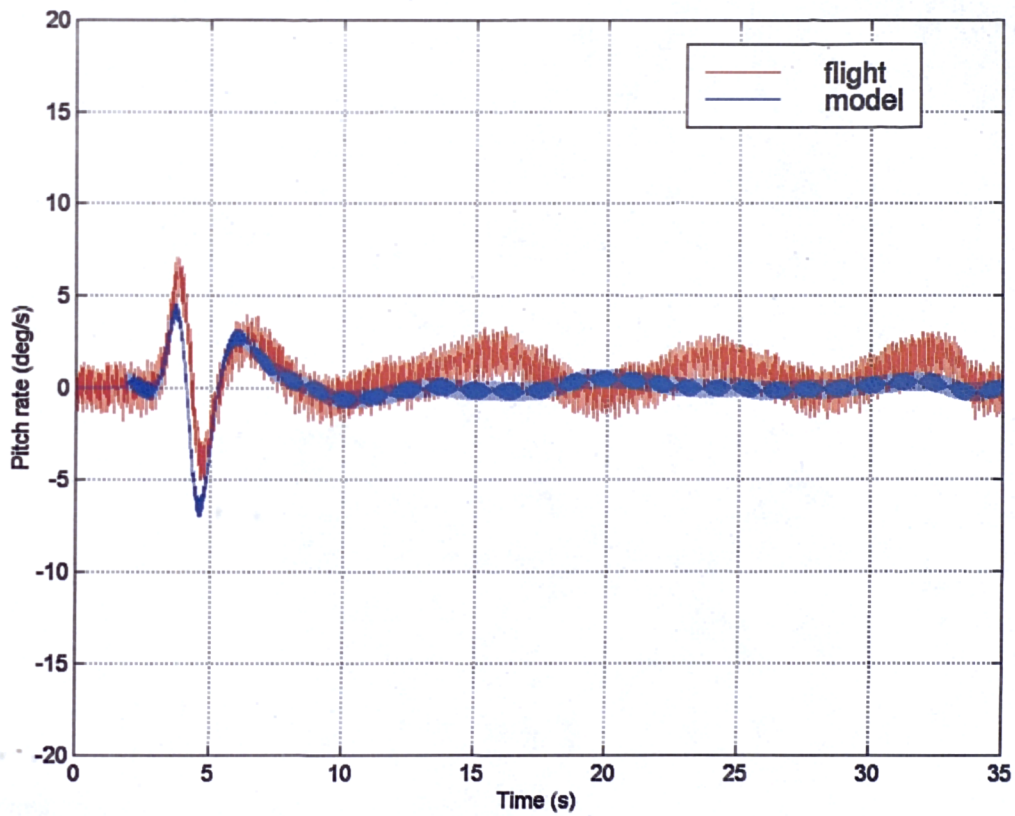
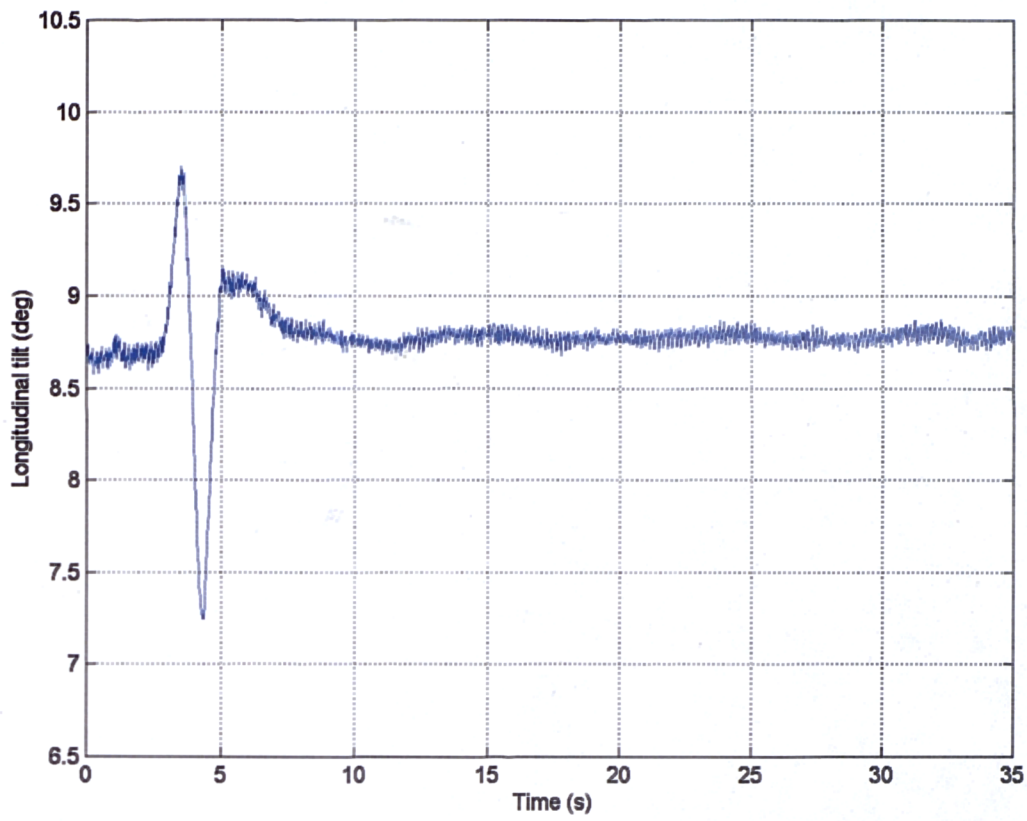
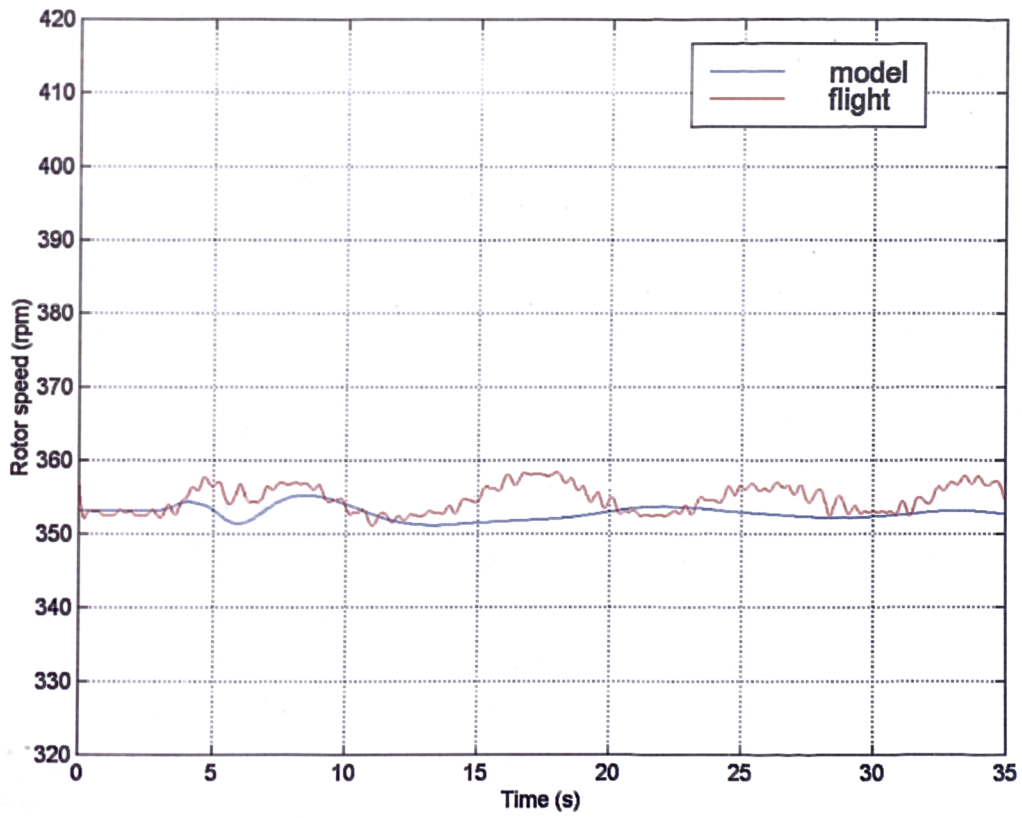
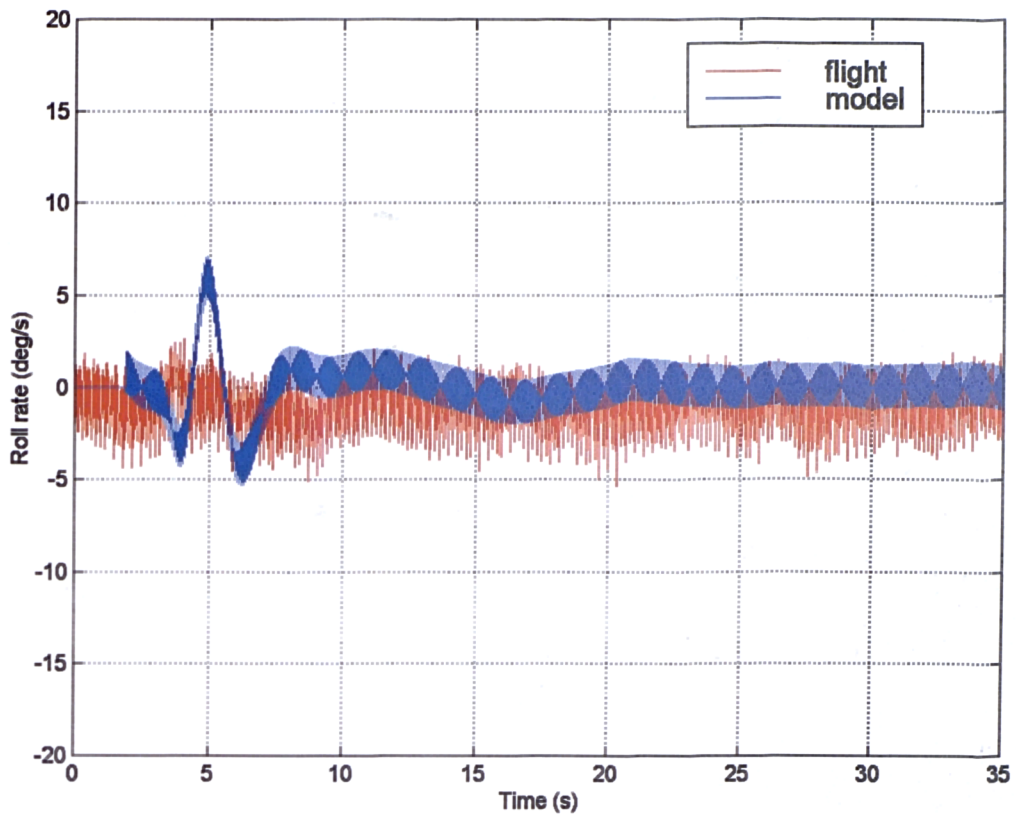


Figure 5.13 (cont.)



**Figure 5.14: Model and flight data response to longitudinal tilt (40 mph)**



**Figure 5.14 (cont.)**

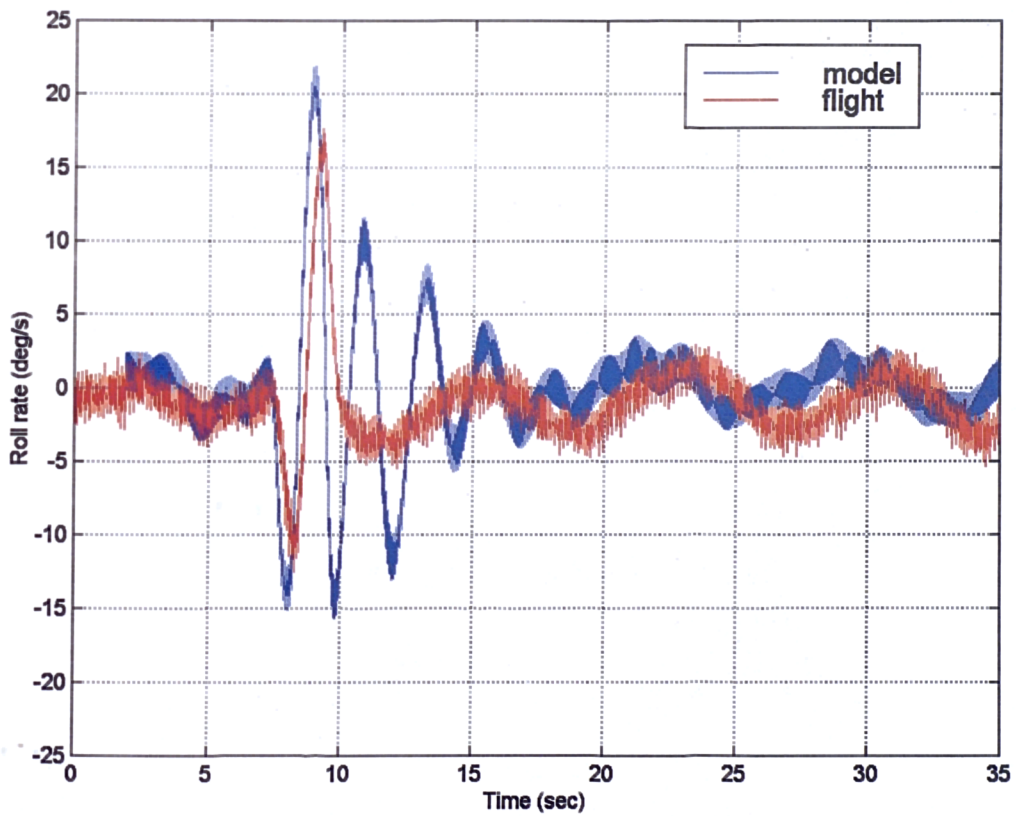
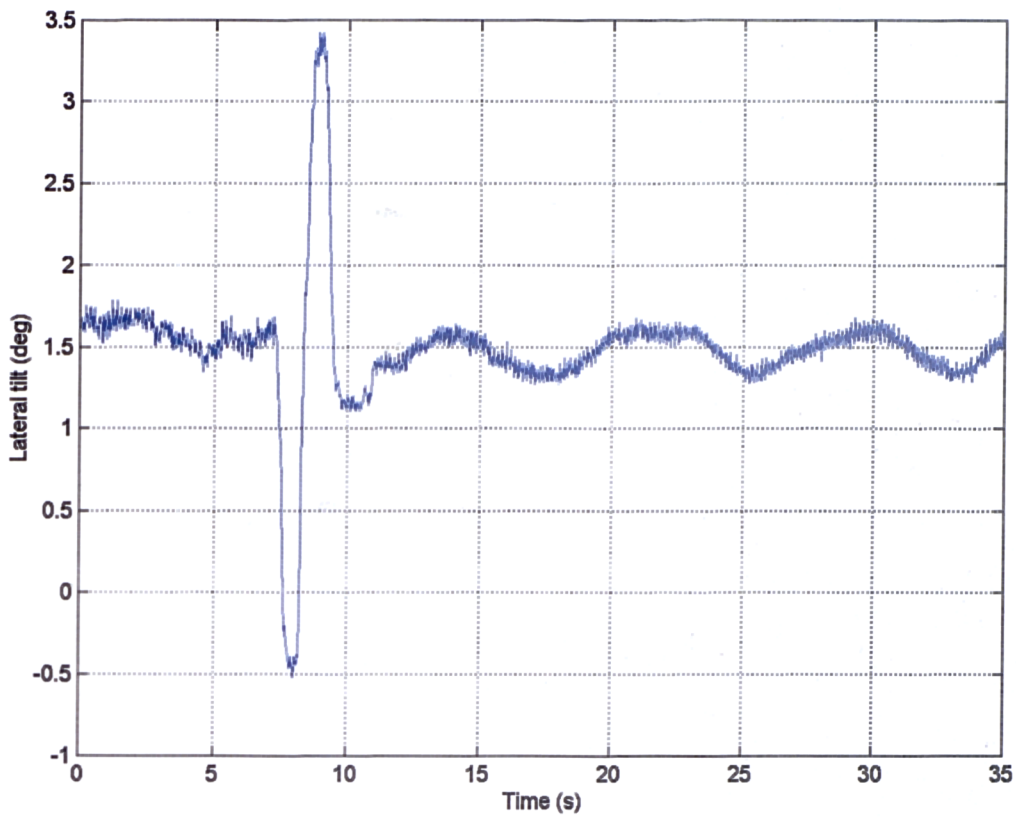


**Figure 5.15: Model and flight data response to lateral tilt (60 mph)**

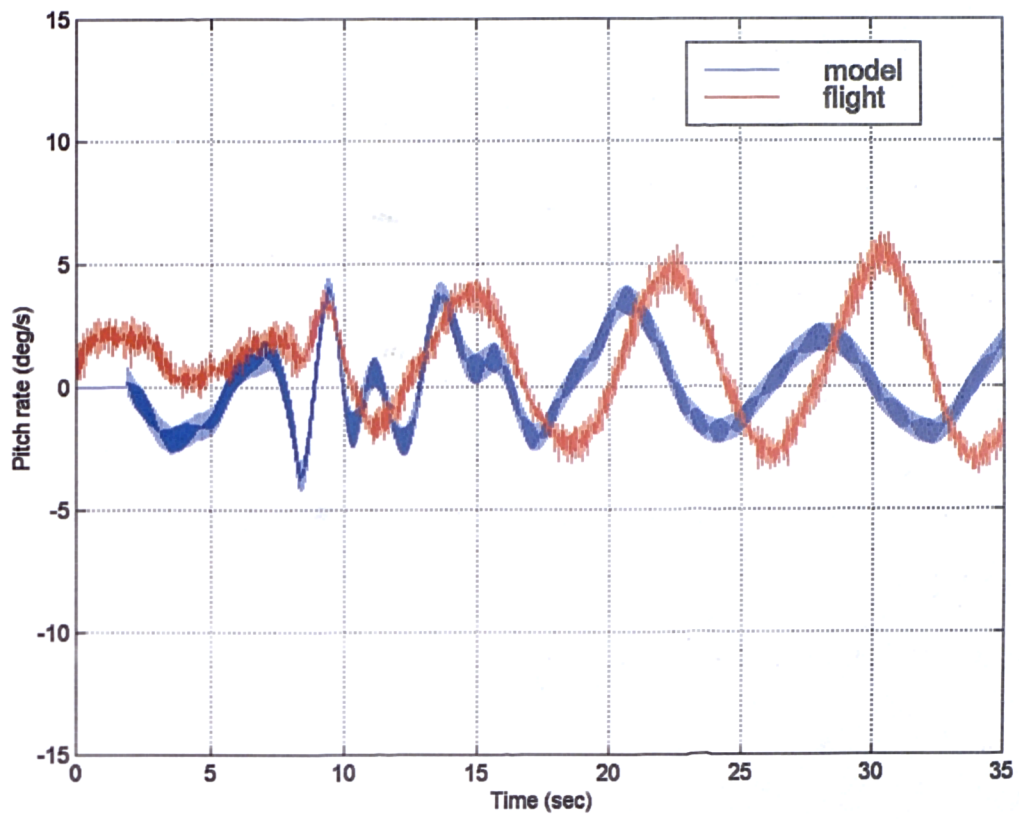


**Figure 5.15 (cont.)**

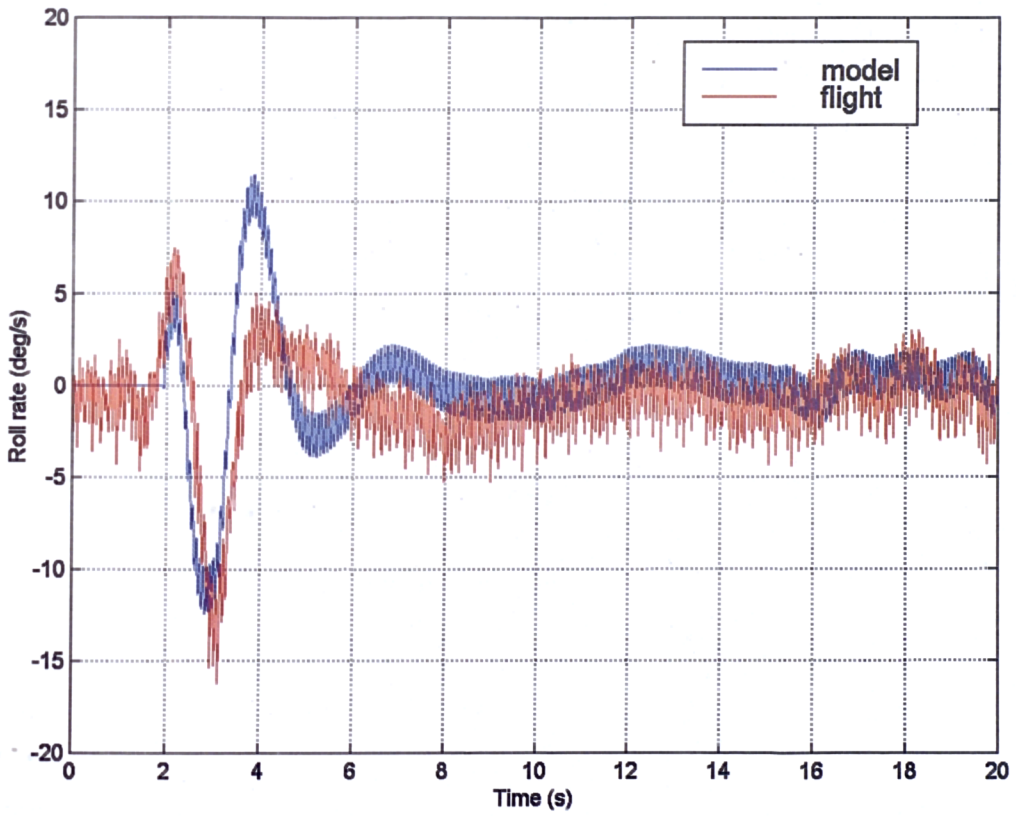
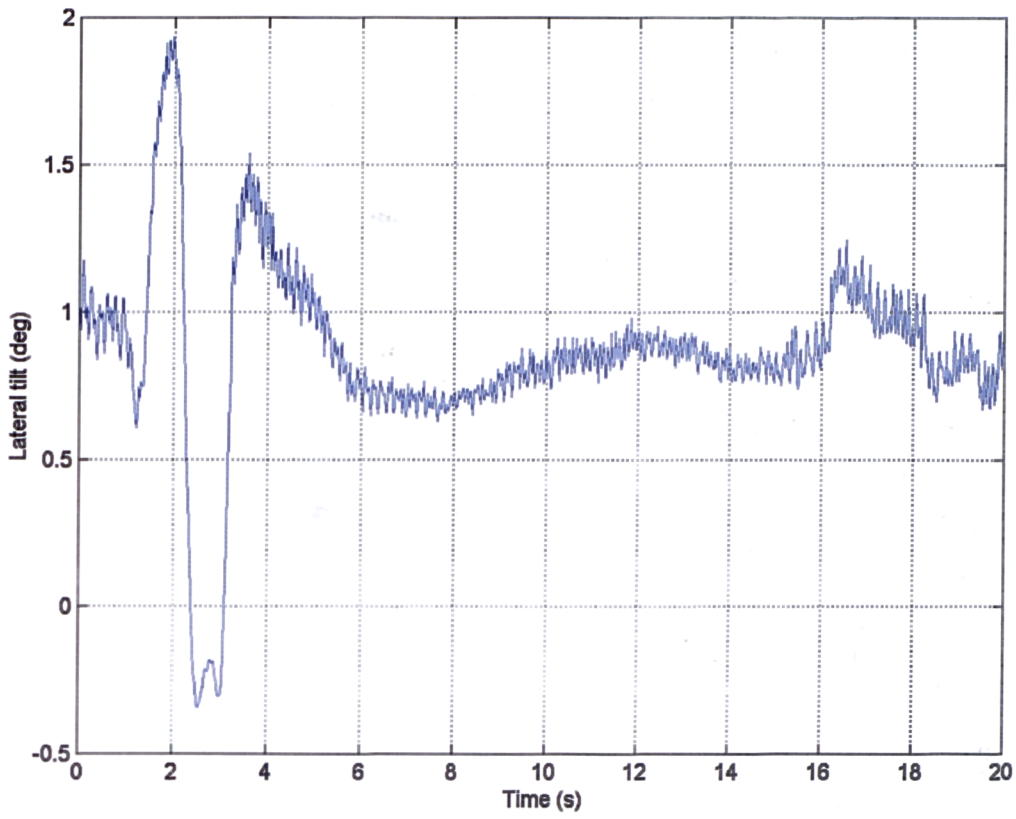


**Figure 5.16: Model and flight data response to lateral tilt (40 mph)**

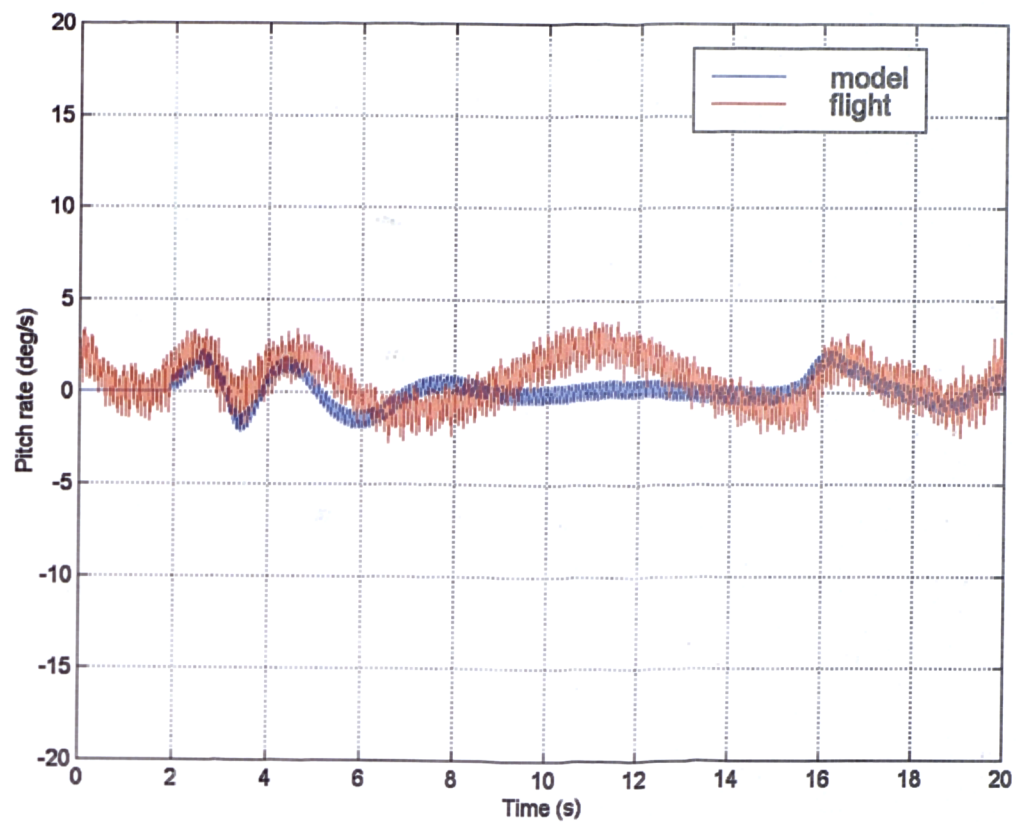


**Figure 5.16 (cont.)**



**Figure 6.1: Gyroplane ready for take off (Carlisle)**



**Figure 6.2: Gyroplane ready for take off (Bournemouth)**

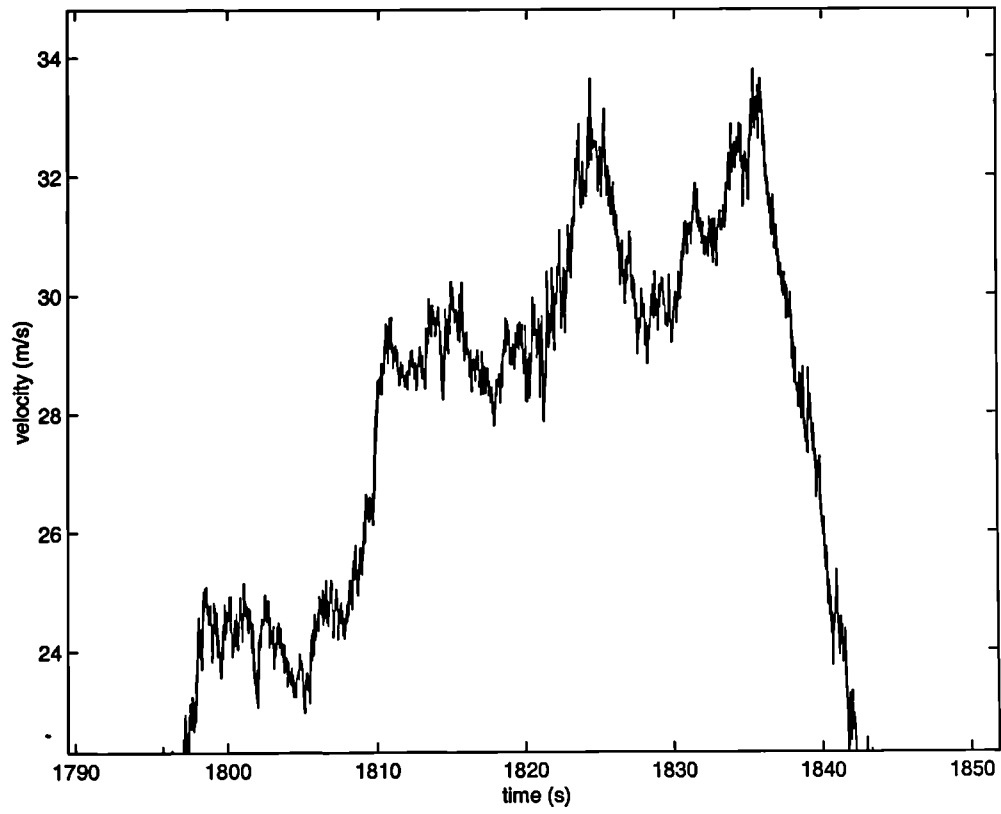
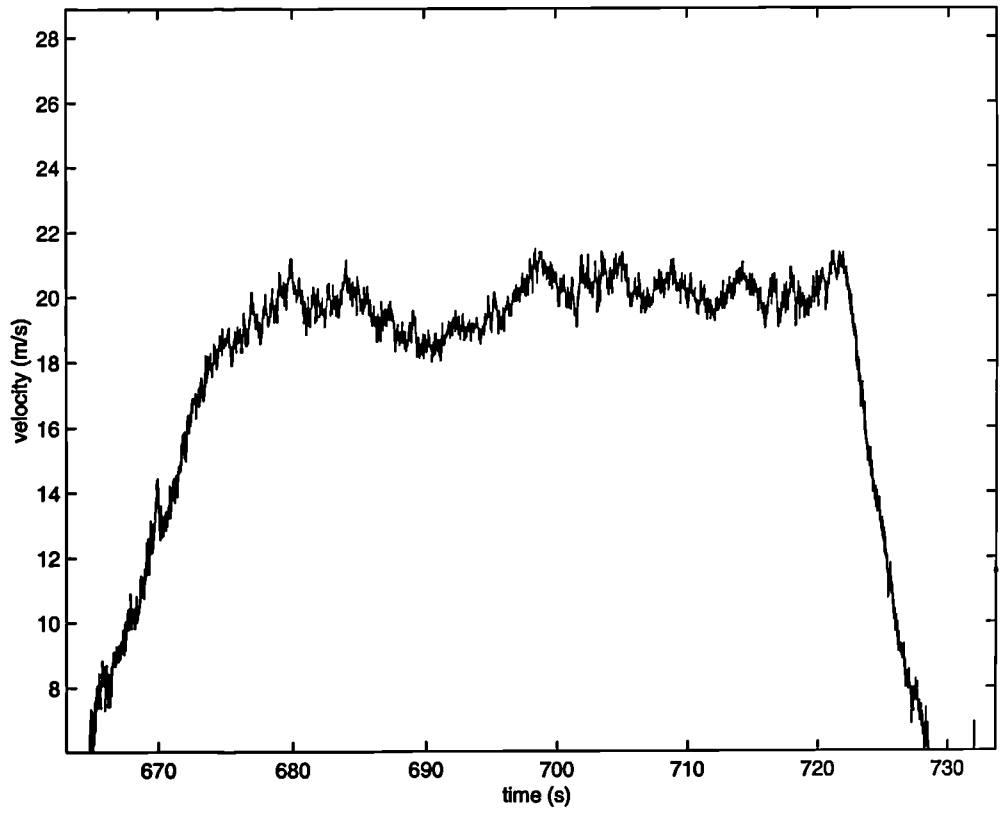


**Figure 6.3: 20 m/s and 31 m/s trim comparisons**

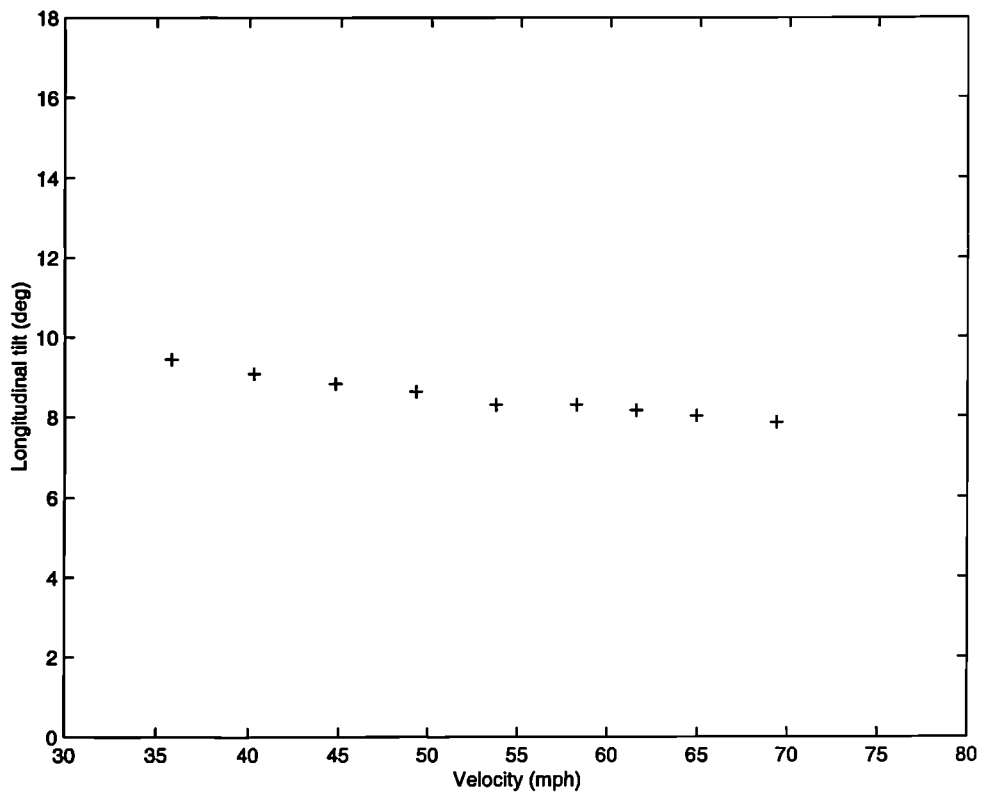
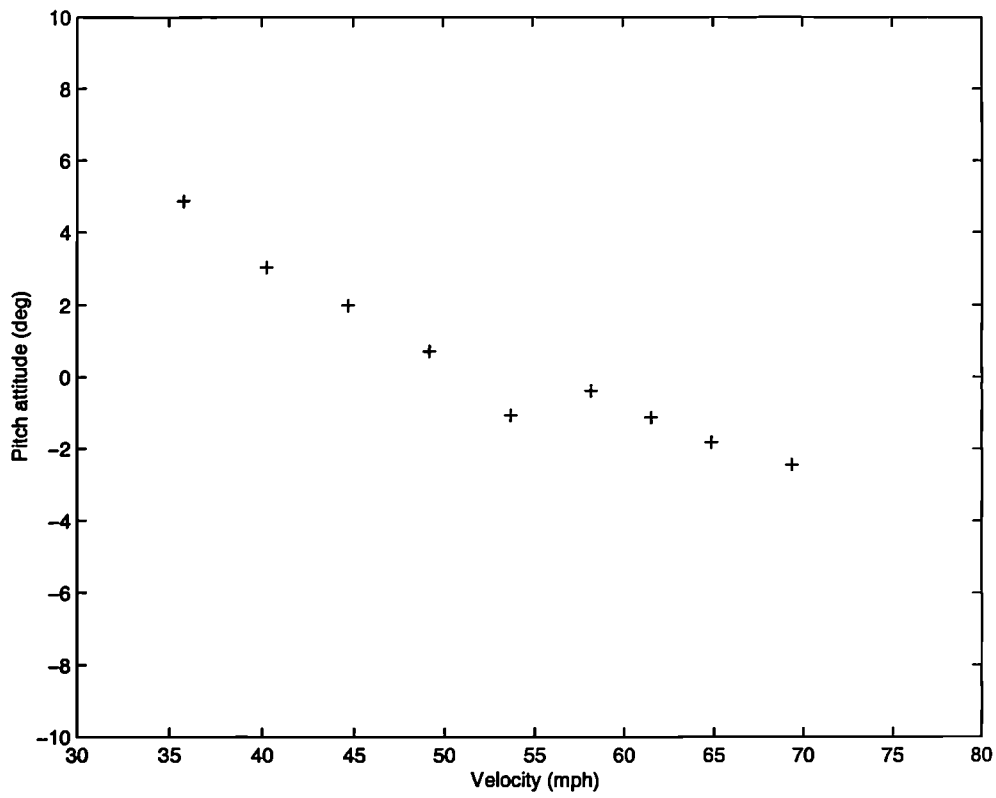


**Figure 6.4: Longitudinal tilt and pitch attitude trim values**

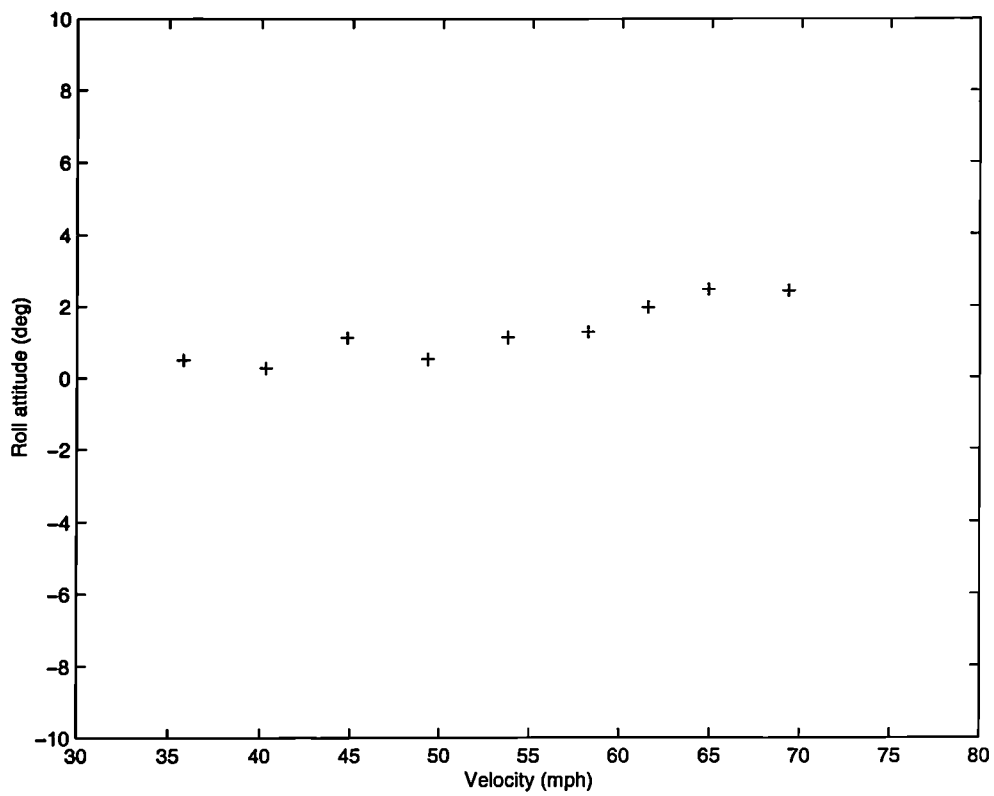
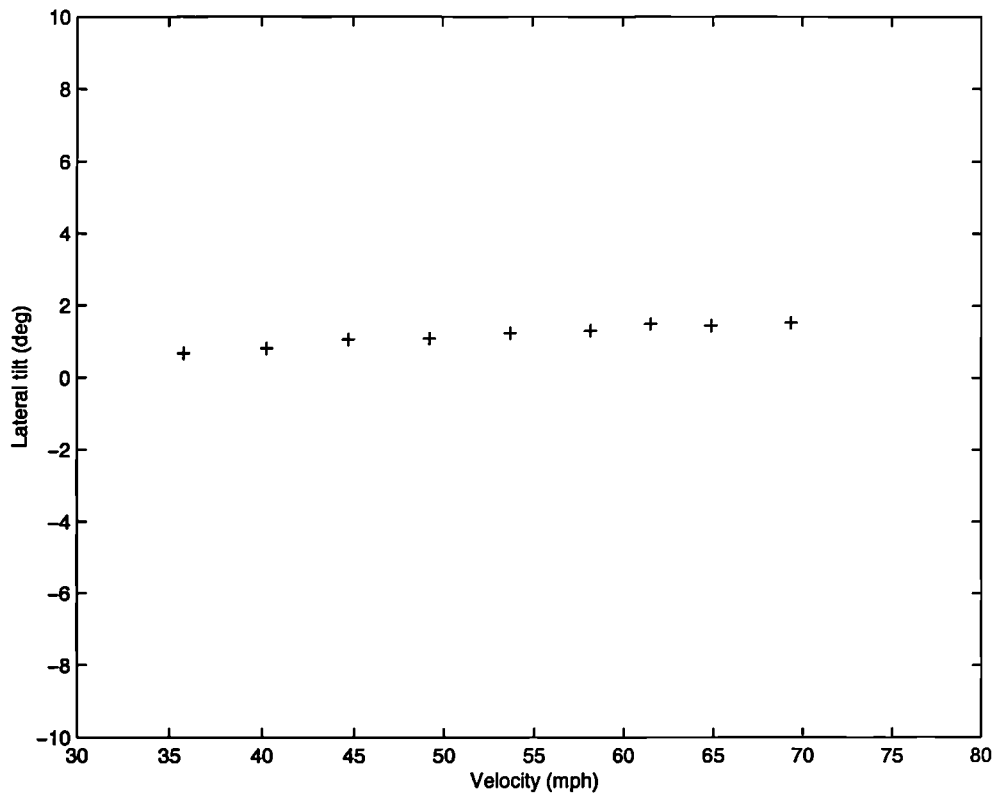


**Figure 6.5: Lateral tilt and roll attitude trim values**

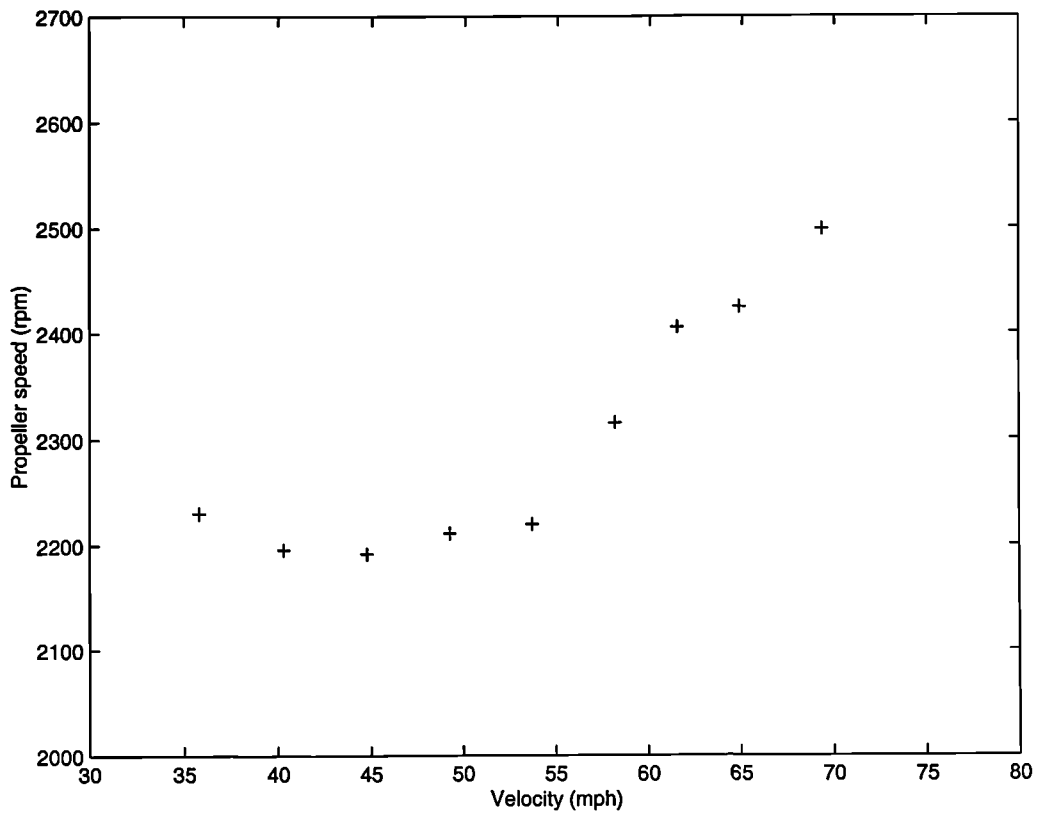
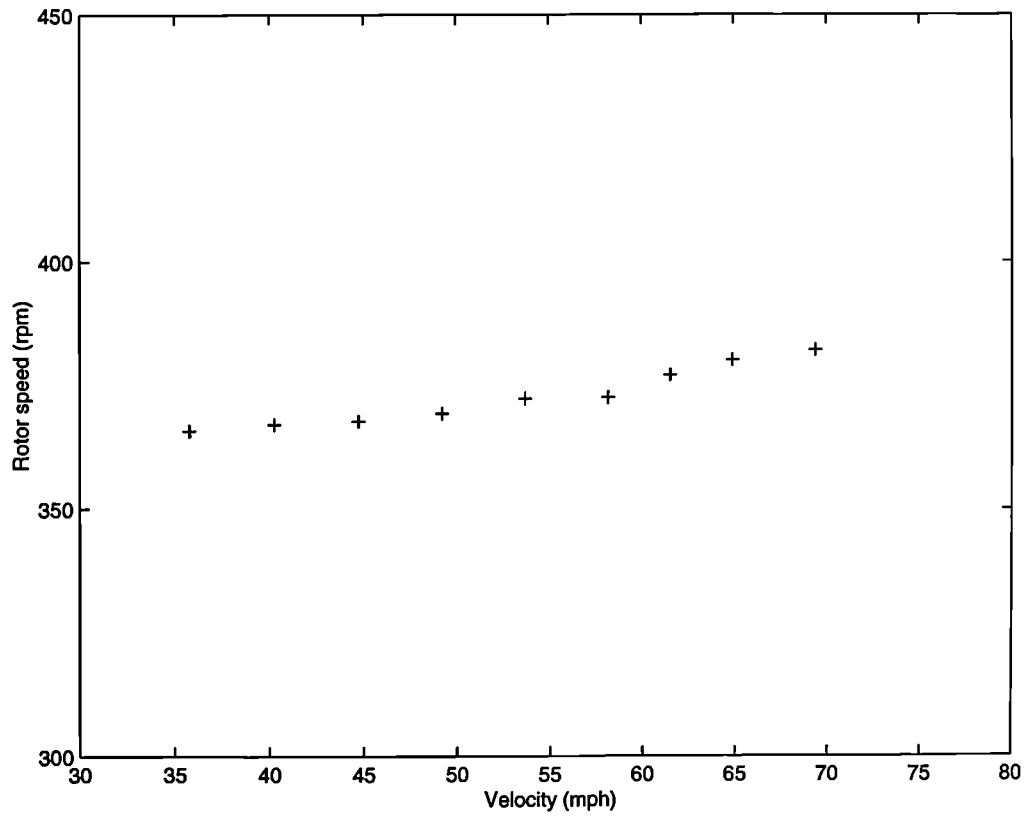


**Figure 6.6: Rotor speed and propeller rpm trim values**

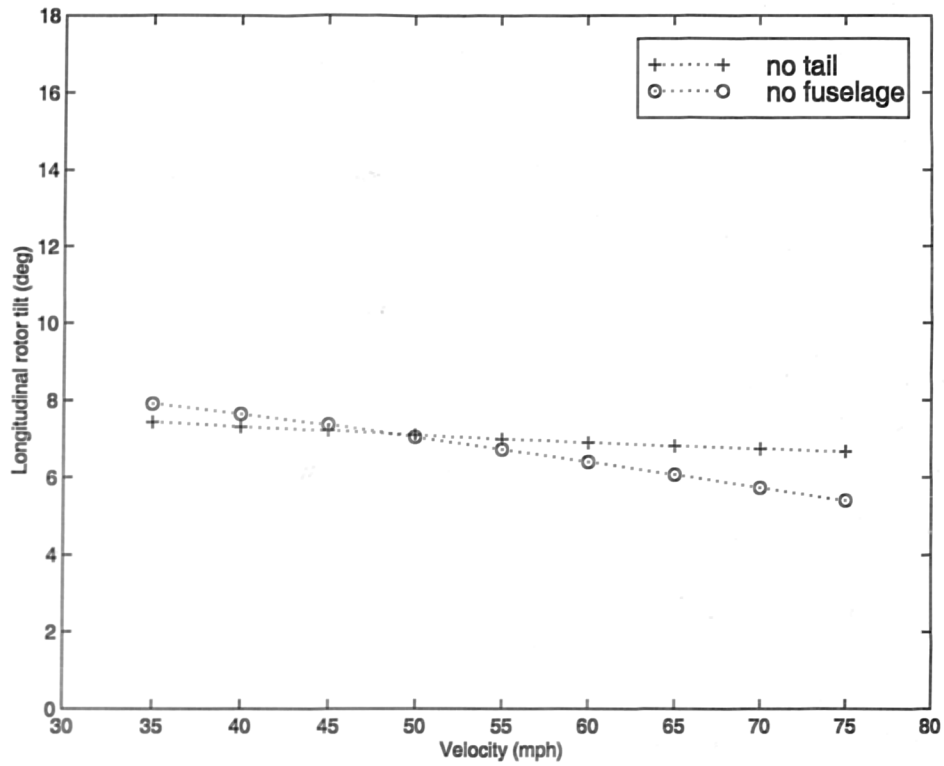


**Figure 6.7: Tailplane and fuselage effect on static stability**

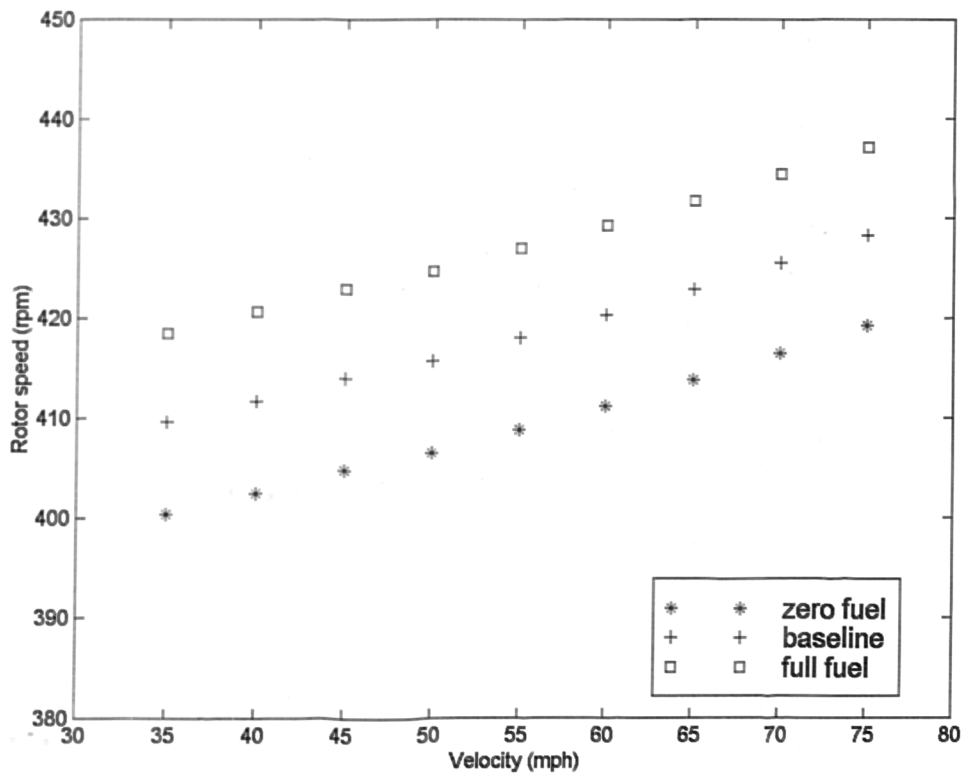


**Figure 6.8: Mass effect on rotor speed**

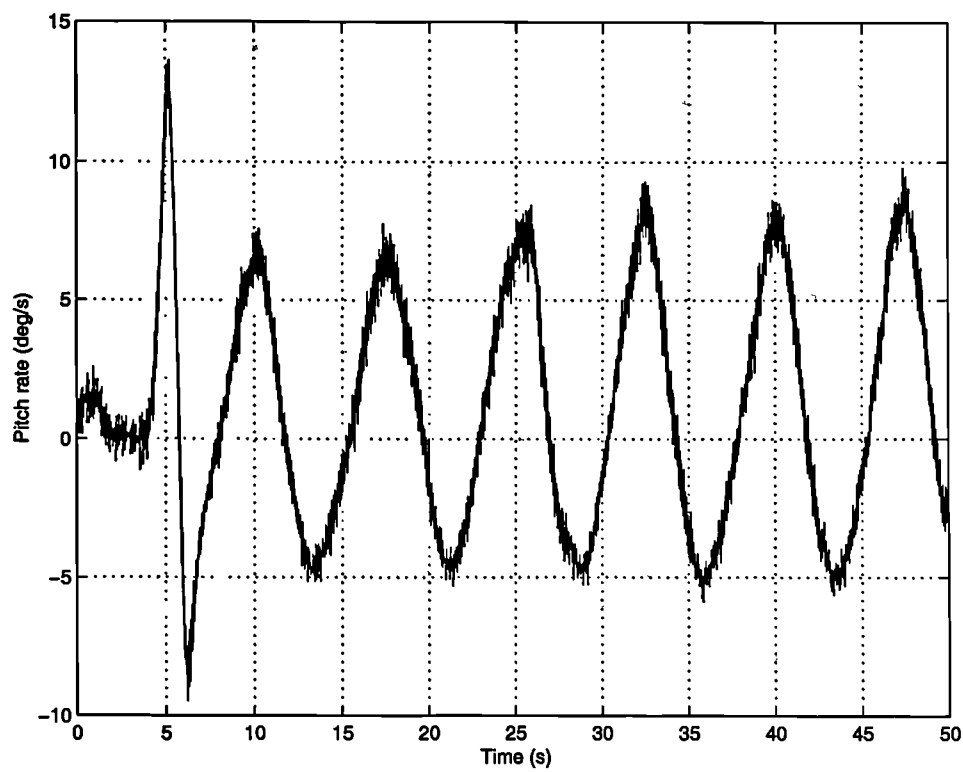
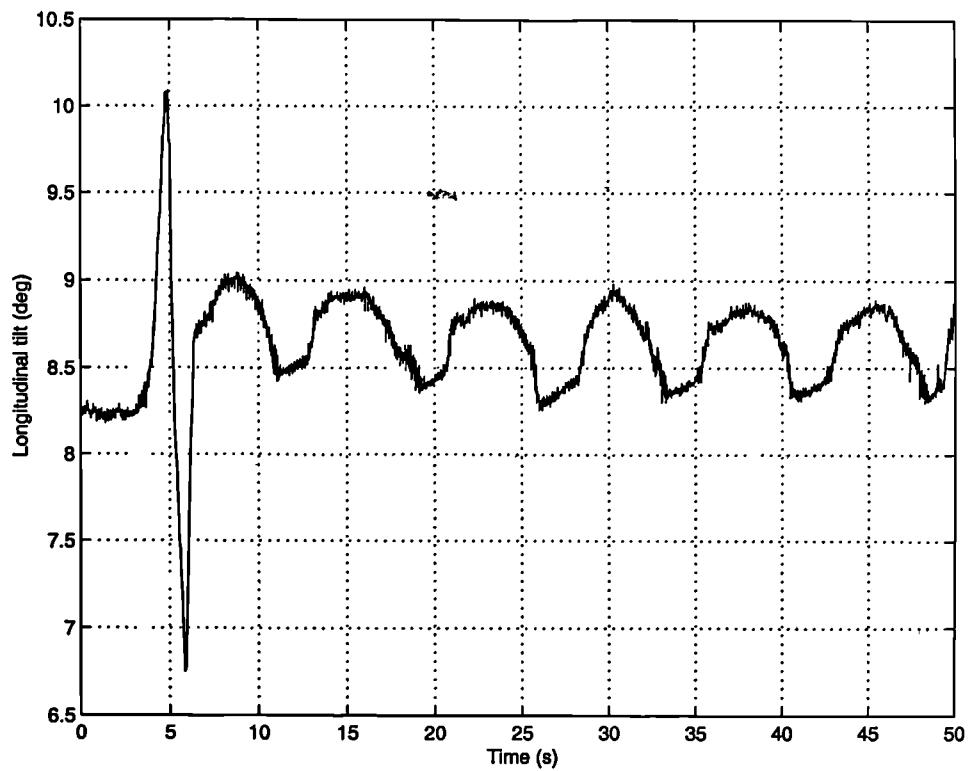


**Figure 6.9: Longitudinal tilt doublet responses**

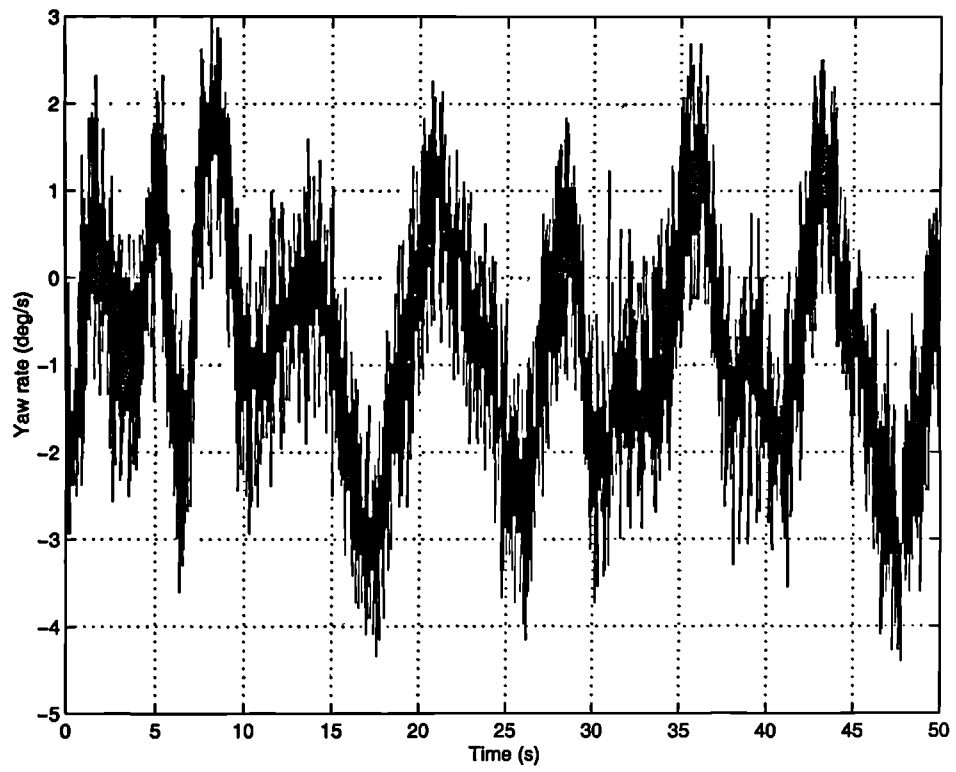
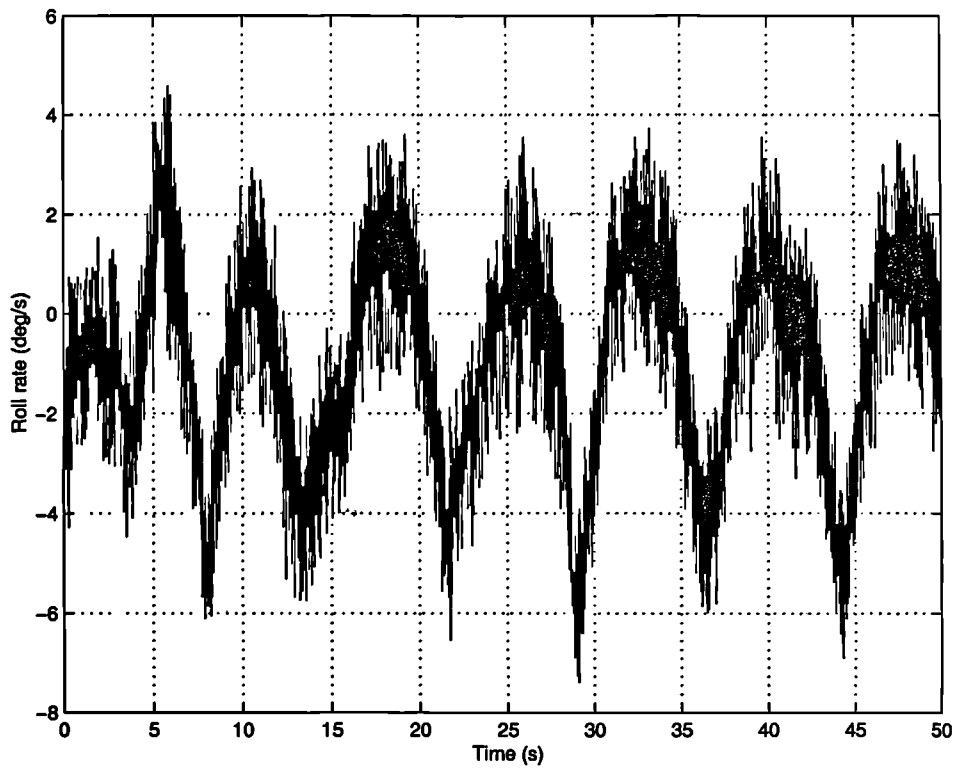


**Figure 6.9 (cont.)**

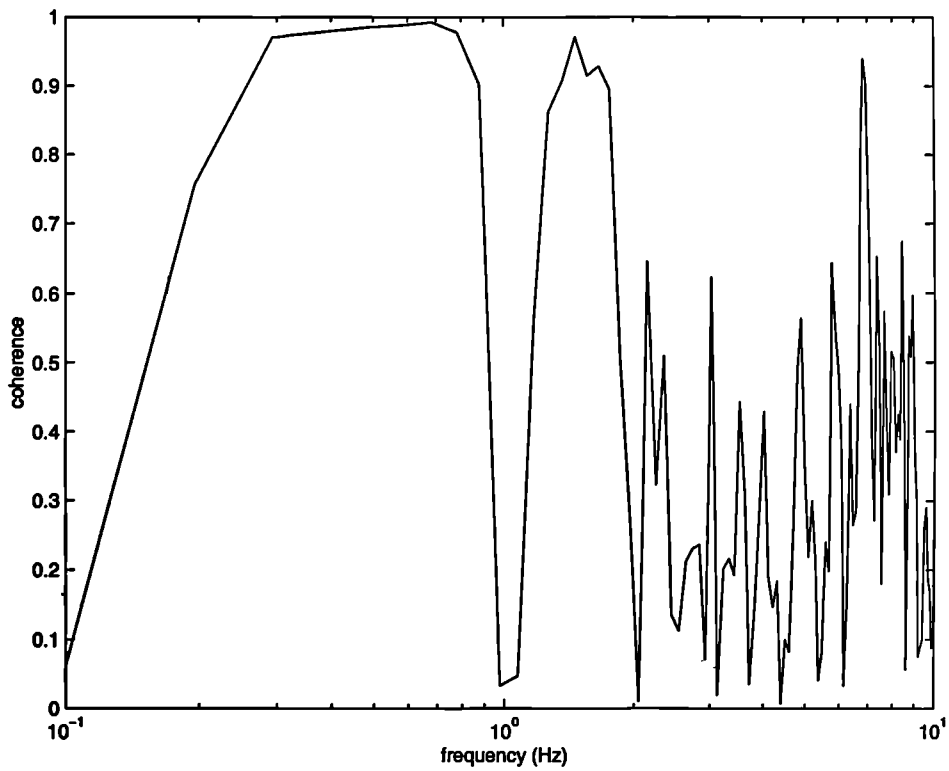


**Figure 6.10: Pitch rate coherence with longitudinal rotor tilt**

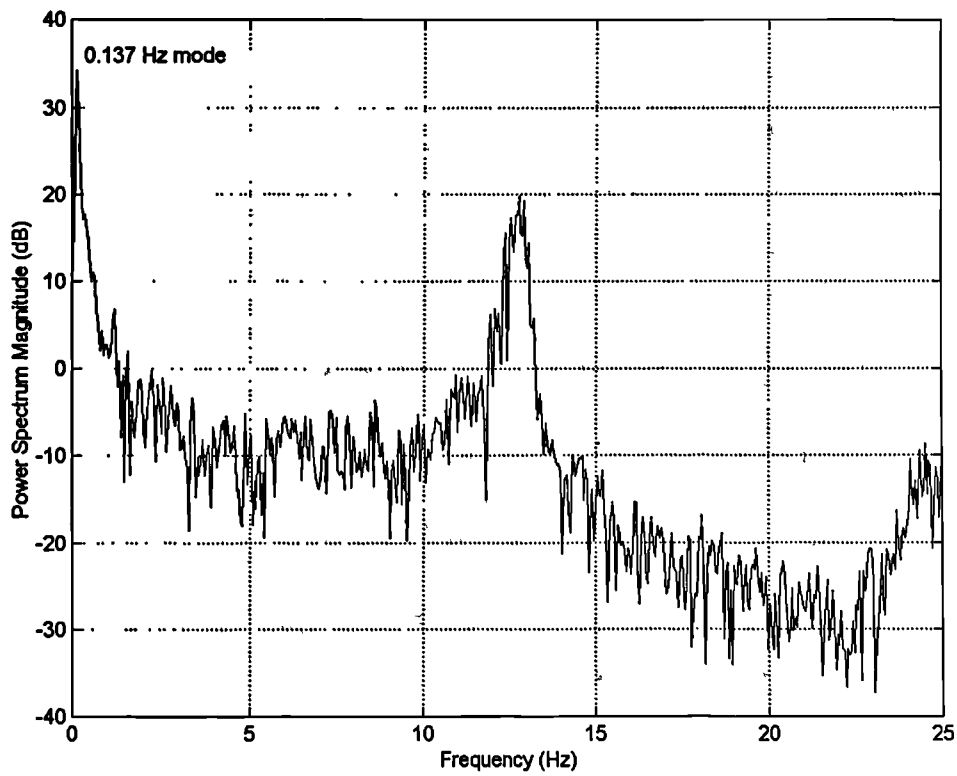


**Figure 6.11: Spectral analysis of angle of attack during longitudinal doublet manoeuvre**

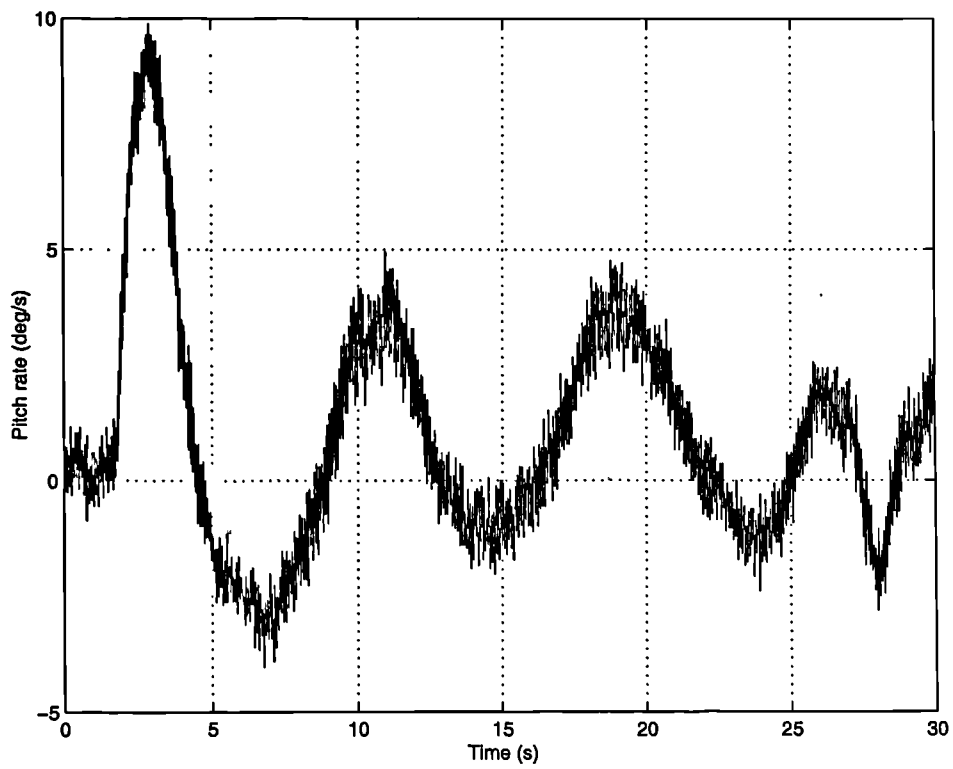
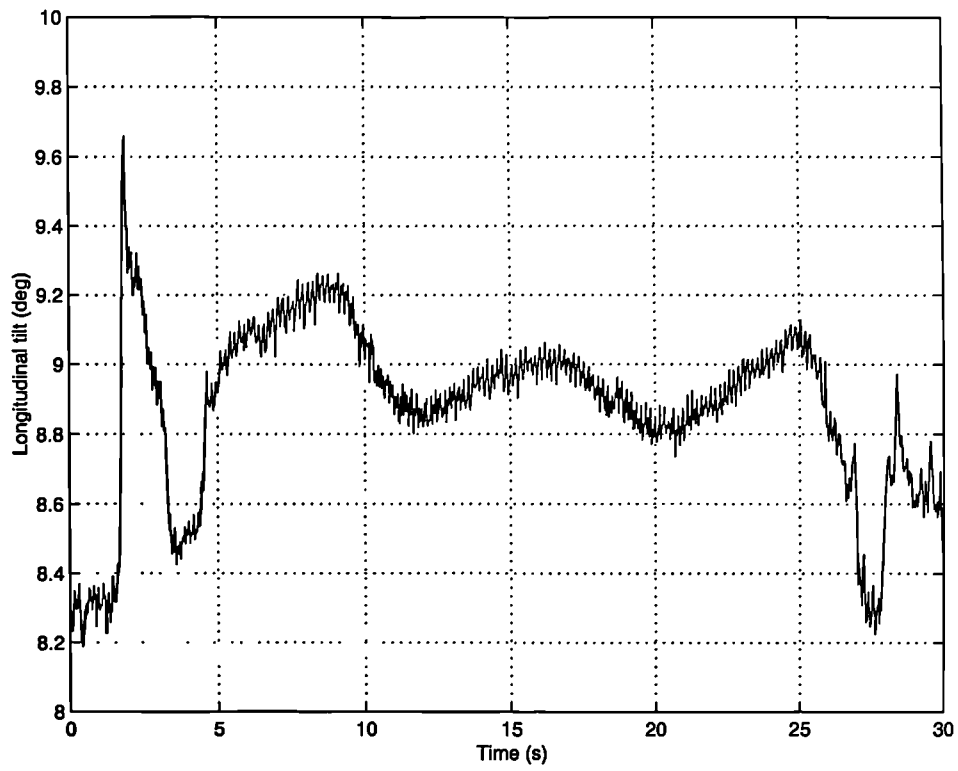


**Figure 6.12: Phugoid response**

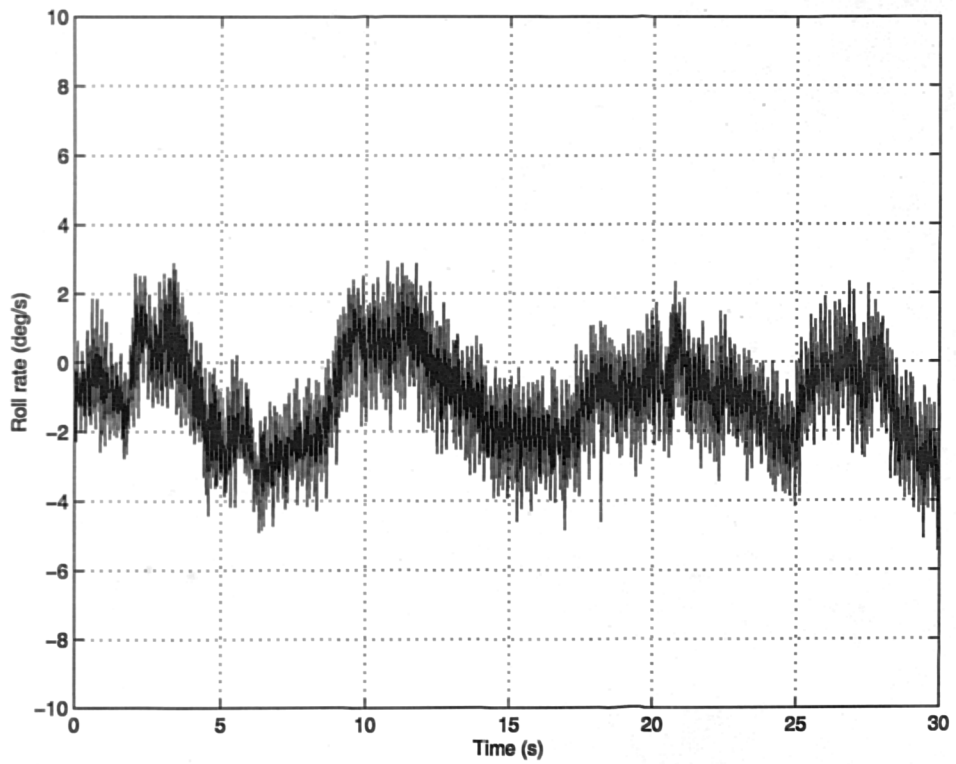
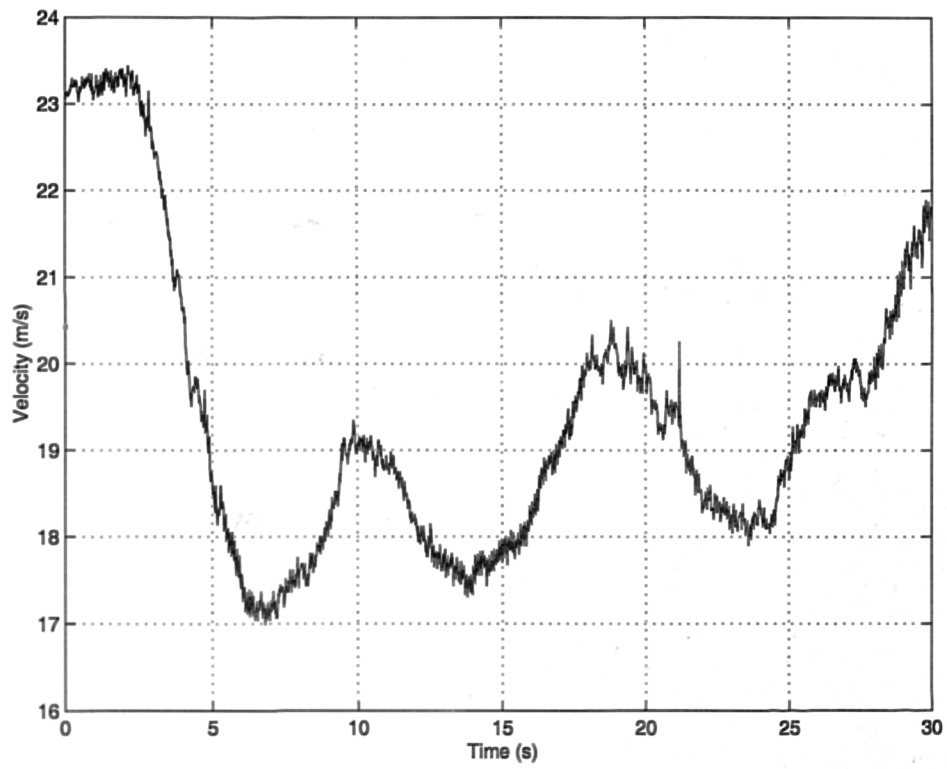


**Figure 6.12 (cont.)**

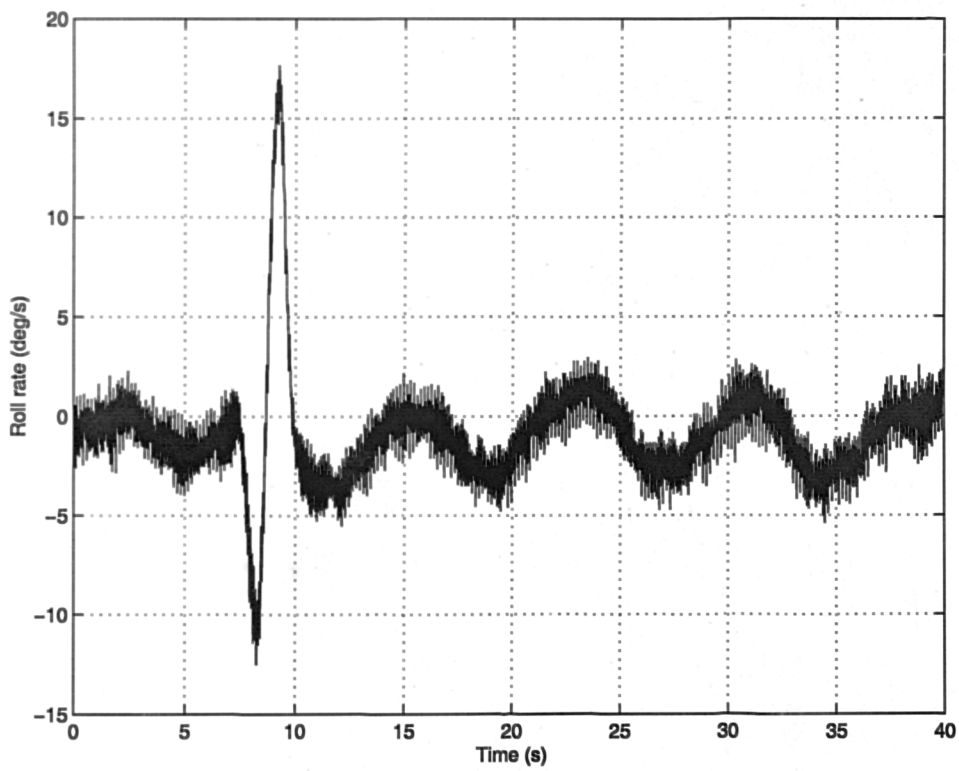
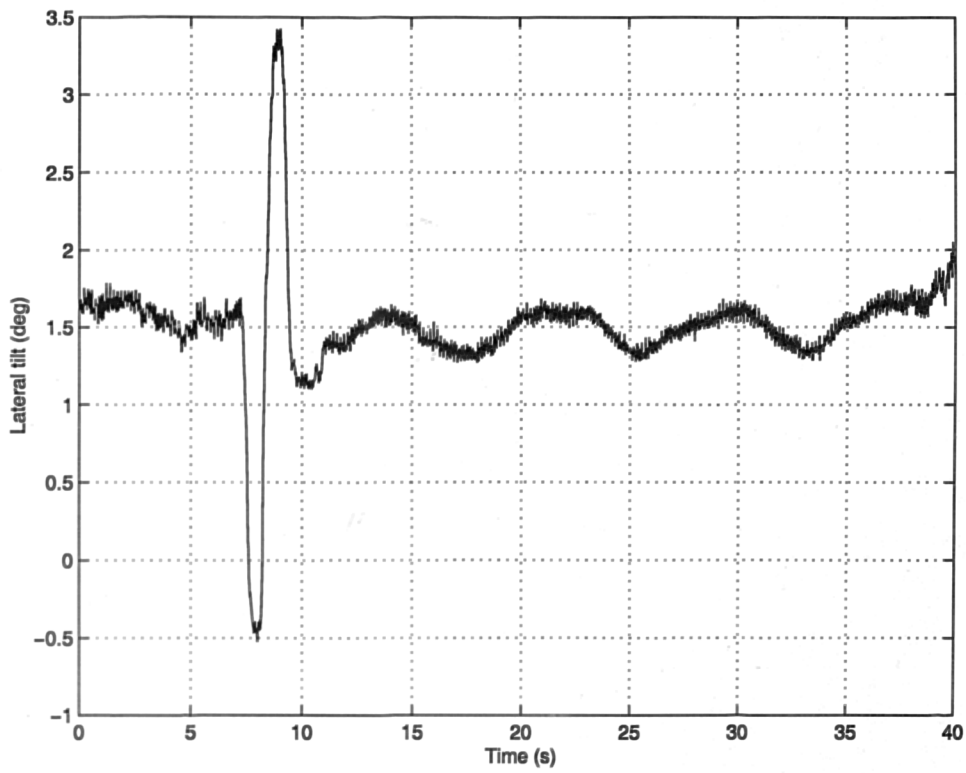


**Figure 6.13 Lateral tilt response**

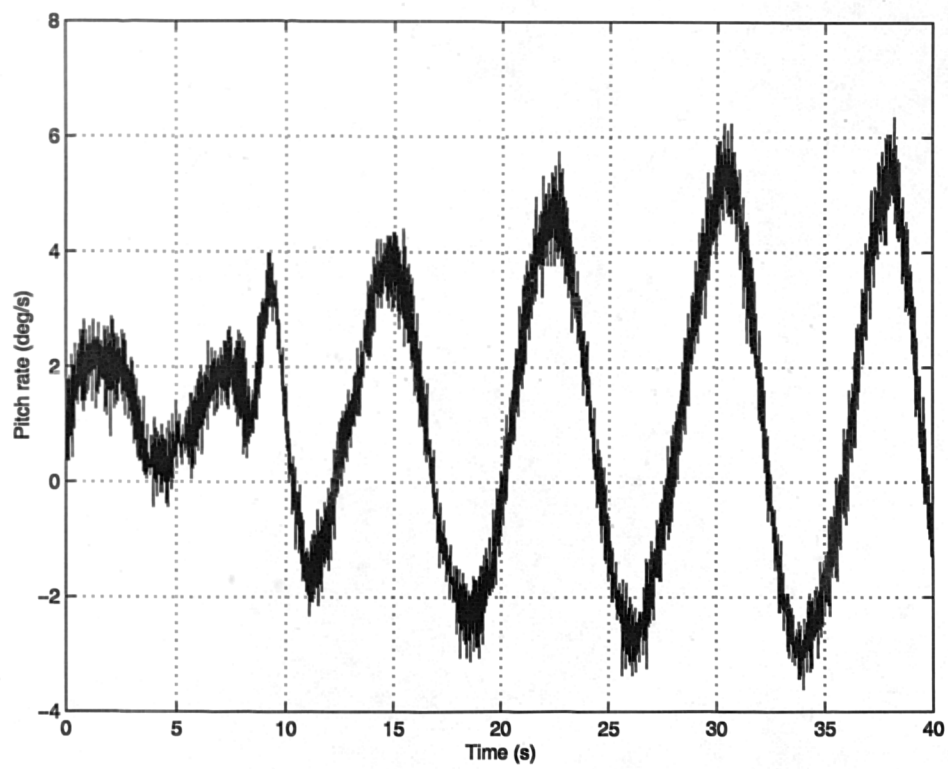
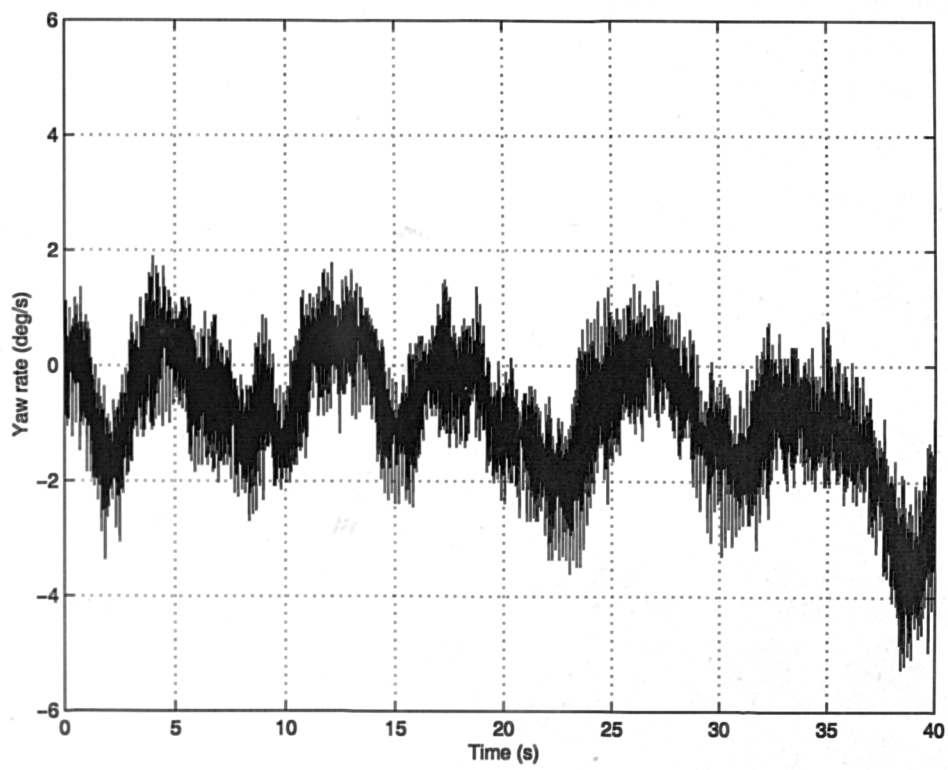


**Figure 6.13 (cont.)**

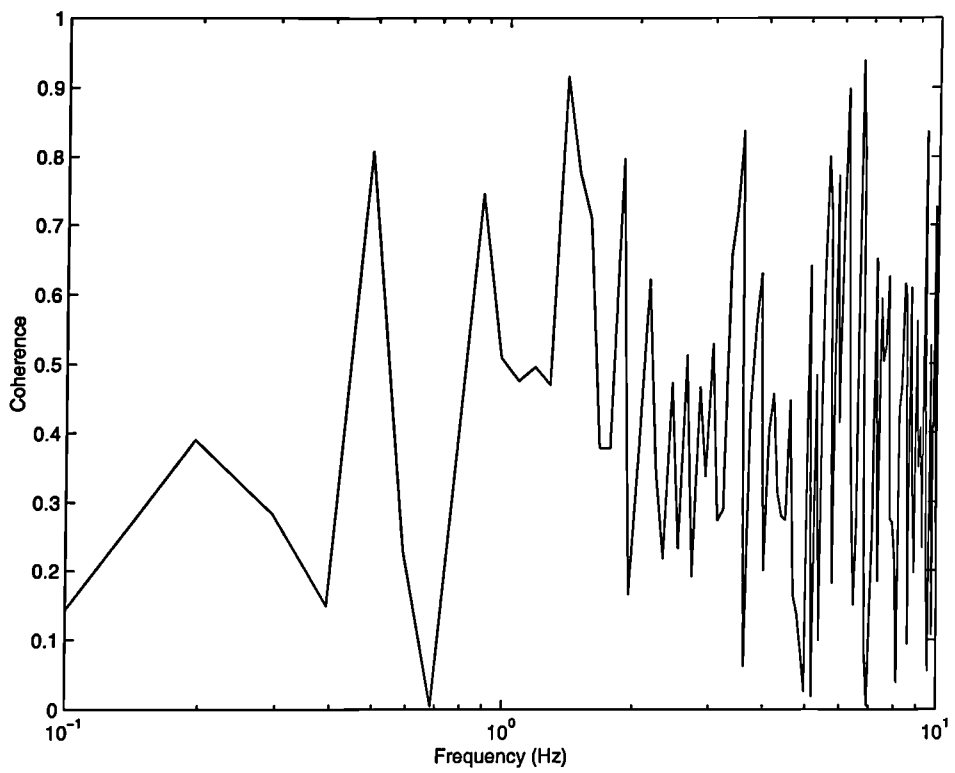
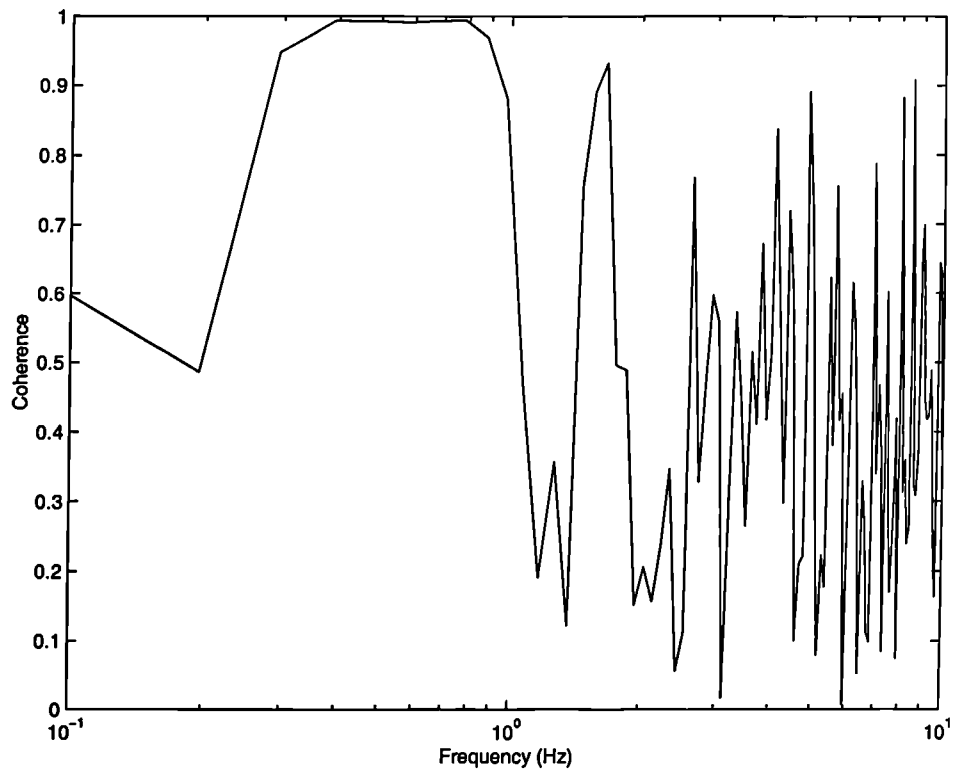


**Figure 6.14: Roll rate and yaw rate coherence with lateral rotor tilt**

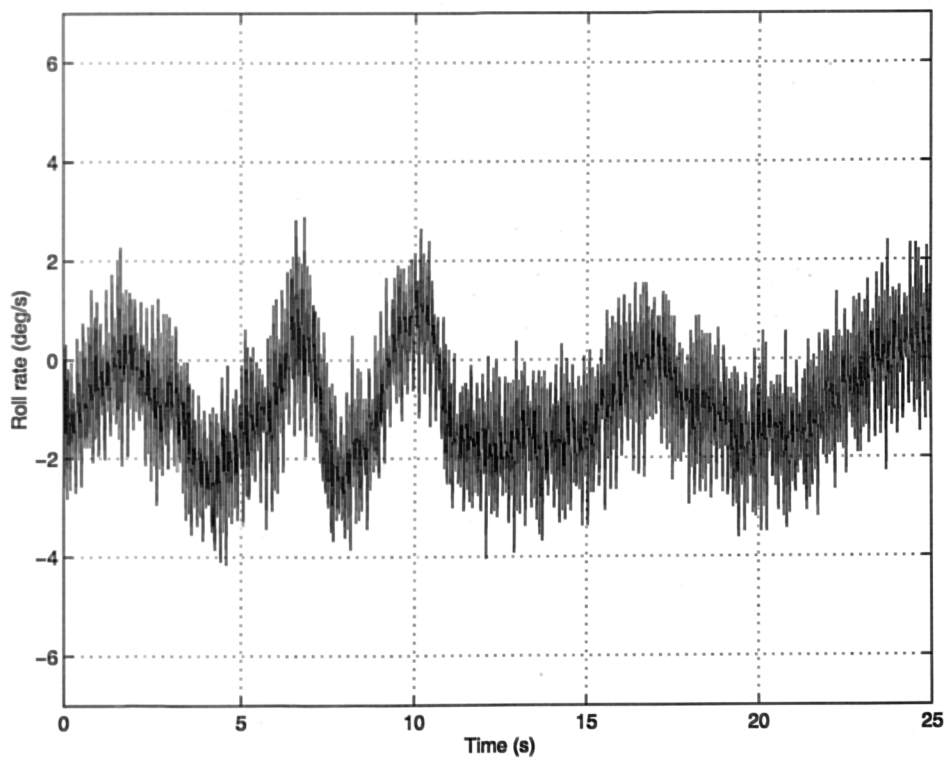
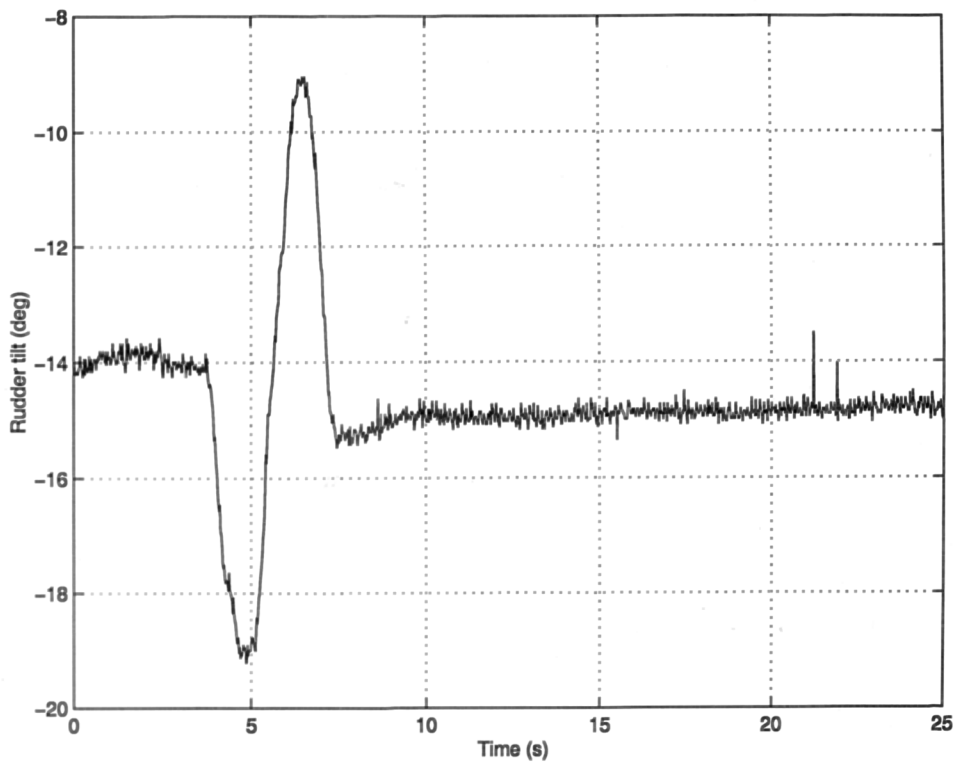


**Figure 6.15: Rudder tilt doublet response**

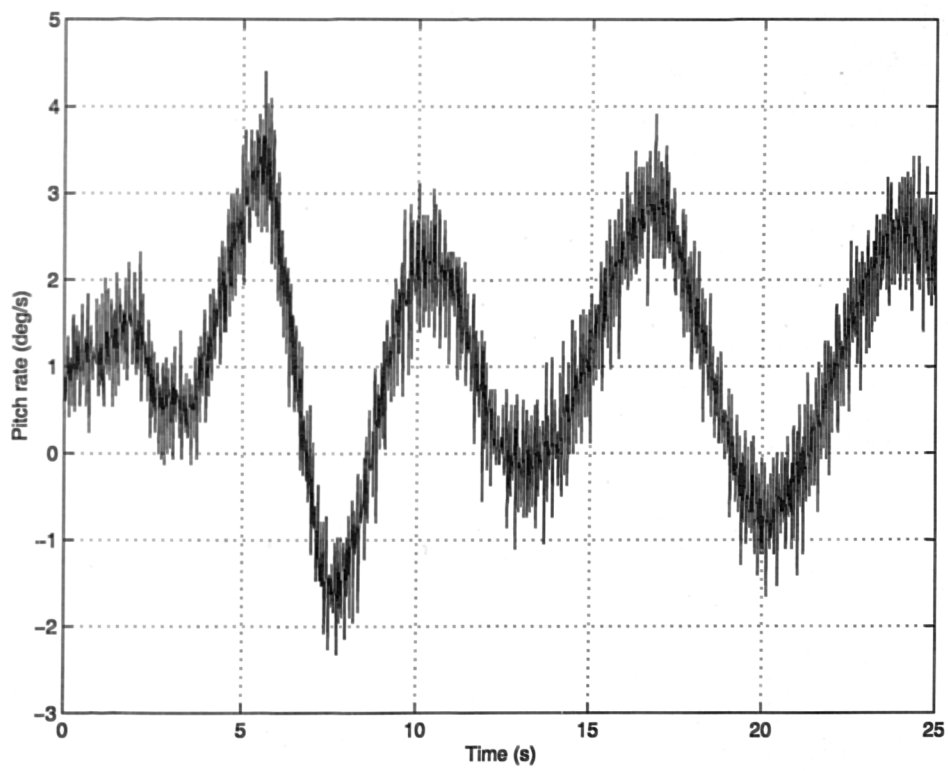
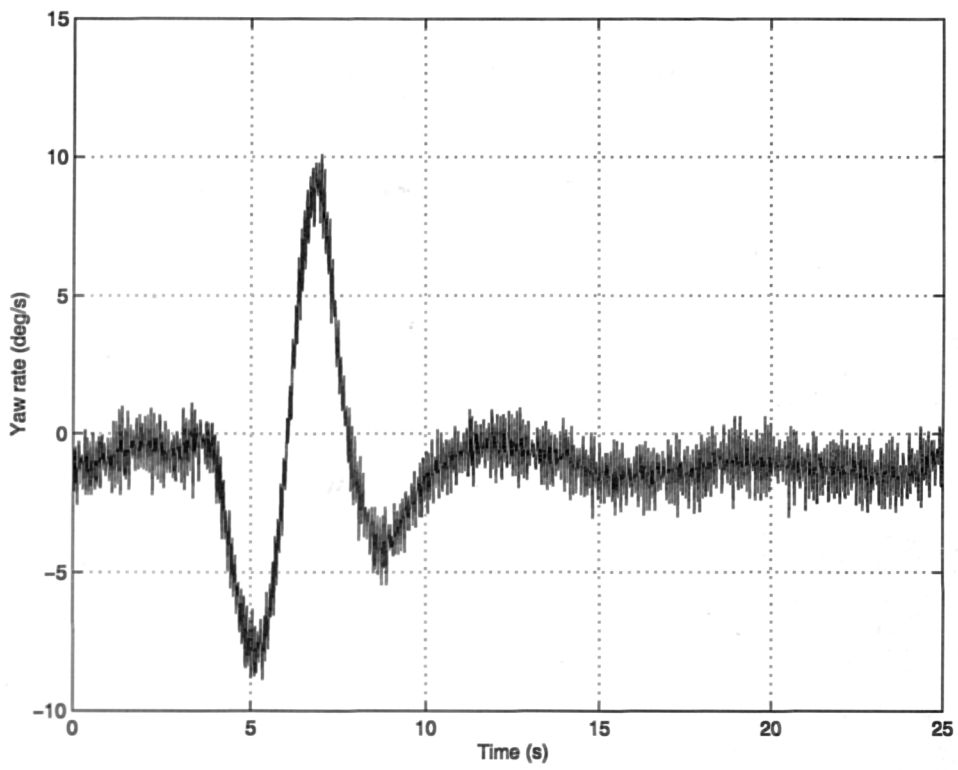


**Figure 6.15 (cont.)**

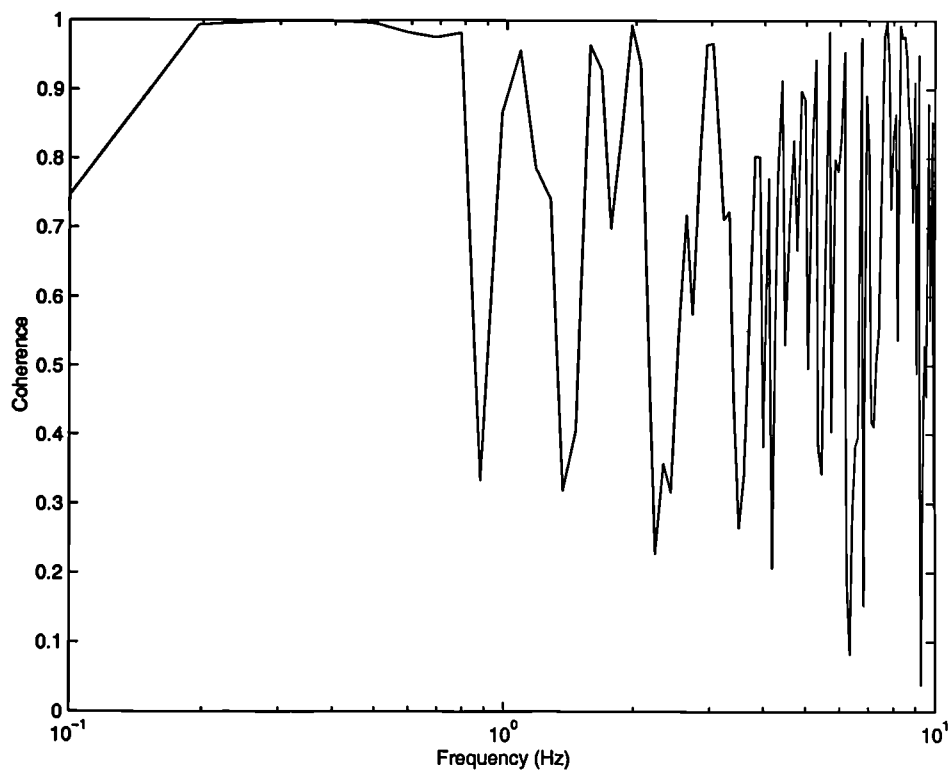
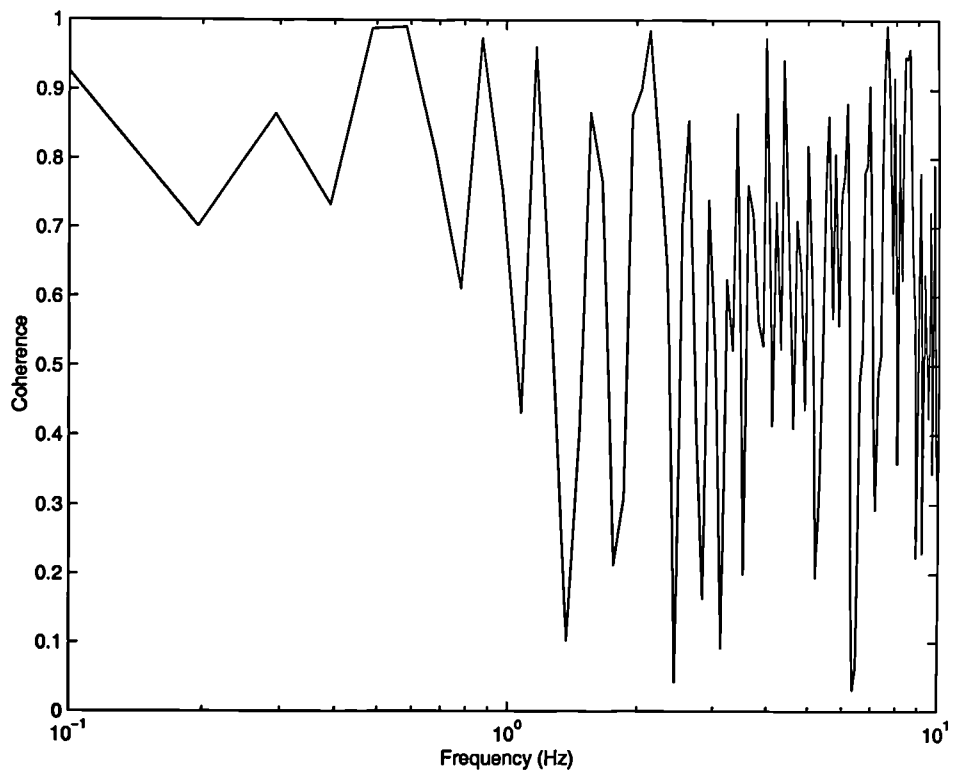


**Figure 6.16: Roll rate and yaw rate coherence with lateral rotor tilt**

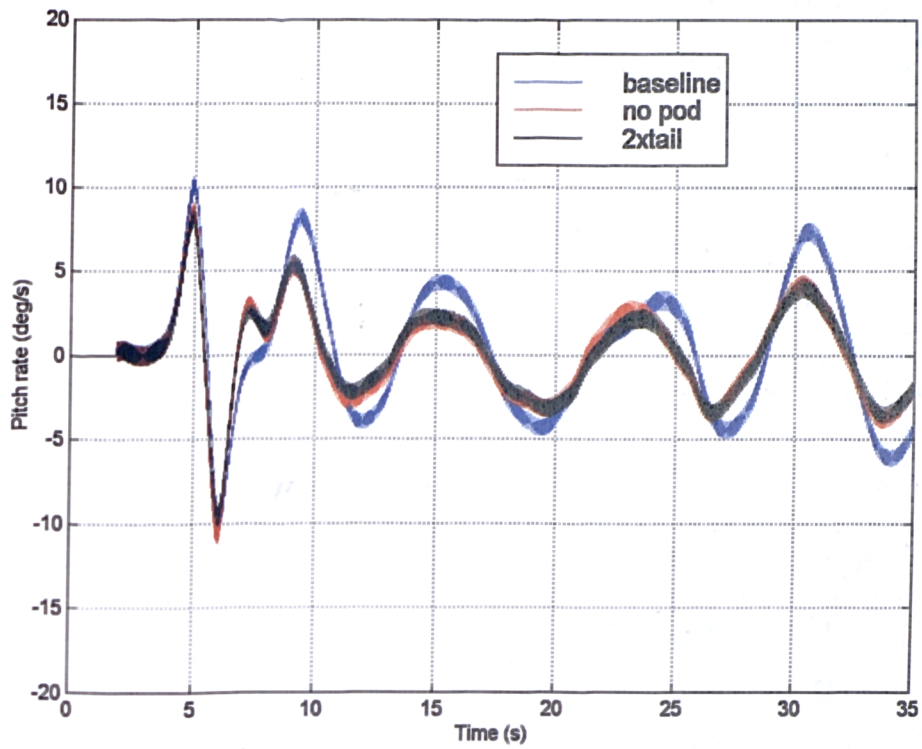


**Figure 6.17: Effect of configuration characteristics on pitch rate response**

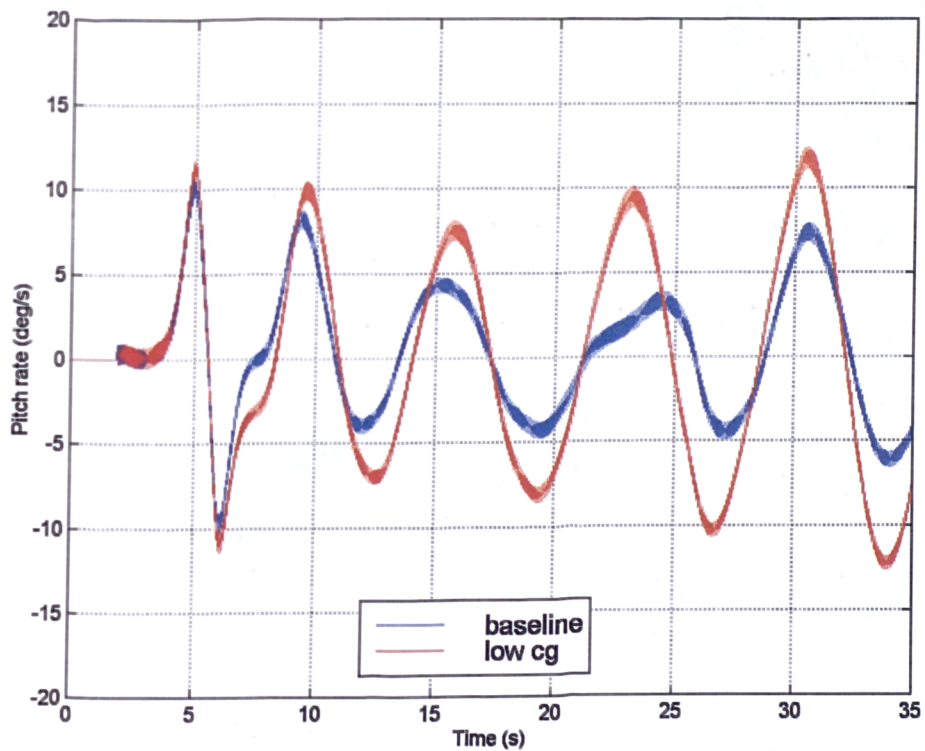


**Figure 6.18: Effect of 10cm vertical cg shift below baseline on pitch rate response**

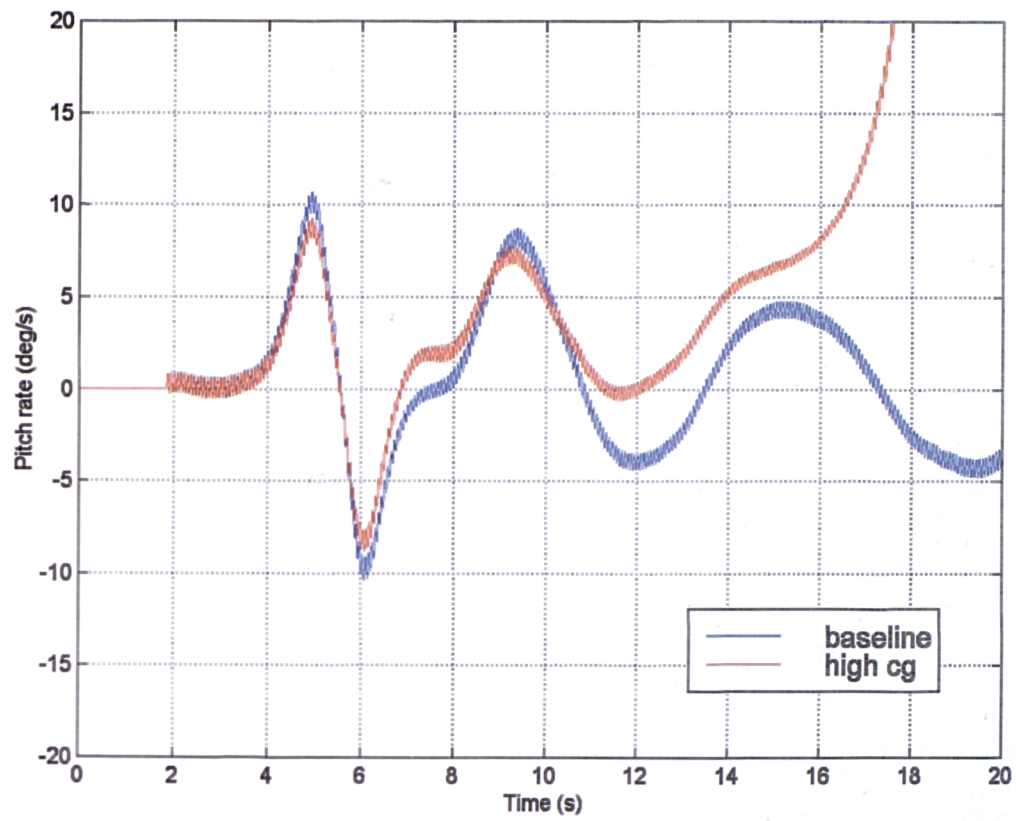


**Figure 6.19: Effect of 10cm vertical cg shift above baseline on pitch rate response**

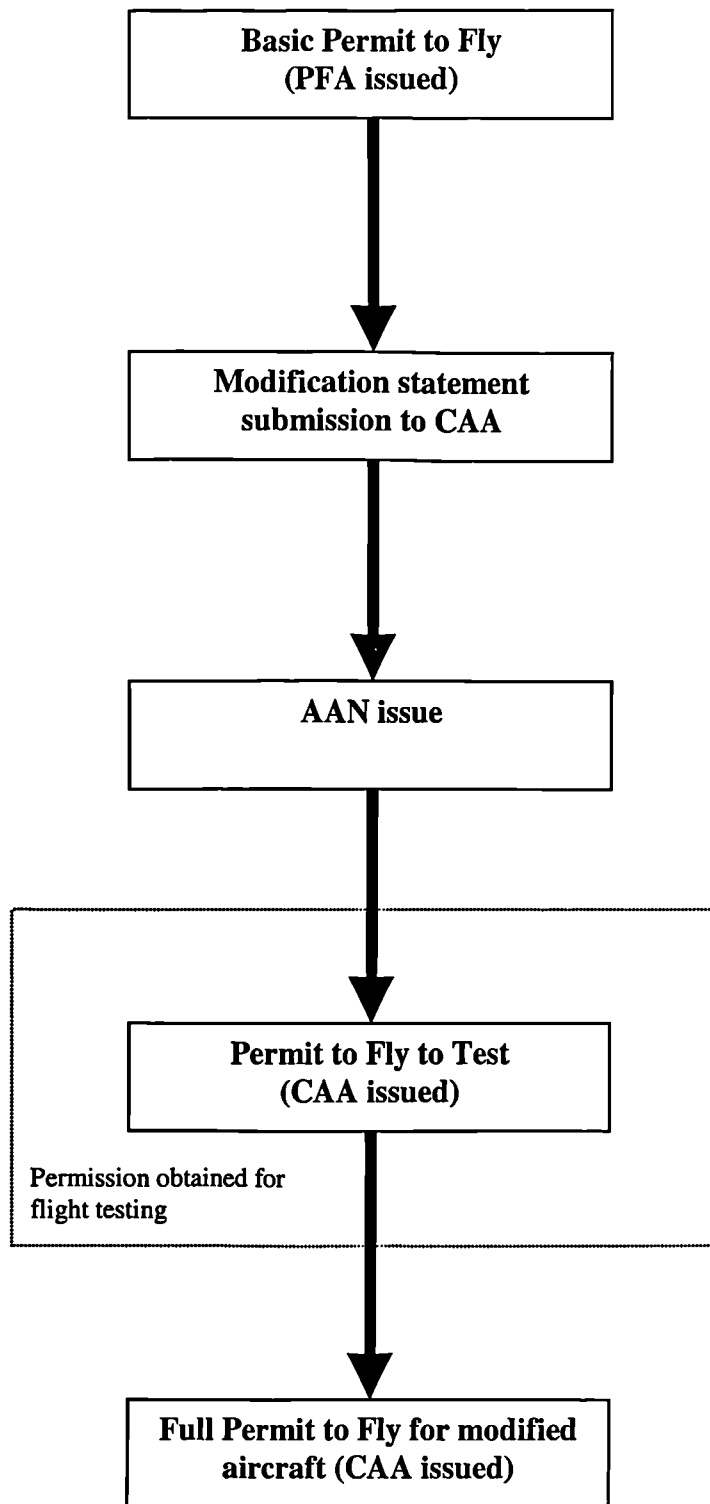


**Figure A3.1: Certification process stages**

## REFERENCES

AGARD [1991]: AGARD Advisory Report 280, "Rotorcraft System Identification", Sep. 1991.

AGARD [1995]: AGARD Flight Test Techniques Series, "Introduction to Flight Test Engineering", AGARDograph 300, Vol. 14, 1995.

Anderson [1999]: Anderson, D., "Active Control of Turbulence-Induced Helicopter Vibration", PhD Thesis, University of Glasgow, 1999.

Anon [1991]: Anon, "Airworthiness Review of Air Command Gyroplanes", Air Accidents Investigation Branch Report, Sept. 1991.

Anon [1993]: Anon, "British Civil Airworthiness Requirements, Section T, Light Gyroplane Design Requirements", Civil Aviation Authority Paper No. T 860 Issue 2, Jul. 1993.

BASE [1995]: British Aerospace (Systems & Equipment) Ltd., "Vibrating Structure Gyroscopes Principles of Operation", MC1481 Issue 1, Oct. 1995.

Black [1988]: Black, C. G., "A Methodology for the Identification of Helicopter Mathematical Models from Flight Data based on the Frequency Domain", Phd Thesis, University of Glasgow, 1988.

Black & Murray-Smith [1989]: Black, C. G., Murray-Smith, D. J., "A Frequency-Domain System Identification Approach to Helicopter Flight Mechanics Model Validation", Vertica, Vol. 13, No. 3, pp 343-368, 1989.

Bramwell [1976]: Bramwell, A. R. S., "Helicopter Dynamics", Arnold, London, 1976.

CAA [1994]: Houston, S. S., Thomson, D. G., Coton, F., "The Aerodynamics of Gyroplanes", CAA Contract No. 7D/S/1125, Progress Report Phases 1-3, 1994-1997.

Chen [1990]: Chen, R. T. N., "A Survey of Non-Uniform Inflow Models for Rotorcraft Flight Dynamics and Control Applications", *Vertica*, Vol. 14, No. 2, pp 147-184, 1990.

Coton et al [1998]: Coton, F., Smrcek, L. and Patek, Z., "Aerodynamic Characteristics of a Gyroplane Configuration", *Journal of Aircraft*, pp 247-279, 1998.

Doyle & Thomson [2000]: Doyle, S. A., Thomson, D. G., "Modification of a Helicopter Inverse Simulation to Include an Enhanced Rotor Model", *Journal of Aircraft*, Vol. 37, No. 3, pp 536-538, 2000.

Gaonkar & Peters [1988]: Gaonkar, G. H., Peters, D. A., "A Review of Dynamic Inflow Modelling for Rotorcraft Flight Dynamics", *Vertica*, Vol. 12, No. 3, pp 213-242, 1988.

Glauert [1926]: Glauert, H., "A General Theory of the Autogyro", *Aeronautical Research Committee Reports and Memoranda No. 1111*, Nov. 1926.

Glauert & Lock [1928]: Glauert, H., Lock, C. N. H., "A Summary of the Experimental and Theoretical Investigations of the Characteristics of an Autogyro", *Aeronautical Research Committee Reports and Memoranda No. 1162*, Apr. 1928.

Hamel [1991]: Hamel, P. G., "Introduction and Overview", *AGARD AR 280*, pp 1-1/1-4, Sep. 1991.

Hearing [1995]: Hearing, E.A., "Airdata Measurement and Calibration", *AGARD Flight Test Techniques Series, "Introduction to Flight Test Engineering"*, *AGARDograph 300*, Vol. 14, pp 11-1/11-11, 1995.

Houston [1994]: Houston, S. S. "Validation of a non-linear individual blade rotorcraft flight dynamics model using a perturbation method," *The Aeronautical Journal*, Vol. 98, No. 977, pp 260-266, Aug/Sept 1994.

Houston [1996]: Houston, S. S., "Longitudinal Stability of Gyroplanes", *The Aeronautical Journal*, Vol. 100, No.991, pp. 1-6, 1996.

Houston [1998a]: Houston, S. S., "Identification of Autogyro Longitudinal Stability and Control Characteristics", *Journal of Guidance, Control, and Dynamics*, Vol. 21, No. 3, pp 391-399, 1998.

Houston [1998b]: Houston, S. S., "Identification of Autogyro Lateral/Directional Stability and Control Characteristics from Flight Test", *Proc. Instn. Mech. Engrs*, Vol. 212, Part G, *Journal of Aerospace Engineering*, pp 271-285, 1998.

Houston [2000]: Houston, S. S., "Validation of a Rotorcraft Mathematical Model for Aytogyro Simulation", *Journal of Aircraft*, Vol. 37, No. 3, pp 403-409, 2000.

Houston [2001]: Houston, S. S., "Analysis of Rotorcraft Flight Dynamics in Autorotation", University of Glasgow, Department of Aerospace Engineering, Internal Report No. 0104, Feb. 2001.

Houston & Thomson [1997]: Houston, S. S., Thomson, D.G., "Flight Investigation of Gyroplane Longitudinal Flight Dynamics", *Proceedings of the 23d European Rotorcraft Forum*, Sept. 1997.

Houston & Thomson [1999]: Houston, S. S., Thomson, D.G., "Identification of Gyroplane Stability and Control Characteristics", *RTO SCI Symposium on "System Identification for Integrated Aircraft Development and Flight Testing"*, RTO MP-11, pp 31-1/31-11, March 1999.

Jones [1958]: Jones, J. P., "The influence of the wake on the flutter and vibration of rotor blades", *Journal of the Royal Aeronautical Society*, Vol. 64, December, 1958.

Johnson [1980]: Johnson, W., "Helicopter Theory", Princeton University Press, 1980.

Kaletka [1991]: Kaletka, J., "Instrumentation and Data Processing", *AGARD AR 280*, pp 5-3, Sep. 1991.

Klein [1989]: Klein, V., "Estimation of Aircraft Aerodynamic Parameters from Flight Data", Journal of Progress in Aerospace Sciences, No. 1, Vol. 26, 1989.

LabView [1997]: "Labview Data Acquisition Basics Manual", National Instruments Corporation, Edition May 1997.

Leishman [2000]: Leishman, J. G., "Principles of Helicopter Aerodynamics", Cambridge University Press, 2000.

Lock [1927]: Lock, C. N. H., "Further Development of Autogyro Theory Parts I and II", Aeronautical Research Committee Reports and Memoranda No. 1127, Mar. 1927.

Lock & Townhead [1927]: Lock, C. N. H., Townhead, H. C. H., "Wind Tunnel Experiments on a Model Autogyro at Small Angles of Incidence", Aeronautical Research Committee Reports and Memoranda No. 1154, Mar. 1927.

Lopez-Diez et al [1999]: Lopez-Diez, J., Cuerno-Rejado, C. and Lopez-Ruiz, J.L., "Study of Competitive Missions for Autogyros", Proceedings of the 25th. European Rotorcraft Forum, Rome, Italy, Sept. 1999.

Matlab [1996]: "Using Matlab", The MathWorks, Inc., Edition December 1996.

McKay [1999]: McKay, K., "Technical Evaluation Report", RTO SCI Symposium on "System Identification for Integrated Aircraft Development and Flight Testing", RTO MP-11, pp T1-T12, March 1999.

McKillip [1990]: McKillip, R. M., Chih, M. H., "Instrumented Blade Experiments Using a Light Autogyro", Proceedings of the 16th. European Rotorcraft Forum, Glasgow, Scotland, Sept. 1990.

Moulder et al [1979]: Analysis of Aircraft Stability, and Control Measurements", Moulder, J. A., AGARD Lecture Series LS-104, Paper 5, 1979.

Murray-Smith [1991]: Murray-Smith, D. J., "Flight Test Procedures", AGARD AR 280, pp 5-2, Sep. 1991.

National Instruments [1997]: National Instruments Reference Catalogue, 1997.

Newman [1994]: Newman, S., "The Foundations of Helicopter Flight", Edward Arnold, 1994.

Padfield [1981]: Padfield, G.D., "On the Use of Approximate Models in Helicopter Flight Mechanics", *Vertica*, Vol. 5, No. 3, pp 243-259, 1981.

Padfield [1986]: Padfield, G. D., "Integrated System Identification Methodology for Helicopter Flight Dynamics", "System Identification and its Application for Rotorcraft" panel, 42nd Annual Forum of the American Helicopter Society, Washington DC, June 1986.

Padfield [1996]: Padfield, G. D., "Helicopter Flight Dynamics", Blackwell Science, 1996.

Pegg [1969]: Pegg, R. J., "A Flight Investigation of a Lightweight Helicopter to Study the Feasibility of Fixed-Collective-Pitch Autorotations" , NASA TN D-5270, pp. 14, June 1969.

Peters & HaQuang [1988]: Peters, D. A., HaQuang, N., "Dynamic Inflow for Practical Applications", *Journal of the American Helicopter Society*, Technical Note, pp 64-68, October 1988.

Pitt & Peters [1981]: Pitt, D. M., Peters, D. A., "Theoretical Prediction of Dynamic Inflow Derivatives", *Vertica*, Vol. 5, pp 21-34, 1981.

Plaetschke et al [1979]: Plaetschke, E., Schulz, G., "Practical Input Signal Design", AGARD LS 104, Paper 3, 1979.

Prouty [1990]: Prouty, R., "Helicopter Performance, Stability and Control", Krieger Publishing, 1990.

RTO [1999]: RTO SCI Symposium on "System Identification for Integrated Aircraft Development and Flight Testing", RTO MP-11, March 1999.

Rutherford [1997]: Rutherford, S., "Simulation Techniques for the Study of the Manoeuvring of Advanced Rotorcraft Configurations", PhD Thesis, University of Glasgow, 1997.

Schad [1965]: Schad, J. L., "Small Autogyro Performance", Journal of the AHS, Vol. 10, pp 39-43, 1965.

Schrage [1991]: Schrage, D., "System Identification Roadmap", AGARD AR 280, pp 3-1, Sep. 1991.

Sedon [1990]: Sedon, J., "Basic Helicopter Aerodynamics", BSP Professional Books, 1990.

Segner [1973]: Segner, D. R., "AH-56A Compound Helicopter Autorotation Characteristics", Society of Experimental Test Pilots, Technical Review, vol. 11, no. 2, pp 29-47, 1973.

Spathopoulos et al [1998a]: Spathopoulos V. M., Houston, S. S., Thomson, D. G., "Flight Dynamics Issues relating to Autogyro Airworthiness and Flight Safety", Proceedings of the American Helicopter Society 54th Annual Forum, May 1998.

Spathopoulos et al [1998b]: Spathopoulos, V. M., Houston, S. S., Thomson, D. G., "The Calibration and Testing of the GBWTP Montgomerie Gyroplane Instrumentation", University of Glasgow, Department of Aerospace Engineering, Internal Report No. 9823, July 1998.

Stivers & Rice [1946]: Stivers, L. S., Rice, F. J., "Aerodynamic Characteristics of Four NACA Airfoils Sections Designed for Helicopter Rotor Blades", NACA Wartime Report, RBL5K02, Feb 1946.

Tischler et al [1986]: Tischler, M. B., Kaletka, J., "Modelling XV-15 Tilt-Rotor Aircraft Dynamics by Frequency and Time domain Identification Techniques",

AGARD Flight Mechanics Panel Symposium on Rotorcraft Design for Operations, Paper No. 9, Amsterdam, October 1986.

Vleghert [1995]: Vleghert J. P. K., "Performance", AGARD Flight Test Techniques Series, "Introduction to Flight Test Engineering", AGARDograph 300, Vol. 14, pp 13-1/13-14, 1995.

Wheatley [1934]: Wheatley, J. B., "An Aerodynamic Analysis of the Autogyro Rotor with a Comparison Between Calculated and Experimental Results", NACA TR 487, 1934.

Wheatley & Hood [1935]: Wheatley, J. B., Hood, M. J. "Full-scale Wind Tunnel Tests of a PCA-2 Autogyro Rotor", NACA TR 515, 1935.

Young [1978]: Young, C., A, "Note on the Velocity Induced by a Helicopter Rotor in Vortex Ring State", RAE Tech Report 78125, 1978.

